The Roles of Ecological Opportunity and Incumbency Effects in the Macroevolution of the Luzon Island, Philippines "Old Endemic" Murine Rodents

A DISSERTATION
SUBMITTED TO THE FACULTY OF
UNIVERSITY OF MINNESOTA
BY

Dakota Michael Rowsey

IN PARTIAL FULFILLMENT OF THE REQUIREMENTS
FOR THE DEGREE OF
DOCTOR OF PHILOSOPHY

Sharon A. Jansa

May 2019

ACKNOWLEDGMENTS

This work is the result of extensive collaboration with and assistance from many people over the past five years. Of principal importance is the collaboration and assistance of my advisor, Sharon Jansa, who gave me the guidance needed when I was uncertain about which direction to take, but the freedom to develop my own intellectual creativity and find my research niche. I have valued her kind but direct approach to providing advice and feedback on my work. I also appreciate her role as a stalwart advocate of my research over the past few years, and indeed my career, no matter the trajectory I was focused on at the time. I hope that the work that results from this dissertation is only the beginning of a long and productive research collaboration.

I would also like to thank Lawrence Heaney for his critical role in ensuring my success. I do not want to understate the role his fieldwork played in making my work possible – the contribution he has made solely in providing the specimens I have used for my dissertation is one of critical importance. However, of just as much benefit to me as having access to specimens necessary to complete this research was the advice and broader perspective on scientific research he has given me. Of special note to me was the following advice: “learn to cultivate a love of writing,” which I have tried to model since I first heard it. As with Sharon, I greatly look forward to our future research endeavors.

My patient and longsuffering committee members, Keith Barker, David Fox, and Kieran McNulty helped me tap into the intellectual merit and rigor of my research questions, but just as importantly they provided me with complementary perspectives to

my research, ways of looking at my result through different lenses, and ideas for augmenting my analyses. The feedback they had, along with that of the members of the Barker-Jansa lab group over the years, including Matthew Dufort, Michael Wells, Juan Díaz-Nieto, Danielle Drabeck, Carmen Martin, Tyler Imfeld, Shanta Hejmadi, Ryan Keenan, and Gabriele Ilarde, substantially improved this dissertation. Carmen Martin deserves additional acknowledgment due to her patient coaching on molecular lab technique during the beginning of my graduate career.

I am grateful to the museum staff and curators who have lent their time and specimens for me to use. These include the late Danilo Balete and William Stanley as well as John Phelps and Adam Ferguson (FMNH); Neil Duncan, Eleanor Hoeger, Eileen Westwig, Nancy Simmons, and Robert Voss (AMNH); Leo Joseph and Alex Drew (ANWC); Darrin Lunde and Megan Krol (USNM); and Judith Chupasko (MCZ). Pierre-Henri Fabre provided useful sequence data and Brian Bagley provided training and assistance to use the University of Minnesota's XRCT scanner.

Funding for my research was provided by several sources, including an American Society of Mammalogists Grant-in-Aid of Research, the Joyce Davenport Fellowship in Natural History, the Florence Rothman Fellowship, and the Dayton Wilkie Fellowship, the latter three of which were awarded to me by the Bell Museum of Natural History. Fellowship support awarded to me by the Bell Museum included the Dayton Fellowship and the Simons Fellowship. I am also grateful for the Research Assistant and Curatorial Assistant positions awarded to me by Keith Barker and Sharon Jansa.

I would also like to thank my friends scattered across the globe, including Kelly Flanders, Axton Moore, Shaun Emsley, and Jason and Sarah Culp, as well as local friends and cohort members, including Rachel King, John Cossette, and Tyler and Melissa Imfeld. They helped me always remember that there is a time and a place for work and for rest, and that finding the right balance is crucial.

Finally, I would like to thank my parents, grandparents, siblings, aunts, and uncles, for the constant words of encouragement, king cakes, homemade soups, and other things that kept me warm during the Minnesota winters both literal and figurative.

DEDICATION

This dissertation is dedicated to Kristie Rowsey, whose fortitude and force of will inspire me, and to Renee Rogers, whom I wish could see her son today.

ABSTRACT

The evolutionary theory of adaptive radiation posits that lineages that experience a breadth of available resources in the absence of competition, known as ecological opportunity, should diversify to specialize on aspects of these available resources. The rapid evolution decelerates as niches fill in a static, spatially limited system, resulting in an assemblage of ecologically distinct species. Despite evidence to support this mode of diversification, little attention has been given to how this process unfolds in systems with multiple, ecologically similar colonizing lineages. The primary-colonizing, or incumbent, lineage, through exploiting niches in the absence of competitors, may serve to depress the rates and patterns of species and ecological diversity of subsequent colonists.

In this dissertation, I explored four aims that seek to test whether the evolution of two clades of rodents endemic to Luzon Island, Philippines, Chrotomyini and Phloeomyini, exhibited evolution consistent with incumbency effects held by Phloeomyini and placed on secondary-colonizing Chrotomyini. First, I determined whether the rates of lineage diversification of the two Luzon Old Endemic (LOE) clades were consistent with reduced ecological opportunity in secondarily-colonizing Chrotomyini, resulting in lower rates of species accumulation. My results instead indicate that Chrotomyini has experienced a faster rate of diversification inconsistent with incumbency effects. Second, I tested whether the mandible of the LOE rodents, as a proxy for diet, exhibits rates of evolution consistent with lower ecological opportunity for Chrotomyini as well as patterns of diversity consistent with clade-specific partitioning of morphological variation. I found that both LOE clades evolved disparate mandible shapes

at a similar rate, apart from outlying genus *Rhynchomys*, but that the two clades occupy nearly discrete areas of morphospace. Third, I tested whether the shape of the humerus can be used to approximate locomotory niche in a similar way to linear measurements of the ulna, metacarpal, and phalanx, to determine whether the morphology associated with locomotory strategy in the two LOE clades is convergent on shared locomotory mode. I found that although the humerus predicts some aspects of locomotory strategy, a substantial proportion of shape variation is reflected by different adaptations within shared locomotory category, thus providing a complement to, rather than replacement for, distal forelimb measurements. Finally, I tested whether the observed lack of mandibular shape overlap between the two LOE clades is consistent Chrotomyini being limited by Phloeomyini in terms of the area of morphospace it could diversify into and whether the ancestral chrotomyine lineage may have exhibited morphology disparate from Phloeomyini, thus facilitating its colonization and subsequent diversification. I found that the patterns of mandibular shape variation in the two LOE clades are consistent with the establishment of a biotic filter, meaning that Chrotomyini's success on Luzon was facilitated by persistent ecological distinction from incumbent Phloeomyini.

This dissertation illustrates that subfamily-related clades can experience substantial ecological distinction both within and between each clade. This distinction can permit repeated colonization of spatially constrained systems: as long as each colonizing clade remains ecologically distinct, evolution may proceed uninhibited by inter-clade competitive effects. Incumbency effects may thus more strongly influence the community assembly of species in a system than their evolutionary rates.

TABLE OF CONTENTS

LIST OF TABLES

LIST OF FIGURES

INTRODUCTION

THE ROLES OF ECOLOGICAL OPPORTUNITY AND INCUMBENCY EFFECTS IN THE MACROEVOLUTION OF THE LUZON ISLAND, PHILIPPINES "OLD ENDEMIC" MURINE RODENTS

Adaptive radiation through ecological opportunity has formed the cornerstone of macroevolutionary biology, explaining patterns of diversity across spatial and temporal scales. This process is typically facilitated by colonizing a depauperate system or evolution of a novel trait that allows exploitation of previously inaccessible niches. In either case, the focal lineage can rapidly diversify to specialize on aspects of these niches, with decelerating evolutionary rates as they are filled. The result of this process is a diverse assemblage of ecologically distinct species, in many cases endemic to a geographically isolated system (Losos et al. 1998; Gillespie 2004; Lack 1947).

Adaptive radiation has typically been explored with respect to a single lineage that colonizes an isolated system, such as an oceanic island, and subsequently diversifies to specialize on niches according to the model of ecological opportunity (Parent and Crespi 2009; Reddy et al. 2012). However, comparatively little attention has been given to how lineage and ecomorphological evolution unfold in systems that are colonized multiple times by closely related lineages. This repeated colonization may change the resultant biodiversity of the system because the primary-colonizing, or incumbent, lineage may affect the rates of species and phenotypic evolution of subsequent colonists

in several ways. First, non-incumbents may be limited in terms of how quickly they change over time: colonizing an already occupied system may mean that the secondary colonists exhibit less ecological opportunity than incumbents. Second, the ecomorphological diversity of non-incumbents may be constrained to be distinct from that of primary colonists to limit competition for finite niches. Finally, incumbent clades may prevent ecologically similar lineages from invading the system in the first place by competitively excluding these potential colonists – a process known as biotic filtering (Urban and De Meester 2009).

Testing these predictions for how active incumbency influences adaptive evolution requires a study system to meet four key requirements. First, three clades must be included, where one clade is the incumbent and one is the secondary colonist on a system. The non-incumbent must be sister to an incumbent lineage on another system – this provides the expectation of what the non-incumbent may have been able to do in the absence of competitive effects (a control group of sorts). Second, the three clades must be reasonably closely related so that they can be expected to compete for access to niches. Third, each clade must be reasonably diverse – this provides statistical power to test these hypotheses. Fourth, the focal system occupied by the clades potentially engaging in incumbency-influenced evolution must be spatially small enough to promote competition for finite resources.

The two broadly sympatric clades of Luzon Island "Old Endemic" (LOE) murine rodents of the Philippines, Phloeomyini and Chrotomyini, along with the third allopatric clade of Sahul "Old Endemic" (SOE) rodents, satisfy these requirements well. Incumbent

Phloeomyini and secondary-colonizing Chrotomyini colonized Luzon Island within the past 15 million years and subsequently diversified to a group of over 40 species (Jansa et al. 2006; Schenk et al. 2013). This species assemblage constitutes approximately 80% of the native non-flying mammal species on an island, which, at approximately 110,000 square kilometers, is only slightly larger than the size of Cuba. Previous studies illustrate that Phloeomyini and Chrotomyini may have colonized Luzon several million years apart, establishing the expectation that Phloeomyini may have limited chrotomyine access to niches. Furthermore, Chrotomyini's sister relationship to SOE, the incumbent murine radiation of New Guinea, Australia, and Melanesia, provides the expectation of potentially realizable evolution in the absence of murine competitors.

In this dissertation, I examine multi-clade macroevolution from several perspectives with respect to how species and ecological diversity accumulate in spatially limited systems, with an emphasis on how incumbency effects may limit the ability of secondary colonizing clades to persist and radiate. In Chapter 1, I infer a new phylogenetic tree of subfamily Murinae to examine whether the rates of lineage diversification in the two LOE clades are consistent with an ecological opportunity model. I also test whether Chrotomyini exhibited a lower lineage diversification rate than Phloeomyini due to their status as secondary colonists. In Chapter 2, I use the shape of the mandible, a trait approximating dietary niche, to ask similar questions regarding the evolutionary tempo and mode as in Chapter 1: specifically, whether both clades evolved under a decelerating evolutionary model and whether Chrotomyini had a limited rate of mandibular shape evolution. I also examine whether the distribution of mandibular

variation is consistent with Chrotomyini and Phloeomyini partitioning niches between clades. In Chapter 3, I examine the relationship between humerus shape and locomotory variables to determine whether the diversity of humerus shapes among LOE species best approximates ecological adaptation to distinct locomotory strategies or parallel evolution that differs among genera. Finally, in Chapter 4, I test whether the diversity of mandibular shape in the two LOE clades is consistent with Chrotomyini being unable to radiate into areas of morphospace being occupied by Phloeomyini as well as whether Chrotomyini may have been ancestrally ecologically distinct from Phloeomyini, potentially facilitating the successful colonization of the non-incumbent clade. My work thus provides the most in-depth test of incumbency effects to date with specific focus given to multiple evolutionary processes and perspectives.

CHAPTER 1. DIVERSIFICATION RATES OF THE "OLD ENDEMIC" MURINE RODENTS OF LUZON ISLAND, PHILIPPINES ARE INCONSISTENT WITH INCUMBENCY EFFECTS AND ECOLOGICAL OPPORTUNITY[1]

Introduction

The factors that contribute to species and ecological diversity are of central concern in evolutionary biology. One of the key triggers shown to contribute to cladogenesis and morphological evolution is ecological opportunity, or the availability of unoccupied niches for a lineage to diversify into (Schluter 2000a; Yoder et al. 2010). This opportunity can be generated by several factors, including dispersal to a depauperate ecosystem, such as an oceanic island (Baldwin and Sanderson 1998, Reddy et al. 2012; Borregaard et al. 2017) or an evolutionary innovation that provides relief from existing competition (Wainwright et al. 2012). Ecological opportunity can facilitate adaptive radiation, rapidly producing a variety of ecologically and morphologically diverse species (Lack 1947; Gillespie 2004; Losos 2011). When examined in a phylogenetic context, ecological opportunity may manifest as a pattern of diversity-dependent cladogenesis, in which lineage diversification rates decrease as competition for available niches increases during a radiation (Nee et al. 1992; Rabosky and Lovette 2008; Skipwith et al. 2016). The phylogenetic signature left by this process can be detected by analyzing the branching

[1] Reproduced with permission from Rowsey, D. M., L. R. Heaney, and S. A. Jansa. 2018. Diversificaiton rates of the "Old Endemic" murine rodents of Luzon Island, Philippines are inconsistent with incumbency effects and ecological opportunity. Evolution 72:1420-1435.

patterns of the focal clade using standard diversification rate analyses (Rabosky 2006; Rabosky 2014).

The influence of competition in shaping diversity has been explored for unfolding adaptive radiations in a variety of natural systems, especially islands, and previous studies have provided support for its effects on the rate of species accumulation (which I refer to as diversification rates) and morphological change over time (which I refer to more broadly as phenotypic evolutionary rates) (Whittaker and Fernandez-Palacios 2007). For example, Schluter and Grant (1983) showed that community assembly of *Geospiza* finches is functionally overdispersed, which minimizes interspecific competition for limited food resources. In a taxonomically broad study, Schluter (2000b) used a meta-analysis approach to examine the prevalence of ecological character displacement, or the divergence in phenotype associated with niche differentiation in closely related species, in natural systems. His results indicated this phenomenon is common and strongly supported in taxa such as *Gasterosteus* sticklebacks, *Geospiza* finches, and heteromyid rodents of the North American desert southwest, although direct causal links between interspecific competition and phenotypic change were often lacking (Schluter 2000b). In this regard, Parent and Crespi (2009) determined intraspecific variation in Galápagos *Bulimulus* land-snail shell shape was negatively correlated with the number of congeners occurring in the same habitat type and positively correlated with food resource heterogeneity. Finally, several recent studies of lineages on oceanic islands have detected patterns of lineage diversification consistent with declining ecological opportunity, including Hawaiian leafhoppers (Bennett and O'Grady 2013), New

Caledonian geckos (Skipwith et al. 2016), and Philippine frogs (Blackburn et al. 2013). In sum, these studies provide evidence that resource availability in the absence of competition can expand the intraspecific variation that may promote the evolution of ecologically distinct species and thus result in increased lineage diversification as well as morphological evolution.

Nevertheless, most studies to date have focused on the evolution of a single lineage and have not addressed how diversification is affected when a system contains multiple, ecologically similar, radiating lineages. Just as density dependence can slow diversification within a single radiating lineage, one can predict that the presence of an ecologically similar lineage may reduce the rate of diversification of a second lineage that disperses to the system. If the colonizing events were asynchronous, the later-dispersing clade may experience a lower diversification rate proportional to the extent of diversification of the primary lineage at the time of secondary colonization. The macroevolutionary advantage held by this primary colonizing lineage is an example of an incumbency effect, whereby a lineage gains an advantage simply by being present in an area first (Case 1991; Alroy 1996).

Whereas this study focuses on the role of incumbency at the macroevolutionary scale, historically, incumbency (or priority) effects were hypothesized as a mechanism to explain alternative stable states in community assembly. In this context, the presence of certain species can alter, whether positively or negatively, the ability of other species to become established (Sutherland 1974). This theory has been extended to suggest that community assembly can be altered simply by the order of colonization of the constituent

species (Drake 1991). The ability of a lineage to colonize given the existence of a competitor is dependent on several factors, including habitat availability, presence of predators, and relatedness of invading species to incumbent species (Fukami 2007; Louette and De Meester 2007; Tan et al. 2012). These short-term ecological effects on community composition, when extended over large temporal scales, may result in differences in evolutionary process between primary and secondary colonizing lineages.

From this macroevolutionary perspective, incumbency effects can be examined in two different types of systems: those that have been released from incumbency effects through extinction of competitors or dispersal to a novel environment, and those in which lineages come into competition due to secondary colonization. A popular example of diversification after extinction of a competing lineage is the Cretaceous-Paleogene (K-Pg) extinction and subsequent ecological release of mammals during the Cenozoic (O'Leary et al. 2013, but see dos Reis et al. 2014). Similarly, Darwin's finches provide a classic example of diversification after dispersal to a competitor-deficient system (Burns et al. 2014). In both cases, the focal lineage undergoes rapid diversification after existing incumbency effects—in the form of competing lineages—have been removed. Detecting such examples requires analysis of diversification rates either in the context of a densely sampled fossil record or with a phylogenetic perspective that includes both dispersing lineages as well as source taxa. Alternatively, incumbency effects on diversification may occur when two lineages come into contact through independent colonizations of a system. In this case, one might expect secondary colonists to experience reduced ecological opportunity— and resulting lower diversification rates—compared to primary

colonists. Detecting incumbency effects in this case requires a robust phylogenetic framework for the two interacting clades, along with analyses of diversification patterns and rates. In addition, researchers must also make prima facie arguments that the two lineages are ecologically similar enough to potentially compete over limited resources. Systems that satisfy these biological and methodological requirements for either approach are relatively rare, meaning there is much to learn about how incumbency and ecological release affect diversification.

Despite the relative scarcity of studies in which multiple ecologically similar clades have colonized a system, several authors have used this approach to test for incumbency effects at continental scales in birds, fishes, and mammals, examining both rates of lineage diversification (Betancur-R. et al. 2012; Schenk et al. 2013) and morphological evolution (Jønsson et al. 2015; Alhajeri et al. 2016), with mixed support for incumbency affecting diversification. However, the geographic scale at which incumbency may be important in diversification remains an open question. For example, in a study of muroid rodents, Schenk et al. (2013) found some evidence for ecological opportunity affecting diversification at the continental scale for South American muroids, but little evidence for ecological opportunity or incumbency effects in other geographic regions. This study did not examine these processes at the scale of individual islands, and in some cases aggregated archipelagic and continental regions with endemic rodent assemblages (e.g., Southeast Asia), potentially masking more localized patterns of diversification. Furthermore, the analysis of continent-sized landmasses, rather than more spatially limited systems, may be too broad for the detection of adaptive radiation and/or

incumbency effects at relatively short timescales. If the breadth of land area and niches available to a clade are sufficiently large or temporally dynamic, interspecific competition may be outweighed by other factors affecting diversification, such as phylogenetically conserved range limits and climatic or geological vicariant events (Goldberg and Lande 2007; Ribas et al. 2007; Derryberry et al. 2011).As a result, the hypothesis that incumbency limits ecological opportunity and slows diversification may best be tested at finer geographic scales, with clades that are more likely to be competing for niches, to measure its importance in determining the species diversity of natural systems.

The endemic rodents of Luzon Island, Philippines afford the opportunity to test hypotheses regarding incumbency and diversification rates at a spatially limited scale. The endemic murine rodents of Luzon have been the subject of extensive field and museum studies in recent decades (reviewed in Heaney et al. 2016a,b) and are an exceptional instance of endemism and diversification following repeated colonization, with up to six colonization events since the middle Miocene (Jansa et al. 2006). The two oldest colonizing lineages, Phloeomyini and Chrotomyini, are referred to as the Luzon "Old Endemic" radiations and comprise the majority (nearly 90%) of native non-volant mammalian diversity on Luzon. These two clades exhibit substantial variation in body size, diet, and other traits, both within and between each clade, yet species in each clade typically occur sympatrically in high-elevation montane and mossy forest (Heaney et al. 2016a). Importantly, the Luzon Old Endemic (LOE) rodents are not sister clades within Murinae and appear to have colonized Luzon several million years apart during the

middle Miocene (Jansa et al. 2006; Schenk et al. 2013; Rowe et al. 2016). An estimated four additional rodent colonizations of Luzon have occurred within the last 5 million years; these four independent colonization events resulted in less diverse, primarily low-elevation clades that are collectively referred to as the "New Endemic" murine rodents (Jansa et al. 2006; Kyriazis et al. 2017). Despite extensive surveys cataloging Luzon's mammalian biodiversity, the LOE rodents lack a comprehensive species-level phylogeny. The absence of this phylogeny obscures the relationships within each clade, the history of island colonization and intra-island diversification, as well as estimates of lineage diversification and phenotypic evolutionary rates.

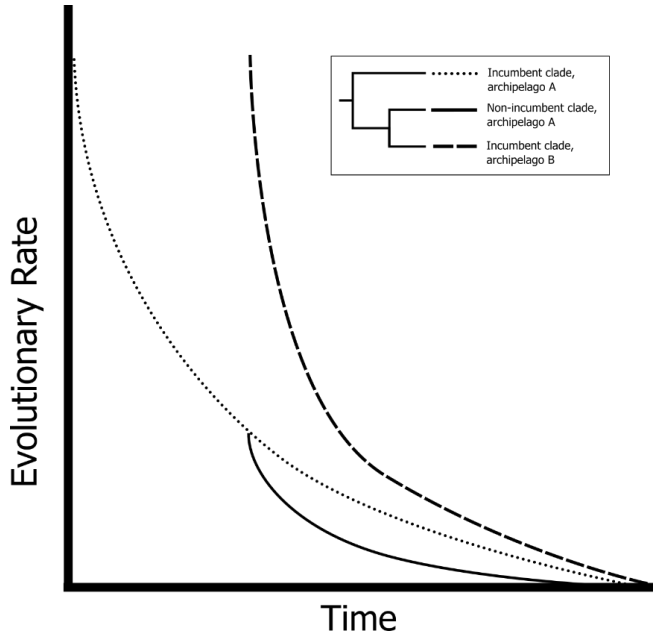

Figure 1.1. Diversification rates-through-time for a three-clade scenario supporting ecological opportunity and incumbency driving diversification. A phylogenetic tree illustrates the relationships among two incumbent clades and a secondary-colonizing clade. The dotted line represents the incumbent clade in the focal system, the solid line represents the second colonizing clade in the focal system, and the dashed line represents an incumbent clade of a different system which is sister to the secondary-colonizing clade of the focal system. All clades follow a model of diversity-dependent cladogenesis, suggesting ecological opportunity is the driving diversification process, but the secondary colonist has a lower diversification rate than both the incumbent lineage and its sister lineage.

In addition to generating the first species-level phylogeny of these two clades, I use the LOE rodents to test several predictions of how incumbency and ecological opportunity impact lineage diversification using finely sampled molecular phylogenies and macroevolutionary inference. If ecological opportunity and incumbency have played an important role in the diversification of LOE rodents, I first expect to recover temporally decelerating diversification rates in both clades consistent with clade-specific, diversity-dependent cladogenesis. Second, if the two clades share a background diversification rate, I expect the secondary colonizing clade (i.e., Chrotomyini) to experience a decrease in that rate. Third, since the two potentially competing clades are not sister clades, I expect to find a lower diversification rate in the secondary colonizing clade relative to its sister clade (Figure 1.1). This is because the secondary colonizing lineage must compete with the primary colonizing clade as well as with other descendant species of its own lineage. Recovering support for this prediction would implicate colonization of Luzon in the decreased diversification rate of Chrotomyini, rather than a decreased diversification rate inherited prior to colonization. The disparity in diversification rate is most easily testable if the secondary-colonizing clade's sister lineage is a primary colonist of another system. In this case, Chrotomyini are sister to the Sahul Old Endemic (SOE) rodents, so named for their range which includes New Guinea and Australia (Rowe et al. 2008). This clade does not overlap in distribution with either focal clade and may exhibit ecological opportunity consistent with an absence of potential competitors.

Materials and Methods

Taxon sampling.

We sampled 204 murid rodent species, including 39 species of Luzon Old Endemic (LOE) rodents, nine species of Old Endemic rodents from elsewhere in the Philippine archipelago, and three species of Luzon "New Endemic" rodents to generate a comprehensive phylogeny of LOE species in the context of broader Murinae. I included all species of murids currently known from Luzon except *Batomys dentatus*, *Crunomys fallax*, and *Tryphomys adustus*. The first and second of these are known only from the holotypes, and the third from a small number of specimens without easily sampleable genetic material (Heaney et al. 2016a).

Sequences from additional murid species were chosen primarily from publicly available sources obtained from previous studies (Steppan et al. 2005; Rowe et al. 2008; Benson et al. 2013; Schenk et al. 2013; Pagès et al. 2016; Rowe et al. 2016; P.-H. Fabre, Université Montpellier II, personal communication, August 2017) and were included to place the Philippine murine radiations in the context of murid phylogeny and to provide the best possible divergence date estimates given available fossil data. I selected taxa from subfamilies Gerbillinae, Deomyinae, and Lophiomyinae as outgroups based on their close phylogenetic proximity to Murinae (Schenk et al. 2013; Pagès et al. 2016; Steppan and Schenk 2017).

DNA extraction and sequencing.

We sampled seven loci at varying coverage for the species in this dataset: the entire mitochondrial gene cytochrome b (CYTB, 1144 bp), exon 11 of breast cancer activating gene 1 (BRCA1, 2784 bp), exon 10 of growth hormone receptor (GHR, 937 bp), exon 1 of interphotoreceptor retinoid-binding protein (IRBP, 1300 bp), recombination activating gene 1 (RAG1, 3040 bp), parts of exons 2 and 3 and the intervening intron of acid phosphatase 5 (ACP5, 450 bp), and intron 7 of β-Fibrinogen (FGB7, 794 bp). For newly generated sequences, tissues were obtained from vouchered specimens held at the Field Museum of Natural History (FMNH) and the Smithsonian National Museum of Natural History (USNM). DNA was extracted using a DNeasy Blood and TissueKit (Qiagen,Germantown, MD).We amplified genes using PCR with the following primers for each locus: CYTB: MVZ05a and UMMZ04 (Smith and Patton 1991; Jansa et al. 1999); GHR: GHRF1 (GHREXON10 in Adkins et al. 2001) and GHREND (Adkins et al. 2001); IRBP: IRBPA and IRBPB (Stanhope et al. 1996); FGB7: FGB7F1 (5' ACGGCATGTTCTTCAGCACG 3'); and FGB7R1 (5' ATCCCTTCCAGTTCATCCACAC 3'). These sequence data have been submitted to the GenBank database under accession numbers MH330617-MH330660. All BRCA1, RAG1, and ACP5 sequences were obtained from previous studies. The concatenated sequence matrix was deposited in TreeBase under accession number 22736; GenBank numbers of sequences used in these phylogenetic analyses can be found in Appendix Table 1.1. All genes were amplified by PCR with a touchdown protocol optimized for each locus (Jansa and Weksler 2004). Amplicons were sequenced using Sanger

sequencing from both template strands. Sequencing was performed by GENEWIZ (South Plainfield, NJ) and the resultant reads were assembled in Geneious R10 (Biomatters Ltd., Auckland, New Zealand). Consensus DNA sequences were aligned using MUSCLE (Edgar 2004) and concatenated for phylogenetic analysis.

Phylogenetic inference.

We used PartitionFinder version 1.1.1 (Lanfear et al. 2012) to determine the best-fitting scheme of nucleotide partitioning and corresponding substitution models. The partitioning scheme varied depending on the analytical approach. For maximum likelihood analyses, I specified candidate partitions for each codon position within each exon and one partition for each intron for a total of 20 potential partitions. For the Bayesian estimation of phylogeny, multiple partitions for each locus produced schemes that prevented Markov-Chain Monte Carlo (MCMC) convergence. Because of this, I used a simpler model allowing one partition for each locus, other than ACP5, for which I proposed one partition for the exons and one for the internal intron. Candidate substitution models were selected based on those implemented in RAxML (Stamatakis et al. 2008) and BEAST 2 (Bouckaert et al. 2014), and compared using the Bayesian Information Criterion (BIC; Schwarz 1978).

We inferred murine phylogeny using maximum likelihood in RAxML v8.2.9, using resources of the CIPRES Science Gateway (Stamatakis et al. 2008; Miller et al. 2010). Variants of the general time reversible model allowing for among-site rate heterogeneity were applied to each partition (GTR with invariant sites and gamma-

distributed rates; Gu et al. 1995). I specified 10 independent searches from randomly-generated starting trees, and nodal support was assessed using 1000 bootstrap permutations conducted using each of 10 starting trees.

Bayesian estimation of phylogeny was conducted using BEAST version 2.4.2 (Bouckaert et al. 2014) on the concatenated data partitioned by locus using the best scheme selected by PartitionFinder. I linked tree models across all partitions, allowed site models to vary among partitions, and estimated separate log-normally-distributed relaxed uncorrelated clock models for CYTB and the nuclear loci (Drummond et al. 2006).To provide divergence date estimates in absolute time, I specified uniform age priors on specific taxa as follows, based on fossil age estimates provided in Kimura et al. (2015): The "*Mus*-*Arvicanthis*" split: 11.1-12.3 million years ago (Ma); the most recent common ancestor (MRCA) of the *Arvicanthis*, *Otomys*, and *Millardia* divisions: 8.7-10.1 Ma; the MRCA of Murini: 7.3–8.3 Ma. I additionally applied a log-normally-distributed prior on the age of Gerbillinae + Deomyinae with 95% quantiles of 16.0–23.0 Ma (Thomas et al. 1982; Schenk et al. 2013). I specified a Yule tree prior with an estimated birth rate given an exponential prior with the initial mean set to 10. All other priors were left with default values. The BEAST analysis was conducted on the CIPRES Science Gateway (Miller et al. 2010) using four additional runs for 1.7×10^8 generations, with trees sampled independent runs: one run for 3.1×10^8 generations and three every 50,000 generations. Parameter convergence was analyzed using Tracer v1.6, with the first 10% of trees discarded as burn-in from each run before combining. The first 2.2×10^8 of the resulting 7.4×10^8 sample generations was subsequently discarded. In total, 1.0×10^5 trees were

generated from this remaining distribution. A maximum clade credibility (MCC) tree was generated from this posterior tree distribution using TreeAnnotator version 2.4.0 (Bouckaert et al. 2014). In addition to generating concatenated trees, I generated gene trees for each locus in BEAST, the MCC trees for which are reported in Appendix Figures 1.1-1.6.

Estimates of Luzon colonization times.

We used the Bayesian posterior tree distribution to estimate colonization times for each of the five Luzon rodent groups I sampled. For the LOE rodents, I calculated the interval of colonization as the time between the stem and crown ages of the clade, corresponding to the maximum and minimum colonization times for each clade. These times were calculated across the 95% highest posterior density (HPD) of divergence times for each clade. I generated probability distributions by populating 0.2 My bins between the maximum and minimum age for each estimate with the normalized proportion of trees in which the given date fell between the stem and crown ages of a clade. Because intra-island speciation events were unavailable to sample for the three New Endemic rodent colonization events, I calculated the maximum colonization ages for these species as the divergence date between each Luzon species and their non-Luzon sister lineage. The distribution of times for each clade was plotted to visualize the probability of independent colonization.

Testing for diversity-dependent cladogenesis and diminished ecological opportunity.

To assess the role of ecological opportunity in diversification, I first assessed whether the pattern of diversification was consistent with expectations of diversity-dependent cladogenesis for each LOE rodent clade. This model predicts initially rapid speciation that diminishes toward the present as ecological opportunity declines. I visualized lineages-through-time (LTT; Nee et al. 1992) of the two Philippine Old Endemic clades after non-Luzon species were pruned from the MCC tree to determine whether the rate of speciation was approximately constant on a logarithmic scale. Under diversity-dependent cladogenesis, lineages are expected to accumulate nonlinearly on a logarithmic scale, with a decrease in slope over time. This change in branching times was quantified using the gamma (γ) statistic applied to each LOE clade, which tests the null hypothesis that the rate of speciation is constant through time. Estimating a γ value less than the critical value of –1.645 (at $\alpha = 0.05$) indicates that speciation events are closer to the root of the reconstructed phylogeny, and thus that the majority of diversification took place earlier in the clade's history, than would be expected under a pure birth diversification process (Pybus and Harvey 2000). This method assumes complete species-level sampling of the clades of interest. While I am reasonably confident that the sampling of LOE species is near completion, the sampling of SOE rodents is far from complete. As such, I could not meaningfully perform this analysis on the SOE rodents. I performed these analyses using the *ape* and *phytools* packages in R (Paradis et al. 2004; Revell 2012; R Core Team 2015).

We also tested for temporally decelerating diversification rates using a model-fitting approach. I compared the fit of five evolutionary models, including a Yule diversification model, a constant-rate birth-death model, and time-dependent rate models with decreasing speciation rates (SPVAR), increasing extinction rates (EXVAR), or both (BOTHVAR; Yule 1924; Nee et al. 1994; Rabosky 2006). The fit of these models was compared using the Akaike information criterion corrected for small sample sizes (AICc; Akaike 1974; Hurvich and Tsai 1989), with the model with the highest Akaike weight (*w*) accepted as the best. Model fitting was conducted using the laser package of R using default parameter settings for each function (Rabosky 2006). To ensure that model selection was not driven by the choice of a Yule tree prior in my BEAST analysis, I performed an additional model selection analysis using a distribution of trees sampled under a birth–death prior with the topology constrained to that of the original tree (samples generated: 2.9×10^8, trees generated: 2.9×10^5). As with the LTT analysis, I did not perform diversification model fitting using on the SOE rodents, for which I lack species-level sampling.

To test for incumbency effects, I assessed whether the secondary colonizing clade (Chrotomyini) has a lower diversification rate than either (1) the incumbent clade that occupies the same system (Phloeomyini) as well as (2) its sister clade (the SOE), which diversified across Sahul in the absence of an earlier-arriving clade of murine competitors. I estimated diversification rate parameters for these three, independent radiations using a likelihood-based framework that accounts for lineage-specific sampling probabilities (Alfaro et al. 2009; estimated using modified MEDUSA code from Jansa et al. 2014). For

this analysis, I pruned the MCC tree to include the two focal groups in each test. Furthermore, I pruned the SOE clade to genus level (i.e., by removing *Pogonomys macrourus* and *P. sylvestris*) and enumerated the species represented by each genus according to Musser and Carleton (2005) supplemented by Rowe et al. (2008) and Rowe et al. (2016). Pruning two of the three species of *Pogonomys* was necessary due to incomplete phylogenetic sampling of this genus and uncertainty associated with relationships of these unsampled species to the three species that were sampled. I then estimated the maximum likelihood parameter values and 95% confidence interval on the net diversification rate ($r = \lambda - \mu$, where λ represents speciation rate and μ represents extinction rate) and extinction fraction ($\varepsilon = \mu/\lambda$) for each clade. This confidence interval was approximated by generating the likelihood surface up to 3 log-likelihood units from the maximum likelihood estimate of these parameters. If incumbency has affected diversification of Chrotomyini, I would expect this clade to exhibit a lower net diversification rate than both Phloeomyini (the competing clade) and the SOE rodents (its sister clade, which radiated elsewhere without other murine competitors). Statistical significance for the difference in rates is inferred if the maximum likelihood estimate (MLE) of diversification rate for one clade falls outside an interval described by 3 log-likelihood units around the MLE for the other.

Finally, as an additional approach to testing these three diversification rate hypotheses, I examined rate heterogeneity using Bayesian Analysis of Macroevolutionary Mixtures v2.5.0 (BAMM; Rabosky 2014) to test differences in diversification rate for each clade of LOE rodents, while allowing for time-dependent diversification rates and

clade-specific sampling probabilities. I used a backbone species sampling probability of 0.89. This value was calculated as the ratio of the estimated number of species within murine genera sampled in the phylogenetic analysis out of the total number of murine species, effectively accounting for the proportion of murine rodents in genera unsampled in the phylogenetic analysis. I also determined genus-specific sampling probabilities to account for unsampled species within sampled genera. In both cases, murid species richness was determined using Musser and Carleton (2005), supplemented by additional sources for many genera (Appendix Table 1.2).

We used initial parameters suggested by the setBAMMPriors function of the R package *BAMMtools* (Rabosky et al. 2014) and conducted an MCMC analysis for 10^8 generations, saving one in every 1000 states. I discarded 10% of samples of the resultant distribution as burn-in and subsampled the remaining samples to 5000. I then examined the 95% credible shift set of this distribution to determine support for rate shifts on branches leading to the clades containing LOE rodents. I interpreted support for diversification driven by ecological opportunity as recovering diversity-dependent cladogenesis with a higher initial diversification rate in the LOE rodent clades compared to the background diversification rate. Conversely, I interpreted support for diminished ecological opportunity as recovering a rate shift followed by decreasing diversification rates along the branch leading to Chrotomyini.

Table 1.1. Partitions best supported by model comparison using PartitionFinder v1.1.1 (Lanfear et al. 2012).

Partition	Model	Coding positions
RAxML 1	GTR+I+Γ	CYTB pos 1
RAxML 2	GTR+I+Γ	CYTB pos 2
RAxML 3	GTR+I+Γ	CYTB pos 3
RAxML 4	GTR+I+Γ	GHR pos 1, IRBP pos 2, RAG1 pos 1, ACP5 exon pos 2
RAxML 5	GTR+I+Γ	GHR pos 2, IRBP pos 3, RAG1 pos 2, ACP5 exon pos 3
RAxML 6	GTR+Γ	GHR pos 3, BRCA1 pos 3, FGB7
RAxML 7	GTR+Γ	IRBP pos 1, RAG1 pos 3
RAxML 8	GTR+Γ	BRCA1 pos 1, BRCA1 pos 2, ACP5 exon pos 1
RAxML 9	GTR+I+Γ	ACP5 intron
BEAST 1	GTR+I+Γ	CYTB
BEAST 2	K80+I+Γ	GHR
BEAST 3	SYM+I+Γ	IRBP
BEAST 4	GTR+Γ	BRCA1
BEAST 5	SYM+I+Γ	RAG1
BEAST 6	SYM+I+Γ	Acp exon
BEAST 7	HKY+I+Γ	Acp intron
BEAST 8	GTR+Γ	FGB7

Results

Phylogenetic relationships among murines.

The PartitionFinder analysis identified nine nucleotide partitions for maximum likelihood (ML) analysis and eight for the Bayesian analysis as the best fit models given the candidate partitions (Table 1.1). Among the OE rodents, bootstrap support values in ML analysis were comparatively weakest within the genus *Apomys*, with other areas of weak support including divergences within *Chrotomys*, *Musseromys*, and *Soricomys* (Figure 1.2). Bayesian nodal support values were generally stronger than their ML counterparts (>0.95) apart from some areas of weak support within *Chrotomys*, *Musseromys*, and *Soricomys* (Figure 1.3). The phylogenetic relationships I recovered among OE rodents were generally consistent with previous studies (Jansa et al. 2006;

Schenk et al. 2013; Justiniano et al. 2015; Rowe et al. 2016). A single exception occurred in the placement of *Apomys minganensis*, which I recovered as sister to *Apomys abrae* and *Apomys datae* compared to the placement as sister to the clade containing *A. brownorum* and *A. sacobianus* as estimated in previous work (Justiniano et al. 2015). Interestingly, the phloeomyine genera *Crateromys* and *Batomys* were not reciprocally monophyletic. *Crateromys australis*, a species endemic to Dinagat Island and represented only by the species holotype, was placed in a well-supported clade containing the other two species of Greater Mindanao phloeomyines, *Batomys salomonseni* and *Batomys hamiguitan*. The remaining *Batomys* and *Crateromys* species found on Luzon and Panay have a robust sister relationship (Figs. 2 and 3).

Among relevant non-Philippine Asian murines, the phylogenetic placement of *Vandeleuria* and *Millardia* remains uncertain. My study corroborates previous molecular studies that fail to find the suggested alliance of *Vandeleuria oleracea* with *Chiropodomys* that has been postulated based on dental characters (Musser and Carleton 2005) and instead strongly supports a sister-taxon relationship between *Chiropodomys* and the clade containing Chrotomyini + SOE murines (Schenk et al. 2013; Steppan and Schenk 2017). Otherwise, the phylogenetic position of *Vandeleuria* is not secure in any molecular analysis to date (Schenk et al. 2013; Pagès et al. 2016; this study). Likewise, the placement of *Millardia* (represented here by *M. kathleenae*) varies depending on analytical approach (Figure 1.3; see also Schenk et al. 2013), and is also not well supported by any analysis of any molecular dataset to date.

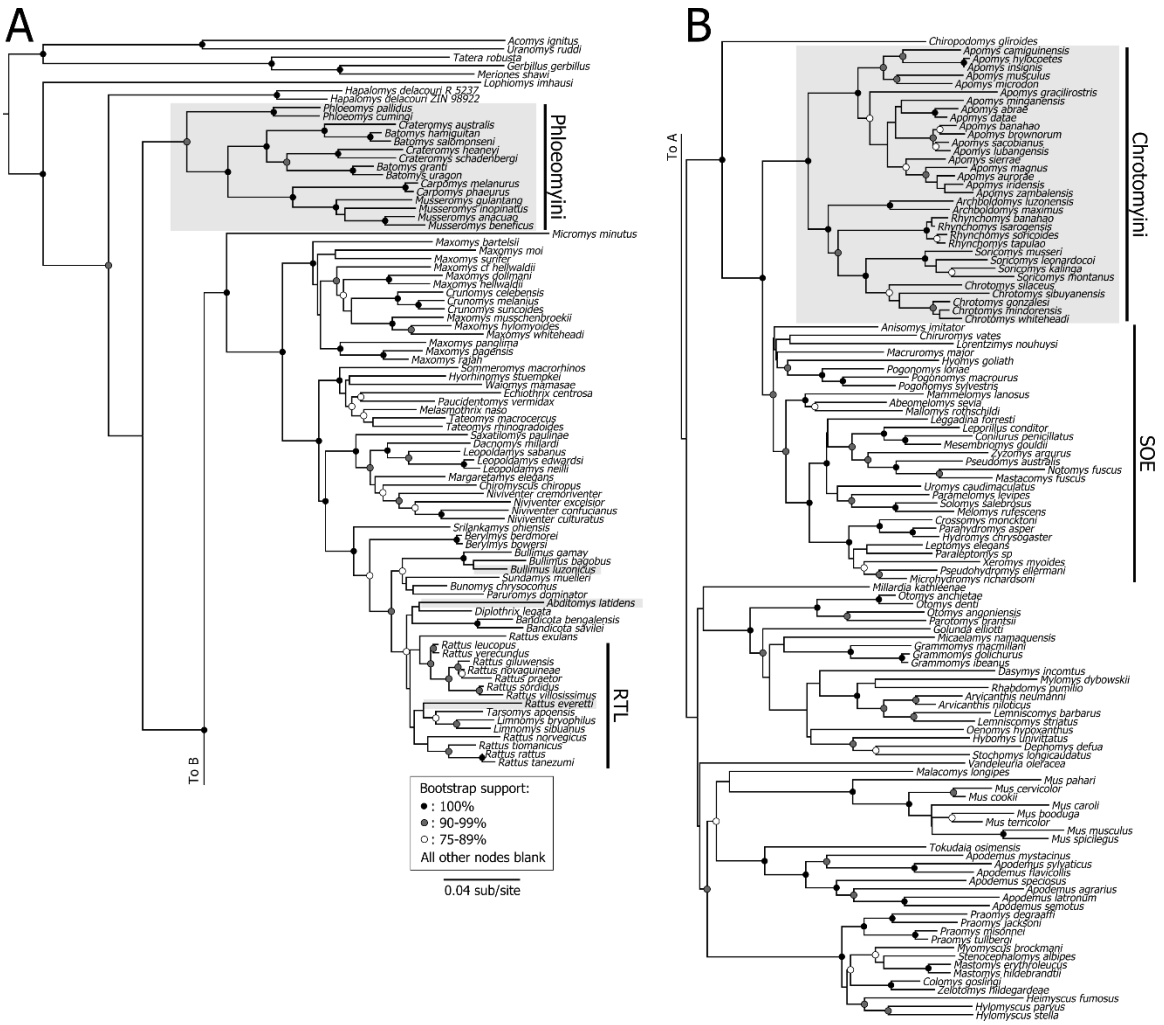

Figure 1.2. Maximum likelihood tree topology generated from concatenated sequence data. Branches are proportional to number of nucleotide substitutions. Dots at nodes correspond to bootstrap support (BS): BS = 100%: black, 90% ≤ BS < 100%: gray, 75% ≤ BS < 90%: white, BS < 75%: blank. Clades containing Luzon-endemic murines are enclosed in gray boxes. Sahul Old Endemics (SOE) and *Rattus-Tarsomys-Limnomys* (RTL) are abbreviated for clarity.

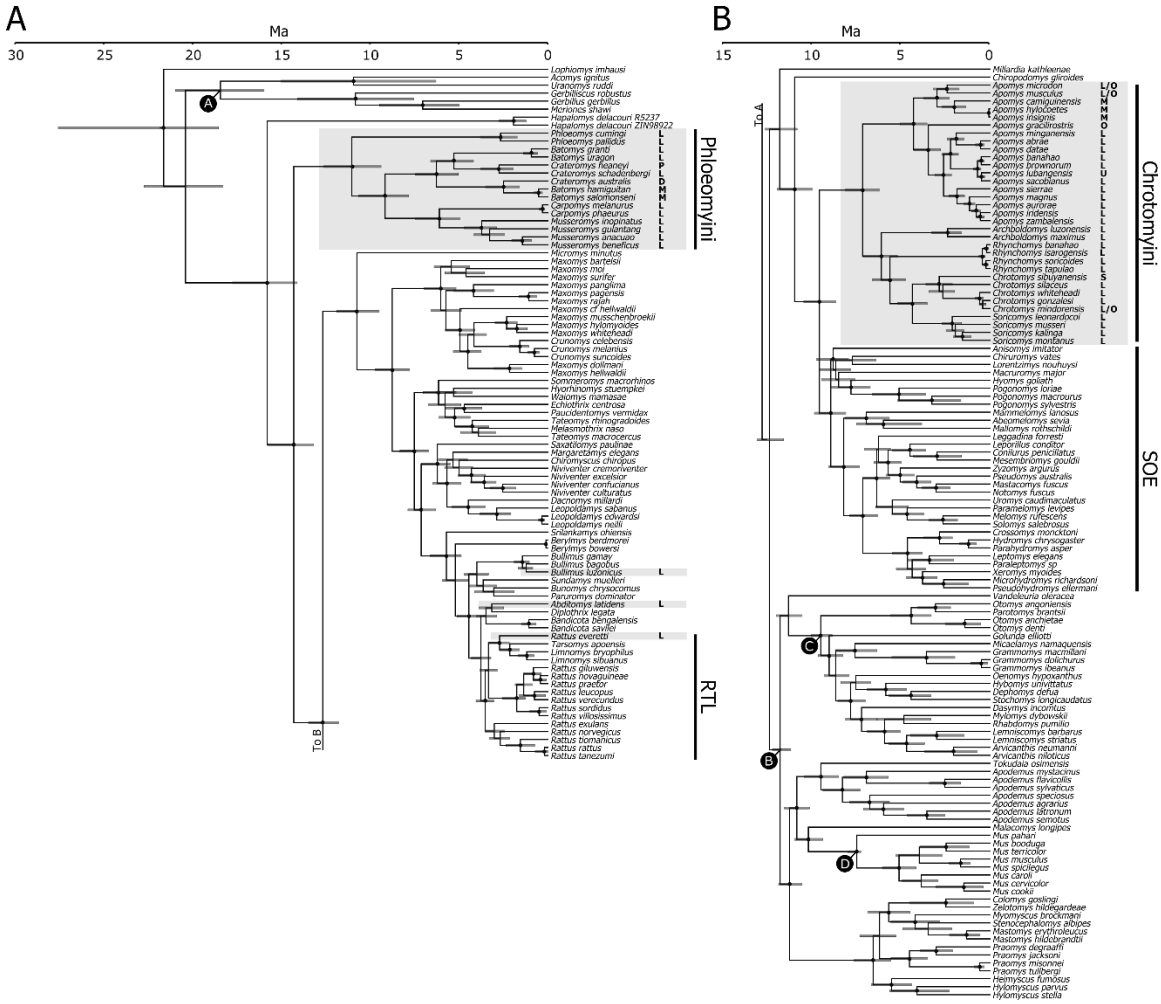

Figure 1.3. Time-calibrated maximum clade credibility (MCC) tree generated from concatenated sequence data. Nodes with ≥0.95 PP are indicated with a dot. Bars at nodes represent 95% highest posterior density (HPD) intervals for node ages. Nodes constrained with fossil data (Thomas et al. 1982; Kimura et al. 2015) are indicated with letters circumscribed by black circles. Clades containing Luzon-endemic murines are enclosed in gray boxes. Letters adjacent to taxon names correspond to the endemic faunal region of the species. L: Luzon Island, P: Panay I., D: Dinagat I., M: Mindanao I., O: Mindoro I., S: Sibuyan I., U: Lubang I. Sahul Old Endemics (SOE) and Rattus-Tarsomys-Limnomys (RTL) are abbreviated for clarity.

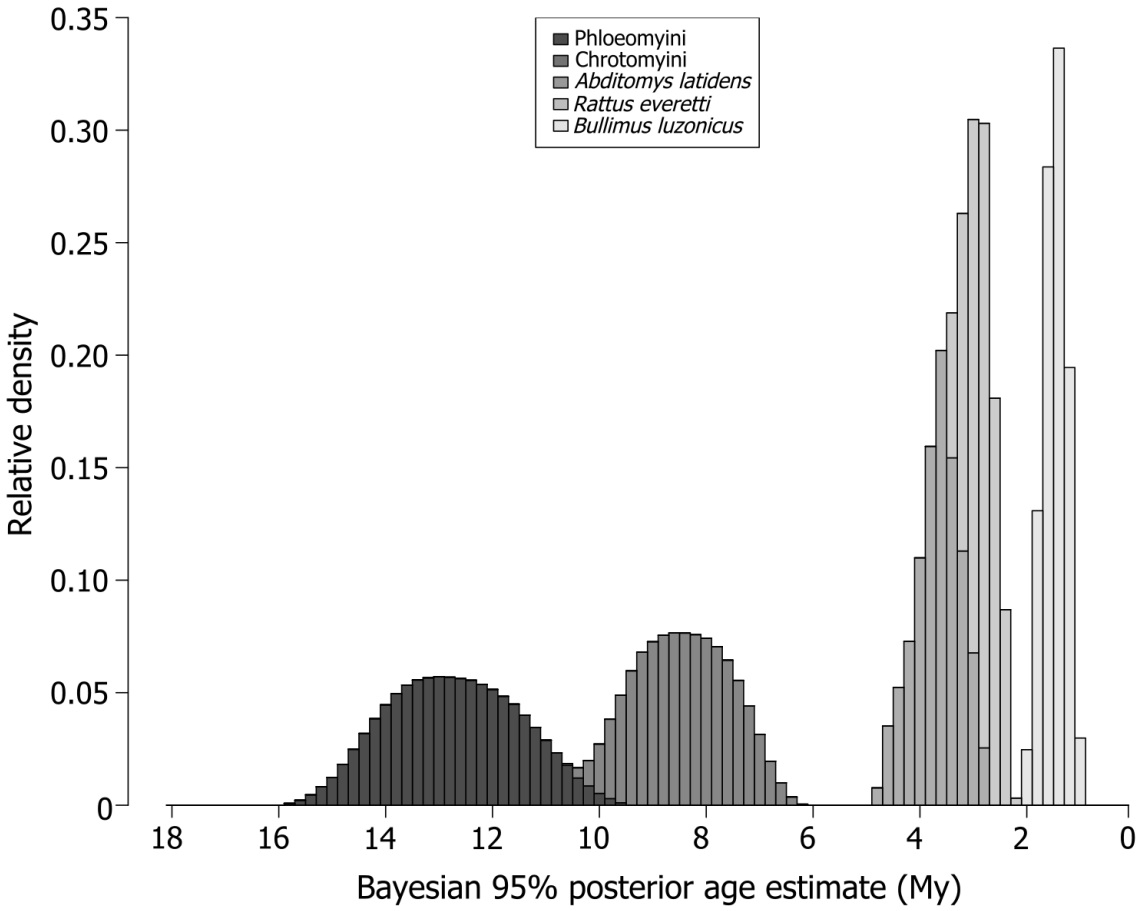

Figure 1.4. Histogram of inferred colonization ages for each clade of murine colonists on Luzon Island. Bars represent cladewise probability of colonization during 0.2 My intervals. Intervals for Phloeomyini and Chrotomyini represent 95% HPD of minimum and maximum age estimates inferred from crown and stem clade ages respectively. Intervals for *Abditomys latidens*, *Rattus everetti*, and *Bullimus luzonicus* are inferred from ages of divergence from their non-Luzon sister taxa and thus represent maximum colonization ages.

Estimates of Luzon colonization times.

Median estimates of colonization time for the LOE rodents were 12.8 ± 1.2 and 8.4 ± 0.9 Ma for Phloeomyini and Chrotomyini, respectively, with a median difference in crown clade age of 3.9 ± 0.9 My, suggesting Phloeomyini were present on Luzon at least 3 My prior to Chrotomyini. I obtained mean maximum colonization age estimates of

Luzon for the New Endemic rodents of 3.6 ± 0.4, 2.8 ± 0.3, and 1.4 ± 0.2 Ma for the lineages *Abditomys latidens*, *Rattus everetti*, and *Bullimus luzonicus*, respectively. No overlap in distribution of colonization times occurred between the Old Endemic and New Endemic groups (Figure 1.4). The colonization ages between Phloeomyini and Chrotomyini exhibited only slight overlap: 3.6% of the phloeomyine 95% HPD overlappped with 7.4% of the chrotomyine density, for a pooled probability density of 5.2%, suggesting time-staggered colonization between the two Old Endemic clades was likely (Figure 1.4).

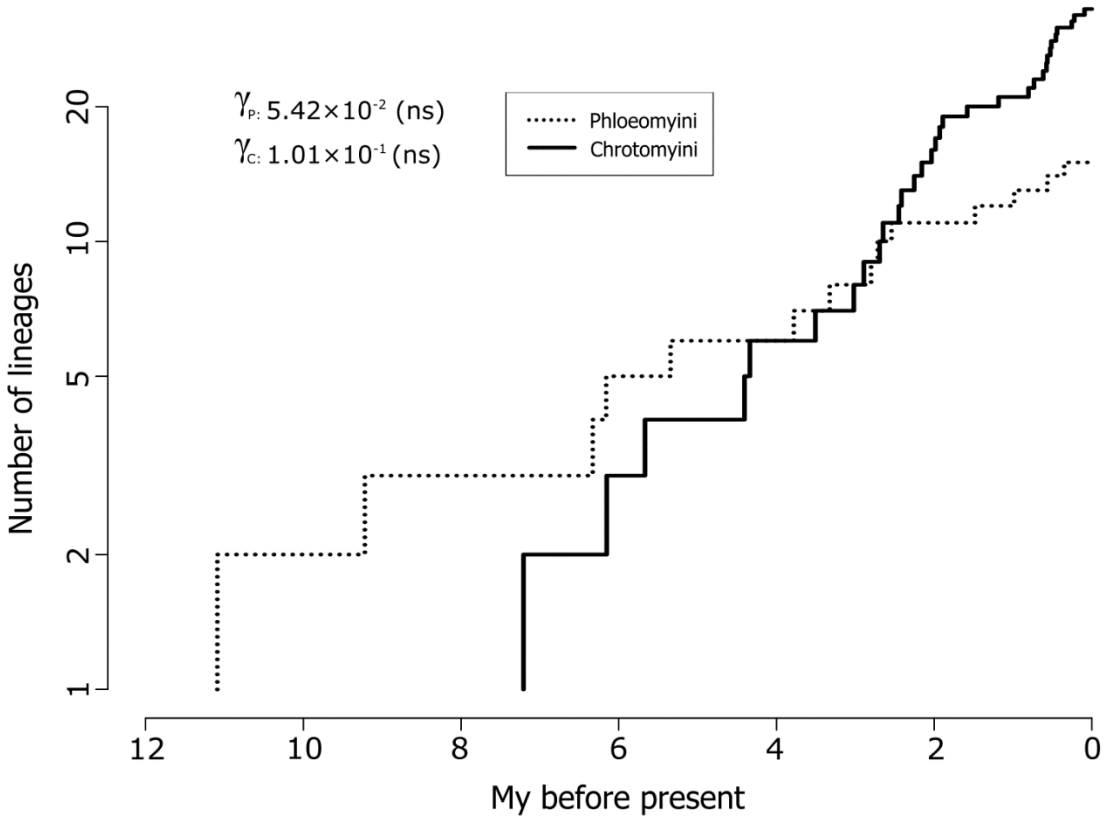

Figure 1.5. Lineage-through-time plots for Luzon Phloeomyini and Chrotomyini. The branching times for each clade could not be distinguished from that of a constant-rate process.

Diversity-dependent cladogenesis and diminished ecological opportunity.

LTT plots and γ–statistics for the Luzon representatives of each Old Endemic clade (i.e., excluding taxa occurring on other Philippine islands) failed to show any signal of temporally dynamic diversification rates (Phloeomyini: $\gamma_P = 5.42\times10^{-2}$, $P = 0.96$; Chrotomyini: $\gamma_C = 1.01\times10^{-1}$, $P = 0.91$; Figure 1.5). Furthermore, I recovered a Yule diversification process, rather than time-variable processes, as the best-fit model of lineage diversification for each LOE group (Phloeomyini: $\ln(L)_P = -10.27$, $AICc_P = 22.99$, $w_P = 0.78$; Chrotomyini: $\ln(L)_C = 15.20$, $AICc_C = -27.96$, $w_C = 0.77$). Also contrary to my predictions, I recovered a net diversification rate (r) of Luzon Chrotomyini more than double that of Luzon Phloeomyini using this model selection approach ($r_P = 0.16$, $r_C = 0.41$). The best-fit model did not differ when conducted using an MCC tree generated under a birth–death tree prior ($\ln(L)_P = -10.33$, $AICc_P = 23.10$, $w_P = 0.78$; $\ln(L)_C = 12.83$, $AICc_C = -23.21$, $w_C = 0.78$).

Likelihood estimation of diversification rate parameters for the two LOE clades corroborated the differences in rate parameters obtained using my model selection approach, with a difference in maximum likelihood estimates (MLE) >3 log-likelihood units for each clade (Figure 1.6A, Table 1.2). Rate parameter comparisons for Chrotomyini and SOE rodents, by contrast, suggested the two clades evolved under processes with comparable diversification rates and similarly low extinction fractions (Figure 1.6B, Table 1.2). The MLE for all clades under a birth–death process was not significantly different from the maximum likelihood assuming a Yule process ($D_P = 0.88$, $P = 0.35$, df = 1; $D_C = 0.036$, $P = 0.85$, df = 1; $D_S = 0.050$, $P = 0.82$, df = 1). Both

comparisons failed to support the hypotheses that diversification of Chrotomyini was depressed with respect to either Phloeomyini or the SOE rodents.

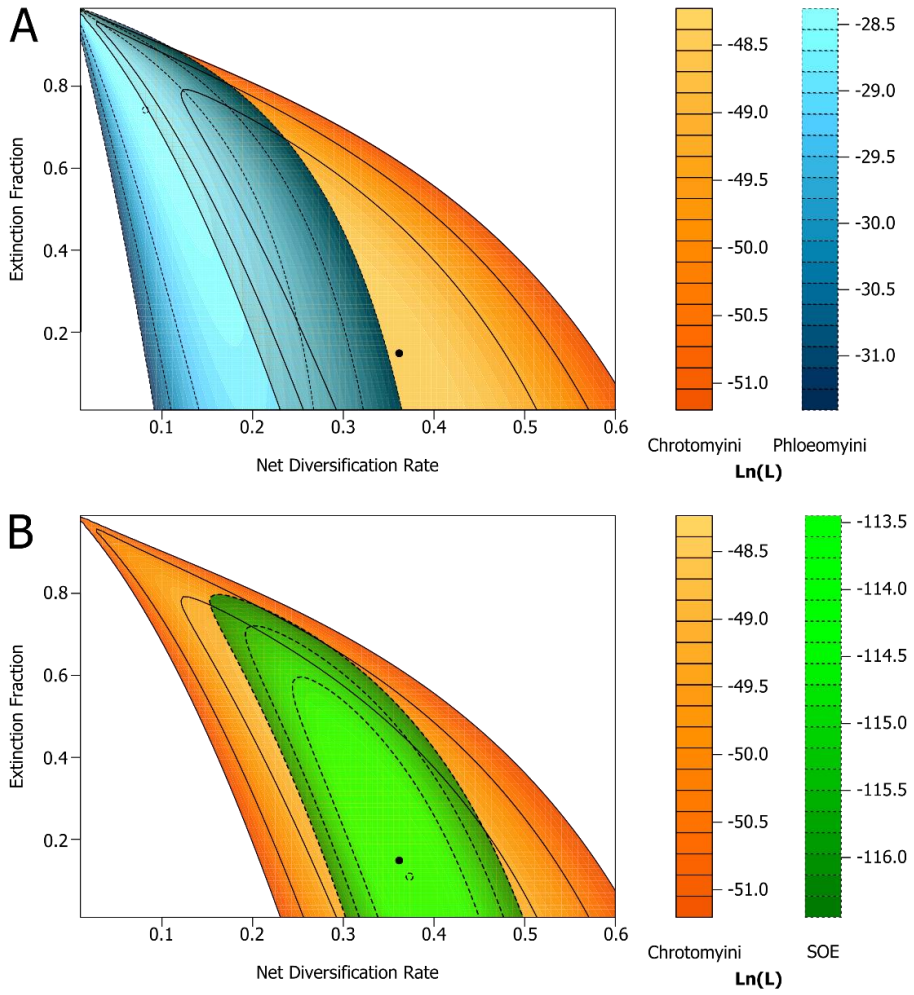

Figure 1.6. Comparison of the net diversification rate ($r = \lambda - \mu$) and extinction fraction ($\varepsilon = \mu/\lambda$) parameters inferred using MEDUSA for each of three murine clades. Panel (A) compares the Luzon Chrotomyini (orange, solid lines, filled point) and Phloeomyini (blue, dashed lines, empty circle), whereas 6B compares the Luzon Chrotomyini with the Sahul Old Endemic (SOE) rodents (green, dashed lines, empty circle). Higher likelihood values are represented with brighter colors. The variation in the size of the likelihood surface stems from variation in uncertainty of parameter estimates for each clade. The maximum likelihood estimate (MLE) for each clade is shown with a point and –1, –2, and –3 log-likelihood unit contours are shown with lines. The parameter area within three log-likelihood units approximates a 95% confidence interval of each clade's MLE, and recovering a MLE outside of the interval of the other clade suggests that the two exhibit distinct evolutionary processes.

Table 1.2. Diversification rate parameters inferred for Phloeomyini, Chrotomyini, and Sahul Old Endemic (SOE) rodents using MEDUSA and BAMM.

	MEDUSA			BAMM		
Lineages/My	Phloeomyini	Chrotomyini	SOE	Phloeomyini	Chrotomyini	SOE
Speciation rate (λ)	3.2×10^{-1}	4.2×10-1	4.2×10^{-1}	3.0×10-1	2.9×10^{-1}	3.0×10^{-1}
Extinction rate (μ)	2.3×10^{-1}	6.3×10^{-2}	4.6×10^{-2}	1.0×10^{-2}	1.0×10^{-2}	8.8×10^{-3}
Diversification rate (r)	8.1×10^{-2}	3.6×10^{-1}	3.7×10^{-1}	2.9×10^{-1}	2.8×10^{-1}	2.9×10^{-1}
Extinction fraction (ε)	0.74	0.14	0.11	3.4×10^{-2}	3.5×10^{-2}	3.0×10^{-2}

Analysis of diversification rates using BAMM suggests nearly constant diversification rates for the majority of Murinae (Figure 1.7). I recovered strong support for a model allowing rate heterogeneity in the murine tree, with the largest posterior-to-prior ratio supporting three rate shifts (Bayes factor: 108.8, but such models were rarely sampled). Instead, both the maximum a posteriori (MAP) rate-shift configuration and modal number of shifts inferred in my BAMM analysis suggest two diversification rate shifts. These rate shifts were proposed in similar locations across the 95% credible-shift set. First, I recovered an increasing extinction rate along the branch leading to *Lophiomys imhausi* (the sole representative of Lophiomyinae), yielding a lower net diversification rate compared to the rest of Muridae. Second, an additional shift with increased speciation and extinction rates occurred along the branch leading to the *Rattus*-*Tarsomys*-*Limnomys* (RTL) division, yielding an increased net diversification rate Appendix Figure 1.7. The remainder of the tree exhibits a slowly declining net diversification rate with near-zero extinction, with an average time-integrated diversification rate of 0.30 lineages/My across the posterior distribution. In contrast to the nearly twofold difference

in rates inferred from the ML analyses reported above, this analysis recovers nearly identical average diversification rates for Phloeomyini and Chrotomyini (r_P = 0.29, r_C =0.28; Table 1.2). The 95% credible-shift set included 38 distinct rate shift configurations, but were largely similar to one another and the MAP configuration. Rate shifts were frequently sampled along the split between *Lophiomys* and remaining Muridae, with a lower net diversification rate than the remaining Muridae, and in the core *Rattus* division, with higher diversification rates than the background diversification process (Appendix Figure 1.8). Consistent with my maximum likelihood analyses of diversification rates (Figure 1.6), I failed to recover support for the hypotheses of lowered diversification rates in Chrotomyini compared to either Phloeomyini or the SOE rodents. Although I recovered slowly declining diversification rates for both LOE clades, the generating process is identical for most of the remainder of the murine tree.

Discussion

Estimates of Luzon colonization times.

In reconstructing the first species-level phylogeny of LOE rodents, I provide evidence that colonization of Luzon by these two major rodent groups was temporally staggered. Previously, a two-phase model for colonization of Philippine Old Endemic versus New Endemic rodents was supported, but individual clades within each of these groups could not be temporally differentiated (Jansa et al. 2006). This study refines this

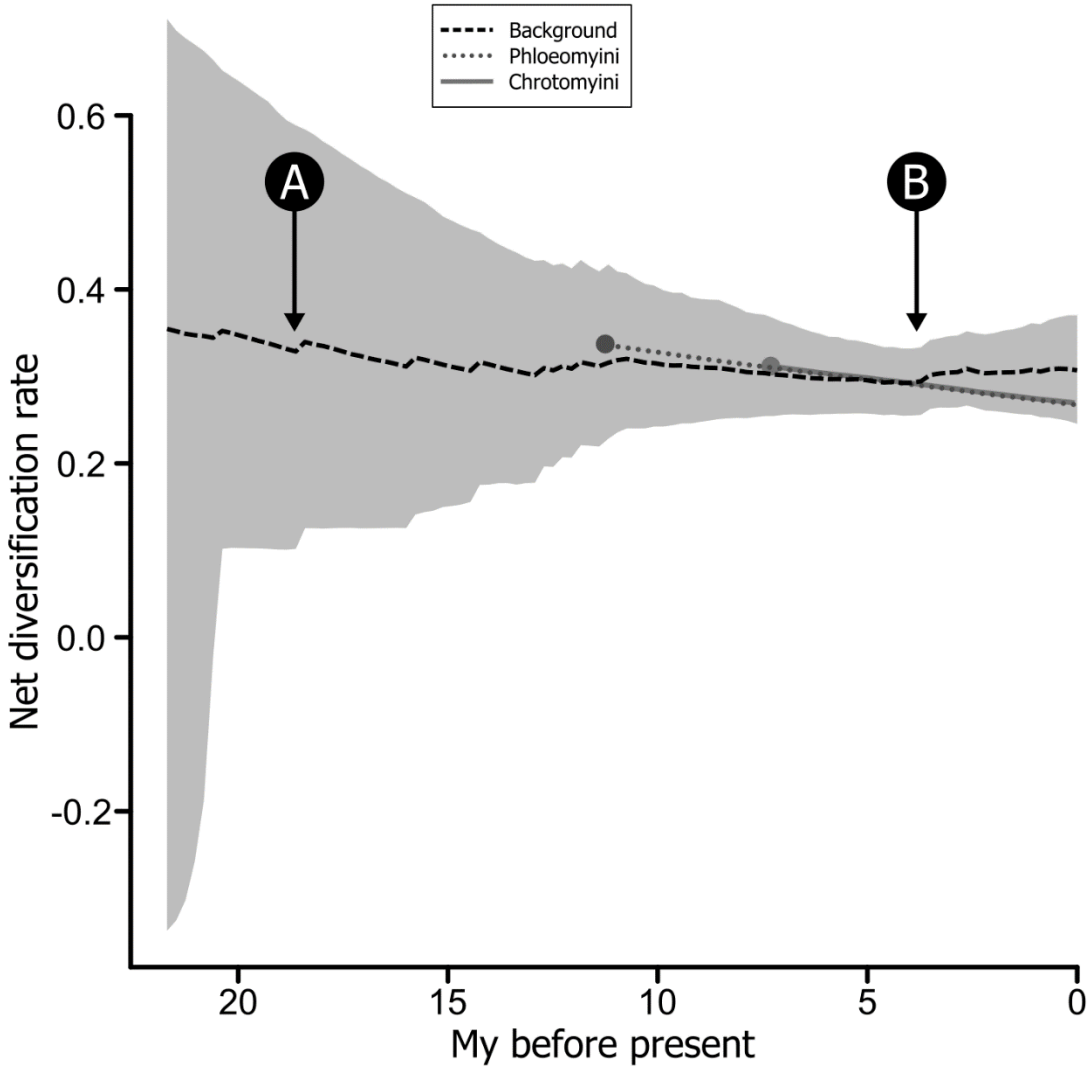

Figure 1.7. Diversification rate-through-time of Murinae and out-groups inferred from the distribution of BAMM rate configurations. Dashed line represents net diversification rate for the entire tree inferred from the average of the posterior (time-integrated rate: 0.30 lineages/My); gray envelope indicates the 95% confidence interval of the estimate. The dotted gray line indicates average diversification rate inferred for Phloeomyini (0.29 lineages/My) and the solid gray line indicates the inferred rate of Chrotomyini (0.28 lineages/My), with circles at the clade origin for clarity. Lettered circles indicate inferred rate shift positions based on the maximum a posteriori (MAP) rate shift configuration: (A) extinction rate increase along branch leading to *Lophiomys imhausi*; (B) speciation and extinction rate increase along branch leading to the *Rattus-Tarsomys-Limnomys* (RTL) division.

estimate by temporally separating the invasion of Luzon by Phloeomyini from that of

Chrotomyini, and provides the first step in differentiating the timing of colonization of the Luzon New Endemics, suggesting independent colonization of *Bullimus luzonicus* from *Abditomys latidens* and *Rattus everetti* (based on maximum clade ages; Figure 1.4). Recovering Phloeomyini and Chrotomyini as colonizing millions of years apart provides the basis for the prediction that competition for niches was potentially weaker for the phloeomyines compared to the chrotomyines.

Diversity-dependent cladogenesis and diminished ecological opportunity.

For this study, I sought to test three predictions regarding how ecological opportunity, diminished in secondary colonists by incumbency of another clade, alters lineage diversification. First, I tested whether diversity-dependent cladogenesis provided a good fit for the diversification of the two clades of LOE rodents, but failed to recover any evidence of temporally decelerating cladogenesis. My BAMM analysis recovered slightly decreasing diversification rates through time for both Chrotomyini and Phloeomyini, but this process appears to be no different from the remainder of Murinae (excluding *Rattus-Tarsomys-Limnomys*, which show accelerated rates of diversification). Based on these results, I conclude that species diversification of LOE rodents is not consistent with expectations of ecological opportunity presented by colonizing a new landmass.

The second prediction I tested was that Chrotomyini should exhibit lower diversification rates than Phloeomyini, due to incumbency effects. Two lines of evidence suggest that this was not the case. First, I did not detect a change in diversification rate in

the murine phylogeny between these two clades in the BAMM analysis (Figure 1.7). Second, although I did recover a significant difference in diversification rate using maximum-likelihood analysis, this difference was not in the expected direction: the estimated diversification rate of Chrotomyini in these analyses was up to fourfold faster than that of Phloeomyini (Figure 1.6, Table 1.2). Recovering, at minimum, similar diversification rates, or as I found, a much higher diversification rate in Chrotomyini, directly contradicts the expectation that a colonizing clade is prevented from achieving comparable diversity to an incumbent lineage.

Our final prediction was that Chrotomyini should exhibit a lower diversification rate than their sister clade, the Sahul Old Endemics, which constitutes the earliest rodent colonists of the Sahul region. Comparing these two clades allowed me to explore how chrotomyine diversification may have unfolded in the absence of primary colonists on Luzon. Again, in contrast to my predictions, the two clades had diversification rates consistent with evolution under a single macroevolutionary process. The uniformity I recovered provides an additional line of evidence that Chrotomyini were not limited in their diversification by colonizing Luzon after Phloeomyini. My failure to recover support for any of the three predictions that formed the basis of this study point to the conclusion that the diversification history of the Luzon Old Endemic rodents is more prominently influenced by factors other than incumbency effects. The dominant pattern for the LOE rodents, and the majority of Murinae, is a constant or slowly decelerating diversification rate with a relatively low apparent extinction rate.

The patterns illustrated in these two clades of island rodents corroborate the patterns found for rodents in continental systems (Schenk et al. 2013). These authors found that incumbency effects, whereby secondary colonists exhibit diminished diversification rates compared to primary colonists, were the exception rather than the rule among muroid rodents. The authors recovered diversity-dependent cladogenesis among South American muroid rodents with strong support, and among the SOE rodents with weak support, but found no support for secondary colonists having decreased diversification rates in any of their biogeographic categories. In aggregate, these findings suggest that incumbency's influence on lineage diversification may be easily overshadowed by other phenomena (Derryberry et al. 2011; Schenk et al. 2013). With this context in mind, there are several mutually compatible scenarios that could be responsible for the observed diversification history of the LOE. I outline three below.

First, Phloeomyini may have not had enough time for sufficient speciation to occur to impose incumbency effects on Chrotomyini. To assess how much diversification could have occurred within Phloeomyini before Chrotomyini arrived on Luzon, I simulated the number of phloeomyine lineages present at the inferred median colonization age of Chrotomyini. Based on the diversification rates inferred using MEDUSA and BAMM, I performed 100 constant-rate birth–death simulations, which yielded an average of three species present for each set of assumed rates (simulations performed using *TESS* in R; Hoehna 2013). The relatively low rate of early cladogenesis among Phloeomyini is further supported by my failure to recover diversity-dependent cladogenesis as the best-supported diversification model for this clade. Additionally, if

density-independent time-for-speciation processes were the dominant mechanism of early diversification in this clade, as suggested by my analyses, then I would not expect the rapid early cladogenesis predicted under a model of ecological opportunity (Stephens and Wiens 2003; Rabosky 2012). As a result, the relatively low early diversity of phloeomyine species may not have exhibited a strong enough competitive pressure on the secondary colonists to depress their diversification.

Second, the extent of geographic dynamism may be too great to impose realistic ecological limits on species diversity, even at the scale of a single island. Numerous studies encompassing a variety of clades illustrate that allopatric speciation is a prevalent mode of diversification on continental landmasses (Ribas et al. 2007; Derryberry et al. 2011; Giarla and Jansa 2014). At large, geographically complex spatial scales, vicariance or dispersal events facilitate diversification without increasing interspecific competition (Esselstyn et al. 2009; Maestri et al. 2016; Pavan et al. 2016). Thus, geographic scale and isolation likely influence the mechanism by which diversification occurs, as has been suggested in the tropical Andes (Hutter et al. 2017). Despite the limited space afforded to colonists of Luzon compared to continental radiations, the patterns of LOE diversification were more consistent with a mechanism of allopatric speciation, where species diversity is able to accumulate nearly constantly, offset slightly by background extinction rates. This conclusion is consistent with the observation that Luzon, as a volcanic oceanic island, has had a markedly dynamic history: tectonic uplift, sea level fluctuations, and volcanism have all contributed to substantial changes in available land area and suitable habitat (Hall 2013; Heaney et al. 2016a). This temporal dynamism may mean speciation

is driven less by competition for niches and more by dispersal to newly available habitat generated by geological processes, specifically, the montane "islands" formed by volcanism and tectonic uplift over the past 15 million years. Importantly, these montane islands, while originally isolated from one another in the form of individual oceanic islets, probably coalesced into their contemporary configuration only within the last 5 million years (Heaney et al. 2016a). Considering many of the species-level divergences in both LOE clades began after Luzon's coalescence, and that sister species within either clade often occupy nonadjacent ranges (Heaney et al. 2016b), I suggest that a mixture of over-land and over-water dispersal to other mountain ranges on Luzon has been at least as important in LOE evolutionary history as processes of ecological specialization and differentiation, and that lowland habitat presents a prominent, but not insurmountable, dispersal barrier to most LOE species. The patterns of allopatric speciation I propose are supported in several clades of Southeast Asian mammals (Esselstyn et al. 2009; Achmadi et al. 2013; Justiniano et al. 2015), suggesting that the climatic and geological dynamism of this region may be paramount in explaining its biodiversity.

Third, the effects of incumbency may still be apparent in this system, but they are acting not on diversification history, but rather on patterns of phenotypic diversity. If true, one may still recover diversity-dependent trait evolution with decreased rates of phenotypic evolution among secondary colonists. This hypothesis seems intuitive, considering phenotypic evolution driven by ecological opportunity forms the basis for adaptive radiation theory (Parent and Crespi 2009; Mahler et al. 2010), but it remains to be tested in this system. In the context of incumbency, the rate of morphological

evolution may be suppressed in secondary colonists, although lineage diversification (via allopatric speciation) is unaffected, yielding many ecologically similar species. Alternatively, incumbent clades may filter secondary colonists in favor of those lineages occupying distinct regions of ecomorphospace. The resulting morphological variation may be such that cladewise overlap is minimized (Jønsson et al. 2015). In the context of the LOE rodents, the colonizing ancestor of Chrotomyini may have been ecologically distinct enough to facilitate coexistence through divergent evolutionary trajectories. For example, comparative analysis of Floridian *Quercus* oaks suggests that, within ecological communities, individual species are less ecologically similar and more phylogenetically distant than would be expected by chance (Cavender-Bares et al. 2004). The phylogenetic and ecological overdispersion reported by these authors may extend more broadly to the island scale such that, for a lineage to successfully invade, it must be phenotypically distinct enough from other lineages to minimize competition. Preliminary evidence to support this prediction stems from field observations suggesting the LOE rodent clades differ in their modal dietary and habitat preferences: members of Phloeomyini are primarily arboreal herbivores whereas chrotomyine species are predominantly terrestrial animalivores (Heaney et al. 2016a).

One additional aspect that is also worth considering is the potential impact the two Old Endemic clades have had on the diversification of the Luzon New Endemics. I did not include these more recent colonists in these analyses, because they lack species diversity due to their relatively recent origin on Luzon. Nevertheless, these recently colonizing species do exhibit substantial ecological differences from the LOE rodents. As

an example, the New Endemics are typically found either in low elevation or disturbed habitats. Their distribution may be the result of competitive exclusion by the Luzon Old Endemics, which are concentrated in high elevation, primary montane forest habitats (Heaney et al. 2016a). The ecological disparity may otherwise stem from an ongoing taxon cycle in which the two colonization regimes are in different stages: the Old Endemics may have achieved relative stasis due to their comparatively ancient colonization and subsequent ecological specialization; in contrast, the New Endemics, due to recent colonization, represent an incipient taxon expansion (Ricklefs and Bermingham 2002). Whether the differences in habitat use is the result of active exclusion by the LOE rodents or habitat preferences among the Luzon New Endemics remains to be discovered, but could shed additional light on how incumbency alters macroevolutionary processes and community assembly.

Conclusions

The extent to which ecological interactions among species and clades influence macroevolutionary processes is an important question for understanding the origination and maintenance of biodiversity. My study examined whether incumbency of another clade diminishes the rate at which secondary colonists diversify while also providing the most complete record of Luzon Old Endemic rodent phylogenetic diversity. I did not recover a signal of incumbency-mediated diversification, but there is still the potential for inter-clade interactions to have shaped the diversification of both. Given the complexity of natural systems, many processes have likely contributed to the evolution of species

diversity to varying degrees over the history of Luzon Island, including incumbency effects, within-clade interspecific competition, and allopatric speciation through island and/or montane habitat hopping (Heaney et al. 2016b). Nevertheless, I argue that ecological opportunity does not appear to be the primary mechanism determining the generation of species among these mammals and propose that incumbency effects may only be detectable in spatially limited scales that have remained geologically and climatically static over evolutionary time.

CHAPTER 2. TEMPO AND MODE OF MANDIBULAR SHAPE AND SIZE EVOLUTION REVEAL MIXED SUPPORT FOR INCUMBENCY EFFECTS IN TWO CLADES OF ISLAND-ENDEMIC RODENTS (MURIDAE: MURINAE)[2]

Introduction

Adaptive radiation theory proposes that ecological opportunity, in which a lineage has access to an abundance of resources unused by competitors, can generate rapid evolutionary change to specialize on niches. The availability of unexploited niches promotes intraspecific variation necessary to accumulate new, ecologically distinct species (Parent and Crespi 2009) and may arise either from colonization of a depauperate ecosystem (Givnish et al. 2009) or from an evolutionary innovation that frees the lineage from existing competition to some degree (Wainwright et al. 2012). Over time, the radiation unfolds as intraspecific variation becomes partitioned into diverse species through disruptive selection in sympatry or adaptation in allopatry toward the resources on which they have specialized (Bolnick 2004; Tobias et al. 2014). From a quantitative standpoint, this theory suggests that release from competition is followed by an initially rapid occupation of available niches that declines over time as the opportunity for subsequent diversification decreases, resulting in a historical pattern of an initial burst of phenotypic evolution that decelerates toward the present (Mahler et al. 2010; Burbrink and Pyron 2011; Derryberry et al. 2011).

[2] Reproduced with permission from Rowsey, D. M, L. R. Heaney, and S. A. Jansa. 2019. Tempo and mode of mandibular shape and size evolution reveal mixed support for incumbency effects in two clades of island-endemic rodents (Muridae: Murinae). Evolution. doi: 10.1111/evo.13737

Despite developments in the ability to detect the historical signal of within-lineage adaptive radiation, the ecomorphological diversification of closely related lineages that colonize a system independently is insufficiently explored. Multiple colonizing lineages may serve to limit ecological opportunity because each group of colonists may compete with one another for available niches. If two colonization events by similar lineages are asynchronous, I should expect the lineage which arrived first to experience greater ecological opportunity than the secondary invader. Additionally, I might also expect the descendants of this initial colonist to competitively exclude potential invaders that are too ecologically similar (biotic filtering: Gillespie 2004; Emerson and Gillespie 2008). The advantage a primary colonizing lineage has over subsequently-invading, ecologically similar lineages is known as an incumbency effect (Alroy et al. 1996; Jablonski and Sepkoski 1996; Bambach et al. 2002). Incumbency effects can range in strength and scale from limiting colonization ability, to reducing abundance, to even facilitating colonization of subsequently-colonizing lineages, and as a result has highly variable effects depending on the system and spatiotemporal scale of interest (Almany 2004; Fukami 2004; Louette and De Meester 2007); nevertheless, the persistence of incumbency effects and the ability of subsequent clades to escape them requires further investigation.

Studies that have examined the macroevolutionary signature left by incumbency effects fall under two broad categories. First, several studies have examined clades that have escaped from incumbency effects, whether through a mass extinction event in the competing lineage (Bambach et al. 2002; Webb 1985; Engel et al. 1998) or dispersal to a

competitor-deficient system (ecological release: Schluter 2000a). Importantly, studies following this approach often consider the focal clade in isolation, and rarely integrate the diversification history of this clade with respect to its close relatives. This lack of integration limits the ability to infer the history of competition prior to release from the effect. Second, researchers have inferred macroevolutionary dynamics from two potentially interacting radiations, but the scale of these studies is often too geographically broad, potentially limiting the ability to detect incumbency effects. In particular, previous studies have used this approach to examine the signature of incumbency effects at continental scales, usually recovering idiosyncratic patterns inconsistent with persistent inter-clade competition (Jønsson et al. 2015; but see Betancur-R. et al. 2012). For example, Schenk et al. (2013) and Alhajeri et al. (2016) used muroid rodents to test whether secondary colonists of continental systems experienced lower diversification rates and limited rates of ecological morphological evolution, respectively. These studies, in sum, recovered little support for decelerating rates of evolution in most systems, suggesting that the ecological opportunity model poorly explains the mode of evolution in Muroidea. However, studies such as these that focus on continental scales of macroevolution undoubtedly oversimplify the community structure and geologic history of the regions in question, especially for regions as biologically and geologically dynamic such as southeast Asia (Goldberg and Lande 2007; Ribas et al. 2007). Exploring these geographic regions at finer scales, with constituent clades that are more likely to compete with one another due to more recent phylogenetic divergence, may yield insights about macroevolutionary pattern and process that would otherwise be obscured. Lineages

occupying oceanic archipelagic systems present ideal opportunities to test these hypotheses due to the potential for complex colonization history, spatial limitations, and striking adaptations arising from rapid evolution (Emerson 2002; Filardi and Moyle 2005; Schenk et al. 2013).

With this in mind, I chose to examine macroevolutionary incumbency effects at a fine spatial scale using two clades of "Old Endemic" murid rodents native to Luzon Island in the Philippines. Specifically, I examined evolution of mandibular morphology, because mandibular shape serves as a proxy for dietary niche, particularly with respect to differences associated with specialization on consuming invertebrates, seeds, or foliage (Grossnickle and Polly 2013; Maestri et al. 2016; Verde Arregoitia et al. 2016). Luzon is an oceanic island that began emerging as a continuously dry-land area approximately 25 million years ago (Hall 2013). Since its formation, the island has been colonized an estimated six times by murine rodents, including the five colonization events identified by Jansa et al. (2006) and Rowsey et al. (2018): Phloeomyini, Chrotomyini, *Abditomys*, *Bullimus*, and *Rattus everetti*, and a potential sixth by *Crunomys fallax*. The first two invading lineages, Phloeomyini (*sensu* Lecompte et al. 2008) and Chrotomyini (considered by Lecompte et al. 2008 to be a member of Hydromyini and containing *Apomys*, *Archboldomys*, *Chrotomys*, *Rhynchomys*, and *Soricomys*; Rowsey et al. 2018), colonized between two and six million years (My) apart at approximately 12.8 and 8.4 million years ago (Ma) respectively (Rowsey et al. 2018). These two clades subsequently diversified to constitute nearly 90% of the rodent diversity on Luzon (Heaney et al. 2016b). My previous analyses recovered no support for incumbency-influenced lineage

diversification rates in these clades; however, rates of ecomorphological diversification for these lineages remains unexplored.

Prior field studies suggest that Phloeomyini and Chrotomyini greatly differ in dietary disparity: whereas the incumbent Phloeomyini range from generalist herbivores (i.e. eating some amount of fruits, seeds, and vegetative material), to bamboo foliage specialists, to specialists on thick-coated seeds, most species within secondary-colonizing Chrotomyini vary mostly on a spectrum from omnivory to specializing on earthworms and soft-bodied arthropods (Heaney et al. 2016a, b). This apparent disparity in dietary variation begs several questions. First, is the partitioning of dietary variation the result of either depressed evolutionary rates or biotic filtering effects acting on Chrotomyini? Second, have incumbency effects acted on morphological evolution without a comparable signal in the lineages' diversification history? Finally, if inter-clade competition has influenced the morphological evolution of these two clades, is there evidence that Chrotomyini has exhibited a rapid change in evolutionary process to escape the incumbency effects imposed by Phloeomyini?

To address these questions, I quantified mandibular shape and size for the constituent species of these two lineages. The analysis of mandibular variation in the phylogenetic framework established by Rowsey et al. (2018) allows me to test whether dietary evolution has occurred according to different processes for primary compared to secondary colonists. Specifically, I tested five predictions regarding how incumbency effects may have altered mandibular morphological evolution. First, I examined whether the two Luzon "Old Endemic" (LOE) clades occupied distinct areas of mandibular shape

and size morphospace. I expect to observe this pattern if the ancestor for secondary-colonizing Chrotomyini could only establish itself on Luzon because it was distinct enough from the Phloeomyine lineages present on the island at the time, in other words, if Chrotomyini passed a biotic filter. Second, I tested whether either LOE clade evolved according to an "early burst" model of evolution, which predicts decreasing rates of morphological evolution over time (Harmon et al. 2010). Recovering decelerating evolution would suggest that morphological evolution is linked to the availability of ecological (specifically dietary) niches. Third, I tested whether morphological evolution in these two clades has exhibited discrete shifts to new "quantum zones" (Simpson 1953), as may be expected if Chrotomyini has evolved to escape incumbency effects imposed by Phloeomyini. Fourth, I tested whether extant morphological diversity in Chrotomyini resulted from greater convergent evolution than in Phloeomyini. If ecological incumbency plays a role in constraining chrotomyine morphospace occupancy, and by extension, niche evolution, one may expect to recover denser clustering of morphological variability, such that chrotomyines convergently resemble each other to a greater extent than phloeomyines do. Finally, I tested whether Chrotomyini exhibited lower rates of morphological evolution than Phloeomyini, assuming that no shifts in evolutionary rate occurred prior to colonization. I expected to recover this pattern if Chrotomyini had less ecological opportunity due to the diversification that had already occurred within Phloeomyini.

Materials and Methods

Taxon sampling and morphometric data sampling.

We photographed and landmarked a total of 337 mandibles representing 41 species, comprising all described Luzon Old Endemic (LOE) rodent species and two species undescribed at the time of writing. Specimens were sampled from the American Museum of Natural History (AMNH), the Field Museum of Natural History (FMNH), the Harvard University Museum of Comparative Zoology (MCZ), and the United States National Museum of Natural History (USNM). Only individuals with all molars completely erupted in both the cranium and mandible were chosen for study. The right ramus of the mandible was photographed on its buccal surface such that the anterior and posterior margins of the mandible (excluding the incisor) were coplanar. For specimens with mandibles damaged such that landmarks could not be taken, I used the left ramus if fewer landmarks would be lost and mirrored the image before data collection. The complete list of specimens sampled is presented in Appendix Table 2.1.

To account for intraspecific variation, I included multiple individuals from distinct geographic regions (e.g., different mountains and provinces) when available. When possible, I included two males and two females from each sampling locality, or four individuals if two of each sex were unavailable. Although they were included for my initial analyses of mandibular variation, I pruned *Batomys dentatus* and the single undescribed *Apomys* and *Rhynchomys* species from the comparative analyses of morphological evolution as no molecular phylogenetic data were available for these three species. Nearly all of my samples were obtained from rodents occurring on Luzon and

minor outlying islands connected by shallow channels, although I included four individuals (out of 31 total) of *Chrotomys mindorensis* from Mindoro Island. I also excluded from the study old endemic species that are not found on Luzon, including five species of *Apomys* and the Greater Mindanao *Batomys* + *Crateromys* clade.

Geometric morphometric analysis and morphospace occupancy.

All morphometric data were collected using the *geomorph* package in *R* (Adams and Otárola-Castillo 2013, R Core Team 2015). Twelve landmarks were collected from each mandible to quantify functional variation in mandibular morphology, based in part on landmarks used in previous studies (Figure 2.1 inset; Hautier et al. 2011, Grossnickle and Polly 2013). I estimated the positions of missing landmarks on applicable specimens using the thin-plate spline method implemented in the estimate.missing function of *geomorph* (Gunz et al. 2009), using the average configuration of completely represented conspecific mandibles as the reference to compute incomplete specimens. These landmark configurations were subjected to a generalized Procrustes analysis (GPA; Gower 1975, Rohlf and Slice 1990) to minimize differences among specimens due to scaling, translation, and rotation. These superimposed specimens were then analyzed using a principal component analysis (PCA) to determine variables that provided the greatest contribution to the variance of the dataset. In addition to shape data, I retained logarithmically-transformed centroid size to analyze as a univariate trait to determine whether size and shape evolution displayed different signals of ecological opportunity or incumbency effects. Centroid size, or the square root of the summed distances from each

landmark to the center of the landmark configuration, is a univariate measure used to rescale all specimens to a common size as a part of GPA. To ensure this was a reasonable proxy for body size, I regressed log-transformed centroid size against log-transformed head-and-body length.

Previous studies suggest that analysis of principal components can be misleading if phylogenetic relationships are unaccounted for (Revell 2009). However, I chose to present my results using standard PCA scores for three reasons. First, phylogenetic PCA requires specification of an underlying evolutionary model to compute the evolutionary variance-covariance matrix of the traits in question, and a primary goal of this study is inferring the evolutionary model responsible for generating the mandibular morphology of the focal clades. Second, whenever possible, I analyzed mandibular shape using approaches that determine multivariate distances among each species' GPA-transformed landmarks, which is equivalent to analyzing the entire component space generated under standard or phylogenetic PCA; this is because the phylogenetic rotation preserves Procrustes distances among specimens in multivariate space (Polly et al. 2013). Finally, when multivariate distance-based methods were unavailable for an analysis of interest, I used methods that can account for phylogenetic covariance among principal component axes whenever possible. Analyzing principal component axes using univariate comparative methods can incorrectly specify the model the data were generated under, regardless if phylogenetic transformations are performed (Uyeda et al. 2015). Due to the rapid proliferation of estimated parameters of multivariate analyses as more traits are examined and the relatively few species in Phloeomyini (11 species for which

phylogenetic information was available), the rate-matrix-based multivariate analyses were limited to the first two principal component axes. The first two component axes for each clade-specific rotation account for 68.7% of chrotomyine shape variation and 58.9% of phloeomyine shape variation. I report results of the analyses generated under phylogenetic PCA in Appendix Tables 2.5-2.7 and Appendix Figures 2.1-2.2 of this article and emphasize that they do not change my conclusions.

Using the *R* packages *ape* and *phytools* (Paradis et al. 2004; Revell 2012), I imported the maximum clade credibility (MCC) chronogram from Rowsey et al. (2018) to provide time-scaled evolutionary relationships with which I could conduct the comparative analyses. This tree was pruned to include only the focal taxa (i.e. the LOE rodents; Figure 2.2). As the first step in my morphometric analysis, I observed whether the patterns of morphological overlap in mandibular shape and size were consistent with biotic filtering, with areas of morphospace partitioned between clades, using phylomorphospace analysis of shape morphology (Klingenberg and Ekau 1996, Sidlauskas 2008) and a histogram of log-transformed centroid size to visualize the distribution of morphological variation. Recovering clade-specific morphospace partitioning would suggest that the assembly of the Luzon murine community is the result of inter-clade competitive factors and that the successful establishment of Chrotomyini may be the result of persistent ecological distinction between the two clades.

Clade-specific mode of mandibular evolution.

To test whether the evolution of mandibular shape and size was consistent with decelerating ecological opportunity, I first partitioned the morphological data by LOE clade. For the analyses of shape evolution, I performed a principal component analysis on the GPA-transformed data for each clade. The first two PC axes for each clade were then fitted to a constant-rate Brownian Motion model of evolution (BM; Felsenstein 1985) and a time-decelerating "early burst" model of trait evolution (EB; Pagel 1999, Blomberg et al. 2003, Harmon et al. 2010) in a multivariate, maximum likelihood rate-matrix framework implemented in the *mvMORPH* package in *R* (Clavel et al. 2015, R Core Team 2015). These models were compared using a likelihood ratio test for each clade. It is important to note that, because I rotated each clade's mandibular shape separately, I did not compare the evolutionary rates between clades as a part of this analysis. For the analysis of size evolution, I performed a similar clade-specific model-fitting procedure using univariate BM and EB candidate models, likewise determining support using a likelihood ratio test for each clade. I additionally plotted multivariate shape and size disparity through time, measured in average pairwise Euclidean distances among species in subclades present at a given time in the tree, to visualize temporal changes in morphological evolution for each clade (Harmon et al. 2003). Average subclade disparity values near zero indicate each subclade accounts for relatively little disparity of the entire clade as a whole, meaning variation is clustered within subclades. Likewise, values near one indicate each subclade accounts for a large proportion of the total disparity of the clade, meaning variation is dispersed among subclades.

In a complementary approach to this model-fitting test, I used a model adequacy approach to determine how well these best-fit models actually described trait evolution in each clade. This method, implemented in the R package *arbutus*, computes a series of metrics from the supplied data given an evolutionary model (Pennell et al. 2015). These metrics are compared to a distribution of simulated statistics to detect deviations from expected patterns given the model, for example, whether trait evolution is correlated with aspects of the tree topology or branch lengths. Deviations from the expected distributions suggest that the model inadequately describes aspects of trait evolution. As this approach has not been implemented in a multivariate framework, I calculated the model adequacy for each component axis and size separately using the *geiger* package in R (Harmon et al. 2008).

We additionally determined whether shape and size evolution in each clade exhibited evolutionary jumps along PC1, PC2, and centroid size. To do this, I compared the fit between a constant-rate BM process and a Lévy process that models rapid evolutionary jumps corresponding to a shift in evolutionary mode (Landis et al. 2013). I inferred model parameters and tested model fit using *Levolution* (Duchen et al. 2017). This program uses an expectation maximization (EM) approach to optimize model parameters given a range of jump strength (α) values from which to sample using a grid search procedure, followed by a Markov-Chain Monte Carlo (MCMC) estimation of rate shifts given the tree. This algorithm requires initial values for the Brownian motion model as well as initial parameters for the Poisson rate (λ) and jump strength (α) of jumps between parameter distributions. I specified initial BM parameters according to the

maximum likelihood estimations for PC1, PC2, and centroid size evolution independently, initial Poisson rates (1 for PC1 and centroid size, 0.01 for PC2) and a distribution of 20 jump strength values ranging from 1 to 1000 for all traits, with an additional set of 20 strengths sampled ranging from 1 to 400 for PC2. For each α, the EM algorithm ran for a maximum of 100 iterations to optimize and was considered converged if two test statistics could not reject a model of no trend among parameter values (test statistic $T < 2$) and the parameter values exhibited approximately equal sign changes in slope between iterations (i.e. random fluctuations, test statistic $N > 0.5$). Parameter value sampling of the MCMC under both EM and the sampling of rate shift configurations on the tree were conducted with 10,000 samples, with samples retained after every 20 steps and the first 200 samples discarded as burn-in.

We also tested whether phloeomyine incumbency constrained the available morphospace for Chrotomyini to occupy, increasing convergence among species within that clade. To do so, I compared the clade-specific covariance of pairwise Euclidean distances among PC 1-5 and pairwise patristic distances from the MCC tree ($\text{cov}(d,p) = x$). This covariance measures the extent to which sister species resemble each other more than non-sister species. A positive covariance suggests that sister species tend to resemble each other more so than non-sister species (prevalent phylogenetic signal), whereas a negative covariance suggests that non-sister species are more similar to one another than sister species (prevalent convergence). I compared the difference between clade-specific covariances ($x_P - x_C$) to 1000 results simulated under a clade-independent multivariate BM model ($x_{max} - x_{min}$). I interpreted support for increased convergent

evolution among Chrotomyini as recovering an observed covariance ratio greater than 95% of the absolute values of simulated differences.

Clade-specific tempo of mandibular evolution.

In addition to examining patterns of diversification, I tested whether rates of mandibular shape and size evolution (σ^2) were diminished in Chrotomyini because of limited ecological opportunity, using two different approaches. In the first, I fit PC1-2 and log-transformed centroid size to candidate single-rate or multi-rate models of multivariate BM trait evolution in a rate-matrix-based likelihood framework. I tested four different partitioning schemes. The first two schemes constitute the null and alternative models testing whether evolution along these component axes is consistent with incumbency effects: 1) a single-rate BM model and 2) a two-rate model partitioned by clade. Additionally, I also sought to test whether the evolutionary rate for Chrotomyini is better modeled with a discrete process for *Rhynchomys*, which has a strikingly distinct morphology compared to the other LOE rodents, and thus included 3) a two-rate model partitioning the chrotomyine genus *Rhynchomys* versus the remaining LOE rodents. Finally, I tested whether the morphological evolution of these two clades is the result of both incumbency effects and evolutionary innovation of *Rhynchomys* and thus I included 4) a three-rate model partitioning Phloeomyini, *Rhynchomys*, and remaining Chrotomyini. The transitions between rate categories were generated using stochastic character mapping repeated 100 times for each model (Revell and Collar 2009). This approach calculates the position along a branch that confers the maximum likelihood of

change in evolutionary rate along a branch in a phylogeny. This likelihood is computed using a priori designated rate categories and the evolutionary variance-covariance matrix of the PC and centroid size data (Revell and Collar 2009). I assigned equal prior probabilities for all root states and allowed rate category to change at any point along the respective branch. The model with the best placement of rate regimes was determined using the Akaike weight (*w*) calculated from the average of $n = 100$ AICc scores for each partitioning scheme (Akaike 1974; Hurvich and Tsai 1989).

Our second approach to assessing clade-specific evolutionary rates involved comparing evolutionary rates between groups in a distance-matrix-based framework (Adams 2014a). This approach has the advantage of permitting analysis of trait matrices with high dimensionality relative to the number of taxa in each group. The evolutionary rate ratio of Phloeomyini to Chrotomyini $\left(\frac{\sigma^2_{\text{mult(P)}}}{\sigma^2_{\text{mult(C)}}}\right)$ was computed from multivariate distances among species' GPA-transformed shape variables for each clade. This observed ratio was compared to those generated under a simulated distribution of rate ratios under a clade-independent BM process. This analysis was repeated for size evolution as it is still applicable under this distance-based framework. Recovering an observed ratio of evolutionary rates much greater than those generated under the simulated process would indicate that each clade evolved according to a different evolutionary process. In the context of clade-specific rates, I expect to recover a rate ratio favoring Phloeomyini if Chrotomyini experienced less ecological opportunity.

Results

Morphospace occupancy.

Our principal component phylomorphospace analysis illustrates the mandibular shape diversity among Luzon murines (). Chrotomyini tend to exhibit slender mandibles with prominent, dorsally-set coronoid and condyloid processes and thin, posteriorly-projecting angular processes. By contrast, phloeomyines exhibit stout, compressed mandibles and prominent, shield-like angular processes with comparatively shorter and broader coronoid and condyloid processes. The PCA illustrates the high dimensionality of mandibular shape: the first eight component axes account for 90.2% of the variance in the dataset. PC1 primarily represents anterior-posterior telescoping versus compression of the mandible, whereas PC2 captures positioning and size of the coronoid/condyloid processes relative to the angular process (Figure 2.1). These axes accounted for 37.4% and 19.2% of dataset variance respectively. The morphospace occupancy of each clade along the first two PCs was almost entirely without overlap. This between-clade partitioning of morphospace illustrates the distinct mandibular morphology, presumably reflecting dietary disparity, of the two clades. PC3, which captured 10.0% of the dataset variation, primarily represents the inflection point of the anterior margin of the coronoid process (landmark 4), a landmark which exhibited substantial intraspecific variation. PC4 captured 7.7% of the dataset variation and represents the orientations of the fossae adjacent to the condyloid process. PC5 captured 5.6% of the dataset variation and primarily corresponds to relative compression versus expansion of the angular process, in

other words, the distances between landmarks 10 and 11. Components 3-5 did not exhibit cladewise clustering.

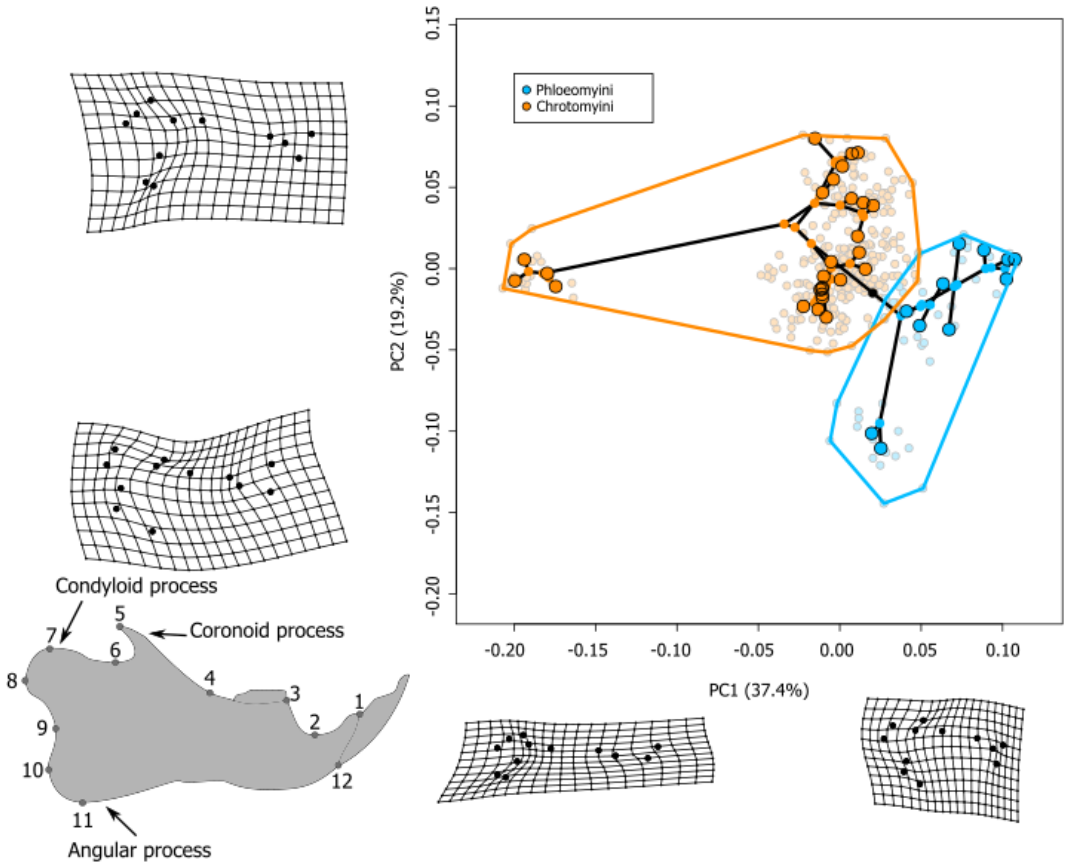

Figure 2.1. PC1 and PC2 of mandibular morphology for 41 Luzon Old Endemic rodent species (n = 337). Opaque enclosed circles represent species averages, with open circles the inferred ancestral state under Brownian Motion evolution. Branches connecting points represent relationships among species according to pruned MCC tree from Rowsey et al. (2018; Figure 2). Transparent points represent individual specimens, the extremes of which are indicated with convex hulls for each clade. Thin-plate splines along axes show specimens with extreme scores and illustrate differences along these axes. Bottom-left: lateral view of a mandible indicating landmarks taken. Landmarks taken include: 1. Anterodorsal apex of incisive alveolus; 2. Ventral nadir of diastema between incisor (I1) and first molar (M1); 3. Anterior margin of M1 alveolus; 4. Junction of coronoid process with body of mandible, defined by point at which a straight line following coronoid process first meets the body; 5. Posterodorsal apex of coronoid process; 6. Ventral nadir between coronoid and condyloid processes; 7. Anterodorsal apex of condyloid process; 8. Posterior apex of condyloid process; 9. Anterior nadir between condyloid and angular processes; 10. Posterior apex of angular process; 11. Ventral apex of angular process; 12. Anteroventral apex of incisive alveolus.

Log-transformed centroid size was highly correlated with log-transformed head and body length (adjusted R^2: 0.919). As such, I used log-transformed centroid size as a proxy for body size in subsequent analyses because these data were available for all specimens. Centroid size varied substantially within and between clades (Figure 2.2), but particularly within Phloeomyini, which exhibited three distinct size categories: the small *Musseromys*; the mid-sized *Batomys* and *Carpomys*; and the large *Crateromys* and *Phloeomys*. In Chrotomyini, I found two size classes, the first comprising the small *Apomys* (subgenus *Apomys*), *Archboldomys,* and *Soricomys*; and the second including the mid-sized *Apomys* (subgenus *Megapomys*), *Chrotomys*, and *Rhynchomys* (Figure 2.2).

Clade-specific mode of mandibular evolution.

The goal of the first test of incumbency effects was to determine whether the rate of mandibular shape evolution decelerated over time, which would be consistent with the expectations of an adaptive radiation scenario. Mandibular shape evolution within Phloeomyini did not support a decelerating, early burst (EB) model of evolution: the maximum likelihood estimate of phloeomyine evolution under EB evolution yielded a rate deceleration parameter $\beta = 0$, rendering it equivalent to a constant-rate model ($\ln(L)_{BM} = 44.07$, $\ln(L)_{EB} = 44.07$, $D = 0$, df = 1, $p \approx 1$, Table 2.1). By contrast, a model of decelerating evolutionary rate was supported for Chrotomyini ($\ln(L)_{BM} = 133.4$, $\ln(L)_{EB} = 136.5$, $D = 6.21$, df = 1, $p = 1.27 \times 10^{-2}$, Table 2.1). The average rate of evolution was higher in Chrotomyini than in Phloeomyini along both PC axes (Table 2.1). Model adequacy results suggested these models fit each clade well, with the

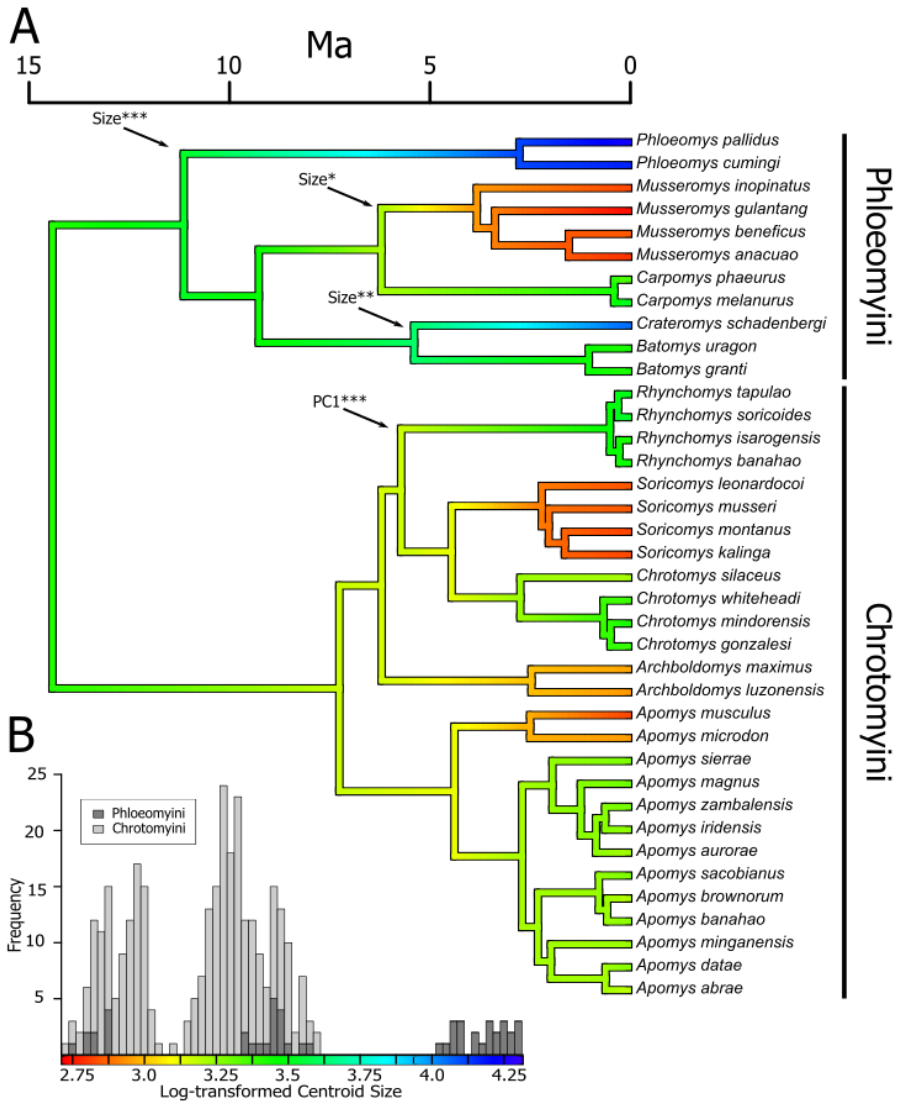

Figure 2.2. A: phylogram illustrating relationships among Luzon old endemic rodents in relation to average log-transformed centroid size. Three additional species included in the phylomorphospace analysis (*Batomys dentatus*, *Apomys sp.*, and *Rhynchomys sp.*) are not shown as no molecular data were available. Tree pruned from the Bayesian MCC tree inferred by Rowsey et al. (2018). Cooler colors indicate larger size and ancestral states were reconstructed based on maximum likelihood Brownian motion model parameters. Arrows indicate branches inferred to exhibit shifts in evolutionary mode and are labeled with the trait inferred to exhibit the shift. ***: posterior probability (PP) ≥ 0.95; **: PP ≥ 0.9; *: PP ≥ 0.85. B: histogram of log-transformed centroid size for the mandibular dataset (n = 337).

Table 2.1. Likelihood ratio tests (LRT) of decelerating morphological evolution fitted to PCs 1 and 2 of mandibular shape. Statistically significant result of LRT suggests a decelerating rate model of evolution better describes the rate of evolution in the given clade. An asterisk indicates the likelihood ratio *D* is statistically significant at $\alpha = 0.05$.

	Phloeomyini		**Chrotomyini**	
$\ln(L)_{BM}$[a]	44.07		133.4	
$\ln(L)_{EB}$[b]	44.07		136.5	
D[c]	0		6.211*	
d.f.	1		1	
Parameter values	**PC1**	**PC2**	**PC1**	**PC2**
σ_0^2 (initial rate)	4.23×10^{-4}	1.92×10^{-4}	1.32×10^{-3}	1.13×10^{-3}
$\bar{\sigma}^2$(average rate)	4.23×10^{-4}	1.92×10^{-4}	7.12×10^{-4}	6.10×10^{-4}
θ (ancestral state)	3.64×10^{-3}	-2.79×10^{-3}	1.96×10^{-2}	1.60×10^{-2}
β (deceleration parameter)	N/A		-0.349	

a: log-likelihood, Brownian motion model of evolution
b: log-likelihood, early burst model of evolution
c: $D = 2 \times (\ln(L)_{EB} - \ln(L)_{BM})$

only poorly-modeled aspects of trait variation occurring in PC1 evolution in Chrotomyini: with marginal significance, the EB model for this axis did not adequately account for among-branch rate heterogeneity ($C_{VAR} = 0.9672$, $p = 0.05395$) and trait-value-associated rate heterogeneity ($S_{ASR} = 6.129$, $p = 0.05195$; Appendix Table 2.2).

Interestingly, I lost all support for an early burst model of evolution when *Rhynchomys* was pruned from the dataset, instead inferring identical parameter estimates under the EB model to the BM model and a deceleration parameter $\beta = 0$. This suggests that the support for an early burst model is driven entirely by the highly divergent morphology of *Rhynchomys.* The disparity-through-time (DTT) of multivariate shape corroborates this, illustrating a steep plummet in within-clade disparity at the time of splitting of *Rhynchomys* from the remaining chrotomyines, suggesting that at that point the average subclade does a poor job explaining the total amount of variation in the dataset (Figure 2.3A). By contrast, Phloeomyini exhibits a strong decrease in average

within-clade disparity at the first split within this clade, corresponding to the distinctiveness of *Phloeomys*. In both clades, subsequent to the splits of these outlying lineages, remaining speciation events do little to contribute to within-clade disparity, except for a brief spike near the present in Phloeomyini, corresponding to the speciation of the morphologically similar species of *Batomys* followed by a decline corresponding to the recent split between morphologically distinct *Carpomys* species (Figure 2.3A).

Table 2.2. Likelihood ratio tests (LRT) of decelerating morphological evolution fitted to log-transformed centroid size. Statistically significant result of LRT suggests a decelerating rate model of evolution better describes the rate of evolution in the given clade. An asterisk indicates the likelihood ratio *D* is statistically significant at $\alpha = 0.05$.

	Phloeomyini	**Chrotomyini**
$\ln(L)_{BM}$	-3.193	21.84
$\ln(L)_{EB}$	-2.959	24.35
D	0.4689	5.033^{*}
d.f.	1	1
σ_0^2 (initial rate)	2.13×10^{-2}	5.13×10^{-2}
$\bar{\sigma}^2$ (average rate)	2.13×10^{-2}	2.68×10^{-2}
θ (ancestral state)	3.64	3.12
β (deceleration parameter)	N/A	-0.437

The clade-specific univariate analysis of log-transformed centroid size recovered a difference between clades in the best-fit model of size evolution, with Phloeomyini again favoring a constant-rate BM model and Chrotomyini favoring an EB model (Table 2.2). Both of these models were found to adequately describe the data, with no violations of model summary statistics. Unlike the results of shape evolutionary rate, the support for an EB model was robust to pruning *Rhynchomys* from the analysis ($\ln(L)_{BM} = 19.37$, $\ln(L)_{EB} = 21.61$, $D = 4.478$, df = 1, $p = 0.0344$). Interestingly, almost all size evolution occurred within the first three million years of the clade's existence on Luzon (Figure

2.3B), roughly corresponding to genus-level divergence in the MCC tree generated by Rowsey et al. (2018). As with mandible shape, DTT of Phloeomyini size showed a large decrease in average within-clade disparity at the first split within this clade, corresponding to *Phloeomys*, and all subsequent splits failed to substantially contribute to within-clade disparity (Figure 2.3B).

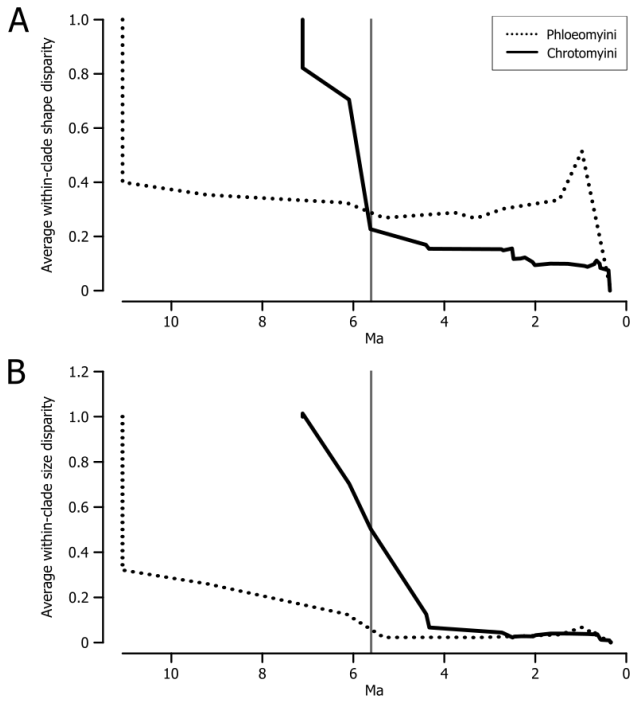

Figure 2.3. Disparity-through-time plots (Harmon et al. 2003) for multivariate mandibular shape (A) and logarithmically-transformed centroid size (B). Within-clade disparity was measured as the ratio between the average pairwise Euclidean distances of each subclade node present at a given time in the clade's history and the average pairwise Euclidean distance among species in the entire clade.

We recovered strong support for an evolutionary model that allowed shifts among evolutionary modes compared to a single-rate BM process for PC1, PC2, and centroid size (Table 2.3). With respect to mode-shift locations, I detected high posterior probability (PP) for a shift in evolutionary mode along PC1 on the branch of the

phylogeny leading to *Rhynchomys* and evidence for three independent shifts in centroid size evolution in Phloeomyini with varying support (Figure 2.2A). I did not recover strong support for shifts along any branch with respect to PC2 despite recovering strong support for this model.

Table 2.3. Likelihood ratio tests (LRT) of BM versus Lévy evolution of mandibular shape (PC1 and PC2) and size. An asterisk indicates the likelihood ratio D is statistically significant at $\alpha = 0.05$. Note that although I recovered strong support for a Lévy process along PC2, I did not recover high posterior probability for any evolutionary shifts on the tree.

	PC1	**PC2**	**Centroid Size**
$\ln(L)_{BM}$	86.25	84.89	12.10
$\ln(L)_{L}$	106.6	95.45	28.90
D	40.76^{*}	21.12^{*}	33.61^{*}
d.f.	2	2	2
σ_0^2 (initial rate)	6.123×10^{-5}	9.851×10^{-5}	1.526×10^{-3}
θ (ancestral state)	3.062×10^{-2}	-4.215×10^{-2}	3.390
α (jump strength)	538.9	43.00	205.9
λ (jump rate)	1.009×10^{-2}	3.008×10^{-2}	9.218×10^{-2}

Our final analysis comparing the mode of evolution between Chrotomyini and Phloeomyini tested whether Chrotomyini exhibited greater convergent evolution than did Phloeomyini resulting from limited morphospace availability. Although Phloeomyini exhibited a larger covariance of PC1-5 Euclidean distances and patristic distances than did Chrotomyini ($x_P = 0.179$, $x_C = 0.139$, $x_P - x_C = 4.05 \times 10^{-2}$), the difference between these covariances was statistically non-significant when compared to those simulated under a single-rate BM model (mean $x_{sim.max} - x_{sim.min} = 2.68 \times 10^{-1}$, $p = 0.90$; Figure 2.4A). Similarly, convergence in size evolution did not exhibit a significant difference between clades ($x_P = 1.72$, $x_C = 3.06 \times 10^{-1}$, $x_P - x_C = 1.41$, $x_{sim.max} - x_{sim.min} = 1.29$, $p = 0.35$; Figure 2.4B). Thus, I failed to support incumbency as forcing an increase in convergent evolution among Chrotomyini in either size or shape evolution.

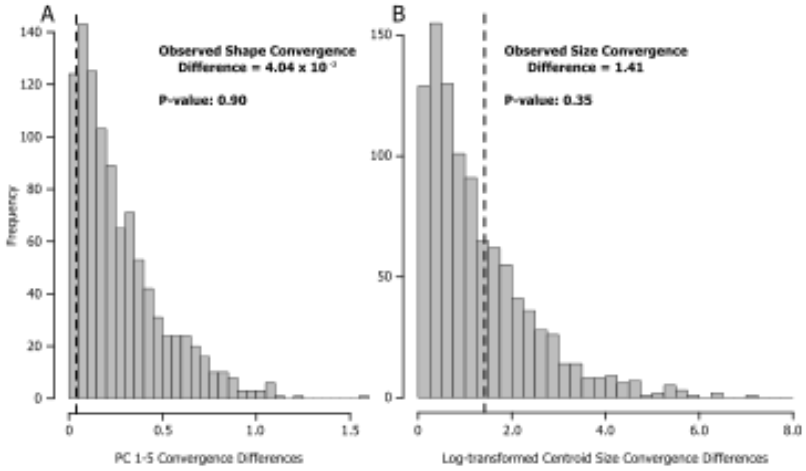

Figure 2.4. Histograms showing distribution of differences in clade-wise covariances between Euclidean and patristic distances as a comparison of convergence between clades. Figure 2.4A illustrates differences in PC 1-5 shape convergence. Figure 2.4B illustrates differences in convergences based on Log-transformed centroid size. The dashed line indicates the observed difference in covariances between Phloeomyini and Chrotomyini, and the gray bars represent differences simulated under a clade-independent Brownian Motion process.

Clade-specific tempo of mandibular evolution.

Our next series of analyses tested the hypothesis that the two clades differ from each other in their rate of mandibular evolution. Among the candidate models of single- versus multi-rate BM evolution, the best-fit model for the first two PCs was a two-rate model parameterizing *Rhynchomys* and the remainder of LOE rodent species under discrete rate categories, with moderate support (Appendix Table 2.3). Most simulated character histories gave strong support for this model over a single-rate model and a two-rate, clade-based model, but a three-rate model with Phloeomyini, *Rhynchomys*, and remaining Chrotomyini as discrete rate categories was supported as the best-fit model in 40% of simulations (w = 0.37. The distance-based simulation approach, which allowed

for multivariate comparisons of shape evolution using all the shape variation captured by the GPA, also revealed little support for clade-specific rates of morphological evolution. Although Phloeomyini exhibited a slightly higher average rate of shape evolution (Phloeomyini: $\sigma^2_{\text{mult(P)}} = 5.60\times10^{-5}$, Chrotomyini: $\sigma^2_{\text{mult(C)}} = 4.56\times10^{-5}$, $\frac{\sigma^2_{\text{mult(P)}}}{\sigma^2_{\text{mult(C)}}} = 1.23$), the observed ratio of multivariate evolutionary rates was not larger than expected under a single-rate model (mean $\frac{\sigma^2_{\text{mult(max.sim)}}}{\sigma^2_{\text{mult(min.sim)}}} = 1.17$, $p = 0.24$, Figure 2.5A).

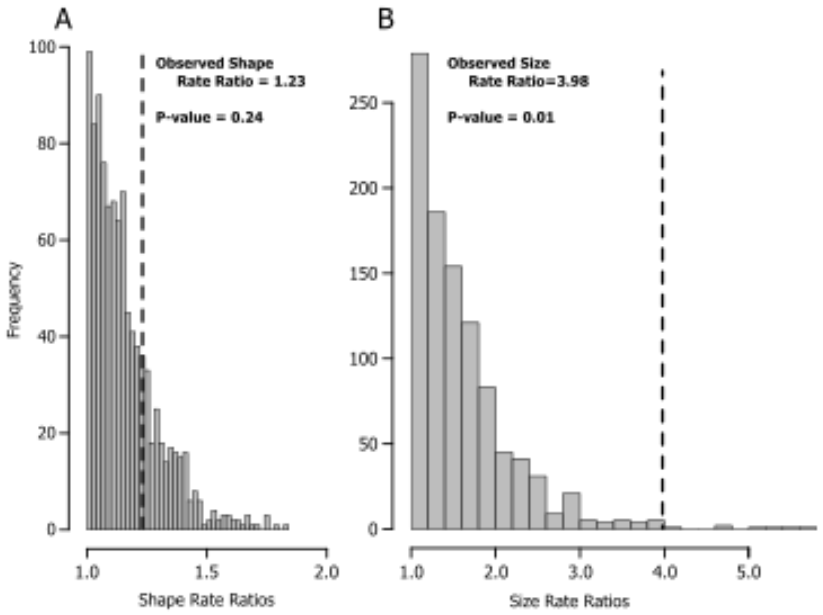

Figure 2.5. Histograms of simulated clade-wise evolutionary rate ratios for multivariate shape data (A) and log-transformed centroid size (B). Bars represent bins of 999 calculated ratios simulated under a single-rate Brownian motion process. Dashed line indicates the observed ratio of evolutionary rates of Phloeomyini to Chrotomyini.

In contrast to shape evolution, size evolution was best explained by a two-rate, clade-specific model (ln(L) = 16.55, k = 3, AICc = -26.41, w = 0.68; Appendix Table 2.4). This result is corroborated by recovering significantly higher rate of size evolution

for Phloeomyini than expected under a single-rate process ($\sigma^2_{\text{size(P)}} = 2.20\times10^{-2}$, $\sigma^2_{\text{size(C)}} = 5.52\times10^{-3}$, $\frac{\sigma^2_{\text{mult(P)}}}{\sigma^2_{\text{mult(C)}}} = 3.98$, mean $\frac{\sigma^2_{\text{size(max.sim)}}}{\sigma^2_{\text{size(min.sim)}}} = 1.61, p = 0.01$, Figure 2.5B). Recovering this significantly lower rate of size evolution within Chrotomyini is consistent with incumbency effects and represents evidence of evolutionary rates consistent with this hypothesis among LOE murines.

Discussion

Our results suggest a complex relationship among incumbency effects, ecological opportunity, and morphological evolution (Table 2.4). Rather than inherently constraining the tempo or mode of evolution of secondary colonists, incumbency's strongest effects on morphological evolution appear to be establishing an initial biotic filter on subsequently colonizing lineages. This is best illustrated in the shape phylomorphospace analysis (Figure 2.1), where the two clades exhibit almost no overlap, and the area each clade occupies is consistent with the ancestral chrotomyine lineage being already ecologically distinct with respect to diet from Phloeomyini extant at the time of chrotomyine colonization due to ancient divergence in allopatry (Tobias et al. 2014).

Table 2.4. Summary of hypotheses and conclusions surrounding incumbency effects in the Luzon Old Endemic rodents.

Hypothesis	Conclusion		
	Lineage diversification	**Mandibular shape evolution**	**Body/mandible size evolution**
Secondary colonists occupy distinct areas of trait space from incumbent clades due to biotic filtering of ecologically similar species	Not applicable	**Strongly supported.** Each clade occupies an almost entirely discrete area along PC1-2 (Figure 2.1).	**Supported.** Phloeomyini occupies a unique size class, likely due to energetic constraints imposed by Chrotomyine diet, which indirectly supports a role of incumbency effects (Figure 2.2).
Both incumbents and secondary colonists exhibit decelerating evolutionary rates due to declining ecological opportunity	Not supported. Constant-rate diversification was a better fit for both clades (Rowsey et al. 2018 Figure 2.5).	Not supported. Constant-rate evolution best described Phloeomyini, decelerating rate best described Chrotomyini *but* only due to outlier morphology of *Rhynchomys*.	Not supported. Constant-rate evolution best described Phloeomyini, decelerating rate best described Chrotomyini, which is likely due to dispersal-mediated speciation, rather than ecological speciation.
Secondary clades can shift to new evolutionary modes	Not supported. Constant-rate diversification comparable to their sister clade, the Sahul Old Endemics, was the best fit for Chrotomyini (Rowsey et al. 2018 Figure 2.5).	**Supported.** *Rhynchomys* represents a rapid shift to a highly divergent mandibular morphology with strong support (Figure 2.2A)	Not supported. I recovered evidence for three shifts in mode of size evolution with varying levels of support, but only in Phloeomyini.
Secondary-colonizing clades exhibit more intra-clade convergent evolution than incumbent clades	Not applicable	Not supported. The two clades have similar levels of convergence (Figure 2.4A).	Not supported. The two clades have similar levels of convergence (Figure 2.4B).
Secondary-colonizing clades exhibit lower evolutionary rates than incumbent clades	Not supported. Incumbent Phloeomyini has a lower diversification rate than Chrotomyini (Rowsey et al. 2018 Figure 2.6A).	Not supported. The two clades have similar rates (Figure 2.5A).	**Strongly supported.** Phloeomyini has size evolutionary rate over threefold that of Chrotomyini (Figure 2.5B).

The morphospace occupancy of Chrotomyini is surprising in its diversity. In particular, *Rhynchomys* represents a rapid evolutionary innovation couched among species that are evolving disparate mandibular shapes at a constant, slower, rate (Figure 2.2, Appendix Table 2.3). This rapid evolution in a secondary-colonizing clade illustrates that incumbency does not necessarily restrict the ability for clades to evolve novel morphologies, merely that this morphological variation may be forced to be distinct from that shown by incumbent species. Although species within Chrotomyini are clustered in genera that exhibit disparate mandibular morphology from one another, field studies suggest that many of these species have similar diets (i.e. earthworms and soft-bodied arthropods, Rickart et al. 2011, Rickart et al. 2016, Heaney et al. 2016b). I suspect focused dietary analyses may reveal differences in prey preference among chrotomyine genera (e.g. earthworms versus arthropods). If detailed dietary analyses determine most earthworm mouse species exhibit very similar diets regardless of mandibular morphology, the PCA would suggest that the disparity in mandibular morphology reflects different prey capture strategies or habitat use facilitated by cranial morphology (e.g. fossoriality in *Chrotomys*: Zuri et al. 1999).

The diversity of chrotomyine mandibular morphology compared with their apparent lack of size and dietary diversity contrasts with Phloeomyini, which appear to be evolving disparate sizes coincident with distinct diet types (e.g. large folivores such as *Phloeomys* and small granivores such as *Musseromys*). Bioenergetic demands may favor an increased body size in folivores such as *Phloeomys* and *Crateromys* due to availability of slow-releasing nutrients in leaves. The primarily insectivorous and vermivorous

chrotomyines may be constrained to small and medium body sizes due to the accessibility of high-nutrient prey items at smaller sizes and the infeasible absolute amount of prey biomass needed for subsistence on these diet types as body size increases (Demment and Van Soest 1985; Gittleman 1985; Churchfield 1990, Churchfield 2002). This bioenergetic constraint, along with the observation that all the large-bodied phloeomyines possess some climbing ability, suggests that evolution of increased size is most likely to favor arboreal, folivorous species which occur in habitats with dense canopy foliage. Evolving a larger body size can thus permit access to a more abundant food source than available to vermivores and insectivores (Millar and Hickling 1990). If the observed lack of morphospace overlap is due to diet-related, constrained body size evolution in Chrotomyini, the fourfold lower rates of size evolution and large size class exclusion in this clade would be consistent with phloeomyine incumbency limiting ecological opportunity. However, because body size is correlated with many aspects of organismal behavior and physiology, there are multiple interpretations for the partial lack of overlap I observed. Thus, rather than phloeomyine competition preventing evolution into this large size class, the resultant size distributions may simply be the result of independent radiations due to different evolutionary pathways of least genetic resistance with little influence of inter-clade competition (Schluter 1996). As a result, I cannot definitively link size diversity with interspecific competitive partitioning of habitat and food resources between the two clades.

Our recovery of decelerating body size evolution in Chrotomyini in the face of constant lineage diversification is likely due to a mixture of early ecological

diversification followed by dispersal-mediated speciation in this clade. Early diversification of chrotomyines on Luzon appears to have been accompanied by relatively rapid size evolution, corresponding to genus-level differences in current species diversity (Figure 2.3B). Paleogeological land-area estimates of Luzon suggest the beginning period of intrageneric divergence among Chrotomyines, approximately three to five Ma, was a time of rapid volcanic activity and therefore of both island and mountain building (Hall 2013). This dynamism may have created new habitat that allowed for a shift from ecological size evolution to dispersal-mediated speciation with limited body size evolution (e.g. Justiniano et al. 2015). By contrast, I suspect the lack of support for decelerating evolution in Phloeomyini may stem from lack of intra-island speciation within genera in this clade. For example, whereas many species in the chrotomyine genus *Apomys* appear to have diverged due to intra-island dispersal and subsequent isolation (Justiniano et al. 2015), several members of Phloeomyini have not dispersed from the oldest region of Luzon, the Central Cordillera (e.g. *Carpomys*, *Crateromys*) or appear to have maintained population connectivity across areas that present gene flow barriers to chrotomyine species (*Phloeomys*), resulting in lower species diversity and less power to detect decelerating body size evolution.

Rowsey et al. (2018) recovered a significantly lower diversification rate in Phloeomyini than Chrotomyini despite Phloeomyini's incumbent status. In conjunction with the findings that Phloeomyini not only exhibits a constant rate of size evolution (Table 2.2) but also that this evolutionary rate is much higher than that of Chrotomyini (Figure 2.5B), I suspect that future work examining the relationship between body size

evolution and lineage diversification across a broader sample of murines may find that increased body size may promote dispersal ability and inhibit lineage diversification (Claramunt et al. 2012; Weeks and Claramunt 2014). If this is indeed the case, an inverse relationship between rates of body size evolution and lineage diversification would explain the patterns I recovered better than resulting from incumbency effects and ecological opportunity in the absence of dispersal to other mountains on Luzon.

Previous work among muroid rodents corroborates the results of tempo and mode of mandibular evolution. Alhajeri et al. (2016) tested whether muroid rodents exhibited early burst evolution consistent with declining ecological opportunity following continental colonization in a suite of ecologically-important morphological characters. From a different perspective, Rowe et al. (2016) documented the remarkable convergence among independently-evolving carnivorous rodents that exhibit shrewlike morphology (such as *Soricomys* and *Archboldomys* on Luzon, and *Melasmothrix* on Sulawesi) as well as the bizarre "tweezer-snouted" morphology exhibited by *Rhynchomys* on Luzon and *Paucidentomys* on Sulawesi (Rowe et al. 2016). Both Alhajeri et al. (2016) and Rowe et al. (2016) came to similar conclusions as I did: the classical model of early-burst evolution used to support a hypothesis of adaptive radiation is not the likely mechanism of morphological evolution in muroids broadly, murines specifically, nor even LOE rodents locally. Instead, a constant background process with some major shifts to new adaptive zones appears to provide a better explanation of the observed morphological variation, with similar selective pressures in convergently evolved carnivorous rodents (Table 2.1, Figure 2.2, Appendix Table 2.3).

In response to the growing interest in detecting early bursts in the macroevolutionary history of diverse clades, Moen and Morlon (2014) emphasized two important points for analyzing phenotypic data in the context of ecological opportunity and adaptive radiation, which Alhajeri et al. (2016) noted as potential reasons for not recovering a signal of early burst morphological evolution. First, the time scale on which adaptive radiation often occurs is typically only detectable in recent radiations, such as Darwin's finches (Sato et al. 2001) and the African lake cichlids of Malawi and Victoria (Friedman et al. 2013), with the potential for other processes to obscure this signal at longer time scales, including the scale of LOE evolution. Second, analysis of phenotypic data may be more robust to unsampled extinct taxa in detecting the historical signature of ecological opportunity, compared to analyses of lineage diversification, due to predictable patterns of trait variation among species in constant-rate versus decelerating evolutionary processes (Moen and Morlon 2014). Nevertheless, one can hypothesize a scenario where ecologically similar incumbent lineages may have selectively been driven extinct by subsequent colonists that, through mechanisms such as increased reproductive rate or foraging efficiency by secondary colonists, may have been able to overcome the incumbency effect (i.e., a competition-mediated taxon cycle: Ricklefs and Bermingham 2002). In the absence of fossil data, however, I cannot currently test this hypothesis, and the low extinction rate in Phloeomyini reported by Rowsey et al. (2018) provides some evidence to suggest that this scenario may be unlikely.

Our study focused on the morphological evolution in the two oldest, most species-rich clades on Luzon, which account for the majority of non-volant mammalian species

and morphological diversity in this system. Nevertheless, an estimated four additional murine colonization events have occurred on Luzon after colonization by the LOE rodents, likely within the past two million years (in other words, likely long after most of the ecological differentiation corresponding to genus-level diversification had already occurred; Rowsey et al. 2018). These "new endemic" lineages are ecologically and phylogenetically distinct from the other clades, and available distributional data suggest that these rodents occur primarily in disturbed habitat types where the LOE rodents typically do not occur or are uncommon (Heaney et al. 2016b, Rowsey et al. 2018). Although these clades lack species diversity necessary for comparing tempo and mode of morphological evolution, the patterns of morphospace occupancy may suggest the exclusion from habitat types occupied by most LOE rodents (i.e. old growth montane forest) is the result of ecological similarity to existing colonists.

Another important piece of the puzzle of incumbency effects among Indo-Australian rodents is the phylogenetic background within which Chrotomyini belongs. Chrotomyini is sister to the Sahul Old Endemics, so named for their range encompassing New Guinea, Australia, and Melanesian islands (SOE: Rowe et al. 2008). The incumbent status of the SOE on Sahul may approximate the potential morphological evolution realizable by Chrotomyini in the absence of an incumbent murine clade, given that Phloeomyini is endemic to the Philippines. Interestingly, several SOE genera resemble some members of the two LOE clades, including giant herbivores such as *Hyomys* and shrew-like insectivores such as *Pseudohydromys*. Analysis of phenotypic variation in these clades in a comparative evolutionary framework may reveal the relative importance

of ecological character displacement, biotic filtering, and phylogenetic inertia (Schluter 2000b). In other words, such an analysis may illustrate whether the pattern of extant morphological diversity and diet type among chrotomyines is due to intrinsic (i.e. plesiomorphic) or extrinsic (i.e. incumbency-mediated) canalization of morphological evolution. Additionally, a comparison of the dietary evolution between these clades may provide evidence to suggest the clade-specific partitioning of LOE mandibular morphology is the result of ecological and evolutionary processes to minimize potential competitive effects.

Conclusions

Our analyses of mandibular shape and size evolution illustrate several important conclusions (Table 2.4). First, incumbency effects may manifest both as preventative barriers to colonization by ecologically similar species as well as decreased rates of evolution in secondary colonists, but both patterns need not occur in systems with repeated colonization. Second, decelerating phenotypic evolutionary rates are not a guaranteed consequence of incumbency effects; the ecological opportunity model may be a poor fit for dynamic island systems even if these systems (such as Luzon) are relatively small and isolated. Instead, clades may be able to explore new and innovative areas of morphospace yielding unique morphologies as long as these morphologies remain disparate from existing species. Finally, these results illustrate that the tempo and mode of morphological evolution has differed in some respects from that of lineage diversification: morphospace partitioning and size variation was consistent with incumbency effects whereas lineage diversification was not (Rowsey et al. 2018). The

strength of a macroevolutionary incumbency effect may be as little as requiring differentiation along an ecologically-important trait axis; the results suggest that if this requirement is met, two clades may co-occur with relatively little impact on phenotypic or lineage evolutionary rates. My work in this system contributes to a growing body of research suggesting that species diversity does not always approximate ecological diversity, at a variety of spatiotemporal scales, even when phylogenetic signal is present in the traits being examined (Rowe et al. 2011; Ruta et al. 2013; Mazel et al. 2017; Múrria et al. 2017), and that examining species and morphological diversity may yield different and equally informative insights (Jablonski 2008).

CHAPTER 3. HUMERUS SHAPE OF LUZON, PHILIPPINES "OLD ENDEMIC" MURINE RODENTS IS INFLUENCED BY LOCOMOTORY ADAPTATION AND PARALLEL EVOLUTION

Introduction

The mammalian forelimb is one of the primary interfaces between the organism and its environment. Generally, quadruped limbs comprise the stylopod, zeugopod, and autopod elements, which in the mammalian forelimb translate to the humerus, radius + ulna, and manus, in turn comprising carpal (wrist), metacarpal (palm), and phalangeal (digit) elements. Of these elements examined individually, the humerus is the most structurally complex and houses origination and insertion points for about a dozen muscles and muscle groups that have important uses in food acquisition and handling, stability and weight bearing, and locomotion (MacPherson 1988; Whishaw and Coles 1996; Iwaniuk et al. 1999; Mathewson et al. 2012). On the other hand, the relative lengths of the three podial units, or portions thereof. provide a simple but effective measure for identifying mammalian locomotory niche. Generally speaking, arboreal mammals tend to have relatively long humeri and phalanges and relatively short olecranon processes (promoting range of motion and gripping ability), whereas fossorial and semifossorial mammals tend to exhibit relatively long humeri and olecranon processes but short phalanges (maximizing the mechanical advantage of the zeugopod and autopod to assist with digging), and terrestrial mammals occupy a more middle ground (Howell 1944; Young and Hallgrímsson 2005; Samuels and Van Valkenburgh

2008, Nations et al. in review). While linear measurements of the distal forelimb are often correlated with locomotory niche, their utility is in some cases hampered by challenges associated with small specimens in taking precise measurements and ease by which elements can be lost. It is thus of further interest to determine whether the humerus, as a complex, comparatively large bone, exhibits a similar relationship to measurements on a combination of distal forelimb elements with respect to locomotory niche.

Perhaps because of the utility of simple linear measurements in predicting mammalian niche, most studies examining the evolutionary correlation between adaptive function and the shape of limb elements in mammals have focused on the extreme adaptations required for fossorial taxa. For example, in their examination of scalopine and talpine moles, Sansalone et al. (2018) found the two relatively deeply divergent sister clades experienced differing allometric trajectories and differing patterns of morphospace occupancy, corresponding to a faster rate of humerus shape evolution in Scalopini despite exhibiting a similar fossorial locomotory type to Talpini. Their study illustrated that humerus shape can differ along distinct phylogenetic axes without corresponding to differences in locomotory mode. By contrast, Marcy et al. (2016) found cranial and humeral shape in *Thomomys* pocket gophers was strongly dependent on soil thickness, body size, and clade membership, where the clade containing larger species exhibited distinct allometric relationships from smaller species, and these size differences corresponded to soil-based habitat preferences. These authors concluded variation in

traits associated with locomotion is partitioned not only by clade, but also by size and ecological niche.

These two studies shed light on how closely related fossorial clades partition morphological variation. Their differences in conclusions reveal an important point: temporal and phylogenetic scale affect the ability to predict differences fossorial locomotion based on humerus shape. At shallow phylogenetic scales, morphological traits may predict ecological niche better than at deeper scales because parallel adaptations to different ecological niches are less likely. With this conclusion in mind, further research is necessary to determine whether locomotory modes beyond fossoriality predict humerus shape in a similar fashion.

Given the requirements (and potential structural trade-offs) for locomotion that differ between species that spend a majority of the time grasping and scaling tree limbs, tree trunks, and slopes compared to species that spend considerable time digging for food and shelter or those who exhibit unspecialized ambulatory locomotion, one may expect the shape of the humerus to vary based on accommodating the stresses, power, and range of motion specific to a particular locomotory strategy. For example, structures such as the deltoid tuberosity, which provides muscle attachment for the deltoids (controlling anterior-posterior movement of the humerus), and the epicondyles flanking the joint between the humerus and ulna, which provide attachment points for the triceps, epitrochlearis, and other muscles (providing power for digit extension and flexion), may be broader and flatter in fossorial species than in terrestrial and arboreal species (Lehmann 1963, Elissamburu and De Santis 2011; Appendix Figure 3.1). Among

arboreal species, the humerus head may be more spherical rather than ovoid (i.e. longer than wide) to favor range of motion over stability (Lehmann 1963). Terrestrial species may exhibit intermediate forms to these, with small distal epicondyles associated with limited digital power required for most terrestrial locomotion. These predicted patterns of shape variation may also be correlated with linear measurements taken from the ulna and manus, including relative olecranon length, metacarpal length, and phalanx length, to approximate locomotory strategy.

Testing the ability to predict humerus shape from a broader array of locomotory modes requires careful attention to the taxonomic and geographic scale at which this test is performed. The focal clades must be diverse enough to exhibit substantial variation in locomotory mode while also being relatively closely related. As recovered by Sansalone et al. (2018), if the focal taxa are deeply divergent, variation due to clade membership may be more important in determining humerus shape than locomotory variation. Recovering this pattern may become more likely as phylogenetic scale increases and independent adaptations to locomotory niches become more common. With this consideration in mind, the two clades of "Old Endemic" rodents of Luzon island, Philippines represent ideal candidates for investigating the correlation between humerus shape, distal forelimb morphology, and locomotory strategy in an evolutionary context. These two murine rodent clades, Phloeomyini and Chrotomyini, colonized Luzon Island independently and together constitute an estimated 40 species (Heaney et al. 2016b). The LOE rodent clades exhibit substantial size and ecological heterogeneity, with phloeomyines ranging from the 20 g *Musseromys* to the 2.5 kg *Phloeomys* and

chrotomyines ranging from 20 g *Apomys musculus* to 200 g *Rhynchomys*. The two clades are remarkably diverse in terms of both diet and habitat use, potentially representing two distinct axes along which these clades may have diversified (Rowsey et al. 2019). Importantly, these two clades diverged from one another approximately 13 to 16 million years ago (Ma) yet are both members of subfamily Murinae, providing the intermediate level of relatedness with which one can test the importance of locomotory node versus clade membership in determining humerus shape.

Although the current understanding of precise locomotory strategy is coarse, field surveys and quantitative assessments of digit lengths suggest that all phloeomyines exhibit climbing behavior ranging in frequency from occasionally to nearly exclusively (Heaney et al. 2016b; Nations et al. in review). By contrast, Chrotomyini varies much greater by species in proportion of time spent on trees, on the ground surface, and burrowing (Heaney et al. 2016b). In sum, these two clades of rodents exhibit ecological heterogeneity, reasonable phylogenetic divergence, and evidence from prior studies establishing the correlation between distal forelimb measurements and both categorical and continuous variation in locomotory strategy. This level of diversity permits testing the correlation between humerus shape and locomotory strategy in a way that is broadly applicable to species rich, ecologically diverse subfamily Murinae.

We thus tested the ability of locomotory strategy to predict both humerus shape and distal forelimb measurements with the goal of being able to use humerus variation as a complement or addition to traditional linear morphometrics to quantify ecological variation. I fit multivariate linear models in the phylogenetic comparative framework of

the LOE rodents to determine the strength of correlation between morphometric variables and categorical locomotory variables as well as determined how these traits vary among species within each category and across the phylogeny.

Materials and Methods

Taxon sampling.

We sampled a total of 76 individuals representing 37 species of Luzon Old Endemic rodents (approximately 95% coverage of described LOE species) from the Field Museum of Natural History (FMNH) and the United States Museum of Natural History (USNM). I sampled at least two individuals for all species except *Apomys magnus* and *Carpomys melanurus* and included one male and one female when available. Dry skeletal specimens were preferred in my sampling, but fluid-preserved carcasses were used when no dry specimens were available. The list of sampled specimens and associated metadata can be found in Appendix I.

X-ray computed tomography.

We scanned both skeletal and fluid-preserved specimens using a North Star Imaging X5000 scanner housed at the University of Minnesota Department of Earth Sciences. A total of 26 scans were performed on the sampled specimens to acquire forelimb surfaces. Scanning parameters varied for each scan to maximize the contrast and clarity of the image according to the particularities of each scanning bout. In general, I attempted to maintain the voltage and power consistently near 130 V and 21.0 W

respectively. The imaging frame-rate was also variable and ranged from 1.0 to 2.1 frames per second. I reconstructed three-dimensional volumes for each scan from a series of 1,440 radiographs using the program efX-CT (North Star Imaging, Rogers, Minnesota) and exported these volumes as .TIF stacks for object segmentation.

Object manipulation and segmentation was performed using Avizo 9.4.0 (FEI Company, Hillsboro, Oregon). All specimens were resampled to a common resolution of 40 μm except for *Phloeomys* and *Crateromys* specimens, which were resampled to 120 μm due to their large size. When necessary, scans of the left forelimb were mirrored to maintain a common orientation for all specimens. The segmented humerus, radio-ulna, and manus were exported as .PLY surfaces for geometric morphometric analysis.

Geometric morphometric analysis of the humerus.

Specimens were read into *R* and digitized using the packages *geomorph* and *rgl* (Adams and Otárola-Castillo 2013, Adams et al. 2017, Adler et al. 2017, R Core Team 2018). In total, I collected 41 landmarks on each humerus based on a previous study of 3D geometric morphometric analysis of mammalian humeri (Milne et al. 2009), as well as independently-derived landmarks based on areas of shape variation of interest. I collected landmark data using the following protocol (Table 3.1, Figure 3.1): first, I recorded the positions of 17 fixed landmarks characterizing the outlines of the proximal and distal ends of the humerus. These landmarks were measured five times on each specimen to quantify intra-specimen measurement error. Second, I measured sliding semilandmarks along three curves. I digitized each curve using a series of fixed

landmarks, from which sliding landmarks were drawn along line segments tangent to each fixed landmark (Bookstein 1997). The first of these curves was located along the

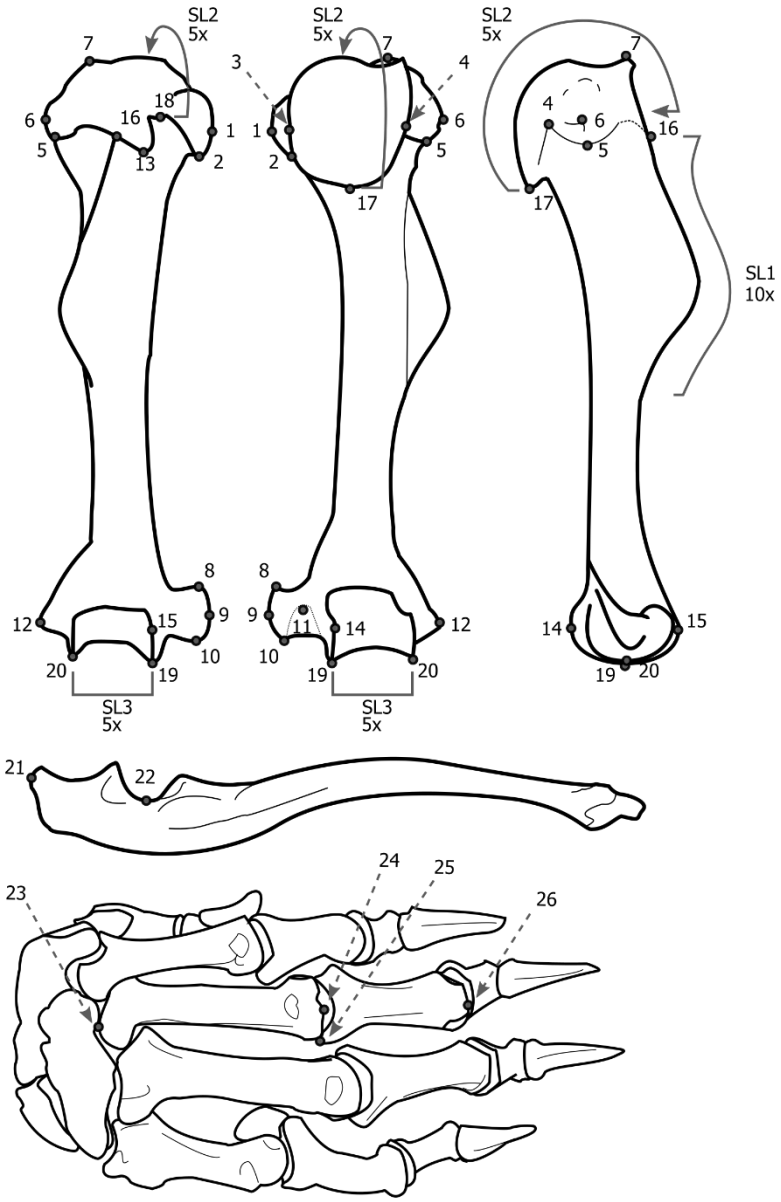

Figure 3.1. Landmarks taken on humerus, ulna, and manus of Luzon old endemic rodent species. Gray lines indicate semilandmark curves. See Table 3.1 for landmark definitions.

deltoid tuberosity and consisted of 30 fixed landmarks from which ten semilandmarks and two anchoring fixed landmarks were collected. The second curve was taken along the circumference of the head of the humerus and was composed of 20-25 fixed landmarks,

Table 3.1. Locations of fixed landmarks taken in geometric morphometric analysis. Lateral/medial descriptors are relative to the midline of the humerus, and proximal/distal descriptors are relative to the joint between the humerus and the scapula.

Landmark	Region	Description
1	Head	Lateral apex of lesser tubercle
2	Head	distal apex of lesser tubercle at suture with surgical neck
3	Head	Medioproximal joint between suture of head, lesser tubercle, and surgical neck
4	Head	Medioproximal joint between suture of head, greater tubercle, and surgical neck
5	Head	Distal apex of greater tubercle at suture with surgical neck
6	Head	Lateral apex of greater tubercle
7	Head	Proximal apex of greater tubercle
8	Distal terminus	Proximal apex of medial epicondyle
9	Distal terminus	Medial apex of medial epicondyle
10	Distal terminus	Distal apex of medial epicondyle
11	Distal terminus	Nadir of medial epicondylar sulcus on posterior face
12	Distal terminus	Lateral apex of lateral epicondyle
13	Head	Anterodistal apex of head of humerus at suture with surgical neck
14	Distal terminus	Posterior apex of medial edge of trochlea
15	Distal terminus	Anterior apex of medial edge of trochlea
16	Body	Intersection of deltoid tuberosity with suture at head of humerus (Anchor of SL curve 1)
End of SL curve 1	Body	Distal insertion of deltoid tuberosity on body of humerus at greatest concavity (Anchor of SL curve 1, landmark discarded)
17	Head	posterodistal apex of head of humerus at suture with surgical neck (Anchor of SL curve 2)
18	Head	Proximal apex of intertubercular groove (Anchor of SL curve 2)
19	Distal terminus	Distal apex of medial edge of trochlea
20	Distal terminus	Distal apex of lateral edge of trochlea (Anchor of SL curve 3)
21	Ulna	Distal apex of olecranon process
22	Ulna	Nadir of trochlear notch
23	Metacarpal 3	Proximal apex on radial side
24	Metacarpal 3	Distal apex
25	Proximal phalanx 3	Proximal apex on radial side
26	Proximal phalanx 3	Distal apex
SL curve 1	Body	Ridge of deltoid tuberosity
SL curve 2	Head	Circumference of articular surface of humerus head
SL curve 3	Distal terminus	Transect of articular surface of trochlea

depending on specimen size, and from which five sliding semilandmarks and two anchoring fixed landmarks were collected. Finally, I digitized 18 fixed landmarks along the width of the trochlea, from which I computed five sliding semilandmarks and two anchoring fixed landmarks. I retained the anchoring fixed landmarks on the ends of the deltoid tuberosity and humerus head curves in subsequent analyses. The resulting humerus dataset contained 21 fixed landmarks and 20 semilandmarks. The landmark configurations for the 17 fixed landmarks were then averaged across the five collection bouts per individual and combined with the semilandmarks and fixed landmark anchors of semilandmark curves.

Preliminary exploratory data analysis indicated that the fixed landmark at the distal end of the deltoid tuberosity, which formed an anchor for sliding semilandmark curve 1, displayed substantially greater variation than all other landmarks in the dataset, which I suspect is due to difficulty of locating its position rather than real differences among specimens. Because this landmark constituted one of the fixed landmark anchors for the deltoid tuberosity sliding semilandmark curve, I did not want to remove the landmark entirely. As a compromise, I retained the landmark as an anchor for computing the sliding semilandmarks but removed it after the curve was generated. During the Procrustes superimposition step, I instead constrained the final sliding semilandmark in this curve to slide along a line segment with fixed landmark 12, which was an easily-characterized fixed landmark. The resulting configurations exhibit semilandmarks that maintain positions along the deltoid tuberosity without introducing considerable measurement error due to difficulty with quantifying the end of the structure.

The configurations of 40 landmarks were transformed using a generalized Procrustes analysis to remove differences among specimens due to isometric scaling, rotation, and translation (GPA; Gower 1975, Rohlf and Slice 1990). I retained log-transformed centroid size, or the average distance between a specimen's landmarks and the center of the shape relative to the mean shape, as a measure of humerus size. I analyzed the superimposed specimens using a principal component analysis (PCA) to visualize the shape variation in the dataset.

Linear morphometric analysis of the distal forelimb

In addition to collecting landmarks on the humerus, I also collected two landmarks on the ulna, to capture length of the olecranon process, and four on the manus, to quantify relative length of the third metacarpal and proximal phalanx. I chose these measurements as several previous studies have indicated that they are useful for discriminating mammals, including rodents, according to locomotory niches (Samuels and Van Valkenburgh 2008, Milne et al 2009, Nations et al. in review). As with the fixed landmarks on the humerus, these landmarks were digitized five times to quantify variation due to measurement error. I calculated the distances between landmarks 21 and 22 on the ulna (corresponding to olecranon length), 23 and 24 (corresponding to digit 3 metacarpal length), and 25 and 26 (corresponding to digit 3 phalanx 1 length; Figure 3.1) and calculated the ratio between phalanx and metacarpal length. I then regressed these linear measurements against log-transformed humerus length, calculated as the distance between landmarks 7 and 19, after re-centering along the LOE phylogenetic mean using

the maximum clade credibility (MCC) tree from Rowsey et al. (2018) (Phylogenetic size correction; Revell 2009). This MCC tree was pruned to include only the focal species in the dataset. These size-regressed residuals thus describe morphological variation while minimizing covariation due to isometric scaling and shared common ancestry.

Locomotory category assignment.

We used a combination of species descriptions, field survey trap success data, and natural history accounts to categorize species based on their locomotory preferences (Heaney et al. 1999, 2016a; Balete et al. 2011, 2013, 2015; Alviola et al. 2011; Duya et al. 2011; Rickart et al. 2011, 2016.) I used five categories: arboreal, terrestrial, semi-fossorial, scansorial (arboreal preference), and scansorial (terrestrial preference), which approximate what is likely continuous variation in locomotory strategy in these rodents. I coded species that exhibited non-significant differences between trap success on the ground and in trees as scansorial, with a habitat preference based on which trapping type was more successful. For example, in a field survey conducted in the Central Cordillera of Luzon, *Batomys granti* was trapped 12 times on the ground surface and twice above ground, yielding a trap site frequency within the expected distribution of no preference ($p = 0.138$; Rickart et al. 2016). I thus coded this species as scansorial with a terrestrial preference.

Testing the correlation among morphometric and ecological variables.

We used the Bayesian time-calibrated phylogenetic tree from Rowsey et al. (2018) to account for shared evolutionary history in the shape data (Figure 3.2). Previous authors have demonstrated concerns with analyzing high-dimensional multivariate data using univariate methods, especially if these methods rely on estimating the evolutionary covariance matrix (Uyeda et al. 2015, Adams and Collyer 2018). To avoid elevated Type I error stemming from estimating parameter-rich multivariate evolutionary models, I constructed the hypothesis tests to use multivariate algebraic generalizations of existing phylogenetic comparative methods.

We tested whether locomotory strategy predicted the morphometric data by constructing two linear models with locomotory strategy as a categorical predictor variable and either humerus shape or distal forelimb measurements as the response variable. I also tested the continuous predictor of relative olecranon length and digit ratios against the response variable of humerus shape to determine whether the continuous variation in distal forelimb measurements had greater power to predict humerus shape than categorical locomotory variables. I then performed a Procrustes phylogenetic ANOVA, which regresses multivariate distances among species' morphology (as the response variables) against predictor variables transformed according to a Brownian Motion process obtained from the phylogenetic tree (Adams 2014b).

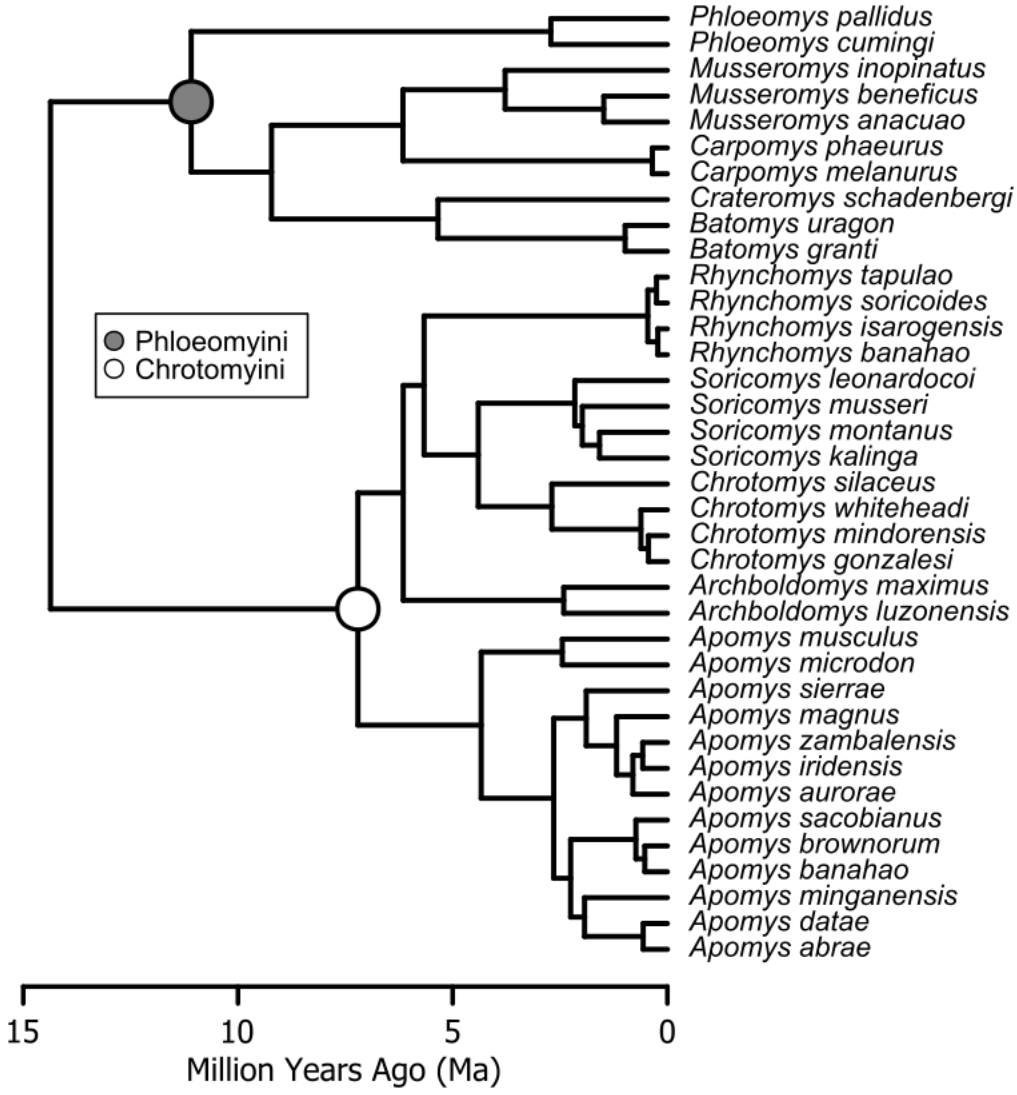

Figure 3.2. Chronogram of LOE rodent relationships used for this study, adapted from the Bayesian Maximum Clade Credibility (MCC) tree inferred by Rowsey et al. (2018).

Effect sizes were determined by permuting morphological data relative to tips in the tree and comparing the observed statistics to statistics generated by adding residuals of the permuted "null" model to fitted values (randomized residual permutation procedure; Collyer et al. 2015). I also used model fitted values and residuals to compare the fit of the

locomotory strategy predictors to the morphometric data. I performed a PCA on model fit and residuals to examine how the variance explained and unexplained by the model was partitioned and to determine what aspects of morphometric variation were best predicted by the model.

Testing the phylogenetic structure of forelimb variation.

The Procrustes distance phylogenetic ANOVA I used to predict humerus shape and distal forelimb proportions assumes that the traits in question evolved according to a constant-rate model of evolution parameterizing variance proportional to time since common ancestry (Brownian Motion: Felsenstein 1987). Modeling trait evolution in this way is necessary to account for correlation between traits that may be indistinguishable from differences in common ancestry. In the case of my analyses, locomotory category may be sufficiently phylogenetically structured such that any correlation with humerus shape or distal forelimb proportions cannot be disentangled from this structure. To test this, I compared the results of the *F*-tests from the phylogenetic Procrustes ANOVA with those from a phylogenetically-naïve permutational MANOVA (nonparametric MANOVA; Anderson 2001) performed using the function *adonis* in the *R* package *vegan* (Jari Oksanen et al. 2018). Recovering a significant predictive value of these input variables from the phylogenetically-naïve MANOVA but not the Procrustes ANOVA would indicate that the variation among LOE rodent forelimbs exhibits insufficient power to detect locomotory shape variation independent from shared common ancestry, thus the predictive value of these variables could be explained simply by phylogenetic correlation.

The Brownian Motion assumption of increasing variance among species as time since common ancestry increases may also not adequately predict shape evolution in the LOE clades. I tested this assumption of whether the variation in the phylogenetic Procrustes ANOVA was phylogenetically clustered even after BM transformation by determining the covariance between patristic distances among tips in the tree and Euclidean distances among residuals from each of the three model fits. These average covariances were compared to distributions of 10000 covariances generated by permuting residuals with respect to tips on the tree. Recovering a covariance between patristic distances and Euclidean distances of residuals for each species greater in magnitude than 5% of the null distribution (or greater in absolute value than 2.5% of one of the tails) would suggest that a Brownian Motion model of evolution, which is used to generate the model coefficients, does not adequately account for distinct responses to similar states in predictor variables. If this covariance is significantly positive, a model parameterizing multiple selective optima, such as an Ornstein-Uhlenbeck model (Butler and King 2004), would provide a better fit for the morphometric data. If this covariance is negative, a model parameterizing repeated convergence and continuous disruptive selection would provide a better fit for these data.

Results

Variation in humerus shape.

The first three principal component axes of humerus shape variation account for 45.2%, 14.6%, and 9.77% of shape variance respectively. The first four component axes comprise over 75% of the dataset variance, but the first 17 component axes are necessary

to account for at least 95% of the dataset variance. PC1 describes the relative sizes of the head and distal terminus to the humerus body (robustness). Positively-loading species tend to have large heads and capitula and distally elongated deltoid tuberosities compared to negatively-loading species (Figure 3.3A). PC2 describes the proximal concavity and distal elongation of the deltoid tuberosity as well as aspects of humerus head length; positively-loading species on this axis tend to have long heads and convex, posteriorly-compressed deltoid tuberosities (Figure 3.3A). PC3 primarily describes the sigmoidality and mediolateral projection of the deltoid tuberosity, with positively-loading species exhibiting large, sigmoidal, laterally-projecting deltoid tuberosities.

These component axes do not appear to univariately or multivariately discriminate among locomotory types. Average deviations from the mean shape based on locomotory type are subtle, especially for the scansorial and terrestrial categories, but arboreal species tend to have slightly less sigmoidal deltoid tuberosities and semifossorial rodents tend to exhibit a slightly more robust humerus than the average shape (Appendix Figure 3.2). Instead, humerus shape illustrates divergent adaptations toward similar strategies (Appendix Figure 3.3). Notably, *Rhynchomys* exhibits exceptionally robust humeri, conferring substantial muscle attachment sites for the insertion of forearm flexor and extensor muscles such as the deltoid, epitrochlearis, and anconeus muscles, despite available evidence suggesting *Rhynchomys* forages among leaf litter, rather than underground, for food (Balete et al. 2007). Along PC1 and PC3, humerus shape appears clustered within genera, with a notable exception being the two species of *Archboldomys* along PC1. However, along PC2, little apparent clustering occurs with respect to either

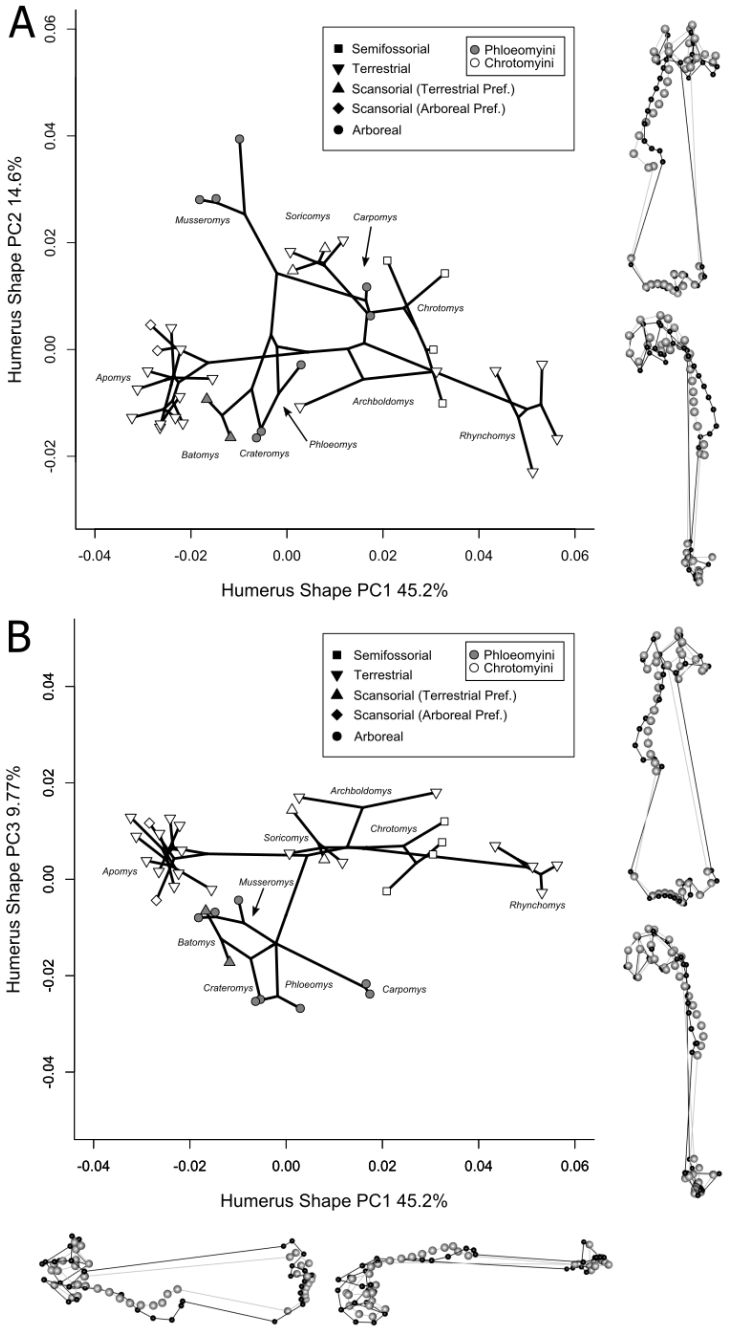

Figure 3.3. Phylomorphospace of principal components 1 and 2 (A) and 1 and 3 (B) of species-averaged humerus shape data. Values for species averages are represented with filled circles, while branches indicate phylogenetic relationships among species. Margins of figure illustrate changes in humerus shape necessary to produce positively-loading (black spheres) and negatively-loading (gray spheres) species. Shape changes are shown in anterior (left, top) and lateral (bottom, right) views.

locomotory type or phylogenetic affinity. Interestingly, PC3 is a univariate discriminator between Phloeomyini and Chrotomyini: apart from *Apomys microdon* compared to *Musseromys inopinatus*, all chrotomyines exhibit more sigmoidal, laterally-projecting deltoid tuberosities than Phloeomyini (Figure 3.3B).

Variation in distal forelimb proportions.

A bivariate plot of phylogenetically size-corrected residuals of olecranon length and digit ratios illustrates some of the discriminatory power of these variables (Figure 3.4). Relative olecranon length qualitatively discriminates semifossorial species, such as *Chrotomys*, and terrestrial species, such as *Apomys* (subgenus *Megapomys*) from scansorial and arboreal species such as *Apomys* (subgenus *Apomys*) and *Musseromys*, and digit ratios appear to discriminate arboreal species from scansorial, terrestrial, and semifossorial species. However, there is clear partitioning of these data with respect to LOE clade membership: of the locomotory types that span both clades (i.e. scansorial in the broad sense), the constituent species exhibit distal forelimb variation consistently similar to other members of their colonizing clade that have different locomotory modes. This may imply that scansorial locomotion is feasible with limited adaptive change from a more specialized locomotory form. Apart from scansoriality, within-clade-and-guild distal forelimb variation appears low compared to among-guild or among-clade locomotory variation.

Testing the correlation among morphometric and ecological variables.

Phylogenetic Procrustes distance ANOVA recovered a non-significant correlation between categorical locomotory variables and both humerus shape as well as distal forelimb measurements. Model fit of ulna and manus measurements exhibited a greater, but still non-significant, relationship with categorical locomotory type than did humerus shape. However, Procrustes ANOVA of distal forelimb proportions yielded a significant correlation with humerus shape, with about 15 percent of humerus shape being explained by variation in digit ratios and about 5 percent of humerus shape being explainable by variation in relative olecranon length (Table 3.2).

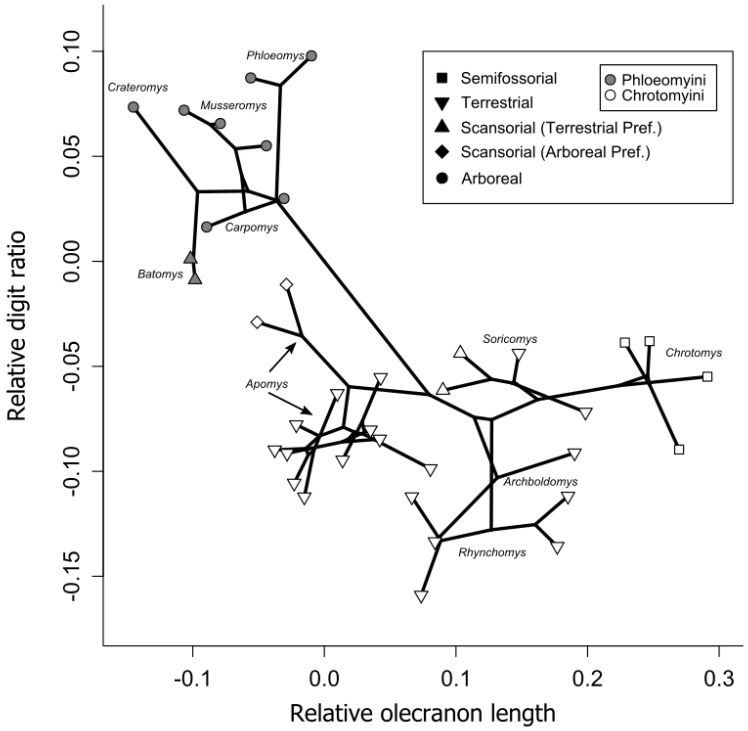

Figure 3.4. Phylomorphospace of relationship between relative olecranon length and ratio proximal phalanx 3 length to metacarpal 3 length. Both variables were previously scaled by humerus length and time since common ancestry. Tips and branches are indicated as in Figure 3.3.

Table 3.2. Summary of Procrustes distance phylogenetic ANOVA on forelimb morphometrics and locomotory category. Model definitions are given in the form response ~ predictors. Predictors demonstrating statistically significant (at critical value $\alpha = 0.05$) correlations with response variable have asterisked *p*-values. Total degrees of freedom for all models: 36.

Model	Predictor	*D.f.*	Sum of Squares	R^2	*F*-score	*Z*-score	*P*-value
Humerus ~ locomotory category	Locomotory category	4	5.93×10^{-4}	0.0329	0.272	-4.23	1.00
Distal forelimb proportions ~ locomotory category	Locomotory category	4	0.0133	0.183	1.79	1.21	0.103
Humerus ~ olecranon length + digit ratio	Olecranon length	1	9.44×10^{-4}	0.0523	2.24	2.86	1.50×10^{-3}*
Humerus ~ olecranon length + digit ratio	Digit ratio	1	0.277×10^{-3}	0.153	6.57	4.52	1.00×10^{-4}*

Figure 3.5 illustrates the principal axes of model fitted values (left column) and model residuals (right column) for each of the three different models (rows), allowing me to see how each model was fit and areas where the model falls short in describing the dataset variation. If the humerus shape strongly reflects locomotory strategy after accounting for shared common ancestry of trait values, one can expect the model fitted values will exhibit discrimination among different locomotory categories and residual errors should be distributed without respect to phylogenetic relationships or locomotory categories (effectively random scatter). The model fit estimate for locomotory type on humerus shape discriminated primarily among within-LOE-clade locomotory category variation, with the first principal axis of the linear model fitting variation primarily within Chorotmyini, and the second axis discriminating between arboreal species and the remaining categories (Figure 3.5A). The residuals for this model appear to be

phylogenetically clustered and appear remarkably similar in overall form to a PCA of raw shape variables: The primary axis of model residuals consisted of two chrotomyine genera within a single locomotory category rather than randomly distributed residuals irrespective of phylogenetic relationships. This result illustrates that these two genera have considerably different humerus shapes from one another despite occupying the same locomotory category and that species within these genera are very similar to one another. A similar pattern occurs along PC2 of model residuals, where the arboreal genera *Phloeomys* and *Crateromys* exhibit distinct shapes from *Musseromys*. With the exception of *Apomys* (*Apomys*) and *Chrotomys*, the remaining species' residuals are oriented similarly to PC1 and PC2 of the shape data (Figure 3.5B). This pattern suggests that categorical locomotory type does a relatively poor job of explaining the principal axes of variation in humerus shape in a phylogenetic context.

For the model of distal forelimb measurements regressed against locomotory category, the model fit displays differences on a continuum of fossoriality to arboreality, with terrestrial and scansorial species intermediate on PC1 of model fit values (Figure 3.5C). Model residuals were much more scattered with respect to phylogenetic relationships, rather than clustered within genera and variable across species with different locomotory categories. This result suggests that distal forelimb proportions among genera with similar locomotory categories varied less than with humerus shape.

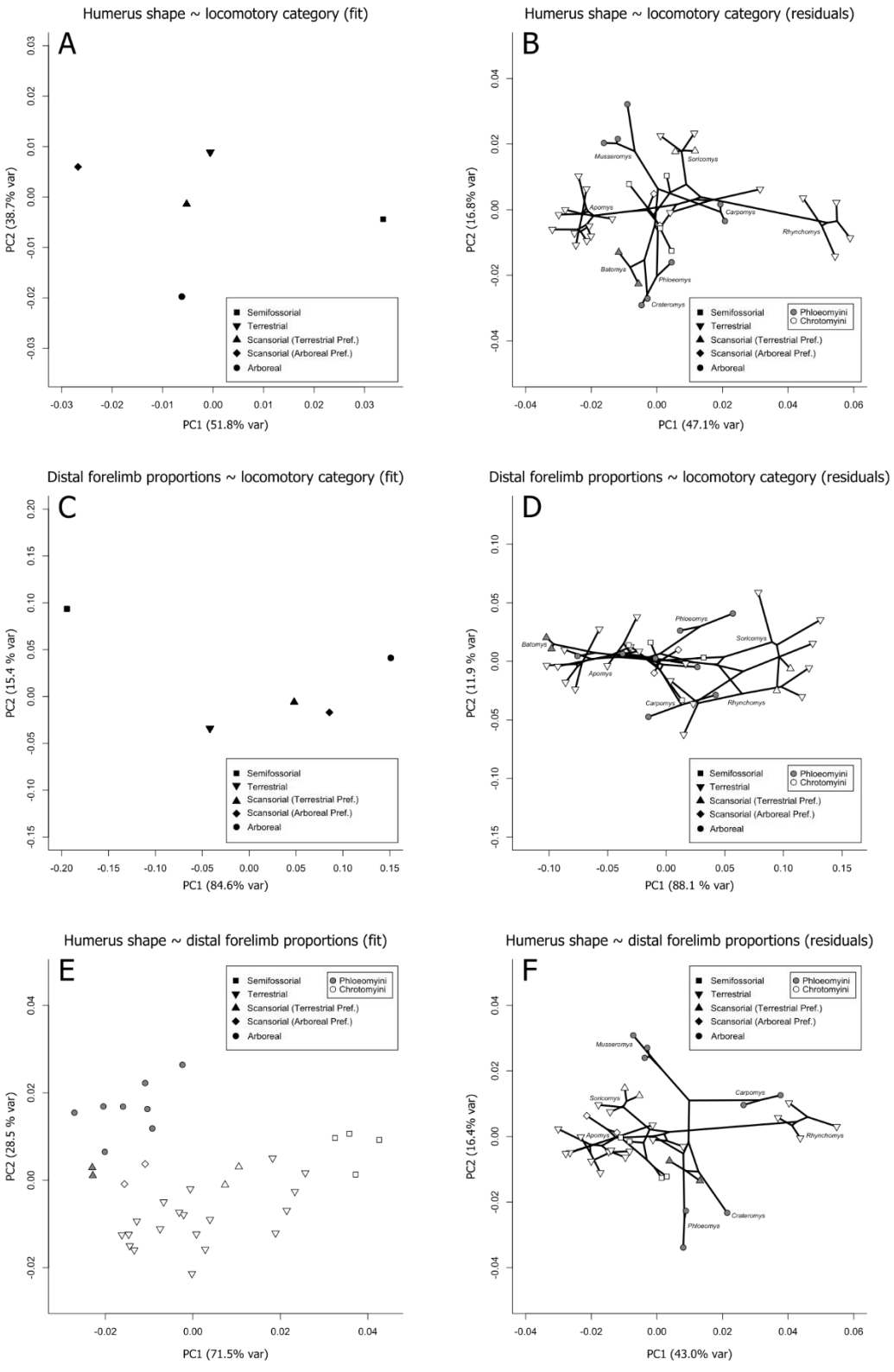
Humerus shape ~ locomotory category (fit)
A
PC2 (38.7% var)
PC1 (51.8% var)
Humerus shape ~ locomotory category (residuals)
B
PC2 (16.8% var)
PC1 (47.1% var)
Musseromys
Soricomys
Apomys
Carpomys
Rhynchomys
Batomys
Phloeomys
Crateromys
Distal forelimb proportions ~ locomotory category (fit)
C
PC2 (15.4 % var)
PC1 (84.6% var)
Distal forelimb proportions ~ locomotory category (residuals)
D
PC2 (11.9 % var)
PC1 (88.1 % var)
Humerus shape ~ distal forelimb proportions (fit)
E
PC2 (28.5 % var)
PC1 (71.5% var)
Humerus shape ~ distal forelimb proportions (residuals)
F
PC2 (16.4% var)
PC1 (43.0% var)
Semifossorial
Terrestrial
Scansorial (Terrestrial Pref.)
Scansorial (Arboreal Pref.)
Arboreal
Phloeomyini
Chrotomyini

Figure 3.5 (Previous). Principal component scores of model fit values (A, C, E) and model residuals (B, D, F) for the three linear models performed. A, B: linear model of humerus shape as a response to locomotory category; C, D: linear model of distal forelimb proportions (i.e. relative olecranon length and digit ratios) as a response to locomotory category; E, F: linear model of humerus shape as a response to distal forelimb proportions. Tips and branches are indicated as in figure 3.3. Genera with distinctive residual scores are labeled near the ancestral node for that genus.

Nevertheless, within-category variation was still the primary component axis of residual variance, with several *Apomys* (*Megapomys*) and two *Rhynchomys* species exhibiting substantial residual variance from one another in the terrestrial category, and the two genera containing terrestrial-biased scansorial rodents occurring on opposite ends of PC1 of residuals (Figure 3.5D).

The model fit of humerus shape regressed against distal forelimb measurements exhibited separation between semifossorial rodents and all other locomotory categories along PC1, and primarily colonizing-clade-based discrimination along PC2 (including separation between rodents categorized as clade-specific groups defined as terrestrial and arboreal). Interestingly, model fitted values for scansorial species with terrestrial preference, the single category occupied by both Phloeomyini and Chrotomyini, did not cluster together, instead resembling their closest relatives. By contrast, arboreal-biased scansorial rodents were situated intermediate to arboreal rodents and their closest relatives, which were categorized as terrestrial (Figure 3.5E). Residuals of this model fit appear to exhibit phylogenetic clustering to a lesser degree than in the model of humerus shape regressed against locomotory type but the general pattern of residual clustering along PC1 and PC2 was similar to that of humerus shape on locomotory category: PC1 of these residuals illustrated *Rhynchomys* as distinct from all other chrotomyines, while *Carpomys* and, to a lesser extent, *Musseromys*, were distinct from the remaining

phloeomyine lineages. PC2 illustrated overlap among all chrotomyines but clustering among all phloeomyine genera apart from *Phloeomys* and *Crateromys* (Figure 3.5F).

Table 3.3. Summary of non-parametric MANOVA on forelimb morphometrics and locomotory category. Model definitions are given in the form response ~ predictors. Predictors demonstrating statistically significant (at critical value $\alpha = 0.05$) correlations with response variable have asterisked *p*-values. Total degrees of freedom for all models: 36.

Model	Predictor	*D.f.*	Sum of Squares	R^2	*F*-score	*Z*-score	*P*-value
Humerus ~ locomotory category	Locomotory category	4	0.0123	0.219	2.24	2.47	6.70×10^{-3}*
Distal forelimb proportions ~ locomotory category	Locomotory category	4	0.462	0.703	18.9	3.72	1.00×10^{-4}*
Humerus ~ olecranon length + digit ratio	Olecranon length	1	0.0126	0.224	11.1	3.72	1.50×10^{-3}*
Humerus ~ olecranon length + digit ratio	Digit ratio	1	5.26×10^{-3}	0.0932	4.64	2.70	1.00×10^{-4}*

Testing the phylogenetic structure of forelimb variation.

Non-parametric, phylogenetically naïve MANOVA yielded significant correlations between all predictor variables and all response variables for all three models (Table 3.3). The relatively high correlations between the variables of interest in these analyses suggest that the lack of significant correlation between locomotory category and morphometric variables in the phylogenetically-informed ANOVA stems more from a lack of power due to underlying correlation between common ancestry and locomotory category than inability to predict forelimb morphology from locomotory type. I also recovered significant positive covariances between residuals of humerus shape and both locomotory category (marginal support: $p = 0.0474$) and distal forelimb proportions

(strong support: $p = 4.10 \times 10^{-3}$) in the Procrustes distance phylogenetic ANOVA (Table 3.4). These significantly positive covariances illustrate that the differences in deviations from the model fit are proportional to the time since common ancestry of the species in question.

Table 3.4. Statistics comparing observed covariance between patristic and Euclidean distances among model fit residuals for each LOE species. Model definitions are given in the form response ~ predictors. Statistically significant (at critical value $\alpha = 0.05$) covariances have asterisked *p*-values.

Model Residuals	cov_{obs}	Mean cov_{perm}	$SD\ cov_{perm}$	*P*-value
Humerus ~ locomotory category	0.0244	4.64×10^{-5}	0.0129	0.0474*
Distal forelimb proportions ~ locomotory category	0.0279	3.36×10^{-4}	0.0356	0.203
Humerus ~ olecranon length + digit ratio	0.0347	8.56×10^{-5}	0.0110	4.10×10^{-3}*

Discussion

Our study sought to examine the ecological and phylogenetic partitioning of morphological variation of the forelimb in the two LOE clades to determine whether humerus shape varies in response to habitat use and locomotory strategy in a similar way to distal forelimb morphology in subfamily-related clades. My results suggest a complex relationship between humerus shape, phylogeny, and ecological variables. The principal axes of LOE humerus shape indicate that some aspects of its variation are partitioned by genus (PC1) and by colonizing clade (PC3), whereas other aspects are distributed without respect to phylogenetic relationships (PC2; Figure 3.3). Two simple linear metrics of distal forelimb shape, by contrast, provided reasonable discrimination between both colonizing clade membership and, to a lesser extent, locomotory category (Figure 3.4). The two genera in the single locomotory category that bridged clade membership,

Batomys in Phloeomyini and *Soricomys* in Chrotomyini, were dissimilar in terms of these measurements, however, instead resembling other members in their own colonizing clade (Figure 3.4; Appendix Figure 3.2).

Our linear models illustrate the two clades exhibit relatively distinct humerus morphology. In other words, phylogenetic relationships strongly influence locomotory mode in predicting both humerus shape and distal forelimb proportions, with no truly arboreal chrotomyines and no semifossorial or truly terrestrial phloeomyines. The significant correlation between both sets of morphometric data and locomotory type when shared common ancestry is not considered indicates that the limited convergence in locomotory strategy among LOE rodent clades limits the power to infer a relationship with humerus shape. The fact that all phloeomyines exhibit some degree of climbing behavior, whereas chrotomyines are much more variable in terms of locomotory strategy, begs the question of whether this variation is the result of different evolutionary modes in either clade, or whether the between-clade disparity in locomotory diversity is the result of inter-clade competitive effects, as has been suggested in terms of patterns of dietary diversity for these rodents (Rowsey et al. 2019).

The residual variation in the linear models illustrates species in different genera with similar forelimb proportions, such as *Apomys* and *Rhynchomys*, have exhibited parallel evolution of distinct humerus shapes (Figure 3.5B). The distinct humerus shapes corresponding to similar model fit values, as visualized by the distribution of species with similar locomotory categories in Figure 3.5, suggest that LOE humerus shape is not the result of a constant homogeneous evolutionary process. More specifically, this pattern

suggests species in each genus are more clustered than expected by the Brownian Motion model of trait evolution used to transform the predictor and response variables. This pattern illustrates that the humerus shape variation in this clade is more likely the result of an evolutionary process in which different genera with the same locomotory category evolved under discrete selective optima or that humerus evolutionary rate has decelerated over time, such that early, genus-level, changes in morphology are greater than more recent, species-level changes (Table 3.4). In either case, this process suggests ecological evolution is decoupled from that of morphological change. This finding contrasts with those of Rowsey et al. (2019), who examined rates and patterns of mandible variation (as a proxy for diet). Whereas the previous study illustrated that shape variation was the result of a single, constant rate process with a discrete shift in mode on the branch leading to *Rhynchomys*, my present analysis suggests the evolution of humerus shape is either the result of multiple selective optima within most of the locomotory categories or that these categories are oversimplified.

The phylogenetic clustering within genera exhibiting a similar locomotory type may be due to distinct humerus shapes performing equally well to accomplish their locomotory tasks, which has the potential to promote phenotypic evolution with limited functional correlation (many-to-one mapping: Wainwright et al. 2005). This decoupling of phenotypic variation from ecological function promotes continuous variation in traits consistent with a comparatively broad, flat biomechanical landscape compared to one-to-one mapped traits and limits the ability to infer function from the trait in question, meaning that trait values can vary freely along a continuum (Alfaro et al. 2005;

Thompson et al. 2017). While the parallel evolution within locomotory categories is reminiscent of many-to-one mapping of humerus shape on locomotory category, I note that the patterns of shape variation unexplained by locomotory differences are partitioned in genus-defined bins rather than along a continuum in the LOE rodents. This pattern is reminiscent of the "quantum evolution" hypothesis proposed by Simpson (1953) where lineages diversify via strong directional selection to occupy multiple "adaptive zones". In the case of the LOE rodents, the intervening gaps in shape space that would generate a continuous pattern of phenotypic variation may be maladaptive due to comparative inefficiencies in locomotion, uncaptured correlates with humerus shape, or both.

An implication of many-to-one mapping is that the traits are relatively free to vary along other functional axes and the optimization of all traits is what determines the distribution of species in morphospace. These functional axes may correspond to fine-scale differences in locomotory strategy uncaptured by the predictor variables, including proportion of bipedal movement and differences in substrate, both of which have been shown to confer differences in humerus length and deltoid tuberosity position in Heteromyid rodents (Price 1993). Interestingly, Price's study, which examined functional morphology in a clade of rodents that vary in the degree of digging, type of substrate, and bipedal versus quadrupedal locomotion used, found that a shift to a mode of bipedal locomotion was associated with significant changes in scapular and humerus dimensions, but not distal forelimb dimensions, suggesting variation in bipedal locomotion may be a mechanism for functional decoupling of these elements.

A caveat of my approach for classifying locomotory niche is that it assumes trapping success rates accurately reflect the locomotory type of the species in question. This assumption is problematic for rare or difficult-to-sample species where, for example, an incidental ground-trapping event constitutes a significant proportion of the total trapping events for a species which spends very little time on the ground. Furthermore, this categorization approach discretizes what is likely continuous variation in habitat use and introduces a component of arbitrary classification into the analysis. These challenges necessitate finding variables that approximate this continuous variation in locomotory strategy in a group with a large diversity of species and locomotory adaptations such as Murinae. My thorough morphometric sampling of two groups of ecologically diverse species in this subfamily shows that the humerus exhibits correlated variation with measurements previously reported to be useful in discriminating niche among phylogenetically diverse groups of rodents, even when accounting for nonindependence of trait values due to shared phylogenetic relationships. I speculate that a broadened sampling scheme with multiple independent transitions among the locomotory categories defined in my dataset would be a logical extension of my work comparing the relative importance of phylogenetic relatedness and ecological adaptation in determining humerus shape.

Conclusions

Our end goal of being able to use humerus shape to approximate continuous variation in locomotory strategy as a complement to or substitute for distal forelimb proportions was partially satisfied. I recovered a significant correlation between these two

morphometric variables, but this correlation notwithstanding, a large component of humerus shape still covaries with time since common ancestry, which contrasts with distal forelimb proportions. My work shows that at this intermediate phylogenetic scale (i.e. including multiple within-subfamily clades), mammalian humerus diversity lies at the intersection of shared common ancestry and adaptation to ecological niches. Whereas humerus shape is perhaps less useful on its own to predict locomotory niche compared to distal forelimb measurements, inclusion of all structures will facilitate a more thorough examination of the factors that contribute to locomotory change. I thus conclude that complex structures, such as the humerus, may exhibit distinct states that confer similar utility, resulting in an apparent breakdown between structure and function when independent transitions to a similar mode are prevalent. Analyses of forelimb evolution should thus include all podial elements to target both the ecological and evolutionary components of variation. Adherence to this strategy in comparative analyses will undoubtedly provide more powerful inferences about ecological diversity is generated and maintained over time.

CHAPTER 4. TROPHIC MORPHOLOGY OF TWO ISLAND ENDEMIC MURINE RODENT CLADES IS CONSISTENT WITH PERSISTENT, INCUMBENT-IMPOSED COMPETITIVE INTERACTIONS

Introduction

In classic examples of adaptive radiation, a single lineage diversifies over time to occupy an array of novel niches, resulting in a group of ecologically and phenotypically distinct species (Rabosky and Lovette 2008; Burbrink and Pyron 2010; Reddy et al. 2012). In such cases, phenotypic diversification is facilitated by adaptive evolution into unoccupied niche space. However, the diversification dynamics that occur when two or more, independent but ecologically similar lineages colonize the same system at different times is not well understood. In this case, primary colonists (the incumbent clade) may prevent phenotypically similar species from invading the system, suggesting that only lineages that are sufficiently distinct from the primary colonists can invade and diversify (Gillespie 2004; Urban and De Meester 2009). This process of biotic filtering could enhance the overall ecological diversity of the system, while at the same time limiting the potential phenotypic diversity attained by secondary colonists. In other words, an incumbent clade may prevent secondary colonists from realizing otherwise attainable phenotypic diversity (Jønsson et al. 2015).

Testing whether incumbent lineages have such filtering and dampening effects on the diversity of subsequent colonists is best accomplished in systems that meet certain rare requirements. First, the colonizing lineages should be ecologically similar enough

that one could reasonably act as a biotic filter for the other. This requirement is most likely to be met by closely related lineages that colonize a system over a relatively short time span, because phylogenetic inertia tends to result in two lineages that resemble one another more than they do distantly related species (Felsenstein 1985; Wiens and Graham 2005; Orzack and Sober 2010). Second, there should be some way to assess the potential phenotypic diversity that these lineages could attain were they to diversify apart from one another. Assessing the potential phenotypic diversity of any clade is a daunting challenge, and it is important to disentangle any intrinsic constraints on the "evolvability" of a clade from external forces of interest, such as competition, that could limit the evolution of otherwise attainable phenotypes (Derrickson and Ricklefs 1988). One way to meet this requirement is to examine diversification of a large clade, part of which is evolving in the presence of potentially competing lineages and part of which is not. Island archipelagoes, which bring together novel assemblages of organisms through different patterns of dispersal and colonization success (Losos et al. 1998; Gillespie 2004) provide one such promising arena for investigation.

The murine rodents (rats and mice) of the Philippines and associated Southeast Asian islands provide a unique opportunity to examine the impact that incumbent lineages have on diversification of later colonists. Notably, Luzon Island – the largest island of the Philippines – has been colonized by murine rodents at least five times (Jansa et al. 2006; Rowsey et al. 2018).The earliest two colonizations occurred approximately 12.8 and 8.4 Ma, respectively, and each has resulted in a phenotypically diverse radiation of species that together are referred to as the Luzon Old Endemics. The first colonization

— known as Phloeomyini (*sensu* Lecompte et al. 2008)— likely invaded Luzon from mainland Asia and appears to be the sister group to the *Mus-Rattus* division of rodents, which contains the bulk of murine diversity (Schenk et al. 2013; Steppan and Schenk 2017; Rowsey et al. 2018). The second colonization — Chrotomyini (*sensu* Rowsey et al. 2018)— is the sister clade to a large group of murines that radiated throughout Australia, New Guinea, and Melanesia (Rowe et al. 2008; Smissen and Rowe 2018). This group – referred to here as the Sahul Old Endemics (SOE) — radiated in the absence of any other incumbent murine linages; in other words, they are the first murine colonists of the islands they inhabit. Therefore, this system seems to meet both requirements for investigating whether incumbent lineages can limit phenotypic diversification: the two Luzon Old Endemic clades are sufficiently closely related to be likely competitors, and the SOE radiation provides an opportunity to examine the diversity Chrotomyini might have achieved had they evolved in the absence of phloeomyine competitors. Prior research has shown that patterns of mandibular diversity may be more likely to exhibit signals of incumbency-influenced evolution than evolutionary rates: although Phloeomyini has not appeared to lower rates of lineage diversification or mandibular shape evolution for non-incumbent Chrotomyini, the two Luzon Old Endemic lineages are morphologically distinct from one another with respect to mandible morphology (Rowsey et al. 2018, 2019). Nevertheless, meaningful interpretation of this distinction requires comparison with the diversity of mandible morphologies attained by the Sahul Old Endemics.

Here, I analyze the trophic diversity of these lineages in a phylogenetic comparative framework to test whether the incumbent lineage on Luzon (Phloeomyini) has shaped initial and persistent phenotypic distinction of the secondary colonizing lineage (Chrotomyini) as compared to its sister taxon (the Sahul Old Endemics). I focus on mandible (lower jaw) shape as an ecologically relevant trait that correlates with food-processing strategy and has proven to be useful for delineating dietary differences among species (Grossnickle and Polly 2013; Verde Arregoitia et al. 2017). I then compare the trophic variation in the two sympatric clades to that of the two incumbent clades to determine whether the contemporary distribution of Chrotomyini forms a biased subset of hydromyine (Chrotomyini + SOE, *sensu* Lecompte et al. 2008) diversity to minimize overlap with incumbent Phloeomyini. Recovering a greater average difference between the two sympatric clades compared to the incumbent clades would suggest that the contemporary diversity of Chrotomyini has been constrained to limit overlap with Phloeomyini.

We then present a novel phylogeny describing hydromyine relationships and divergence times, which I use to infer a distribution of stem chrotomyine ancestral states. In this case, recovering a similar distance among contemporary differences between Chrotomyini and Phloeomyini to differences between Phloeomyini and stem ancestral Chrotomyini would suggest that the distinction between the two LOE clades has been persistent through time.

Materials and Methods

Taxon sampling.

Our molecular dataset consists of DNA sequence data obtained from several previous studies, with additional sequencing performed as needed. I obtained 15 tissue samples from the American Museum of Natural History (AMNH), the Field Museum of Natural History (FMNH), and the Australian National Wildlife Collection (ANWC) to supplement existing molecular sampling. In total, the molecular phylogeny contained 132 samples representing 131 species of Philippine (i.e. including Luzon) Old Endemic and Sahul Old Endemic rodents, including outgroup taxa and *Chiropodomys gliroides*, the sister lineage to Hydromyini (Chrotomyini + SOE).

Our morphometric dataset consisted of two components: LOE and SOE rodents. For the LOE rodents, I used the mandibular morphometric dataset containing 337 specimens representing 41 rodent species obtained in a previous study (Rowsey et al. 2019). This dataset included all described LOE rodent species and two undescribed species. The SOE rodent dataset consisted of 270 specimens representing 85 species for approximately 58 and 86 percent coverage of all currently described species and genera, respectively. These SOE specimens were obtained from the AMNH, FMNH, and the United States Museum of Natural History (USNM). As described in Rowsey et al. (2019), I aged specimens based on eruption and coplanarity of all upper molars and preferred specimens with completely fused basicrania. For the SOE rodents, I attempted to sample four individuals per species with an even sex distribution but relaxed this constraint when suitable specimens were limited. In total, the morphometric dataset

included 607 murine specimens. I photographed the buccal face of the right ramus when possible, but if this ramus was damaged, I used the left ramus and mirrored the resulting image.

Geometric morphometric analysis.

We used the geometric morphometric analytical procedure described by Rowsey et al. (2019) to collect and analyze morphometric data for the SOE rodents that mirrored that of the LOE rodents. I collected 12 fixed landmarks along the outline of the mandible using the R package *geomorph* v. 3.0.5 (Adams and Otárola-Castillo 2013, Adams et al. 2017, *R* Core Team 2018; Figure 4.1). In the cases where a specimen's mandible was damaged, I estimated the positions of missing landmarks using the thin-plate spline algorithm implemented in the estimate.missing function of *geomorph*, using other individuals of the same species as a reference when available or members of the same genus when conspecific specimens were unavailable (Gunz et al. 2009). The complete dataset of landmark configurations, including LOE landmark data, were subjected to a generalized Procrustes analysis (GPA; Gower 1975, Rohlf and Slice 1990) from which I also retained log-transformed centroid size, or the average distance between each landmark and the center of the landmark configuration, as a proxy for body size.

Testing contemporary ecological distinction.

To test whether the mandibular the patterns of LOE mandibular shape variation are consistent with incumbency effects preventing Chrotomyini from invading

phloeomyine-occupied areas of morphospace, I compared the overlap between Chrotomyini and Phloeomyini (sympatric clades) to Phloeomyini and the SOE rodents (incumbent clades). To do this, I first averaged both the GPA-transformed landmark configurations and centroid size by species and performed a PCA on the correlation matrix using these average values. I then calculated the median pairwise distance between the 29 species in Chrotomyini and 12 species in Phloeomyini. This distance was compared to a distribution of distances between Phloeomyini and 10,000 permuted samples of 29 SOE species values to determine whether the distance between the two sympatric clades was significantly greater than that of the two incumbent clades. I also performed this test excluding the chrotomyine genus *Rhynchomys*, which exhibits an extremely disparate morphotype from the remaining rodents in this study and may inflate distances between the two LOE clades. This method thus provides a test of the trait variation realizable by Chrotomyini in the absence of prior murine competition: I expect to recover a significantly larger distance between Chrotomyini and Phloeomyini if phloeomyine incumbency, rather than an inherited phenotypic constraint, could have been responsible for the observed mandibular variation in Chrotomyini, as the incumbent sister clade to Chrotomyini would be able to evolve morphotypes similar to both Phloeomyini and Chrotomyini.

DNA extraction and sequencing.

We performed DNA extractions using a Qiagen DNEasy blood and tissue extraction kit (QIAGEN, Germantown, MD). I sampled four nuclear genes for each

specimen: exon 10 of GHR (growth hormone receptor), exon 1 of IRBP (interphotoreceptor retinoid binding protein), and exon 11 of BRCA1 (breast cancer activating gene 1). I also sequenced the mitochondrial gene CYTB (Cytochrome *b*). I used PCR to amplify each gene using GoTaq Green Master Mix (Promega Corp, Madison, WI) I used a touchdown protocol to amplify GHR and CYTB (Jansa and Weksler 2004). BRCA1 was amplified in three distinct segments, as the locus is over 2,000 base pairs long. Appendix Table 4.1 lists all forward and reverse primers used for each locus. I then submitted amplicons produced from each PCR reaction into GENEWIZ (South Plainfield, NJ) for Sanger sequencing. The resultant reads were assembled in Geneious R7 (Biomatters Ltd., Auckland, NZ).

In addition to these newly-generated sequences, I obtained additional LOE and SOE DNA sequences from previously-sequenced specimens reported in prior studies and broadened the number of loci sampled. I included parts of exons 2 and 3 as well as the intervening intron of acid phosphatase 5 (ACP5), intron 7 of β-Fibrinogen (FGB7), and recombination activating gene (RAG1), all nuclear loci. Sequences of these seven loci from SOE and LOE rodents generated by previous studies (Steppan et al. 2005; Rowe et al. 2008, 2016; Bryant et al. 2011; Schenk et al. 2013; Bryant and Fuller 2014; Pagès et al. 2016; Smissen and Rowe 2018) were obtained from Genbank (Benson et al. 2012). Consensus sequences for each species and each locus were aligned using MUSCLE (Edgar 2004) and concatenated into a single nucleotide alignment. The alignment contained a total of 132 individuals with a maximum concatenated sequence length of 10,462 base pairs.

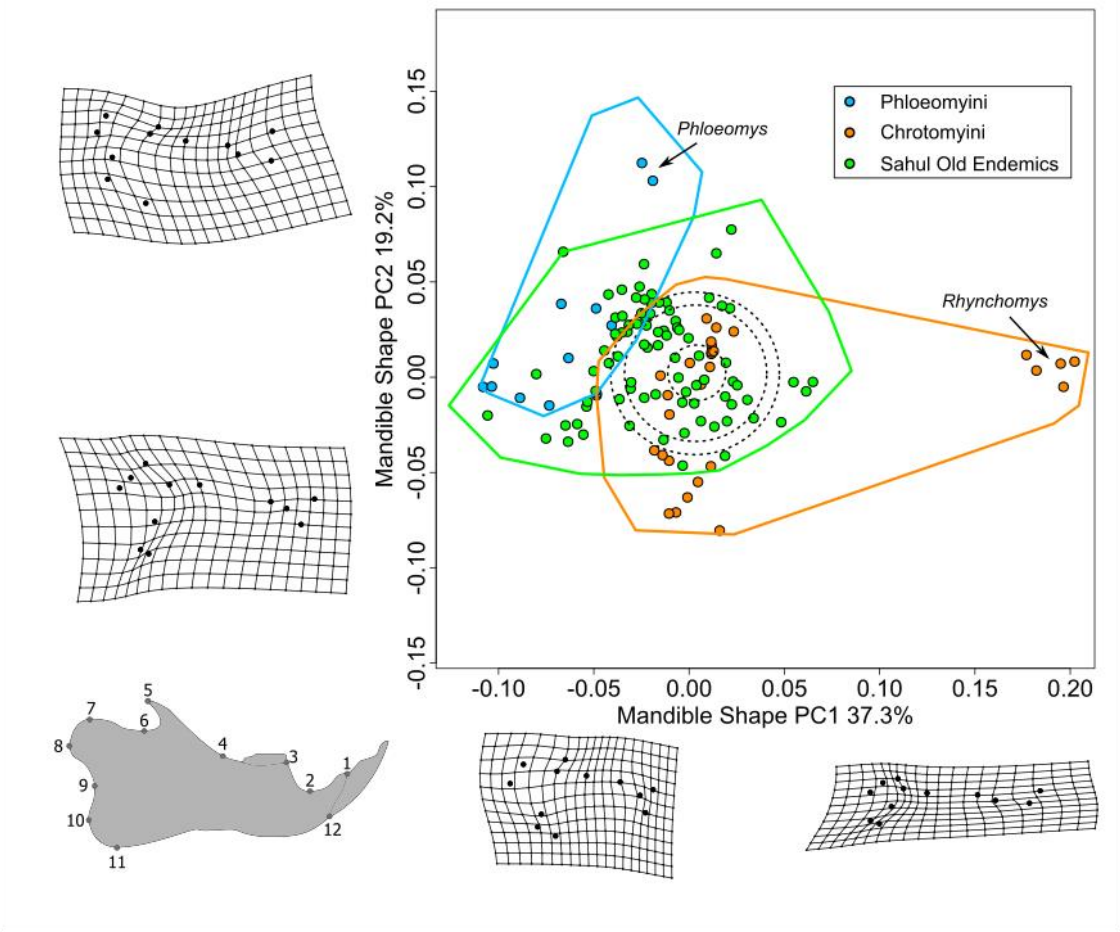

Figure 4.1. PC1 and PC2 of mandibular shape of LOE and SOE rodents, with SOE (green) projected onto the LOE component space. Opaque enclosed circles represent species averages. Convex hulls indicate the extremes of each clade's individual specimens. Dashed ellipses indicate posterior density intervals for estimated ancestral state of stem ancestor of Chrotomyini + SOE, with increasing radii representing 50%, 90%, and 95% highest posterior density respectively. Percentages on axis labels indicate LOE (*i.e.* excluding SOE) dataset variation explained by that axis. Thin-plate splines along axes show specimens with extreme scores and illustrate differences along these axes. Bottom-left: lateral view of a mandible indicating landmarks taken.

Phylogenetic inference.

We used PartitionFinder v2.1.1 (Lanfear et al. 2012) to determine the best-fitting scheme of nucleotide partitions and substitution models using the Bayesian Information Criterion (BIC; Schwarz 1978). I selected gene-level candidate partitions and specified

linked branch lengths among partitioning schemes and selected only substitution models that were supported by BEAST 2 (Bouckaert et al. 2014), choosing the best scheme using the "greedy" algorithm.

We specified separate lognormally-distributed relaxed molecular clock models for the mitochondrial and nuclear locus partitions, allowing nucleotide substitution rates to vary among branches while remaining constant within a branch (Drummond et al. 2006). I used secondary calibration points to date this phylogeny in absolute time by placing a normal prior on the crown ages of Phloeomyini and Chrotomyini based on the distribution of ages inferred by Rowsey et al. (Rowsey et al. 2018), the ages of which were dated themselves based on thoroughly-examined fossil data (Kimura et al. 2015). I specified an exponential speciation rate prior with a mean of 10 using BEAUti v2.4.8 (Bouckaert et al. 2014) and a Yule tree prior (Yule 1924), as recently published phylogenetic analyses encompassing the focal taxa have not indicated that there are high rates of extinction within clades (Rowe et al. 2008, 2016; Rowsey et al. 2018; Smissen and Rowe 2018). I estimated clock rate parameters for the nuclear and mitochondrial partitions but held relative substitution rates fixed at 1, while allowing for substitution rates to vary within loci. This was performed to circumvent problems associated with non-identifiability of nucleotide and clock rate parameters. All other priors were given default values.

We then sampled phylogenetic trees using the Markov-Chain Monte Carlo (MCMC) algorithm implemented in BEAST v. 2.5.2 (Bouckaert et al. 2014) through the CIPRES Science Gateway online portal (Miller et al. 2010). I ran the algorithm for 10^8

samples, storing trees every 10^4 samples with a 20% burn-in. Tracer v1.6 was used to assess convergence of the model parameters, which was defined as an effective sample size (ESS) ≥ 200 (Rambaut et al. 2013). Upon successful convergence of all parameters, I generated the maximum clade credibility (MCC) tree using Tree Annotator v2.4.8 with node ages inferred as the median ages from the 95% highest posterior density of the total set of 8001 trees post burn-in.

Testing ancestral ecological distinction.

As a complement to the test of incumbency-driven morphospace exclusion, I sought to determine whether the ancestor of Chrotomyini and SOE exhibited a mandibular shape distinct from that of Phloeomyini, potentially allowing it to pass a biotic filter to colonize and diversify on Luzon. To test this, I needed to not only estimate a distribution of probable ancestral phenotypes of the common ancestor of Chrotomyini and SOE, but also determine whether the contemporary distances between members of the two LOE (sympatric) clades were similar to the difference between Phloeomyini and the ancestor of the secondary colonizing clade. This analysis was motivated by the observation that the LOE clades occupy almost entirely different regions of morphospace on PC 1-2, which together account for 56.5% of the variation in mandible shape in these two rodent clades (Rowsey et al. 2019).

We performed a PCA on LOE rodent mandibular shape (i.e. excluding SOE) and used the rotation matrix from this PCA to project the SOE morphometric data into the LOE component space. I used this projection to determine whether the SOE rodents filled

areas of morphospace representative of the way the morphological variation of the LOE clades is structured. I then took the average component score of each SOE species.

A challenge associated with estimating the ancestral state of Chrotomyini and SOE is the incomplete sampling of both morphometric and phylogenetic data within SOE, with 58 percent and 52 percent coverage of this radiation respectively. I thus needed to use a method that could account for incomplete taxon sampling to estimate the ancestral state. I performed a MECCA analysis implemented in the *geiger* package, which uses a combination MCMC and approximate Bayesian computation (ABC) algorithm to jointly estimate diversification rate parameters and trait evolution parameters (Slater et al. 2012).

MECCA takes as input a phylogenetic tree, a clade richness vector corresponding to the number of taxa represented by each tip in the tree, and trait means and variances and outputs a posterior distribution of lineage diversification and trait evolutionary model parameters, including rates of trait evolution and root states for the clade of interest. Importantly, MECCA performs univariate analyses of trait and diversification rate parameters. I thus limited the ancestral state reconstructions along PC1 and 2 as opposed to all 24 component axes because I was interested in reconstructing the ancestral state along the axes that exhibit separation between Phloeomyini and Chrotomyini. I recognize that the univariate framework assumes that these trait axes evolved independently, which is likely not the case given the covariation of landmarks within modules of the mandible (Klingenberg et al. 2003), but to my knowledge no method exists to jointly estimate

correlated trait evolutionary rate parameters while accounting for incomplete taxon sampling in both molecular and morphometric data.

We used the MCC chronogram inferred as a part of this study as the phylogenetic framework for this method. I pruned taxa when necessary, including non-Luzon-endemic Phloeomyini and Chrotomyini as well as SOE rodent genera where, despite containing multiple sampled species, the phylogenetic relationships among missing taxa were unknown with respect to sampled species (Appendix Figure 4.3). I enumerated the species in each clade using the species-level taxonomic records from Denys et al. (2017). I then calculated by clade the mean value and interspecific variance as follows: for tips representing a single taxon with molecular and morphometric data, I used the component score as the species mean with zero variance. For incompletely sampled clades exhibiting multiple-species (but not necessarily exhaustive) morphometric sampling coverage, I calculated the mean component score and variance from the taxa that were represented. For incompletely sampled clades containing only a single species sampled with morphometric data, I used the mean component score for the represented species and calculated the interspecific variance as the variance between the sister clade and the focal clade, scaled by the time since common ancestry of the two clades, which is assumed by the Brownian Motion (BM) model of evolution implemented in MECCA (Felsenstein 1985). Finally, for the stem lineage of *Pseudomys* containing *P. johnsoni*, *P. patrius*, and *P. champani*, I calculated the variance as described above and assumed the same component score mean as the average component scores of all sampled lineages in the "crown" *Pseudomys* lineage sister to this clade.

For most datasets, the ABC algorithm used by MECCA is susceptible to inefficient mixing of the MCMC chain when raw summary statistics (*i.e.* trait mean and variance vectors) are used to estimate model parameters due to the sheer number of statistics given by the phylogenetic data (2*N* where *N* is the number of tips in the tree). To overcome this, partial least squares regression is used to maximize the weight of summary statistics that are good predictors of covariation in the original data. The number of PLS components to use is determined based on a calibration step where summary statistics are drawn from the prior distribution of BM model parameters. For this calibration step, I specified uniform priors between -14 and 5 for the log-transformed Brownian rate parameter and -0.2 and 0.2 for root state. Additionally, I specified a two-rate BM model of trait evolution for PC1 based on evidence from Rowsey et al. (2019) that *Rhynchomys* exhibited a shift along its stem branch toward a distinct evolutionary rate. I specified initial diversification rate parameters with 0.42 and 0.0545 lineages per million years for birth and death rates respectively, based on average values for Chrotomyini and SOE reported by Rowsey et al. (2018). I sampled 100,000 calibration statistics for use in PLS regression using these parameter values and ordinated the resultant calibration parameters according to its PLS axes. I determined the number of PLS components to use according to the asymptote of root mean square error plots. For PC1, this amounted to 3 PLS components and for PC2 this amounted to 2 PLS components.

We then ran the full MECCA analysis using the starting values estimated with PLS axes and prior distributions identical to those used in the calibration simulations. I

generated 100,000 samples of parameter values for each trait and applied a post-sampling regression adjustment to refine the precision of the ABC estimate of BM parameter values (ABC-GLM: Leuenberger and Wegmann 2010) using ABCtoolbox (Wegmann et al. 2010), in each case retaining 1000 posterior samples from the procedure. The ancestral state of Chrotomyini and SOE was estimated based on the 50%, 90%, and 95% highest posterior density of sampled root state values for each trait. I performed a similar estimation procedure on the crown ancestor of both Chrotomyini and SOE to visualize the evolution of these traits in the interval of Chrotomyine colonization (Appendix Figure 4.4) but limited this test to the more conservative estimate of the stem ancestor of Chrotomyini and SOE.

Although my sample of morphometric data only contains about 58% of known species in the SOE radiation, I attempted to sample enough generic variation to account for major differences among species while also sampling as many species within species-rich clades as possible such that my sampling was not overdispersed, potentially inflating estimates of evolutionary rate. Using the distribution of 950 estimated ancestral states for PC1 and PC2 from the 95% highest posterior density (HPD) of the ABC-MCMC model inference, I was able to calculate the distance between extant Phloeomyini and these ancestral trait values using 10,000 combinations of ancestral state estimates along PC1 and PC2 sampled with replacement. I computed the distance between these ancestral states and contemporary Phloeomyini to allow for the greatest potential for overlap between this ancestral distribution and the incumbent Luzon clade and thus a more conservative test of biotic filtering. This distribution of distances was compared to the

median pairwise distance in PC axes 1 and 2 of contemporary Phloeomyini and Chrotomyini. This variation thus allowed me to test whether the extant difference between these two clades is significantly greater than the difference between that of the most recent common ancestor of Chrotomyini and SOE. Recovering a greater difference between extant Chrotomyini compared to ancestral Chrotomyini would be consistent with the hypothesis that Chrotomyini has been displaced away from similar trait values to Phloeomyini. By contrast, similar distances between Phloeomyini and contemporary and ancestral Chrotomyini would suggest that the ancestor of SOE and Chrotomyini may have been ecologically distinct from extant Phloeomyini. This latter result would support the hypothesis that a biotic filter is responsible for the ability of Chrotomyini to colonize and diversify on Luzon.

Testing adequacy of models of morphological evolution.

The ancestral state distribution I estimated is susceptible to error if the process that generated the trait variation in these clades is different than that assumed by the model. This becomes relevant if the true ancestor for this clade was actually similar to Phloeomyini and both clades exhibited directional evolution away from this state, as I was unable to infer a constant-rate model of directional trait evolution in the absence of fossil data. I thus wanted to demonstrate that the non-directional model I used adequately described the trait variation to conclude that this variation was not necessarily the result of a model I was unable to test.

We performed model adequacy tests using the *arbutus* package in R to determine how well the parameters of the single- and two-rate BM model inferred using MECCA describe the expected variation in these traits (Pennell et al. 2015). I used the pruned time-scaled tree used in the MECCA analysis alongside the mean component score each tip for PC1 and 2 as the input for this function. To construct the unit tree as a part of this method, I used the median estimates of evolutionary rate from the posterior MECCA distribution to rescale the branches of the phylogeny. Importantly, because I inferred a two-rate model of evolution for PC1 parameterizing an increase in rate along the branch leading to *Rhynchomys*, I rescaled the branch leading to *Rhynchomys* according to the ratio of its inferred evolutionary rate to the backbone of the tree, effectively extending its branch relative to the backbone. It is also important to note that this model assumes that the trait and phylogenetic data are completely sampled, but to my knowledge no method for inferring evolutionary model adequacy exists that can account for the incomplete sampling in SOE.

We then used *arbutus* to calculate six diagnostic statistics and compare these statistics to distributions of statistics generated by simulating trait evolution along the branches in the unit tree provided. Test statistics are as follows, after Pennell et al. (2015): M_{SIG}: mean of squared trait phylogenetically independent contrasts; C_{VAR}: coefficient of variation of the absolute value of the contrasts; S_{VAR}: slope of linear model fitted to absolute value of contrasts against their expected variances; S_{ASR}: slope of linear model fitted to the absolute value of contrasts against the ancestral state of the corresponding node; S_{HGT}: Slope of a linear model fitted to the absolute value of the

contrasts against node depth; D_{CDF}: comparison of contrast distribution to normal distribution with mean 0 and standard deviation equal to the root of the mean of squared contrasts. I was particularly interested in the C_{VAR}, S_{VAR}, and S_{ASR} statistics, as these correspond to unexplained variation in the model due to rate heterogeneity among branches, branch length error in the phylogenetic tree, and evolutionary rate correlated with trait value, all of which could result in incorrect estimates of ancestral states.

Results

Testing incumbency-influenced morphospace exclusion.

Our principal component analysis (PCA) of mandibular shape illustrates the ecomorphological diversity of the three murine clades I studied. The two clades of Philippine rodents do not share mandibular shapes with each other, but species of Sahul Old Endemics exhibit shapes similar to both Luzon clades (Figure 4.1). The first principal component, which describes 37% of the variation in LOE rodent mandible shape, represents an axis of dorsoventral compression and anteroposterior elongation, with positively-scoring species exhibiting slender, elongated mandibles. The second principal component, which describes 19% of the variation, represents the length of the coronoid process relative to the width of the angular process, with positively-scoring species exhibiting reduced coronoid processes and broad, robust angular processes (Figure 4.1). In this visualization of mandibular shape variation (Figure 4.1), Luzon chrotomyines occupy the lower right region of shape space, and have relatively long, slender mandibles with a longer coronoid process and a narrower angular process. On the other hand, Luzon phloeomyines occupy the upper left region of morphospace, with

species means that do not overlap with chrotomyines. This region includes mandibles that are relatively short and robust, with a broad angular process and a reduced coronoid. By contrast, Sahul Old Endemics broadly overlap with both of these clades and include morphologies that appear in both Phloeomyini and Chrotomyini.

We additionally analyzed the distribution of mandibular size independently as this trait may be evolving under a different evolutionary process compared to shape. Nevertheless, distribution of mandibular size variation exhibits a similar pattern to that of shape: specimen-level data of SOE mandibular centroid size overlaps extensively with both Luzon clades, completely encompassing the variation of Chrotomyini and nearly encompassing Phloeomyini. Although Phloeomyini and Chrotomyini exhibit considerable overlap with one another, Phloeomyini occupies a "large" size class to the exclusion of Chrotomyini (Appendix Figure 4.1).

We tested the significance of the contemporary distinction between the two LOE clades by comparing the average Euclidean distance among PC scores of mandibular phenotype (i.e. shape and log centroid size combined). This multivariate distance-based permutation approach enabled the comparison of shape along all component axes simultaneously without overparameterizing a regression model (i.e. as in rate-matrix-based MANOVA). The average distance among PC scores of mandibular phenotype is significantly greater for the comparison between the two Luzon clades than in the incumbent comparison between Phloeomyini and the distribution of permuted samples of SOE (D_{obs} = 7.16, median D_{perm} = 6.58, $p = 4.0 \times 10^{-4}$, Figure 4.2A). This result was robust to exclusion of *Rhynchomys*, which is highly disparate from the remaining rodents

and may contribute to inflation of average between-clade distances (D_{obs} = 7.10, median D_{perm} = 6.57, $p = 2.2 \times 10^{-3}$, Figure 4.2B). These comparisons remain significant even when the comparison is limited to shape variation along the first two component axes of mandibular shape (*i.e.* size excluded) rather than the entire PCA of mandibular form (Appendix Figure 4.2). These results demonstrate that the Luzon Chrotomyini exhibit a limited subset of the variation achieved by the Sahul Old Endemics - a clade that diversified in the absence of other rodent competitors. In particular, chrotomyines do not exhibit the morphologies typical of the Luzon-incumbent Phloeomyini, consistent with phloeomyines acting as a competitor.

Phylogenetic relationships among Philippine and Sahul Old Endemic rodents.

The above comparisons among extant species provide a picture of patterns of morphological variation among extant species in the three murine clades. However, to infer a potential evolutionary mechanism that produced this contemporary distribution of traits, I needed to develop a framework illustrating the evolutionary relationships among the three clades. Using a subset of the sequences and divergence date estimates included in the phylogenetic analysis performed by Rowsey et al. (Rowsey et al. 2018) as a starting point, I performed a time-calibrated Bayesian phylogenetic analysis with expanded sampling among SOE to be able to place the mandibular shape of the three focal clades in an evolutionary context.

Phylogenetic analysis of the seven-gene dataset (Figure 4.3) recovered strong support for most relationships among these rodents as well as estimates of divergence

times that were consistent with previous analyses (Justiniano et al. 2015; Rowsey et al. 2018). The few remaining instances of phylogenetic uncertainty include 1) placement of the two chrotomyine taxa *Chrotomys sibuyanensis* and *Soricomys leonardocoi* relative to other members of their respective genera; 2) resolution of some of the early divergences among SOE genera; and 3) relationships among species of the Sahul Old Endemic genera *Melomys and Paramelomys*. Although these are important questions for future systematic studies to address, the weak support for placement of these species has little influence on the analyses of phenotypic diversification because divergences within these nodes were collapsed for the ancestral state reconstruction.

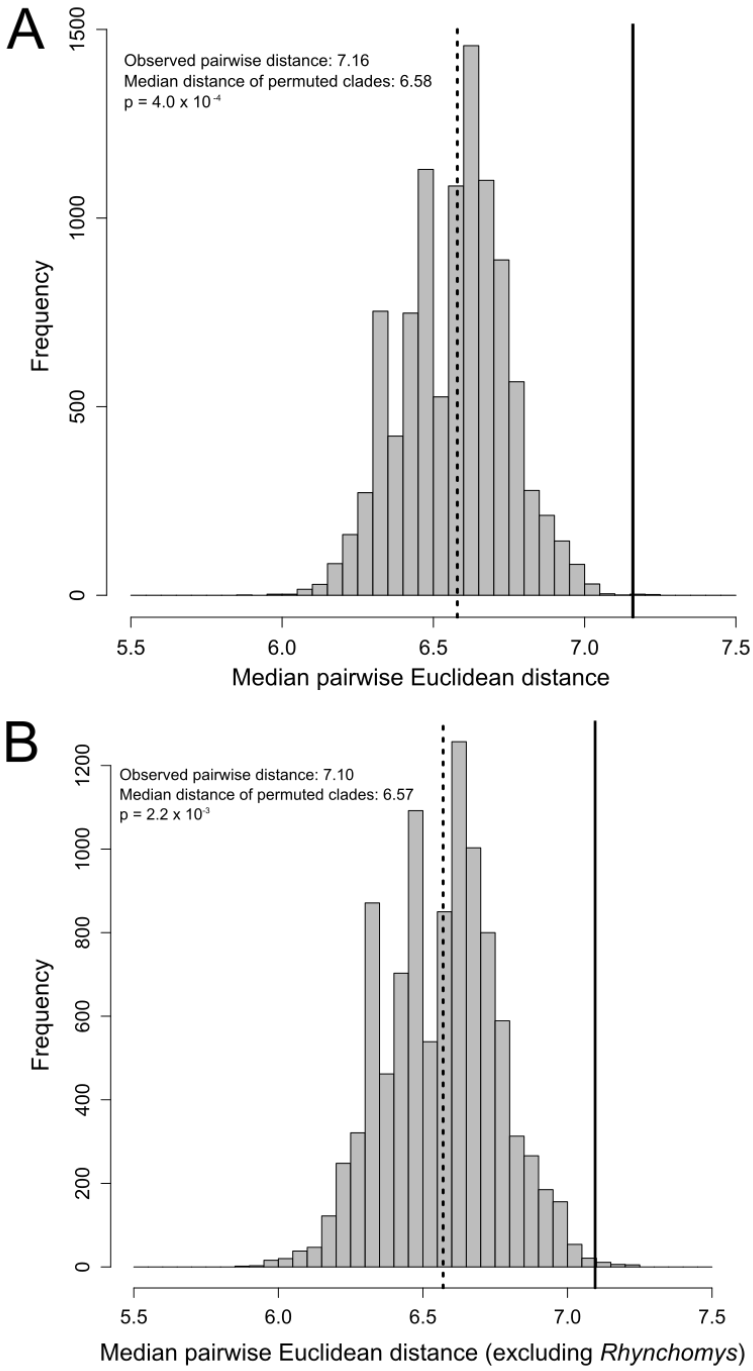

Figure 4.2. Histograms comparing average Euclidean distance in mandible form (i.e. shape and size) between Chrotomyini and Phloeomyini (solid black line) to the distribution of 10,000 average distances between Phloeomyini and permutations of Sahul Old Endemics (gray bars, median: dashed line). (*A*) *Rhynchomys* included, (*B*) *Rhynchomys* excluded.

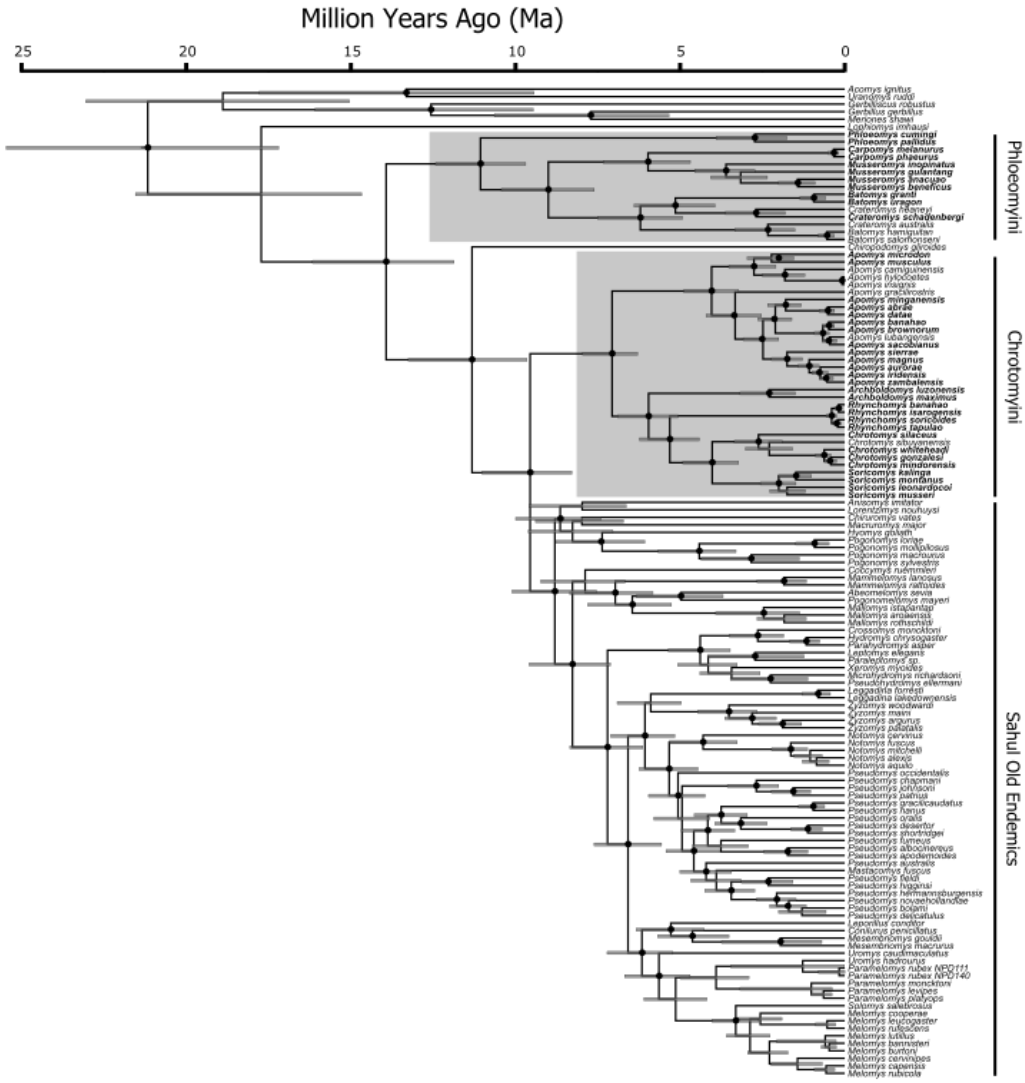

Figure 4.3. Maximum clade credibility tree from BEAST 2 analysis. Bars at nodes indicate 95% highest posterior density interval of node ages. Dots at nodes indicate posterior probability (PP) ≥ 0.95. Gray boxes surrounding clades indicate clades endemic to the Philippines, with bolded names indicating species occurring on Luzon Island.

Testing incumbency-influenced biotic filtering.

The phylogeny I inferred permitted my estimate of ancestral stem chrotomyine mandibular shape. I thus asked whether the ancestral chrotomyine had mandibular morphology distinct from Phloemyini using an evolutionary model estimation procedure that permits incomplete sampling of molecular and phenotypic data and generates a distribution of probable model parameters (including root state estimates) in a Bayesian framework (MECCA: Slater et al. 2012). Recovering a distinct ancestral stem chrotomyine mandibular morphology from Phloeomyini would be consistent with the hypothesis that Chrotomyini's colonization and subsequent diversification on Luzon was made possible by passing a biotic filter.

The distribution of ancestral PC1 and PC2 scores of the ancestor of Chrotomyini and SOE, like that of contemporary Chrotomyini, exhibits little overlap with the distribution of contemporary Phloeomyini on these axes (Figure 4.1). The contemporary distance along PC1-2 does not significantly differ from the distribution of 10000 sampled distances between extant Phloeomyini and this ancestral state interval (D_{obs} = 0.103, median D_{anc} = 0.077, p = 0.27, Figure 4.4A). This result is robust even when I performed an additional MECCA model specification procedure where *Rhynchomys* was excluded (D_{obs} = 0.096, median D_{anc} = 0.154, p = 0.81, Figure 4.4B). The persistent degree of distance between the two clades supports the hypothesis that the successful colonization of Luzon by Chrotomyini could have been due to their ancestral distinction from Phloeomyini.

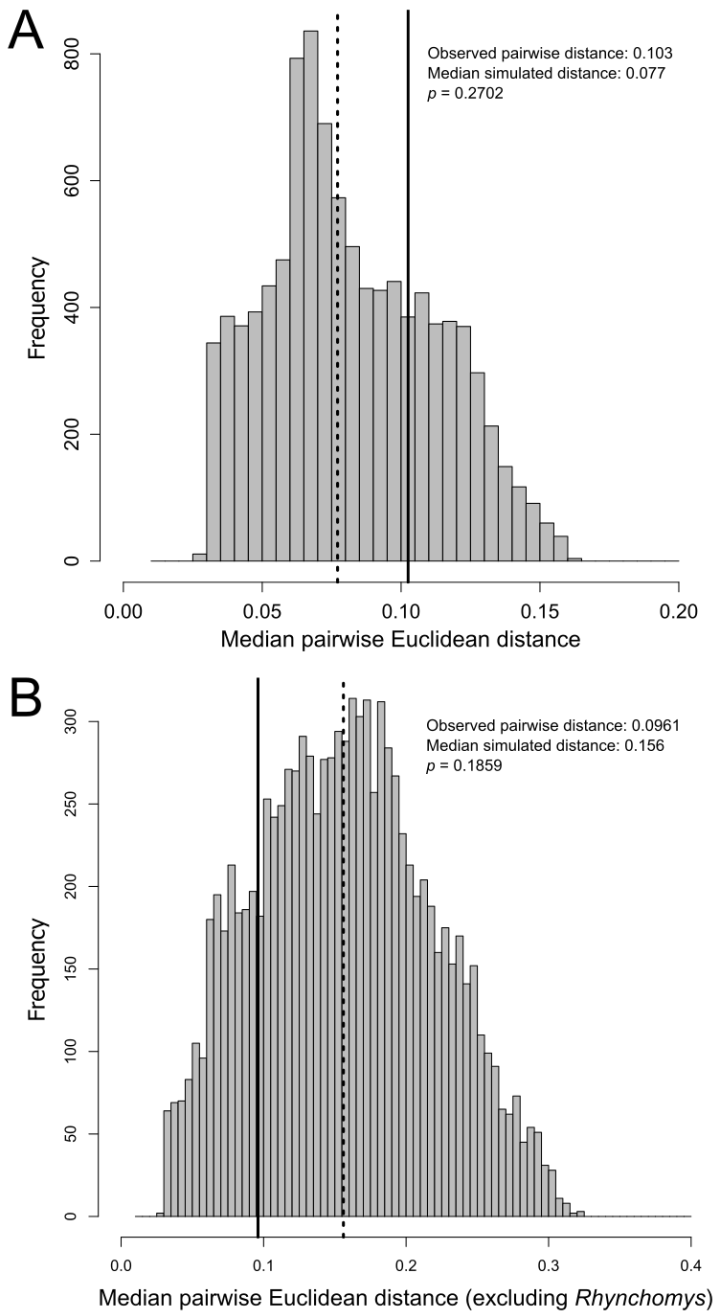

Figure 4.4. Histograms comparing average Euclidean distance in mandible shape along PC1-2 between extant Chrotomyini and Phloeomyini (solid black line) to 10,000 sampled ancestral states along PC1-2 from MECCA posterior distribution (gray bars, median: dashed line). (*A*) *Rhynchomys* included, (*B*) *Rhynchomys* excluded.

MECCA's ancestral state estimations are only accurate insofar as the evolutionary model used to generate the states fits the trait data, given the evolutionary relationships among species. I thus needed to ensure that the ancestral states were not biased due to inconsistencies with the best-fit model of trait evolution and the model used in MECCA. However, the models I infer using MECCA generate *arbutus* model adequacy test statistics within the distribution of simulated statistics in most cases (Pennell et al. 2015). PC1 exhibits violations with respect to M_{SIG}, C_{VAR}, and S_{VAR} statistics, corresponding to a significantly underestimated evolutionary rate, under-parameterized rate heterogeneity along certain branches, and evolutionary rate correlated with branch length (Table 4.1). However, when I recompute these test statistics after removing *Rhynchomys*, the outlying genus along PC1, I lose support for all statistical violations. The model adequacy dependent on inclusion of *Rhynchomys* suggests that the MECCA evolutionary model inadequately parameterizes the difference in rate between the backbone of the supplied tree and *Rhynchomys* leading to an underestimated rate of evolution along the branch leading to *Rhynchomys* and an overestimated rate of trait evolution in the rest of the tree. The evolutionary model along PC2, by contrast, provides a much better fit to the data, with no significant model violations aside from overestimated evolutionary rate (Table 4.1). My consistent recovery of overestimated evolutionary rate may stem from the within-clade variance used to estimate model parameters in MECCA that cannot be easily incorporated into the model adequacy framework. The unobserved variance among tips when simulating distributions of test statistics may lower the estimated rate of evolution in the *arbutus* analysis.

Table 4.1. Results of model adequacy test for evolutionary models used to infer morphological evolutionary rate parameters for change along PC1 and PC2. Means of simulated distributions are indicated in parentheses after the observed value, with statistically significant deviations from the simulated distribution at $\alpha = 0.05$ denoted with asterisks. See methods for definition of test statistics.

Trait axis	Model	M_{SIG}	C_{VAR}	S_{VAR}	S_{ASR}	S_{HGT}	D_{CDF}
PC1	Two-Rate	1.76	0.916	24.7	2.75 (-0.077)	217 (0.910)	0.0800 (0.102)
	BM	(1.00)*	(0.754)*	(0.102)*			
PC2	BM	1.42 (1.00)*	0.774 (0.754)	-15.1 (0.0256)	0.541 (0.0534)	-115 (0.998)	0.0993 (0.103)
PC1 (*Rhynchomys* excluded)	BM	1.15 (1.00)	0.776 (0.753)	15.0 (0.0924)	-5.90 (0.0521)	628 (3.33)	0.0656 (0.106)

Discussion

Our results illustrate persistent cladewise partitioning of morphological variation across the evolutionary history of two sympatric clades. This persistent distinction between the two Luzon "Old Endemic" rodent clades supports the hypothesis that Phloeomyini, as the incumbent murine clade in this system, may have been able to monopolize an area of morphospace such that non-incumbent Chrotomyini must have both been initially distinct from Phloeomyini and was constrained from evolving phloeomyine morphologies present in its close relatives elsewhere. The morphological diversity of SOE, which contains species that resemble members of both Luzon clades, suggests that Chrotomyini may have been able to exploit the niches occupied by Phloeomyini in their absence had it been incumbent.

The pattern of repeated colonization of island systems in non-volant Southeast Asian mammals is not limited to the Luzon "Old Endemic" rodents. Luzon itself has experienced an estimated four additional, more recent colonization events by other rodent lineages. These colonization events have not produced the species and morphological diversity necessary to test whether these "New Endemic" colonizing lineages are

ecologically distinct from the LOE rodents. However, collection records of the most common species of these rodents suggest that they occur almost exclusively in disturbed habitats, where the LOE rodents are typically absent (Heaney et al. 2016b). Detailed comparative morphometric analyses of the diversity of these species may reveal overlapping morphospace occupancy by these New Endemic lineages with the LOE rodents, supporting the hypothesis that a biotic filter established by the LOE rodents excludes the ecologically-similar New Endemics from primary forest habitats on Luzon. This result would also illustrate that incumbency status is relative, and secondary colonizing lineages (such as Chrotomyini) have potential competitive advantages above subsequent colonists (such as the New Endemics). Repeated colonization of island systems by mammals is also not unique to Luzon Island: Sahul was colonized by an additional lineage of murine rodents, which subsequently exhibited an exceptional rate of lineage diversification among the highest recorded in vertebrates (Rowe et al. 2011). However, the rapid lineage diversification of Sahulian *Rattus* has been accompanied by little ecomorphological evolution, warranting investigation as to whether this limited morphological diversity may be due to incumbency effects.

The emerging picture regarding incumbency effects in the evolution of Indo-Australian rodents is one of limited influence on the rates of lineage diversification (Schenk et al. 2013; Rowsey et al. 2018) and trait evolution (Alhajeri et al. 2016; Rowsey et al. 2019). In other words, secondarily colonizing rodent clades appear to be able to diversify without a reduction in evolutionary rate provided they can colonize the system in the first place. However, the patterns observed among Indo-Australian rodents do not

necessarily hold true across other lineages. For example, in aquatic systems, secondary colonists can experience limited ecological opportunity and subsequent diversification compared to incumbent lineages, leading to depressed evolutionary rates in non-incumbent clades contrary to what has unfolded in Indo-Australian rodents (Betancur-R. et al. 2012; Múrria et al. 2018). In North American canids, younger lineages appear to have driven incumbent lineages extinct, in a reversal of the expectations set by ecological incumbency (Silvestro et al. 2015). This analysis also reveals the potential impact that geographic scale and isolation have on recovering patterns consistent with biotic filtering and subsequent clade-specific partitioning. A previous analysis on continent-wide assemblages of passerine birds revealed limited effects of colonization order and subsequent ecological evolution on the patterns of morphospace occupancy (Jønsson et al. 2015). These results illustrate that incumbency can quickly become obscured by other factors, such as allopatric speciation and limited competition between focal clades, when examining ecological diversity and community assembly at increasingly broad geographic and taxonomic scales (Jablonski 2008). As more examples of evolution influenced by incumbency effects are explicitly tested in an evolutionary framework, the relative roles of phylogenetic and ecological similarity among potentially-competing niches, as well as the role spatial scale plays in my ability to recover these dynamics, should be explored.

Although my results strongly support the hypothesis of evolution influenced by a persistent biotic filter in the Luzon Old Endemic rodents, my approach is constrained by the lack of fossil information available for these three clades. Inferences of evolutionary

process based solely on extant taxa can only provide potential explanations that may be inaccurate upon discovering fossil evidence inconsistent with this hypothesis. In this case, if a fossil chrotomyine was recovered I could compare the fit of a standard Brownian Motion model versus a model exhibiting an evolutionary shift away from Phloeomyini (Pagel 1999). Nevertheless, the model adequacy test illustrates that the extant variation in mandibular morphology is adequately described by non-directional BM model of evolution, particularly once *Rhynchomys* is removed from the dataset (Table 4.1), meaning that a trend model need not be invoked to explain the patterns in the data.

Our results also indicate merely that the patterns I observe in this system are consistent with the processes I sought to test; other potential explanations for the patterns I observe may exist. My ability to compare the evolution of LOE to SOE relies on the assumption that SOE rodents rests on the assumption that the three clades experience similar ecological opportunity. I assume that SOE provides a realistic expectation for the evolution of Chrotomyini if this clade did not experience competition with Phloeomyini. A potential criticism of my approach is that SOE may have experienced greater ecological opportunity due to greater available land area, and thus a greater potential exploitation of morphospace. However, I recovered SOE occupied an overlapping, but not eclipsing, area of morphospace with the LOE rodents, suggesting that the SOE rodents did not have the ability to diversify into a broader array of niches than LOE.

Our study examined incumbency effects from the standpoint of the secondary-colonizing Chrotomyini in part because of the easily-tractable sister-clade comparison

between Chrotomyini and SOE. However, my work begs the question as to what has influenced the morphological variation among phloeomyines. There are two potential mechanisms that may have imposed fixed limits on phloeomyine variation. First, Phloeomyini may exhibit intrinsic (plesiomorphic) constraints that limit their ability to evolve out of a herbivorous morphotype. Testing this hypothesis would require comparing the evolutionary pattern and process between Phloeomyini and its sister clade. Unfortunately, Phloeomyini is sister to the incredibly species rich and geographically widespread *Mus*/*Rattus* division within Murinae. This sister relationship precludes a comparison of evolutionary pattern and process due to conflation of geographic and ecological sources of evolutionary variability. However, assuming that there are no intrinsic evolutionary constraints within Phloeomyini (i.e. Phloeomyini and Hydromyini exhibit the same potentially realizable trophic diversity), Phloeomyini could have been able to evolve mandibular shapes consistent with an animalivorous diet relatively quickly but did not because chrotomyine colonization either blocked their evolution into an animalivorous niche or drove the phloeomyine species in these trophic niches to extinction. However, testing these two hypotheses is difficult unless a fossil definitively attributable to Phloeomyini was uncovered with chrotomyine-like mandibular shape.

The question of macroevolutionary determinism is one of the greatest centers of evolutionary debate and the degree of determinism is likely at the intersection of many processes idiosyncratic with respect to the system (Losos et al. 1998; Blount et al. 2008; Burbrink et al. 2012; Meyer et al. 2012). This question is preeminently important in understanding the evolution of the focal rodents and the broader murine fauna of

Southeast Asia. The areas of morphospace exclusive to the LOE clades might suggest that incumbency may promote evolutionary novelty in the absence of other determining factors, as illustrated by the novelty exhibited by *Phloeomys* and *Rhynchomys*. Despite this pattern of apparent uniqueness, Indo-Australian rodents exhibit repeated convergence on similar morphotypes with respect to diet, including four independent transitions to carnivory with similar diagnostic cranial shape (Rowe et al. 2016) and gigantism potentially associated with arboreal herbivory (Rowsey et al. 2019). A promising area of research may be determining the relative importance of incumbency effects versus the dynamic archipelagic environment in which the Indo-Australian murines are found in influencing the repeated evolution of exaggerated ecomorphological variation.

Biotic filtering has been previously demonstrated to be an important factor in the community assembly of island-endemic and continentally-distributed faunas alike (Gillespie 2004; Rabosky et al. 2011). The patterns of mandibular form variation in the three murine clades I studied illustrate that incumbency may establish a biotic filter for subsequently colonizing lineages in this system as well. Furthermore, along with the results of previous studies of Luzon murines, my results indicate that incumbency effects are more likely to influence the patterns of morphological diversity than they are rates of lineage diversification or morphological evolution, with non-incumbent clades diversifying relatively freely after colonization despite the constraining influence of incumbent clades on morphospace occupancy (Rowsey et al. 2018, 2019). I conclude that clades that pass a biotic filter may be forced to exhibit persistent ecological distinction

from the incumbent clade, but as long as this distinction is maintained, evolution may proceed relatively uninhibited.

Conclusions

The explicit influence of incumbency effects on macroevolutionary processes is a relatively nascent line of inquiry. Potential incumbency effects have typically been investigated by examining rates of evolution in co-occurring clades at continental scales, yielding little support to date. The patterns of morphological evolution in Luzon rodents provide a unique perspective that illustrates incumbency effects may be more feasible to detect at relatively small spatial scales, and that they are more likely to manifest in patterns of community assembly and ecomorphological diversity than in evolutionary rates *per se*. My results suggest that non-incumbents may be able to radiate uninhibited, provided these colonists consistently maintain ecological distinction from incumbents.

CONCLUSION

THE INFLUENCE OF INCUMBENCY EFFECTS ON THE MACROEVOLUTION OF ISLAND-ENDEMIC FAUNA

This dissertation tested the hypothesis that, in spatially limited island systems, primary colonizing (incumbent) lineages may serve to limit the evolution of ecologically-similar subsequent colonists. In Chapter 1, I found that the rates of lineage diversification of secondary colonizing Chrotomyini were inconsistent with both a model of decelerating evolution representative of ecological opportunity as well as an absolute lower rate than Phloeomyini or SOE due to Chrotomyini's status as non-incumbents. In Chapter 2, I recovered similar results with respect to rates of mandibular shape evolution: neither Chrotomyini nor Phloeomyini exhibited rates of evolution that slowed over time, nor did mandibular shape evolution slow over time. These results indicate that incumbency effects and ecological opportunity have not influenced the rates of evolution in the two clades of LOE rodents very strongly. These expected patterns may not have been recovered due to one of the fundamental assumptions of adaptive radiation theory: habitat availability is assumed to be static over time. This assumption does not hold for the Luzon system, whose dynamic history is marked by periods of rapid changes in available area, heterogeneity, and habitat complexity (Hall 2013; Heaney et al. 2016a). These changes in habitat area may have facilitated dispersal-mediated speciation with limited necessary phenotypic evolution responsible for the patterns I observed in these two chapters.

In Chapter 3, I determined that humerus shape is strongly influenced by individual genera exhibiting parallel evolution within different locomotory modes – genera exhibiting similar locomotory strategies in some cases exhibited humerus shapes more different from one another than did genera in different locomotory categories. The ecological distinction between the two LOE clades was retained in their humerus shape, but the lack of repeated convergence in locomotory mode between Phloeomyini and Chrotomyini limited my power to infer humerus shape from locomotory strategy. My results indicate that humerus shape may confer similar functional performance with multiple distinct shapes, potentially causing a decoupling between form and function and freeing the shape to specialize on other functional variables not captured in this study. Nevertheless, humerus shape illustrates an axis other than mandibular morphology on which these two clades are dissimilar. This dissimilarity may have either promoted Chrotomyini's ability to colonize the system or have been forced to limit the competition between these two clades.

In Chapter 4, I recovered consistent partitioning of morphospace between the two LOE clades consistent with the hypothesis that Chrotomyini represents only a subset of the morphospace this clade could have occupied to limit competition with Phloeomyini. Furthermore, I recovered a persistent lack of overlap with Phloeomyini such that the stem ancestor for Chrotomyini was likely distinct from the morphology Phloeomyini currently exhibits. I thus conclude that incumbency effects may present consistent barriers to non-incumbents, constraining the diversity of these clades to limit competition with incumbents.

This work presents a detailed analysis of the macroevolution of two island-endemic clades from multiple perspectives, including evolutionary rates and patterns of diversity, while also examining these perspectives with respect to multiple characters, specifically lineage diversification, mandibular evolution, and forelimb evolution. My goal was to provide a detailed examination of an insular fauna with a complex history potentially influenced by competitive, phylogenetic, and geological factors in determining their diversity. This research illustrates that, in an island as geologically dynamic as Luzon, the classical model of adaptive radiation is not necessarily a good fit for predicting species and phenotypic diversity. Potentially due to limited sustained competition for niches, rates of evolution have not varied predictably with respect to colonizing clade. However, my work also illustrates that even with the potential for prominent dispersal away from centers of competition over the course of Luzon's history, the patterns of morphological diversity and island-level community assembly are consistent with non-incumbents being restricted in their diversity. I conclude that as long as non-incumbents remain ecologically distinct from incumbents, they may colonize and radiate in a system without depressed evolutionary rates.

BIBLIOGRAPHY

Achmadi, A. S.; J. A. Esselstyn, K. C. Rowe, I. Maryanto, and M. T. Abdullah. 2013. Phylogeny, diversity, and biogeography of Southeast Asian spiny rats (*Maxomys*). Journal of Mammalogy 94(6):1412-1423.

Adams, D. C. 2014a. Quantifying and comparing phylogenetic evolutionary rates for shape and other high-dimensional phenotypic data. Sys. Biol. 63:166-177.

Adams, D. C. 2014b. A method for assessing phylogenetic least squares models for shape and other high-dimensional multivariate data. Evolution 68: 2675-2688.

Adams, D. C. and M. L. Collyer. 2018. Multivariate phylogenetic comparative methods: evaluations, comparisons, and recommendations. Syst. Biol. 67:14-31.

Adams, D. C., M. L. Collyer, A. Kaliontzopolou, and E. Sherratt. 2017. Geomorph: Software for geometric morphometric analyses. R package version 3.0.5. https://cran.r-project.org/package=geomorph.

Adams, D. C., and E. Otárola-Castillo. 2013. Geomorph: An r package for the collection and analysis of geometric morphometric shape data. Methods Ecol. Evol. 4:393–399.

Adkins, R. M., E. L. Gelke, D. Rowe, and R. L. Honeycutt. 2001. Molecular phylogeny and divergence time estimates for major rodent groups: evidence from multiple genes. Mol. Biol. Evol. 18:777–791.

Adler, D., D. Murdoch, O. Nenadic, S. Urbanek, M. Chen, A. Gebhardt, B. Bolker, G. Csardi, A. Strzelecki, and A. Senger. 2017. rgl: 3D Visualization Using OpenGL. R package version 0.98.1. https://CRAN.R-project.org/package=rgl.

Akaike, H. 1974. A new look at the statistical model identification. IEEE Trans. Auto. Cont. 19: 716-723.

Alfaro, M. E., D. I. Bolnick, and P. C. Wainwright. 2005. Evolutionary consequences of many-to-one mapping of jaw morphology to mechanics in labrid fishes. Am. Nat. 165:E140-E154.

Alfaro,M. E., F. Santini, C. Brock, H. Alamillo, A. Dornburg, et al. 2009. Nine exceptional radiations plus high turnover explain species diversity in jawed vertebrates. Proc. Nat. Acad. Sci. USA 106:13410–13414.

Alhajeri, B. H., J. J. Schenk, and S. J. Steppan. 2016. Ecomorphological diversification following continental colonization in muroid rodents (Rodentia: Muroidea). Biol. J. Linn. Soc. 117:463–481.

Almany, G. R. 2004. Priority effects in coral reef fish communities of the Great Barrier Reef. Ecology 85:2872-2880.

Alroy, J. 1996. Constant extinction, constrained diversification, and uncoordinated stasis in North American mammals. Palaeogeo., Palaeoclim., Palaeoecol. 127:285-311.

Alviola, P. A., M. R. M. Duya, M. V. Duya, L. R. Heaney, and E. A. Rickart. 2011. Mammalian diversity patterns on Mount Palali, Caraballo Mountains, Luzon. Fieldiana 2:61-74.

Anderson, M. J. 2001. A new method for non-parametric multivariate analysis of variance. Aust. Ecol. 26:32-46.

Baldwin, B. G., and M. J. Sanderson. 1998. Age and rate of diversification of the Hawaiian silversword alliance (Compositae). Proc. Nat. Acad. Sci. USA 95:9402–9406.

Balete, D. S., P. A. Alviola, M. R. M. Duya, M. V. Duya, L. R. Heaney, et al. 2011. The mammals of the Mingan Mountains, Luzon: evidence for a new center of mammalian endemism. Fieldiana 2:75-87.

Balete, D. S., L. R. Heaney, P. A. Alviola, and E. A. Rickart. 2013. Diversity and distribution of small mammals in the Bicol volcanic belt of southern Luzon Island, Philippines. Nat. Mus. Philipp. J. Nat. His.. 1:61-86.

Balete, D. S., L. R. Heaney, E. A. Rickart, R. S. Quidlat, and J. C. Ibanez. 2008. A new species of *Batomys* (Mammalia: Muridae) from eastern Mindanao Island, Philippines. Proc. Biol. Soc. Wash. 121:411-428.

Balete, D. S., E. A. Rickart, and L. R. Heaney. 2006. A new species of the shrew-mouse, *Archboldomys* (Rodentia: Muridae: Murinae), from the Philippines. Syst. Biodiv. 4:489-501.

Balete, D. S., E. A. Rickart, and L. R. Heaney. 2012. *Archboldomys* (Muridae: Murinae) reconsidered: a new genus and three new species of shrew mice from Luzon Island, Philippines. Am. Mus. Nov. 3754:1-60.

Balete, D. S., E. A. Rickart, L. R. Heaney, and S. A. Jansa. 2015. A new species of *Batomys* (Muridae, Rodentia) from southern Luzon Island, Philippines. Proc. Biol. Soc. Wash. 128:22-39.

Balete, D. S., E. A. Rickart, R. G. B. Rosell-Ambal, S. Jansa, and L. R. Heaney. 2007. Descriptions of two new species of *Rhynchomys* Thomas (Rodentia: Muridae: Murinae) from Luzon Island, Philippines. J. Mamm. 88: 287-301.

Bambach, R. K., A. H. Knoll, and J. J. Sepkoski, Jr. 2002. Anatomical and ecological constraints on Phanerozoic animal diversity in the marine realm. Proc. Nat. Acad. Sci. USA 99:6854-6859.

Bennet, G. M., and P. M. O'Grady. 2013. Historical biogeography and ecological opportunity in the adaptive radiation of native Hawaiian leafhoppers (Cicadellidae: Nesophrosyne). J. Biogeogr. 40:1512–1523.

Benson, D. A., M. Cavanaugh, K. Clark, I. Karsch-Mizrachi, D. J. Lipman, J. Ostell, and E. W. Sayers. 2012. GenBank. Nucleic Acids Res. 41:D36–D42.

Betancur-R., R., G. Ortí, A. M. Stein, A. P. Marceniuk, and R. A. Pyron. 2012. Apparent signal of competition limiting diversification after ecological transitions from marine to freshwater habitats. Ecol. Lett. 15:822–830.

Blackburn, D. C., C. D. Siler, A. C. Diesmos, J. A. McGuire, D. C. Cannatella, and R. M. Brown. 2013. An adaptive radiation of frogs in a southeast Asian island archipelago. Evolution 67:2631–2646.

Blomberg, S. P., T. Garland, and A. R. Ives. 2003. Testing for phylogenetic signal in comparative data: behavioral traits are more labile. Evolution 57:717-745.

Blount, Z. D., C. Z. Borland, and R. E. Lenski. 2008. Historical contingency and the evolution of a key innovation in an experimental population of Escherichia coli. Proc. Natl. Acad. Sci. 105:7899–7906.

Bolnick, D. I. 2004. Can intraspecific competition drive disruptive selection? An experimental test in natural populations of sticklebacks. Evolution 58:608-618.
Bookstein, F. L. 1996. Landmark methods for forms without landmarks: localizing group differences in outline shape. Med. Image Anal. 1: 279-289.
Borregaard, M. K., I. R. Amorim, P.A.V.Borges, J. S. Cabral, J-M. Fernandez-Palacios, R. Field, L. R. Heaney, H. Kreft, T. J. Matthews, J. M. Olesen, et al. 2017. Oceanic island biogeography through the lens of the General Dynamic Model: assessment and prospect. Biol. Rev. 92:830–853.
Bouckaert, R. R., J. Heled, D. Kühnert, T. Vaughan, C. H. Wu, D. Xie, M. A. Suchard, A. Rambaut, and A. J. Drummond. 2014. BEAST 2: A Software Platform for Bayesian Evolutionary Analysis. PLoS Comput. Biol. 10:1–7.
Bryant, L. M., S. C. Donnellan, D. A. Hurwood, and S. J. Fuller. 2011. Phylogenetic relationships and divergence date estimates among Australo-Papuan mosaic-tailed rats from the Uromys division (Rodentia: Muridae). Zool. Scr. 40:433–447.
Bryant, L. M., and S. J. Fuller. 2014. Pleistocene climate fluctuations influence phylogeographical patterns in Melomys cervinipes across the mesic forests of eastern Australia. J. Biogeogr. 41:1923–1935.
Burbrink, F. T., X. Chen, E. A. Myers, M. C. Brandley, and R. A. Pyron. 2012. Evidence for determinism in species diversification and contingency in phenotypic evolution during adaptive radiation. Proc. R. Soc. B Biol. Sci. 279:4817–4826.
Burbrink, F. T., and R. A. Pyron. 2010. How does ecological opportunity influence rates of speciation, extinction, and morphological diversification in New World ratsnakes (tribe Lampropeltini)? Evolution Figure. 64:934–943.
Burns, K. J., A. J. Shultz, P. O. Title, N. A. Mason, F. K. Barker, J. Klicka, S. M. Lanyon, and I. J. Lovette. 2014. Phylogenetics and diversification of tanagers (Passeriformes: Thraupidae), the largest radiation of Neotropical songbirds. Mol. Phy. Evol. 75:41–77.
Butler, M. A. and A. A. King. 2004. Phylogenetic comparative analysis: a modeling approach for adaptive evolution. Am. Nat. 164: 683-695.
Case, T. J. 1991. Community collapse in metapopulation models with interspecies competition. Biol. J. Linn. Soc. 42:239–266.
Cavender-Bares, J., D. D. Ackerly, D. A. Baum, and F. A. Bazzaz. 2004. Phylogenetic overdispersion in Floridian oak communities. Am. Nat. 163:823–843.
Churchfield, S. 1990. *The Natural History of Shrews*. Cornell University Press, Ithaca, NY.
Churchfield, S. 2002. Why are shrews so small? The costs and benefits of small size in northern temperate *Sorex* species in the context of foraging habits and prey supply. Acta Theriol. 47:169-184.
Claramunt, S., E. P. Derryberry, J. V. Remsen Jr., and R. T. Brumfield. 2012. High dispersal ability inhibits speciation in a continental radiation of passerine birds. Proc. R. Soc. B. 279:1567-1574.
Clavel, J., G. Escarguel, and G. Merceron. 2015. mvMORPH: an R package for fitting multivariate evolutionary models to morphometric data. Meth. Ecol. Evol. 6:1311-1319.

Collyer, M. L., D. J. Sekora, and D. C. Adams. 2015. A method for analysis of phenotypic change for phenotypes describes by high-dimensional data. Heredity 115: 357-365.

Demment, M. W. and P. J. Van Soest. 1985. A nutritional explanation for body-size patterns of ruminant and nonruminant herbivores. Am. Nat. 125:641-672.

Denys, C., P. Taylor, and K. P. Aplin. 2017. Family Muridae. P. *in* D. E. Wilson, T. E. J. Lacher, and R. A. Mittermeier, eds. Handbook of the Mammals of the World Vol. 7: Order Rodentia. Lynx Edicions in association with Conservation International and IUCN, Barcelona.

Derrickson, E. M., and R. E. Ricklefs. 1988. Taxon-Dependent Diversification of Life-History Traits and the Perception of Phylogenetic Constraints. Funct. Ecol. 2:417–423.

Derryberry, E. P., S. Claramunt, G. Derryberry, R. T. Chesser, J. Cracraft, A. Aleixo, J. Pérez-Emán, J. V. Remsen, Jr., and R. T. Brumfield. 2011. Lineage diversification and morphological evolution in a large-scale continental radiation: the neotropical ovenbirds and woodcreepers (Aves: Furnariidae). Evolution 65:2973-2986.

Dos Reis, M., P. C. J. Donoghue, and Z. Yang. 2014. Neither phylogenomic nor palaeontolological data support a Palaeogene origin of placental mammals. Biol. Lett. 10:1–4.

Drake, J. A. 1991. Community-assembly mechanics and the structure of an experimental species ensemble. Am. Nat. 137:1–26.

Drummond, A. J., S. Y. W. Ho, M. J. Phillips, and A. Rambaut. 2006. Relaxed phylogenetics and dating with confidence. PLoS Biol. 4:699–710.

Duchen, P., C. Leuenberger, S. M. Szilágy, L. Harmon, J. Eastman, M. Schweizer, and D. Wegmann. 2017. Inference of evolutionary jumps in large phylogenies using Lévy processes. Syst. Biol. 66:950-963.

Duya, M. R. M., M. V. Duya, P. A. Alviola, D. S. Balete, and L. R. Heaney. 2011. Diversity of small mammals in montane and mossy forests on Mount Cetaceo, Cagayan Province, Luzon. Fieldiana 2:88-95.

Edgar, R. C. 2004. MUSCLE: Multiple sequence alignment with high accuracy and high throughput. Nucleic Acids Res. 32:1792–1797.

Emerson, B. C. 2002. Evolution on oceanic islands: molecular phylogenetic approaches to understanding pattern and process. Mol. Ecol. 11:951-986.

Emerson, B. C. and R. G. Gillespie. 2008. Phylogenetic analysis of community assembly and structure over space and time. Trend. Ecol. Evol. 23:619-630.

Engel, S. R., K. M. Hogan, J. F. Taylor, and S. K. Davis. 1998. Molecular systematics and paleobiogeography of the South American sigmodontine rodents. Mol. Biol. Evol. 15:35-49.

Elissamburu, A. and L. De Santis. 2011. Forelimb proportions and fossorial adaptations in the scratch-digging rodent *Ctenomys*. J. Mamm. 92:683-689.

Esselstyn, J. A., A. S. Achmadi, H. Handika, and K. C. Rowe. 2015. A hog-nosed shrew rat (Rodentia: Muridae) from Sulawesi Island, Indonesia. J. Mamm. 96(5):895-907.

Esselstyn, J., A. S. Achmadi, and K. C. Rowe. 2012. Evolutionary novelty in a rat with no molars. Biol. Lett. 8:6-10.
Esselstyn, J. A., R. M. Timm, and R. M. Brown. 2009. Do geological or climatic processes drive speciation in dynamic archipelagos? The tempo and mode of diversification in southeast Asian shrews. Evolution 63:2595–2610.
Felsenstein, J. 1985. Phylogenies and the Comparative Method. Am. Nat. 125:1–15.
Filardi, C. E. and R. G. Moyle. 2005. Single origin of a pan-Pacific bird group and upstream colonization of Australasia. Nature 438:216-219.
Friedman, M. B. P. Keck, A. Dornburg, R. I. Eytan, C. H. Martin, C. D. Hulsey, P. C. Wainwright, and T. J. Near. 2013. Molecular and fossil evidence place the origin of cichlid fishes long after Gondwanan rifting. Proc. R. Soc. B. 280:20131733.
Fukami, T. 2004. Assembly history interacts with ecosystem size to influence species diversity. Ecology 85:3234-3242.
Fukami, T., H. J. E. Beaumont,X. -X. Zhang, and P. B.Rainey. 2007. Immigration history controls diversification in experimental adaptive radiation. Nature 446:436–439.
Giarla, T. C., and S. A. Jansa. 2014. The role of physical geography and habitat type in shaping the biogeographical history of a recent radiation of Neotropical marsupials (Thylamys:Didelphidae). J. Biogeogr. 41:1547–1558.
Gillespie, R. G. 2004. Community assembly through adaptive radiation in Hawaiian spiders. Science. 303:356–359.
Gittleman, J. L. 1985. Carnivore body size: ecological and taxonomic correlates. Oecologia 67:540-554.
Givnish, T. J., K. C. Millam, A. R. Mast, T. B. Paterson, T. J. Theim, A. L. Hipp, J. M. Henss, J. F. Smith, K. R. Wood, and K. J. Sytsma. 2009. Origin, adaptive radiation and diversification of the Hawaiian lobeliads (Asterales: Campanulaceae). Proc. Roy. Soc. B. 276:407-416.
Goldberg, E. E. and R. Lande. 2007. Species' borders and dispersal barriers. Am. Nat. 170:297-304.
Gower, J. C. 1975. Generalized procrustes analysis. Psychometrika 40:33–51.
Grossnickle, D. M., and P. D. Polly. 2013. Mammal disparity decreases during the Cretaceous angiosperm radiation. Proc. R. Soc. B 280:1–8.
Gu, X., Y. X. Fu, and W. H. Li. 1995. Maximum likelihood estimation of the heterogeneity of substitution rate among nucleotide sites. Mol. Biol. and Evol. 12:546–557.
Gunz, P., P. Mitteroecker, S. Neubauer, G. W. Weber, and F. L. Bookstein. 2009. Principles for the virtual reconstruction of hominin crania. J. Hum. Evol. 57:48–62.
Hall, R. 2013. The palaeogeography of Sundaland and Wallacea since the Late Jurassic.
J. Limno. 72:1-17.
Harmon, L. J., J. B. Losos, T. J. Davies, R. G. Gillespie, J. L. Gittleman, et al. 2010. Early bursts of body size and shape evolution are rare in comparative data. Evolution 64:2385-2396.
Harmon, L. J., J. A. Schulte II, A. Larson, and J. B. Losos. 2003. Tempo and mode of evolutionary radiation in iguanian lizards. Science 301:961-964.

Harmon, L. J., J. T. Weir, C. D. Brock, R. E. Glor, and W. Challenger. 2008. GEIGER: investigating evolutionary radiations. Bioinformatics 24:129-131.
Hautier, L. R. Lebrun, S. Saksiri, J. Michaux, M. Vianey-Liaud et al. 2011. Hystricognathy *vs* sciurognathy in the rodent jaw: a new morphometric assessment of hystricognathy applied to the living fossil *Laonastes* (Diatomyidae). *PLoS ONE* 6:1-11.
Heaney, L. R., D. S. Balete, M. R. M. Duya, M. V. Duya, S. A. Jansa, et al. 2016b. Doubling diversity: a cautionary tale of previously unsuspected mammalian diversity on a tropical oceanic island. Front. Biogeogr. 8:1-19.
Heaney, L. R., D. S. Balete, and E. A. Rickart. 2016a. The Mammals of Luzon Island. Johns Hopkins University Press, Baltimore.
Heaney, L. R., D. S. Balete, E. A. Rickart, M. J. Veluz, and S. A. Jansa. 2009. A new genus and species of small 'tree-mouse' (Rodentia, Muridae) related to the Philippine giant cloud rats. Bull. Am. Mus. Nat. His. 331:205-229.
Heaney, L. R., D. S. Balete, E. A. Rickart, M. J. Veluz, and S. A. Jansa. 2014a. Three new species of *Musseromys* (Muridae, Rodentia), the endemic Philippine tree mouse from Luzon Island. Am. Mus. Nov. 3802:1-27.
Heaney, L. R., D. S. Balete, E. A. Rickart, P. A. Alviola, M. R. M. Duya, et al. 2011. Chapter 1: seven new species and a new subgenus of forest mice (Rodentia: Muridae: *Apomys*) from Luzon Island. Fieldiana 2:1-60.
Heaney, L. R., D. S. Balete, M. J. Veluz, S. J. Steppan, J. A. Esselstyn, A. W. Pfeiffer, and E. A. Rickart. 2014b. Two new species of Philippine forest mice (*Apomys*, Muridae, Rodentia) from Lubang and Luzon Islands, with a rediscription of *Apomys sacobianus* Johnson, 1962. 2014b. Proc. Biol. Soc. Wash. 126(4): 395-413.
Heaney, L. R., E. A. Rickart, R. C. B. Utzurrum, and P. C. Gonzales. 1999. Mammalian diversity on Mount Isarog, a threatened center of endemism on southern Luzon Island, Philippines. Fieldiana 95:1-62.
Heaney, L. R. and B. R. Tabaranza. 2006. A new species of forest mouse, genus *Apomys* (Mammalia: Rodentia: Muridae), from Camiguin Island, Philippines. Fieldiana 106: 14-27.
Hoehna, S. 2013. Fast simulation of reconstructed phylogenies under global, time-dependent birth-death processes. Bioinformatics 29:1367–1374.
Howell, A. B. 1944. *Speed in Animals: Their Specialization for Running and Leaping*. University of Chicago Press, Chicago.
Hurvich, C. M. and C.-L. Tsai. 1989. Regression and time series model selection in small samples. Biometrika. 76:297-307.
Hutter, C. R., S. M. Lambert, and J. J.Wiens. 2017. Rapid diversification and time explain amphibian richness at different scales in the tropical Andes, Earth's most biodiverse hotspot. Am. Nat. 190:828–843.
Iwaniuk, A. N., S. M. Pellis, and I. Q. Whishaw. 1999. The relationship between forelimb morphology and behaviour in North American carnivores (Carnivora). Can. J. Zool. 77: 1064-1074.

Jablonski, D. 2008. Biotic interactions and macroevolution: Extensions and mismatches across scales and levels. Evolution Figure. 62:715–739.
Jablonski, D. and J. J. Sepkoski, Jr. 1996. Paleobiology, community ecology, and scales of ecological pattern. Ecology 77:1367-1378.
Jansa, S. A., F. K. Barker, and L. R. Heaney. 2006. The pattern and timing of diversification of Philippine endemic rodents: evidence from mitochondrial and nuclear gene sequences. Syst. Biol. 55:73–88.
Jansa, S. A., F. K. Barker, and R. S. Voss. 2014. The early diversification history of Didelphid marsupials: a window into South America's "splendid isolation". Evolution 68:684–695.
Jansa, S. A., S. M. Goodman, and P. K. Tucker. 1999. Molecular phylogeny and biogeography of the native rodents of Madagascar (Muridae: Nesomyinae): a test of the single-origin hypothesis. Cladistics 15:253–270.
Jansa, S. A., and M. Weksler. 2004. Phylogeny of muroid rodents: Relationships within and among major lineages as determined by IRBP gene sequences. Mol. Phylogenet. Evol. 31:256–276.
Jari Oksanen, F., G. Blanchet, M. Friendly, R. Kindt, P. Legendre, D. McGlinn, P. R. Minchin, et al. 2018. Vegan: community ecology package. R Package version 2.5-3. https://CRAN.R-project.org/package=vegan
Jønsson, K. A., J. P. Lessard, and R. E. Ricklefs. 2015. The evolution of morphological diversity in continental assemblages of passerine birds. Evolution Figure. 69:879–889.
Justiniano, R., J. J. Schenk, D. S. Balete, E. A. Rickart, J. A. Esselstyn, L. R. Heaney, and S. J. Steppan. 2015. Testing diversification models of endemic Philippine forest mice (Apomys) with nuclear phylogenies across elevational gradients reveals repeated colonization of isolated mountain ranges. J. Biogeogr. 42:51–64.
Kimura, Y., M. T. R. Hawkins, M. M. Mcdonough, L. L. Jacobs, and L. J. Flynn. 2015. Corrected placement of Mus - Rattus fossil calibration forces precision in the molecular tree of rodents. Sci. Rep. 5:1–9. Nature Publishing Group.
Klingenberg, C. P., K. Mebus, and J. C. Auffray. 2003. Developmental integration in a complex morphological structure: How distinct are the modules in the mouse mandible? Evol. Dev. 5:522–531.
Klingenberg, C. P. and W. Ekau. 1996. A combined morphometric and phylogenetic analysis of an ecomorphological trend: pelagization in Antarctic fishes (Perciformes: Nototheniidae). Biol. J. Linn. Soc. 59:143-177.
Kyriazis, C. C., J. M. Bates, and L. R. Heaney. 2017. Dynamics of genetic and morphological diversification in an incipient intra-island radiation of Philippine rodents (Muridae: *Bullimus*). J. Biogeogr. 44:2585-2594.
Lack, D. 1947. Darwin's Finches. Cambridge University Press, Cambridge.
Lanfear, R., B. Calcott, S. Y. W. Ho, and S. Guindon. 2012. PartitionFinder: Combined selection of partitioning schemes and substitution models for phylogenetic analyses. Mol. Biol. Evol. 29:1695–1701.
Lecompte, E., K. Aplin, C. Denys, F. Catzeflis, M. Chades, and P. Chevret. 2008. Phylogeny and biogeography of African Murinae based on mitochondrial and

nuclear gene sequences, with a new tribal classification of the subfamily. BMC Evol. Biol. 8:1–21.
Leuenberger, C., and D. Wegmann. 2010. Bayesian computation and model selection without likelihoods. Genetics 184:243–252.
Landis, M. J., J. G. Schraiber, and M. Liang. 2013. Phylogenetic analysis using Lévy processes: finding jumps in the evolution of continuous traits. Syst Biol. 62:193-204.
Losos, J. B. 2011. *Lizards in an Evolutionary Tree: Ecology and Adaptive Radiation of Anoles*. Univ. of California Press, Berkeley, CA.
Losos, J. B., T. R. Jackman, A. Larson, K. De Queiroz, and L. Rodríguez-schettino. 1998. Adaptive radiations of island lizards. Science 279:2115–2118.
Louette, G. and L. De Meester. 2007. Predation and priority effects in experimental zooplankton communities. Oikos 116:419-426.Lehmann, W. H. 1963. The forelimb architecture of some fossorial rodents. J. Morph. 113:59-76.
Maestri, R., L. R. Monteiro, R. Fornel, N. S. Upham, B. D. Patterson, and T. R. O. de Freitas. 2016. The ecology of a continental evolutionary radiation: is the radiation of sigmodontine rodents adaptive? Evolution 71:610–632.
Maestri, R., B. D. Patterson, R. Fornel, L. R. Monteiro, and T. R. O. de Freitas. 2016. Diet, bite force and skull morphology in the generalist rodent morphotype. J. Evol. Biol. 29:2191-2204.
MacPherson, J. M. 1988. Strategies that simplify the control of quadrupedal stance. I. Forces at the ground. J. Neurophys. 60: 204-217.
Mahler, D. L., L. J. Revell, R. E. Glor, and J. B. Losos, J.B. 2010. Ecological opportunity and the rate of morphological evolution in the diversification of Greater Antillean anoles. Evolution. 64:2731-2745.
Marcy, A. E., E. A. Hadly, E. Sherratt, K. Garland, and V. Weisbecker. 2016. Getting a head in hard soils: convergent skull evolution and divergent allometric patterns explain shape variation in a highly diverse genus of pocket gophers (*Thomomys*). BMC Evol. Biol. 16: 1-16.
Mathewson, M. A., M. A. Chapman, E. R. Hentzen, J. Fridén, and R. L. Lieber. 2012. Anatomical, architectural, and biochemical diversity of the murine forelimb muscles. J. Anat. 221: 443-451.
Mazel, F., A. Ø. Mooers, G. V. Dalla Riva, and M. W. Pennell. 2017. Conserving phylogenetic diversity can be a poor strategy for conserving functional diversity. Syst. Biol. 66:1019-1027.
McGowan, C. P. and C. E. Collins. 2018. Why do mammals hop? Understanding the ecology, biomechanics and evolution of bipedal hopping. J. Exp. Biol. 221:1-10.
Millar, J. S. and G. J. Hickling. 1990. Fasting endurance and the evolution of mammalian body size. Fun. Ecol. 4:5-12.
Miller, M. A., W. Pfeiffer, and T. Schwartz. 2010. Creating the CIPRES Science Gateway for inference of large phylogenetic trees. 2010 Gateway Computing Environments Workshop, GCE 2010. New Orleans, Louisiana.

Milne, N., S. F. Vizcaíno, and J. C. Fernicola. 2009. A 3D geometric morphometric analysis of digging ability in the extant and fossil cingulate humerus. J. of Zool. 278:48-56.
Moen, D. S., D. J. Irschick, and J. J. Wiens. 2013. Evolutionary conservatism and convergence both lead to striking similarity in ecology, morphology and performance across continents in frogs. Proc. R. Soc. B. 280: 1-9.
Moen, D. and H. Morlon. 2014. From dinosaurs to modern bird diversity: extending the time scale of adaptive radiation. PLoS Biol. 12:12-15.
Meyer, J. R., D. T. Dobias, J. S. Weitz, J. E. Barrick, R. T. Quick, and R. E. Lenski. 2012. Repeatability and Contingency in the Evolution of a Key Innovation in Phage Lambda. Science 335:428–432.
Miller, M. A., W. Pfeiffer, and T. Schwartz. 2010. Creating the CIPRES Science Gateway for inference of large phylogenetic trees. 2010 Gatew. Comput. Environ. Work. GCE 2010, doi: 10.1109/GCE.2010.5676129.
Múrria, C., S. Dolédec, A. Papadopoulou, A. P. Vogler, and N. Bonada. 2018. Ecological constraints from incumbent clades drive trait evolution across the tree-of-life of freshwater macroinvertebrates. Ecography (Cop.). 41:1049–1063.
Musser, G. G. and M. D. Carleton. 2005. Family Muridae *in* Wilson, D. E. and D. M. Reeder, eds. Mammal Species of the World: A Taxonomic and Geographic Reference. John Hopkins University Press, Baltimore.
Musser, G. G., L. R. Heaney, and B. R. Tabaranza. 1998. Philippine rodents: redefinitions of known species of *Batomys* (Muridae, Murinae) and description of a new species from Dinagat Island. Am. Mus. Nov. 3237:1-51.
Nee, S., A. Ø. Mooers, and P. H. Harvey. 1992. Tempo and mode of evolution revealed from molecular phylogenies. Proc. Nat. Acad. Sci. USA 89:8322–8326.
Nee, S., R. M. May, and P. H. Harvey. 1994. The reconstructed evolutionary process. Phil. Trans. Roy. Soc. B 344:305–311.
O'Leary, M. A., J. I. Bloch, J. J. Flynn, T. J. Gaudin, A. Giallombardo, N. P. Giannini, S. L. Goldberg, B. P. Kraatz, Z.-X. Luo, J. Meng, et al. 2013. The placental mammal ancestor and the post-K-Pg radiation of placentals. Science 339:662–667.
Orzack, S. H., and E. Sober. 2010. Adaptation, Phylogenetic Inertia, and the Method of Controlled Comparisons. Adapt. Optim. 45–63.
Patton, J. T. and M. H. Kaufman. 1995. The timing of ossification of the limb bones, and growth rates of various long bones of the fore and hind limbs of the prenatal and early postnatal laboratory mouse. J. Anat. 186: 175-185.
Pagel, M. 1999. Inferring the historical patterns of biological evolution. Nature 401:877–884.
Pagès, M., P.-H. Fabre, Y. Chaval, A. Mortelliti, V. Nicolas, K. Wells, J. R. Michaux, and V. Lazzari. 2016. Molecular phylogeny of South-East Asian arboreal murine rodents. Zool. Scr. 45:349–364.
Paradis, E., J. Claude, and K. Strimmer. 2004. APE: analyses of phylogenetics and evolution in R language. Bioinf. 20:289-290.
Parent, C. E. and B. J. Crespi. 2009. Ecological opportunity in adaptive radiation of Galápagos endemic land snails. Am. Nat. 174:898-905.

Pavan, S. E., S. A. Jansa, and R. S. Voss. 2016. Spatiotemporal diversification of a low-vagility Neotropical vertebrate clade (short-tailed opossums, Didelphidae: *Monodelphis*). J. Biogeogr. 43:1299–1309.

Pennell, M. W., R. G. FitzJohn, W. K. Cornwell, and L. J. Harmon. 2015. Model Adequacy and the Macroevolution of Angiosperm Functional Traits. Am. Nat. 186:E33–E50.

Pinto, G., D. L. Mahler, L. J. Harmon, and J. B. Losos. 2008. Testing the island effect in adaptive radiation: rates and patterns of morphological diversification in Caribbean and mainland *Anolis* lizards. Proc. Roy. Soc. B 275:2749–2757.

Polly, P. D., A. M. Lawing, A.-C. Fabre, and A. Goswami. 2013. Phylogenetic principal components analysis and geometric morphometrics. Hystrix, It. J. Mamm. 24:33-41.

Price, M. V. 1993. A functional-morphometric analysis of forelimbs in bipedal and quadrupedal heteromyid rodents. Biol. J. Linn. Soc. 50:339-360.

Pybus, O.G., and P.H. Harvey. 2000. Testing macro-evolutionary models using incomplete molecular phylogenies. Proc. R. Soc. B 267: 2267–2272.

R Core Team. 2015. R: A language and environment for statistical computing. R Foundation for Statistical Computing, Vienna, Austria.

R Core Team. 2018. R: A language and environment for statistical computing. R Foundation for Statistical Computing, Vienna, Austria.

Rabosky, D. L. 2006. LASER: a maximum likelihood toolkit for detecting temporal shifts in diversification rates from molecular phylogenies. Evolutionary Bioinformatics Online 2:273–276.

Rabosky, D. L. 2012. Testing the time-for-speciation effect in the assembly of regional biotas. Methods Ecol. Evol. 3:224–233.

Rabosky, D. L. 2014. Automatic detection of key innovations, rate shifts, and diversity-dependence on phylogenetic trees. PLoS One 9:e89543.

Rabosky, D. L., M. A. Cowan, A. L. Talaba, and I. J. Lovette. 2011. Species Interactions Mediate Phylogenetic Community Structure in a Hyperdiverse Lizard Assemblage from Arid Australia. Am. Nat. 178:579–595.

Rabosky, D. L., M. Grundler, C. Anderson, P. Title, J. J. Shi, J. W. Brown, H. Huang, and J. G. Larson. 2014. BAMMtools: an R package for the analysis of evolutionary dynamics on phylogenetic trees. Methods Ecol. Evol. 5:701–707.

Rabosky, D. L., and I. J. Lovette. 2008. Density-dependent diversification in North American wood warblers. Proc. R. Soc. B 275:2363–2371.

Rambaut, A., A. J. Drummond, and M. A. Suchard. 2013. Tracer MCMC Analysis Package.

Reddy, S., A. Driskell, D. L. Rabosky, S. J. Hackett, and T. S. Schulenberg. 2012. Diversification and the adaptive radiation of the vangas of Madagascar. Proc. R. Soc. B 279:2062–2071.

Revell, L. J. 2009. Size-correction and principal components for interspecific comparative studies. Evolution. 63:3258-3268.

Revell, L. J. 2012. Phytools: an R package for phylogenetic comparative biology (and other things). Methods Ecol. Evol. 3:217-223.

Revell, L. J. and D. C. Collar. 2009. Phylogenetic analysis of the evolutionary correlation using likelihood. Evolution. 63:1090-1100.

Ribas, C. C., R. G. Moyle, C. Y. Miyaki, and J. Cracraft. 2007. The assembly of montane biotas: linking Andean tectonics and climatic oscillations to independent regimes of diversification in *Pionus* parrots. Proc. Roy. Soc. B. 274:2399-2408Rickart, E. A., D. S. Balete, P. A. Alviola, M. J. Veluz, and L. R. Heaney. 2016. The mammals of Mt. Amuyao: a richly endemic fauna in the Central Cordillera of northern Luzon Island, Philippines. Mammalia 80:579-592.

Rickart, E. A., L. R. Heaney, D. S. Balete, and B. S. Tabaranza. 2011. Small mammal diversity along an elevational gradient in northern Luzon, Philippines. Mamm. Biol. 76: 12-21.

Rickart, E. A., L. R. Heaney, S. M. Goodman, and S. A. Jansa. 2005. Review of the Philippine genera *Chrotomys* and *Celaenomys* (Murinae) and description of a new species. Journal of Mammalogy 86(2):415-428.

Rohlf, F. J., and D. E. Slice. 1990. Extensions of the Procrustes Method for the Optimal Superimposition of Landmarks. Syst. Zool. 39:40–59.

Ricklefs, R. E. and E. Bermingham. 2002. The concept of the taxon cycle in biogeography. Glob. Ecol. Biogeogr. 11:353-361.

Rowe, K. C., A. S. Achmadi, and J. A. Esselstyn. 2014. Convergent evolution of aquatic foraging in a new genus and species (Rodentia: Muridae) from Sulawesi Island, Indonesia. Zootaxa. 3815(4):541-564.

Rowe, K. C., A. S. Achmadi, and J. A. Esselstyn. 2016. Repeated evolution of carnivory among Indo-Australian rodents. Evolution Figure. 70:653–665.

Rowe, K. C., K. P. Aplin, P. R. Baverstock, and C. Moritz. 2011. Recent and rapid speciation with limited morphological disparity in the genus Rattus. Syst. Biol. 60:188–203.

Rowe, K. C., M. L. Reno, D. M. Richmond, R. M. Adkins, and S. J. Steppan. 2008. Pliocene colonization and adaptive radiations in Australia and New Guinea (Sahul): Multilocus systematics of the old endemic rodents (Muroidea: Murinae). Mol. Phylogenet. Evol. 47:84–101.

Rowsey, D. M., L. R. Heaney, and S. A. Jansa. 2018. Diversification rates of the "Old Endemic" murine rodents of Luzon Island, Philippines are inconsistent with incumbency effects and ecological opportunity. Evolution. 72:1420–1435.

Rowsey, D. M., L. R. Heaney, and S. A. Jansa. 2019. Tempo and mode of mandibular shape and size evolution reveal mixed support for incumbency effects in two clades of island-endemic rodents (Muridae: Murinae). Evolution. evo.13737.

Ruta, M., K. D. Angielczyk, J. Fröbisch, and M. J. Benton. 2013. Decoupling of morphological disparity and taxic diversity during the adaptive radiation of anomodont therapsids. Proc. R. Soc. B. 280.

Sato, A. C. O'Huigin, H. Tichy, P. R. Grant, B. R. Grant, and J. Klein. 2001. On the origin of Darwin's finches. Mol. Biol. Evol. 18:299-311.

Samuels, J. X. and B. Van Valkenburgh. 2008. Skeletal indicators of locomotor adaptations in living and extinct rodents. J. Morph. 269: 1387-1411.

Sansalone, G., P. Colangelo, T. Kotsakis, A. Loy, R. Castiglia, et al. 2018. Influence of evolutionary allometry on rates of morphological evolution and disparity in strictly subterranean moles (Talpinae, Talpidae, Lipotyphla, Mammalia). J. Mamm. Evol. 25: 1-14.

Schenk, J. J., K. C. Rowe, and S. J. Steppan. 2013. Ecological opportunity and incumbency in the diversification of repeated continental colonizations by muroid rodents. Syst. Biol. 62:837–864.

Schluter, D. 1996. Adaptive radiation along genetic lines of least resistance. Evolution 50:1766-1774.

Schluter, D. 2000a. The ecology of adaptive radiation. New York, NY: Oxford University Press.

Schluter, D. 2000b. Ecological character displacement in adaptive radiation. Am. Nat. 156:S4-S16.

Schluter, D., and P. R. Grant. 1983. Determinants of morphological patterns in communities of Darwin's finches. Am. Nat. 123:175–196.

Schwarz, G. 1978. Estimating the dimension of a model. Ann. Stat. 6:461–464.

Sidlauskas, B. 2008. Continuous and arrested morphological diversification in sister clades of characiform fishes: a phylomorphospace approach. Evolution 62:3135-3156.

Silvestro, D., A. Antonelli, N. Salamin, and T. B. Quental. 2015. The role of clade competition in the diversification of North American canids. Proc. Natl. Acad. Sci. 112:8684–8689.

Simpson, G. G. 1953. *The Major Features of Evolution*. Columbia University Press, New York, 1953.

Skipwith, P. L., A. M. Bauer, T. R. Jackman, and R. A. Sadlier. 2016. Old but not ancient: coalescent species tree of New Caledonian geckos reveals recent post-inundation diversification. J. Biogeogr. 43:1266–1276.

Slater, G. J., L. J. Harmon, D. Wegmann, P. Joyce, L. J. Revell, and M. E. Alfaro. 2012. Fitting models of continuous trait evolution to incompletely sampled comparative data using approximate bayesian computation. Evolution Figure. 66:752–762.

Smissen, P. J., and K. C. Rowe. 2018. Repeated biome transitions in the evolution of Australian rodents. Mol. Phylogenet. Evol. 128:182–191.

Smith, M. F., and J. L. Patton. 1991. Variation in mitochondrial cytochrome b sequence in natural populations of South American Akodontine rodents (Muridae: Sigmodontinae). Mol. Biol. Evol. 8:85–103.

Stamatakis, A., P. Hoover, and J. Rougemont. 2008. A rapid bootstrap algorithm for the RAxML web servers. Syst. Biol. 57:758–771.

Stanhope, M. J., M. R. Smith, V. G. Waddell, C. A. Porter, M. S. Shivji, and M. Goodman. 1996. Mammalian evolution and the interphotoreceptor retinoid binding protein (IRBP) gene: convincing evidence for several superordinal clades. J. Mol. Evol. 43:83–92.

Stephens, P. R., and J. J. Wiens. 2003. Explaining species richness from continents to communities: the time-for-speciation effect in Emydid turtles. Am. Nat. 161:112–128.

Steppan, S. J., R. M. Adkins, and J. Anderson. 2004. Phylogeny and divergence-date estimates of rapid radiations in muroid rodents based on multiple nuclear genes. Syst. Biol. 53(4):533-553.

Steppan, S. J., R. M. Adkins, P. Q. Spinks, and C. Hale. 2005. Multigene phylogeny of the Old World mice, Murinae, reveals distinct geographic lineages and the declining utility of mitochondrial genes compared to nuclear genes. Mol. Phylogenet. Evol. 37:370–388.

Steppan, S. J., and J. J. Schenk. 2017. Muroid Rodent Phylogenetics: 900-species tree reveals increasing diversification rates. PLoS ONE 12:e0183070.

Sutherland, J. P. 1974. Multiple stable points in natural communities. Am. Nat. 108:859–873.

Tan, J., Z. Pu, W. A. Ryberg, and L. Jiang. 2012. Species phylogenetic relatedness, priority effects, and ecosystem functioning. Ecology 93:1164–1172.

Thomas, H., S. Sen, M. Khan, B. Battail, and G. Ligabue. 1982. The Lower Miocene fauna of Al-Sarrar (Eastern Province, Saudi Arabia). Atlal 5:109–136.

Thompson, C. J., N. I. Ahmed, T. Veen, C. L. Peichel, A. P. Hendry, et al. 2017. Many-to-one form-to-function mapping weakens parallel morphological evolution. Evolution 71:2738-2749.

Tobias, J. A., C. K. Cornwallis, E. P. Derryberry, S. Claramunt, R. T. Brumfield, and N. Seddon. 2014. Species coexistence and the dynamics of phenotypic evolution in adaptive radiation. 506:359-363.

Tokita, M., W. Yano, H. F. James, and A. Abzhanov. 2016. Cranial shape and evolution in adaptive radiations of birds: comparative morphometrics of Darwin's finches and Hawaiian honeycreepers. Phil. Trans. R. Soc. B 372:1–17.

Urban, M. C., and L. De Meester. 2009. Community monopolization: local adaptation enhances priority effects in an evolving metacommunity. Proc. R. Soc. B 276:4129–4138.

Uyeda, J. C., D. S. Caetano, and M. W. Pennell. 2015. Comparative analysis of principal components can be misleading. Syst. Biol. 64:677-689.

Verde Arregoitia, L. D., D. O. Fisher, and M. Schweizer. 2017. Morphology captures diet and locomotor types in rodents. R. Soc. Open Sci. 4:1–14.

Veyrunes, F., J. Britton-Davidian, T. J. Robinson, E. Calvet, C. Denys, P. Chevret. 2005. Molecular phylogeny of the African pygmy mice, subgenus *Nannomys* (Rodentia, Murinae, *Mus*): implications for chromosomal evolution. Mol. Phylo. Evol. 36(2):358-369.

Wainwright, P. C., M. E. Alfaro, D. I. Bolnick, and C. D. Hulsey. 2005. Many-to-one mapping of form to function: a general principle in organismal design? Int. Comp. Biol. 42:256-262.

Wainwright, P. C., W. L. Smith, S. A. Price, K. L. Tang, J. S. Sparks, L. A. Ferry, K. L. Kuhnm R. I. Eytan, and T. J. Near. 2012. The evolution of pharyngognathy: a phylogenetic and functional appraisal of the pharyngeal jaw key innovation in Labroid fishes and beyond. Syst. Biol. 61:1001-1027.

Webb, S. D. 1985. Late Cenozoic mammal dispersals between the Americas. *In* F. G. Stehli and S. D. Webb (eds.) *The Great American Biotic Interchange.* Plenum Press: New York. 357-386.

Weeks, B. C. and S. Claramunt. 2014. Dispersal has inhibited avian diversification in Australasian archipelagoes. Proc. R. Soc. B. 281:1-7.

Wegmann, D., C. Leuenberger, S. Neuenschwander, and L. Excoffier. 2010. ABCtoolbox: a versatile toolkit for approximate Bayesian computations. BMC Bioinf. 11:116–116.

Whishaw, I. Q. and B. L. K. Coles. 1996. Varieties of paw and digit movement during spontaneous food handling in rats: postures, bimanual coordination, preferences, and the effect of forelimb cortex lesions. Behav. Brain Res. 77: 135-148.

Whittaker, R. J., and J. M. Fernadez-Palacios. 2007. Island Biogeography: Ecology, Evolution, and Conservation. Oxford Univ. Press, Oxford.

Wiens, J. J., and C. H. Graham. 2005. Niche Conservatism: Integrating Evolution, Ecology, and Conservation Biology. Annu. Rev. Ecol. Evol. Syst. 36:519–539.

Yoder, J. B., E. Clancey, S. Des Roches, J. M. Eastman, L. Gentry,W. Godsoe, T. J. Hagey, D. Jochimsen, B. P. Oswald, J. Robertson, et al. 2010. Ecological opportunity and the origin of adaptive radiations. J. Evol. Biol. 23:1581–1596.

Young, N. M. and B. Hallgrímsson. 2005. Serial homology and the evolution of mammalian limb covariation structure. Evolution 59: 2691-2704.

Young, R. L., T. S. Haselkorn, and A. V. Badyaev. 2007. Functional equivalence of morphologies enables morphological and ecological diversity. Evolution 61: 2480-2492.

Yule, G. U. 1924. A mathematical theory of evolution, based on the conclusions of Dr. J. C. Willis, F.R.S. Philos. Trans. R. Soc. London Ser. B 213:21–87.

Zuri, I., I. Kaffe, D. Dayan, and J. Terkel. 1999. Incisor adaptation to fossorial life in the blind mole-rat, *Spalax ehrenbergi*. J. Mamm. 80:734-741.

APPENDIX 1. SUPPLEMENTARY MATERIAL FOR CHAPTER 1.

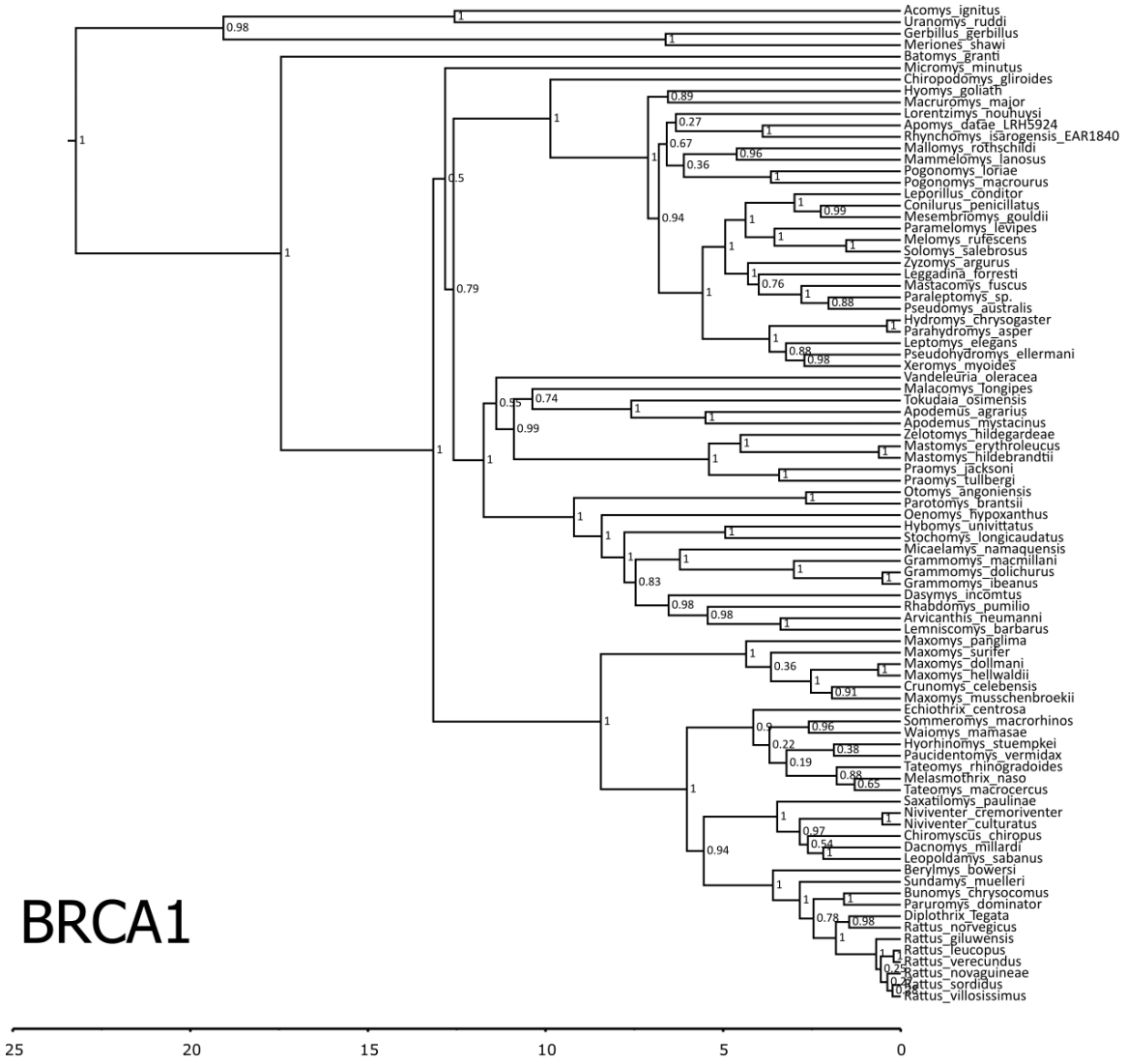

Appendix Figure 1.1. BRCA1 MCC gene tree inferred using BEAST.

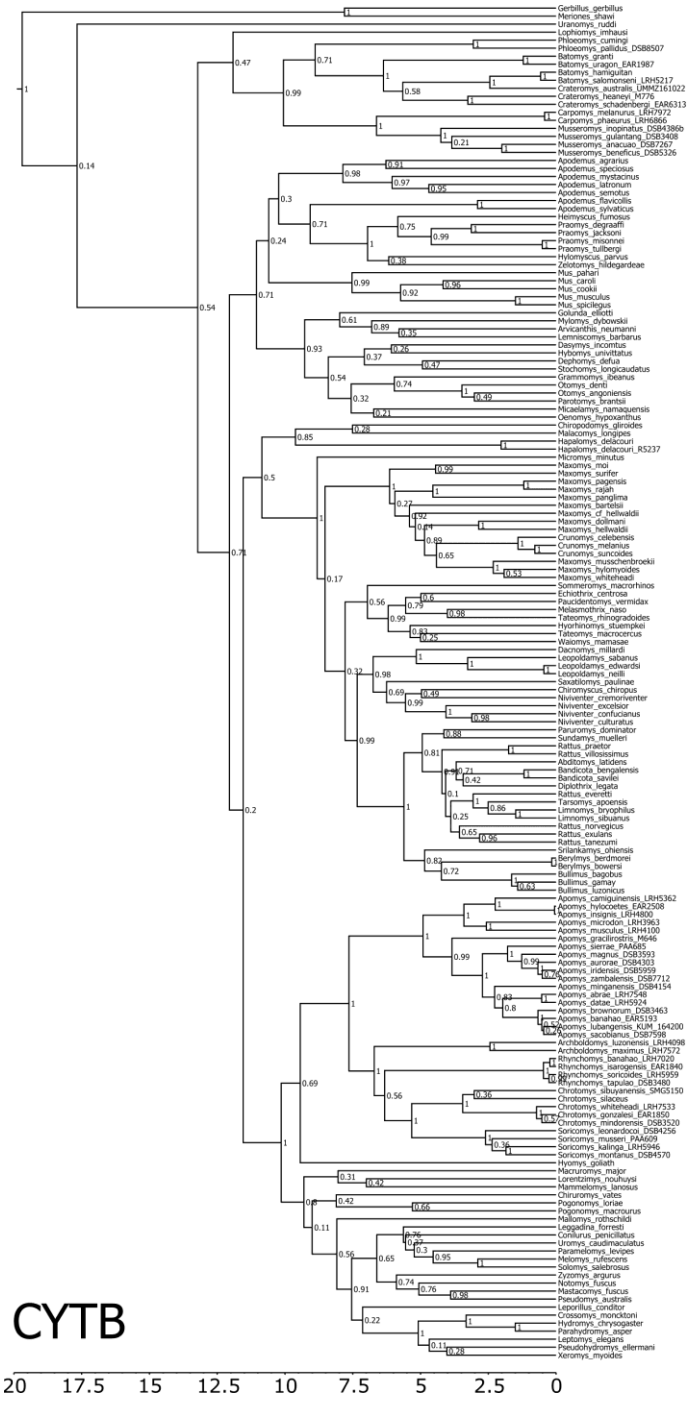

Appendix Figure 1.2. CYTB MCC gene tree inferred using BEAST.

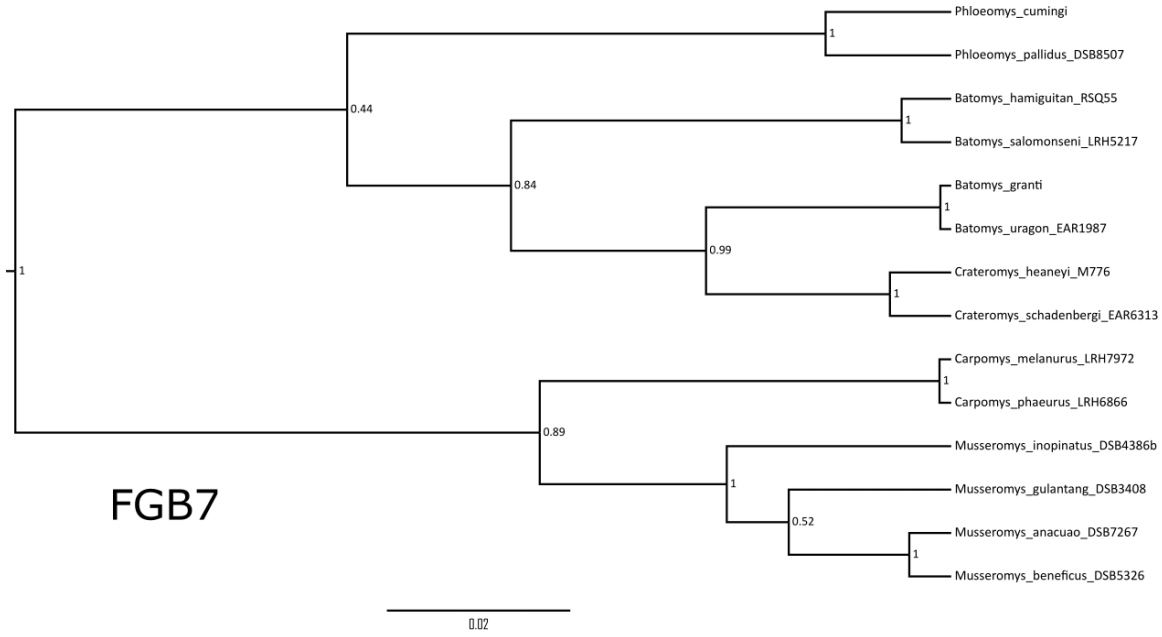

Appendix Figure 1.3. FGB7 MCC gene tree inferred using BEAST.

Appendix Figure 1.4. GHR MCC gene tree inferred using BEAST.

Appendix Figure 1.5. IRBP MCC gene tree inferred using BEAST.

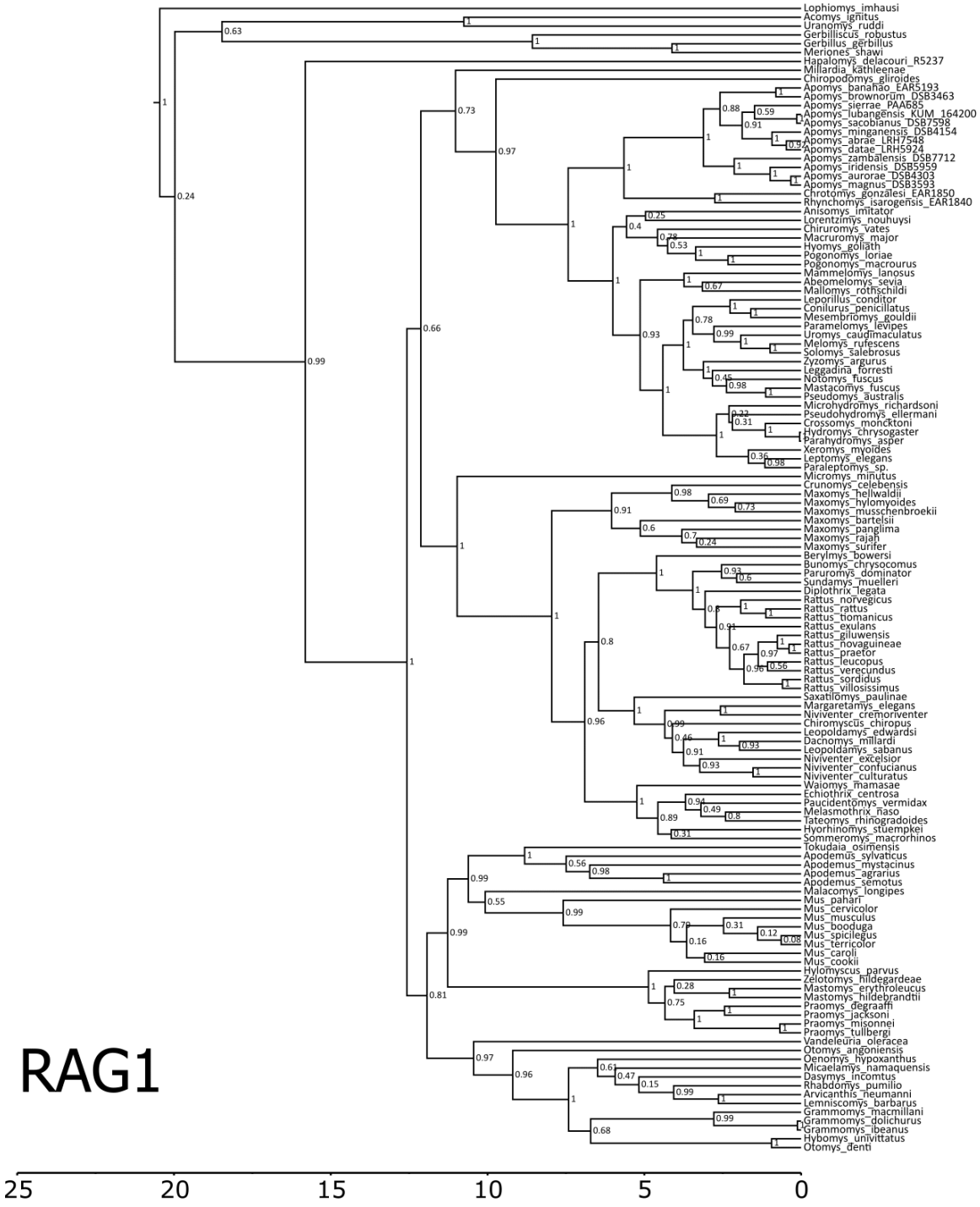

Appendix Figure 1.6. RAG1 MCC gene tree inferred using BEAST.

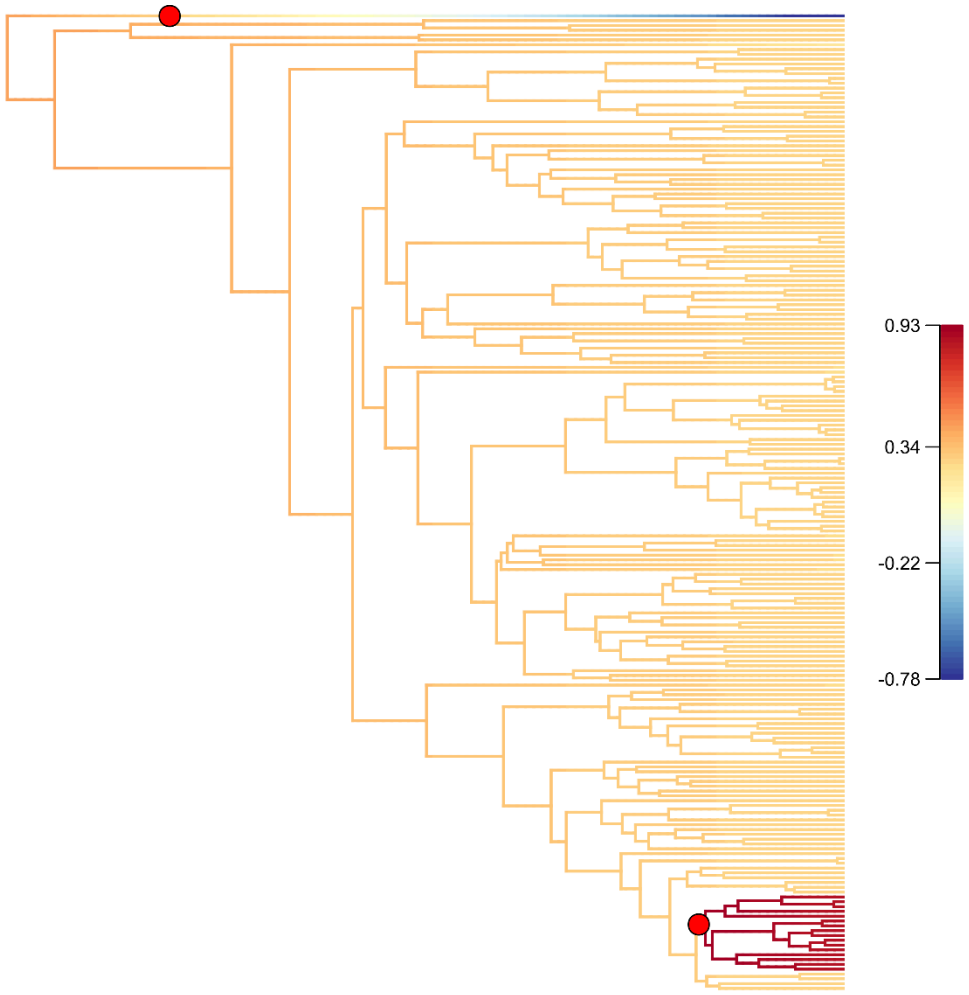

Appendix Figure 1.7. BAMM maximum a posteriori (MAP) rate configuration based on MCC tree. Branches are colored according to their net diversification rate, where warmer colors indicate more rapid diversification. Circles along branches represent inferred diversification rate shifts. A diversification rate shift on the branch leading to Lophiomyinae supports an increasing extinction rate through time, whereas a rate shift on the branch leading to Rattus-Tarsomys-Limnomys supports increased extinction and speciation rates and a higher overall diversification rate. Dashes boxes indicate lineages occurring on Luzon.

Appendix Figure 1.8. BAMM rate shift configurations sorted in order of frequency sampled, totaling 66.3% of the credible shift set. F represents proportion of sample with the given rate configuration. Branches are colored according to inferred net diversification rate, with darker colors representing higher rates. Circles along branches represent inferred rate shifts. Rate shifts were commonly sampled along the divergence from Lophiomyinae and the remainder of the tree and in Rattus-Tarsomys-Limnomys and allies of this clade.

Appendix Table 1.1. Full specimen matrix for phylogenetic analyses. Cells indicate GenBank numbers when available.

Species		cytb	GHR	IRBP	BRCA1	RAG1	Acp5	FGB7	Number Associated with Specimen
Abditomys latidens		Fabre pers. Comm.							
Abeomelomys sevia		EU349730	EU349793	EU349832	EU349682	EU349879	EU349607		
Acomys ignitus		JN247674		KC953348					
Anisomys imitator		EU349732	DQ019052	EU349833		DQ023471			
Apodemus agrarius		EU349658	DQ019054	AB096842	EU349733	DQ023472			
Apodemus flavicollis		JF819967	AM910943	AB032860					
Apodemus latronum		AM945834	GU908445	AB096852					
Apodemus mystacinus		KU375149	DQ019053	KU375167	KC953157	KC953476			
Apodemus semotus		AB033694	DQ019055	AB032862		AB164040			
Apodemus speciosus		AB164486	AB491493	AB032856					
Apodemus sylvaticus		AB033695		AB032863		AB164041			
Apomys abrae		HM371054				KM099834	KM099687		LRH7548 with cytb from LRH6282
Apomys aurorae		HM371036				KM099836	KM099689		DSB4303
Apomys banahao		HM371079				KM099837	KM099690		EAR5193
Apomys brownorum		HM371087				KM099839	KM099692		DSB3463
Apomys camiguinensis		AY324476							LRH5362
Apomys datae		AY324463	KJ607288	EU349836	KC953158	KC953478	KM099694		LRH5924
Apomys gracilirostris		AY324465							M646
Apomys hylocoetes		AY324467		KC953357					EAR2508
Apomys insignis		DQ191467		DQ191492					LRH4800

Apomys iridensis		KM099826				KM099873	KM099721		DSB6057 with RAG1 from DSB5959
Apomys lubangensis		KM099820				KM099867	KM099716		KUM_164200
Apomys magnus		HM371042	KU375161	KU375168		KM099855	KM099705		DSB3593
Apomys microdon		DQ324480	GQ405366	DQ191493					LRH3963
Apomys minganensis		HM371048				KM099859	KM099708		DSB4154
Apomys musculus		DQ191469	GQ405367	DQ191494					LRH4100
Apomys sacobianus		KM099818				KM099862	KM099710		DSB7598
Apomys sierrae		HM371011				KM099866	KM099714		PAA685
Apomys zambalensis		KM099829				KM099877	KM099727		DSB7712
Archboldomys luzonensis		AY687858	GQ405368	DQ191495					LRH4098
Archboldomys maximus		JQ898033	This study	JQ898078					LRH7572
Arvicanthis neumanni		AY349737	AY294948	KC953358	AY349648	AY294946			
Arvicanthis niloticus			KC953243	DQ022386					
Bandicota bengalensis		AM408336	AM910945	AM408331					
Bandicota savilei		HM217385		HM217623					
Batomys granti		Balete *et al.* 2015	This study	This study	EU349838			This study	DSB3851 with BRCA1 from EAR1822
Batomys hamiguitan		Balete *et al. 2015*	This study	This study				This study	RSQ49 cytb, ghr, irbp; RSQ55 fgb7
Batomys salomonseni		Balete et al. 2015	This study	This study				This study	LRH5217
Batomys uragon		DQ191470	This study	DQ191496				This study	EAR1987
Berylmys berdmorei		HM217432		HM217669					
Berylmys bowersi		AM408337			KC953160	DQ023457			

Bullimus bagobus		KX364504	GQ405369	DQ191498					
Bullimus gamay		KX364503	GQ405370	DQ191499					
Bullimus luzonicus		KX364537	GQ405371	DQ191500					
Bunomys chrysocomus			EU349795	EU349839	EU349667	EU349880			
Carpomys melanurus		This study	This study	This study				This study	LRH7972
Carpomys phaeurus		DQ191475	GQ405373	DQ191501				This study	LRH6866
Chiromyscus chiropus		EU349739	EU349796	EU349840	EU349665	EU349881	EU349609		
Chiropodomys gliroides		KJ607274	KJ607289	KJ607299	EU349674	EU349882			
Chiruromys vates		EU349741	KJ607290	KJ607300		EU349883	EU349611		
Chrotomys gonzalesi		EU389742	KJ607291	EU349843		EU349884			EAR1850
Chrotomys mindorensis		JQ898035	This study	This study					DSB3520
Chrotomys sibuyanensis		AY687862							SMG5150
Chrotomys silaceus		AY687859	GQ405377	DQ191502					LRH6894 with cytb from LRH6364
Chrotomys whiteheadi		JQ898045		JQ898074					LRH7533
Colomys goslingi			AM910948	DQ022395					
Conilurus penicillatus		EU349743	DQ019057	EU349844	EU349694	DQ023467			
Crateromys australis		This study							UMMZ161022
Crateromys heaneyi		This study	This study	This study				This study	M776
Crateromys schadenbergi		This study	This study	This study				This study	EAR6313
Crossomys moncktoni		KJ607276	KJ607292	KJ607310		KJ607310			

Crunomys celebensis		KC878028	KC878172	KC878203	KJ607264	KJ607311		
Crunomys melanius		DQ191477	GQ405379	DQ191506				
Crunomys suncoides		DQ191478		DQ191507				
Dacnomys millardi		JQ55897	DQ019058	JQ755961	KC953169	DQ023459		
Dasymys incomtus		EU349744	EU349798	KC878207	EU349653	KC953489		
Dephomys defua		KU375150		KU375169				
Diplothrix legata		AB033696	EU349799	AB033706	EU349670	AB164042	EU349612	
Echiothrix centrosa		KP210088	KP2100090	KP210092	KP2100084	KP210094		
Gerbilliscus robustus			AY294920	AY326113		AY294949		
Gerbillus gerbillus		KR089023	DQ019049	EU349846	EI349700	DQ23452	DQ023416	
Golunda elliotti		AM408338	AM910951	AM408332				
Grammomys dolichurus			EU349800	EU349847	EU349651	EU349887		
Grammomys ibeanus		KJ607277	EU349801	KC953380	KC953174	KC953503	EU349614	
Grammomys macmillani			EU349802	EU349848	KC953175	EU349888	EI349615	
Hapalomys delacouri Genbank		KJ772322		KJ772369				
Hapalomys delacouri R5237		Pages et al. 2016	Pages et al. 2016	Pages et al. 2016		Pages et al. 2016		
Heimyscus fumosus		AF518333	AM910953	DQ022397				
Hybomys univittatus		KJ607278	DQ019059	KC953383	KC953181	DQ023462	DQ023428	
Hydromys chrysogaster		EU349748	EU349804	EU349849	EU349699	EU349889		
Hylomyscus parvus		KU375151	KU375160	DQ022399		DQ023479		
Hylomyscus stella			AM90955	AM408320				
Hyomys goliath		EU349750	EU349805	KC953384	EU349679	EU349891	DQ070375	
Hyorhinomys stuempkei		KP210087	KP210089	KP210091	KP210085	KP210093		
Leggadina forresti		EU349751	DQ019061	EU349850	EU349686	DQ023468	DQ023437	

Lemniscomys barbarus		KU375152	DQ019062	KC953387	KC953184	DQ023461	DQ023426	
Lemniscomys striatus			AM910956	AM408321				
Leopoldamys edwardsi		KJ607279	KY069109	KY068527		KY068692		
Leopoldamys neilli		HM217460		HM217697				
Leopoldamys sabanus		KJ607280	DQ019063	KJ607302	KC953186	KC953153		
Leporillus conditor		EU349752	EU349806	EU349851	EU349692	EU349892	DQ070376	
Leptomys elegans		EU349753	EU349807	EU349852	EU349697	EU349893	EU349619	
Limnomys bryophilus		DQ191479	GQ405380	DQ191508				
Limnomys sibuanus		DQ191480	GQ405381	DQ191509				
Lophiomys imhausi		KR089025		AY326090		KC953514	KR088988	
Lorentzimys nouhuysi		EU349755	GQ405383	KC953392	EU349680	EU349894		
Macruromys major		EU349756	EU349809	EU349853	EU349678	EU349895	EU349620	
Malacomys longipes		EU349757	DQ019064	DQ022393	EU349656	DQ023474		
Mallomys rothschildi		EU349758	EU349810	EU349854	EU349681	EU349896	EU349621	
Mammelomys lanosus		EU349759	EU349811	EU349855	KC953188	EU349897	EU349622	
Margaretamys elegans			KC953274	KC953394		KC953518		
Mastacomys fuscus		EU349760	EU349812	EU349856	EU349687	EU349898	DQ070378	
Mastomys erythroleucus			AM910959	AM408335	KC953189	KC953519		
Mastomys hildebrandti			AY294916	KC953395	AY295001	KC953520		
Maxomys bartelsii		KC878032	KC878173	KC878211		DQ023460		
Maxomys cf. hellwaldii		KC878039	KC878174	KC878212				
Maxomys dollmani		KC878035	KC878175	KC878213	KC607265			

Maxomys hellwaldii		KC878044	KC878176	KC878214	KJ607314	KJ607266		
Maxomys hylomyoides		kC878050	KC878179	KC878218		KJ607315		
Maxomys moi		JN105094	KF154081	JN105086				
Maxomys musschenbroekii		KJ607281	KJ607293	KJ607304	KJ607267	KJ607316		
Maxomys pagensis		KC878128	KC878186	KC878225				
Maxomys panglima		KC878129	KC878187	KC878226	KJ607268	KJ607317		
Maxomys rajah		KC878135	KC878195	KC878228		KJ607318		
Maxomys surifer		HM217445	KM397261	HM217682	KC953190	KM397347		
Maxomys whiteheadi		HQ877148	KC878193	KC878234				
Melasmothrix naso		KJ607283	KJ607295	KJ607306	KJ607270	KJ607319	EU349264	
Melomys rufescens		EU349764	EU349816	EU349860	EU349690	EU349902	EU349626	
Meriones shawi		KR089031	AF332021	KC953400	AF332048	AY294947		
Mesembriomys gouldii			EU349817	EU349861	EU349693	EU349903	DQ070382	
Micaelamys namaquensis		EU349731	AY294914		EU349649	AY294941		
Microhydromys richardsonii			KU375162	KU375170		KU375184		
Micromys minutus		AB0333697	EU349818	AB033710	EU349664	AB125847		
Millardia kathleenae			AM910963	KC953403		EU349905		
Mus booduga				AB125796		Schenk *et al.* 2013 Supplementary Information		
Mus caroli		KU375153		KU375171		KU375177		
Mus cervicolor				AB125799		Schenk *et al.* 2013 Supplementary Information		
Mus cookii		AY057813	KC953279	KC953404		KU375178		

Mus musculus		AF520621	M33324	JX457616		AY214462			
Mus pahari		EU349767	KC953280	AJ698893		EU349906	EU349629		
Mus spicilegus		KU375154	KU375159	AJ698882		KU375179			
Mus terricolor				AB125810		Schenk *et al.* 2013 Supplementary Information			
Musseromys anacuao		Heaney *et al*. 2014	This study	This study				This study	DSB7267
Musseromys beneficus		Heaney *et al*. 2014	This study	This study				This study	DSB5326
Musseromys gulantang		Heaney *et al*. 2009	GQ405384	GQ405364				This study	DSB3408
Musseromys inopinatus		Heaney *et al*. 2014	This study	This study				This study	DSB4386b
Mylomys dybowskii		AF141212	AM901965	EU292146					
Myomyscus brockmani			AM910966	DQ022407					
Niviventer confucianus		KY068648	KY068976	KY068483		KY068648			
Niviventer cremoriventer		KJ607284	DQ019067	KC953417	KC953198	KC953541			
Niviventer culturatus		KY068785	KY068949	KY068456	KC953199	KY068621			
Niviventer excelsior		KY068715	KY068877	KY068383		KY068550			
Notomys fuscus		EU349768	KC953295	EU360811		EU349907	DQ070379		
Oenomys hypoxanthus		EU349769	DQ019069	EU349865	EU349654	EU349908	DQ023464		
Otomys anchietae			GQ405388	AY326101					
Otomys angoniensis		EU349770	EU349819		EU349647	EU349909	EU349630		
Otomys denti		EU874449	KC953305	KC953428		KC953552			
Parahydromys asper		EU349771	EU349820	EU349866	EU349698	EU349910	EU349631		
Paraleptomys sp.			KU375163	KU375172	KU375144	KU375180			

Paramelomys levipes		EU349772	EU349821	EU349867	EU349689	EU349911	EU349632		
Parotomys brantsii		EU349773	AY294912	KC953432	EU349646				
Paruromys dominator		KC878166`	KC878199	KJ607307	KJ607271	KJ607320			
Paucidentomys vermidax		KJ607286	KJ607297	KJ607308	KJ607272	KJ607321			
Phloeomys cumingi		This study	This study	AY326103				This study	cytb and FGB LRH8439; GHR and IRBP EAR1699
Phloeomys pallidus		This study	This study	This study				This study	DSB8507; cytb found in database
Pogonomys loriae		EU349776	EU349823	EU349868	EU349683	EU349912	EU349635		
Pogonomys macrourus		EU349777	EU349824	EU349869	EU349684	EU349913	EU349636		
Pogonomys sylvestris			GQ405389	GQ405365					
Praomys degraaffi		AF518358	KC953315	DQ022410		KC953562			
Praomys jacksoni		EU349778	DQ109071	KC953443	EU349663	DQ023477	DQ070386		
Praomys misonnei		EU519356	KC953316	KC953444		KC953563			
Praomys tullbergi		EU349779	DQ019072	DQ022413	EU349662	DQ023478	DQ070387		
Pseudohydromys ellermani		EU349763	EU349814	EU349858	EU349695	EU349900	EU349623		
Pseudomys australis		EU349780	DQ019073	EU349780	EU349688	DQ023469	DQ070377		
Rattus everetti		DQ191485	GQ405390	DQ191513					
Rattus exulans		DQ191486	DQ019074	KC953446		DQ023455			
Rattus giluwensis				HQ334607	HQ334419	HQ334673			
Rattus leucopus			EU349825		EU349672	EU349914	EU349637		
Rattus norvegicus		EU349782		EU349671	EU349671	AY294938			
Rattus novaguineae			KC953319	KC953447	KC953210	KC953566			
Rattus praetor		DQ191487	GQ405392	KC953448		KC953567			

Rattus rattus			AM910976	HM217606		HQ334643			
Rattus sordidus				HQ334599	HQ334411	HQ334691			
Rattus tanezumi		DQ191488	GQ405393	DQ191515					
Rattus tiomanicus			KC953320	KC953449		KC953568	KR088997		
Rattus verecundus			KC953321		KC953211	KC953961			
Rattus villosissimus		EU349783	EU349826	HQ334576	EU349673	EU349915	DQ070372		
Rhabdomys pumilio			AY294913	EU349871	EU349650	AY294940			
Rhycnhomys isarogensis		AY324462		KC953453	EU349677	AY294944			EAR1840
Rhynchomys banahao		JQ898050							LRH7020
Rhynchomys soricoides		JQ898052							LRH5959
Rhynchomys tapulao		JQ898056							DSB3480
Saxatilomys paulinae		KU375155	KF154067	KU375173	KU375145	KU375181			
Solomys salebrosus		EU349785	EU349827	EU349872	EU349691	EU349917	EU349638		
Sommeromys macrorhinos		KU375156	KU375164	KU375174	KU375146	KU375182			
Soricomys kalinga		JQ898059		This study					LRH5946
Soricomys leonardocoi		JQ898062		JQ898077					DSB4256
Soricomys montanus		JQ898066		JQ898076					DSB4570
Soricomys musseri		JQ898071		JQ898075					PAA609
Srilankamys ohiensis		JN009856	JN009860	JN009857					
Stenocephalomys albipes			AM910977	DQ022404					
Stochomys longicaudatus		EU349786	DQ019076	KC953458	EU349652		DQ070393		
Sundamys muelleri		EU349787	DQ019077	AY3326111	EU349668	DQ023456			
Tarsomys apoensis		DQ191491	GQ405395	DQ191519					

Tateomys macrocercus		KU375157	KU375165	KU375175	KU375147			
Tateomys rhinogradoides		KU375158	KU375166	KU375176	KU375148	KU375183		
Tokudaia osimensis			EU349828	EU349874	EU349659	AB164046	EU349640	
Uranomys ruddi		HM635858	DQ019051	EU360812	EU349642	DQ023454		
Uromys caudimaculatus		EU349789	DQ019079	EU349875		DQ023470	JN114352	
Vandeleuria oleracea			EU349829	EU349876	EU349655	EU349919	EU349641	
Waiomys mamasae		KJ607287	KJ607298	KJ607309	KJ607273	KJ607322		
Xeromys myoides		EU349790	EU349830	EU349877	EU349696	EU349920	DQ070380	
Zelotomys hildegardeae		EU349791	DQ019080	DQ022396	EU349661	DQ23476	DQ070388	
Zyzomys argurus		EU349792	EU349831	EU349878	EU349685	EU349921	DQ070381	

Appendix Table 1.2. Clade-specific sampling probabilities used in the BAMM analysis accompanied by source(s) used for justifying the number of species in the clade.

Taxon	Group	Taxa Included	Sampling Prob.	Total Taxa in Clade	Authority
Abeomelomys_sevia	Abeomelomys	1	1	1	Musser and Carleton (2005), Rowe et al. (2008)
Abditomys_latidens	abtr	1	0.5	2	Musser and Carleton (2005)
Anisomys_imitator	Anisomys	1	1	1	Musser and Carleton (2005), Rowe et al. (2008)
Apodemus_agrarius	Apode	7	0.35	20	Musser and Carleton (2005)
Apodemus_flavicollis	Apode	7	0.35	20	Musser and Carleton (2005)
Apodemus_latronum	Apode	7	0.35	20	Musser and Carleton (2005)
Apodemus_mystacinus	Apode	7	0.35	20	Musser and Carleton (2005)
Apodemus_semotus	Apode	7	0.35	20	Musser and Carleton (2005)
Apodemus_speciosus	Apode	7	0.35	20	Musser and Carleton (2005)
Apodemus_sylvaticus	Apode	7	0.35	20	Musser and Carleton (2005)
Apomys_abrae	Apom	18	0.9	20	Heaney et al. (2016a)
Apomys_aurorae	Apom	18	0.9	20	Heaney et al. (2016a)
Apomys_banahao	Apom	18	0.9	20	Heaney et al. (2016a)
Apomys_brownorum	Apom	18	0.9	20	Heaney et al. (2016a)
Apomys_camiguinensis	Apom	18	0.9	20	Heaney and Tabaranza (2006), Heaney et al. (2016a)
Apomys_datae	Apom	18	0.9	20	Heaney et al. (2016a)
Apomys_gracilirostris	Apom	18	0.9	20	Heaney et al. (2016a)
Apomys_hylocoetes	Apom	18	0.9	20	Steppan et al. (2005), Heaney et al. (2016a)
Apomys_insignis	Apom	18	0.9	20	Steppan et al. (2005), Heaney et al. (2016a)
Apomys_iridensis	Apom	18	0.9	20	Heaney et al. (2014b), Heaney et al. (2016a)
Apomys_lubangensis	Apom	18	0.9	20	Heaney et al. (2014b), Heaney et al. (2016a)
Apomys_magnus	Apom	18	0.9	20	Heaney et al. (2016a)
Apomys_microdon	Apom	18	0.9	20	Heaney et al. (2016a)

Apomys_minganensis	Apom	18	0.9	20	Heaney et al. (2016a)
Apomys_musculus	Apom	18	0.9	20	Heaney et al. (2016a)
Apomys_sacobianus	Apom	18	0.9	20	Heaney et al. (2014b), Heaney et al. (2016a)
Apomys_sierrae	Apom	18	0.9	20	Heaney et al. (2016a)
Apomys_zambalensis	Apom	18	0.9	20	Heaney et al. (2016a)
Archboldomys_luzonensis	ar	2	1	2	Balete et al. (2012)
Archboldomys_maximus	ar	2	1	2	Balete et al. (2012)
Arvicanthis_neumanni	Arvic	2	0.285714	7	Musser and Carleton (2005)
Arvicanthis_niloticus	Arvic	2	0.285714	7	Musser and Carleton (2005)
Bandicota_bengalensis	Ban	2	0.666667	3	Musser and Carleton (2005)
Bandicota_savilei	Ban	2	0.666667	3	Musser and Carleton (2005)
Batomys_granti	bat	2	0.666667	3	Musser *et al*. (1998); Musser and Carleton (2005), Balete et al. (2015)
Batomys_uragon	bat	2	0.666667	3	Musser *et al*. (1998); Musser and Carleton (2005), Balete et al. (2015)
Berylmys_berdmorei	Beryl	2	0.5	4	Musser and Carleton (2005)
Berylmys_bowersi	Beryl	2	0.5	4	Musser and Carleton (2005)
Bullimus_bagobus	Bul	3	0.75	4	Kyriazis et al. (2017)
Bullimus_gamay	Bul	3	0.75	4	Kyriazis et al. (2017)
Bullimus_luzonicus	Bul	3	0.75	4	Kyriazis et al. (2017)
Bunomys_chrysocomus	Bun	1	0.166667	6	Musser and Carleton (2005)
Carpomys_melanurus	ca	2	1	2	Heaney et al. (2016a)
Carpomys_phaeurus	ca	2	1	2	Heaney et al. (2016a)
Chrotomys_gonzalesi	ch	5	1	5	Rickart et al. (2005)
Chrotomys_mindorensis	ch	5	1	5	Rickart et al. (2005)
Chrotomys_sibuyanensis	ch	5	1	5	Rickart et al. (2005)
Chrotomys_silaceus	ch	5	1	5	Rickart et al. (2005)
Chrotomys_whiteheadi	ch	5	1	5	Rickart et al. (2005)
Chiromyscus_chiropus	Chiromyscus	1	1	1	Musser and Carleton (2005)

Chiropodomys_gliroides	Chiropodomys	1	0.166667	6	Musser and Carleton (2005)
Chiruromys_vates	Chiruromys	1	0.333333	3	Musser and Carleton (2005), Rowe et al. (2008)
Colomys_goslingi	Colom	1	1	1	Musser and Carleton (2005)
Conilurus_penicillatus	Conilurus	1	0.5	2	Musser and Carleton (2005), Rowe et al. (2008)
Crateromys_heaneyi	cr	2	0.666667	3	Musser and Carleton (2005)
Crateromys_schadenbergi	cr	2	0.666667	3	Musser and Carleton (2005)
Crossomys_moncktoni	Crossomys	1	1	1	Musser and Carleton (2005), Rowe et al. (2008)
Dacnomys_millardi	Dac	1	1	1	Musser and Carleton (2005)
Dasymys_incomtus	Dasym	1	0.111111	9	Musser and Carleton (2005)
Acomys_ignitus	Deomyinae	2	0.090909	22	Musser and Carleton (2005)
Uranomys_ruddi	Deomyinae	2	0.090909	22	Musser and Carleton (2005)
Dephomys_defua	Depho	1	0.5	2	Musser and Carleton (2005)
Diplothrix_legata	Diplo	1	1	1	Musser and Carleton (2005)
Echiothrix_centrosa	Echio	1	0.5	2	Musser and Carleton (2005)
Gerbilliscus_robustus	Gerbillinae	3	0.028302	106	Musser and Carleton (2005); Steppan and Schenk (2017) for polyphyly
Gerbillus_gerbillus	Gerbillinae	3	0.028302	106	Musser and Carleton (2005)
Meriones_shawi	Gerbillinae	3	0.028302	106	Musser and Carleton (2005)
Golunda_elliotti	Golunda	1	1	1	Musser and Carleton (2005)
Grammomys_dolichurus	Gramm	3	0.076923	39	Musser and Carleton (2005); Steppan and Schenk (2017)
Grammomys_ibeanus	Gramm	3	0.076923	39	Musser and Carleton (2005); Steppan and Schenk (2017)
Grammomys_macmillani	Gramm	3	0.076923	39	Musser and Carleton (2005); Steppan and Schenk (2017)
Hapalomys_delacouri_R5237	Hap	1	0.5	2	Musser and Carleton (2005)
Heimyscus_fumosus	Heimy	1	1	1	Musser and Carleton (2005)
Hybomys_univittatus	Hybom	1	0.142857	7	Musser and Carleton (2005)
Hydromys_chrysogaster	Hydromys	1	0.333333	3	Musser and Carleton (2005), Rowe et al. (2008)
Hylomyscus_parvus	Hylom	2	0.25	8	Musser and Carleton (2005)

Hylomyscus_stella	Hylom	2	0.25	8	Musser and Carleton (2005)
Hyomys_goliath	Hyomys	1	0.5	2	Musser and Carleton (2005), Rowe et al. (2008)
Hyorhinomys_stuempkei	Hyorhinomys	1	1	1	Esselstyn et al. (2015)
Leggadina_forresti	Leggadina	1	0.5	2	Musser and Carleton (2005), Rowe et al. (2008)
Lemniscomys_barbarus	Lemni	2	0.181818	11	Musser and Carleton (2005)
Lemniscomys_striatus	Lemni	2	0.181818	11	Musser and Carleton (2005)
Leopoldamys_edwardsi	Leo	3	0.5	6	Musser and Carleton (2005)
Leopoldamys_neilli	Leo	3	0.5	6	Musser and Carleton (2005)
Leopoldamys_sabanus	Leo	3	0.5	6	Musser and Carleton (2005)
Leporillus_conditor	Leporillus	1	0.5	2	Musser and Carleton (2005), Rowe et al. (2008)
Leptomys_elegans	Leptomys	1	0.25	4	Musser and Carleton (2005), Rowe et al. (2008)
Lophiomys_imhausi	Lop	1	1	1	Musser and Carleton (2005)
Lorentzimys_nouhuysi	Lorentzimys	1	1	1	Musser and Carleton (2005), Rowe et al. (2008)
Macruruomys_major	Macruromys	1	0.5	2	Musser and Carleton (2005), Rowe et al. (2008)
Malacomys_longipes	Malac	1	0.333333	3	Musser and Carleton (2005)
Mallomys_rothschildi	Mallomys	1	0.333333	3	Musser and Carleton (2005), Rowe et al. (2008)
Mammelomys_lanosus	Mammelomys	1	0.5	2	Musser and Carleton (2005), Rowe et al. (2008)
Margaretamys_elegans	Marg	1	0.333333	3	Musser and Carleton (2005)
Mastacomys_fuscus	Mastacomys	1	1	1	Musser and Carleton (2005), Rowe et al. (2008)
Mastomys_erythroleucus	Masto	2	0.222222	9	Steppan et al. (2004); Musser and Carleton (2005)
Mastomys_hildebrandti	Masto	2	0.222222	9	Steppan et al. (2004); Musser and Carleton (2005)
Crunomys_celebensis	MaxCru	15	0.555556	27	Achmadi et al. (2013) suggested potentially 27 species including the ones unable to be sampled
Crunomys_melanius	MaxCru	15	0.555556	27	Achmadi et al. (2013) suggested potentially 27 species including the ones unable to be sampled
Crunomys_suncoides	MaxCru	15	0.555556	27	Achmadi et al. (2013) suggested potentially 27 species including the ones unable to be sampled
Maxomys_bartelsii	MaxCru	15	0.555556	27	Achmadi et al. (2013) suggested potentially 27 species including the ones unable to be sampled

Maxomys_cf._hellwaldii	MaxCru	15	0.555556	27	Achmadi et al. (2013) suggested potentially 27 species including the ones unable to be sampled
Maxomys_dollmani	MaxCru	15	0.555556	27	Achmadi et al. (2013) suggested potentially 27 species including the ones unable to be sampled
Maxomys_hellwaldii	MaxCru	15	0.555556	27	Achmadi et al. (2013) suggested potentially 27 species including the ones unable to be sampled
Maxomys_hylomyoides	MaxCru	15	0.555556	27	Achmadi et al. (2013) suggested potentially 27 species including the ones unable to be sampled
Maxomys_moi	MaxCru	15	0.555556	27	Achmadi et al. (2013) suggested potentially 27 species including the ones unable to be sampled
Maxomys_musschenbroekii	MaxCru	15	0.555556	27	Achmadi et al. (2013) suggested potentially 27 species including the ones unable to be sampled
Maxomys_pagensis	MaxCru	15	0.555556	27	Achmadi et al. (2013) suggested potentially 27 species including the ones unable to be sampled
Maxomys_panglima	MaxCru	15	0.555556	27	Achmadi et al. (2013) suggested potentially 27 species including the ones unable to be sampled
Maxomys_rajah	MaxCru	15	0.555556	27	Achmadi et al. (2013) suggested potentially 27 species including the ones unable to be sampled
Maxomys_surifer	MaxCru	15	0.555556	27	Achmadi et al. (2013) suggested potentially 27 species including the ones unable to be sampled
Maxomys_whiteheadi	MaxCru	15	0.555556	27	Achmadi et al. (2013) suggested potentially 27 species including the ones unable to be sampled
Melasmothrix_naso	Melasmothrix	1	1	1	Musser and Carleton (2005)
Melomys_rufescens	Melomys	1	0.055556	18	Musser and Carleton (2005), Rowe et al. (2008)
Mesembriomys_gouldii	Mesembriomys	1	0.5	2	Musser and Carleton (2005), Rowe et al. (2008)
Micaelamys_namaquensis	Micae	1	0.5	2	Musser and Carleton (2005)
Microhydromys_richardsonii	Microhydromys	1	1	1	Musser and Carleton (2005), Rowe et al. (2008)
Micromys_minutus	Micromys	1	1	1	Musser and Carleton (2005)
Millardia_kathleenae	Milla	1	0.25	4	Musser and Carleton (2005)
Batomys_hamiguitan	mindanaomys	3	0.75	4	Musser *et al*. (1998); Balete *et al*. (2008); Results of this study
Batomys_salomonseni	mindanaomys	3	0.75	4	Musser *et al*. (1998); Results of this study

Crateromys_australis	mindanaomys	3	0.75	4	Musser *et al*. (1998); Results of this study
Mus_booduga	Mus	8	0.205128	39	Musser and Carleton (2005); Veyrunes et al. (2005)
Mus_caroli	Mus	8	0.205128	39	Musser and Carleton (2005); Veyrunes et al. (2005)
Mus_cervicolor	Mus	8	0.205128	39	Musser and Carleton (2005); Veyrunes et al. (2005)
Mus_cookii	Mus	8	0.205128	39	Musser and Carleton (2005); Veyrunes et al. (2005)
Mus_musculus	Mus	8	0.205128	39	Musser and Carleton (2005); Veyrunes et al. (2005)
Mus_pahari	Mus	8	0.205128	39	Musser and Carleton (2005); Veyrunes et al. (2005)
Mus_spicilegus	Mus	8	0.205128	39	Musser and Carleton (2005); Veyrunes et al. (2005)
Mus_terricolor	Mus	8	0.205128	39	Musser and Carleton (2005); Veyrunes et al. (2005)
Musseromys_anacuao	Musseromys	4	1	4	Heaney et al. (2014a)
Musseromys_beneficus	Musseromys	4	1	4	Heaney et al. (2014a)
Musseromys_gulantang	Musseromys	4	1	4	Heaney et al. (2009)
Musseromys_inopinatus	Musseromys	4	1	4	Heaney et al. (2014a)
Mylomys_dybowskii	Mylomys	1	0.5	2	Musser and Carleton (2005)
Myomyscus_brockmani	Myomyscus	1	0.25	4	Musser and Carleton (2005)
Niviventer_confucianus	Niv	4	0.235294	17	Musser and Carleton (2005)
Niviventer_cremoriventer	Niv	4	0.235294	17	Musser and Carleton (2005)
Niviventer_culturatus	Niv	4	0.235294	17	Musser and Carleton (2005)
Niviventer_excelsior	Niv	4	0.235294	17	Musser and Carleton (2005)
Notomys_fuscus	Notomys	1	0.2	5	Musser and Carleton (2005), Rowe et al. (2008)
Oenomys_hypoxanthus	Oenom	1	0.5	2	Musser and Carleton (2005)
Otomys_anchietae	Otomy	4	0.2	20	Musser and Carleton (2005); Steppan and Schenk (2017) for polyphyly

Otomys_angoniensis	Otomy	4	0.2	20	Musser and Carleton (2005); Steppan and Schenk (2017) for polyphyly
Otomys_denti	Otomy	4	0.2	20	Musser and Carleton (2005); Steppan and Schenk (2017) for polyphyly
Parotomys_brantsii	Otomy	4	0.2	20	Musser and Carleton (2005); Steppan and Schenk (2017) for polyphyly
Parahydromys_asper	Parahydromys	1	1	1	Musser and Carleton (2005), Rowe et al. (2008)
Paraleptomys_sp.	Paraleptomys	1	0.5	2	Musser and Carleton (2005), Rowe et al. (2008)
Paramelomys_levipes	Paramelomys	1	0.125	8	Musser and Carleton (2005), Rowe et al. (2008)
Paruromys_dominator	Paruromys	1	1	1	Musser and Carleton (2005)
Paucidentomys_vermidax	Pauci	1	1	1	Esselstyn et al. (2012)
Phloeomys_cumingi	ph	2	1	2	Musser and Carleton (2005)
Phloeomys_pallidus	ph	2	1	2	Musser and Carleton (2005)
Pogonomys_loriae	Pogonomys	3	0.75	4	Musser and Carleton (2005), Rowe et al. (2008)
Pogonomys_macrourus	Pogonomys	3	0.75	4	Musser and Carleton (2005), Rowe et al. (2008)
Pogonomys_sylvestris	Pogonomys	3	0.75	4	Musser and Carleton (2005), Rowe et al. (2008)
Praomys_degraaffi	Praom	4	0.25	16	Musser and Carleton (2005)
Praomys_jacksoni	Praom	4	0.25	16	Musser and Carleton (2005)
Praomys_misonnei	Praom	4	0.25	16	Musser and Carleton (2005)
Praomys_tullbergi	Praom	4	0.25	16	Musser and Carleton (2005)
Pseudohydromys_ellermani	Pseudohydromys	1	0.142857	7	Musser and Carleton (2005), Rowe et al. (2008)
Pseudomys_australis	Pseudomys	1	0.043478	23	Musser and Carleton (2005), Rowe et al. (2008)
Limnomys_bryophilus	RatTarLim	16	0.228571	70	Musser and Carleton (2005); Rowe et al. (2011); Schenk et al. (2013)
Limnomys_sibuanus	RatTarLim	16	0.228571	70	Musser and Carleton (2005); Rowe et al. (2011); Schenk et al. (2013)
Rattus_everetti	RatTarLim	16	0.228571	70	Musser and Carleton (2005); Rowe et al. (2011); Schenk et al. (2013)
Rattus_exulans	RatTarLim	16	0.228571	70	Musser and Carleton (2005); Rowe et al. (2011); Schenk et al. (2013)

Rattus_giluwensis	RatTarLim	16	0.228571	70	Musser and Carleton (2005); Rowe et al. (2011); Schenk et al. (2013)
Rattus_leucopus	RatTarLim	16	0.228571	70	Musser and Carleton (2005); Rowe et al. (2011); Schenk et al. (2013)
Rattus_norvegicus	RatTarLim	16	0.228571	70	Musser and Carleton (2005); Rowe et al. (2011); Schenk et al. (2013)
Rattus_novaguineae	RatTarLim	16	0.228571	70	Musser and Carleton (2005); Rowe et al. (2011); Schenk et al. (2013)
Rattus_praetor	RatTarLim	16	0.228571	70	Musser and Carleton (2005); Rowe et al. (2011); Schenk et al. (2013)
Rattus_rattus	RatTarLim	16	0.228571	70	Musser and Carleton (2005); Rowe et al. (2011); Schenk et al. (2013)
Rattus_sordidus	RatTarLim	16	0.228571	70	Musser and Carleton (2005); Rowe et al. (2011); Schenk et al. (2013)
Rattus_tanezumi	RatTarLim	16	0.228571	70	Musser and Carleton (2005); Rowe et al. (2011); Schenk et al. (2013)
Rattus_tiomanicus	RatTarLim	16	0.228571	70	Musser and Carleton (2005); Rowe et al. (2011); Schenk et al. (2013)
Rattus_verecundus	RatTarLim	16	0.228571	70	Musser and Carleton (2005); Rowe et al. (2011); Schenk et al. (2013)
Rattus_villosissimus	RatTarLim	16	0.228571	70	Musser and Carleton (2005); Rowe et al. (2011); Schenk et al. (2013)
Tarsomys_apoensis	RatTarLim	16	0.228571	70	Musser and Carleton (2005); Rowe et al. (2011); Schenk et al. (2013)
Rhabdomys_pumilio	Rhabd	1	0.5	2	Musser and Carleton (2005)
Rhycnhomys_isarogensis	rhy	4	0.8	5	Heaney et al. (2016a)
Rhynchomys_banahao	rhy	4	0.8	5	Balete et al. (2009), Heaney et al. (2016a)
Rhynchomys_soricoides	rhy	4	0.8	5	Heaney et al. (2016a)
Rhynchomys_tapulao	rhy	4	0.8	5	Balete et al. (2009), Heaney et al. (2016a)
Saxatilomys_paulinae	Sax	1	1	1	Pagès et al. (2016)
Soricomys_kalinga	so	4	1	4	Balete et al. (2006); Balete et al. (2012)
Soricomys_leonardocoi	so	4	1	4	Balete et al. (2012)

Soricomys_montanus	so	4	1	4	Balete et al. (2012)
Soricomys_musseri	so	4	1	4	Balete et al. (2012)
Solomys_salebrosus	Solomys	1	0.25	4	Musser and Carleton (2005), Rowe et al. (2008)
Sommeromys_macrorhinos	Sommeromys	1	1	1	Musser and Carleton (2005)
Srilankamys_ohiensis	Sri	1	1	1	Musser and Carleton (2005)
Stenocephalomys_albipes	Steno	1	0.25	4	Musser and Carleton (2005)
Stochomys_longicaudatus	Stoch	1	1	1	Musser and Carleton (2005)
Sundamys_muelleri	Sundamys	1	0.333333	3	Musser and Carleton (2005)
Tateomys_macrocercus	Tateomys	2	1	2	Musser and Carleton (2005)
Tateomys_rhinogradoides	Tateomys	2	1	2	Musser and Carleton (2005)
Tokudaia_osimensis	Tokud	1	0.5	2	Musser and Carleton (2005)
Uromys_caudimaculatus	Uromys	1	0.166667	6	Musser and Carleton (2005), Rowe et al. (2008)
Vandeleuria_oleracea	Vande	1	0.333333	3	Musser and Carleton (2005)
Waiomys_mamasae	Wai	1	1	1	Rowe et al. (2014)
Xeromys_myoides	Xeromys	1	1	1	Musser and Carleton (2005), Rowe et al. (2008)
Zelotomys_hildegardeae	Zelot	1	0.5	2	Musser and Carleton (2005)
Zyzomys_argurus	Zyzomys	1	0.25	4	Musser and Carleton (2005), Rowe et al. (2008)
Total Rodents in sampled lineages				687	
Total Murines in sampled lineages				558	
Total Murines in unsampled lineages				630	
Sampling Fraction of Backbone				0.885714	

APPENDIX 2. SUPPLEMENTARY MATERIAL FOR CHAPTER 2.

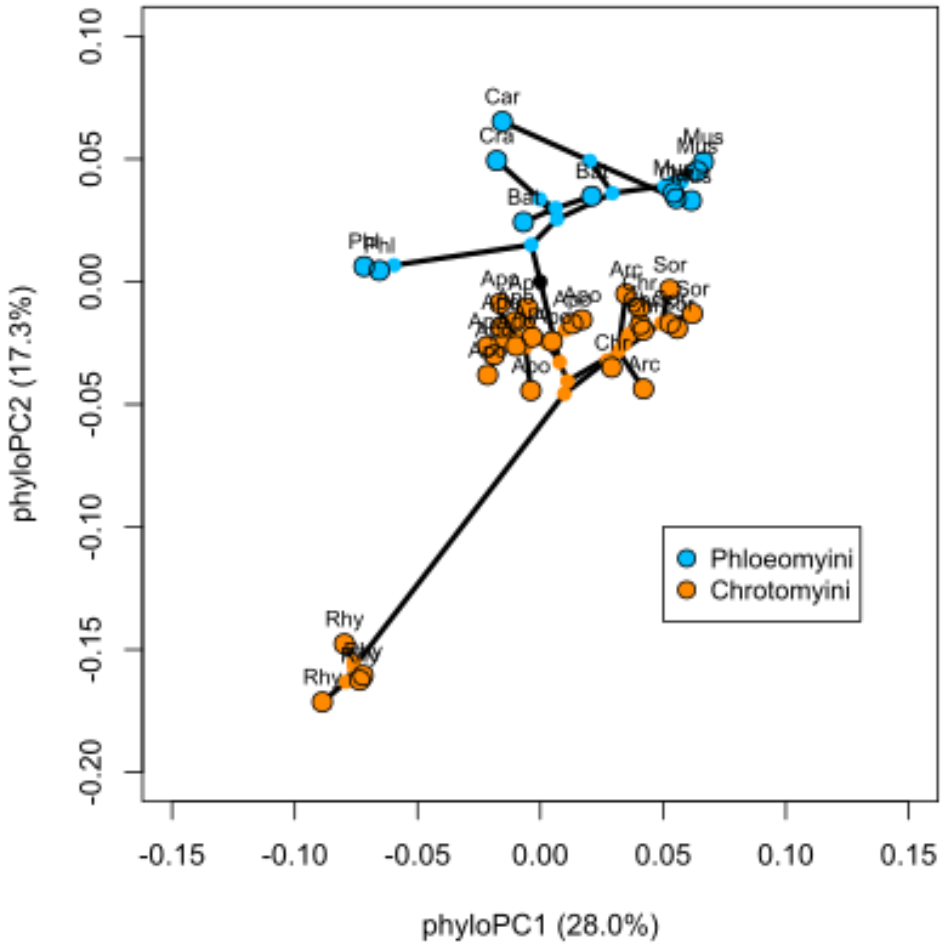

Appendix Figure 2.1. Phylomorphospace of phylogenetically-corrected principal components 1-2 for Luzon Old Endemic rodents.

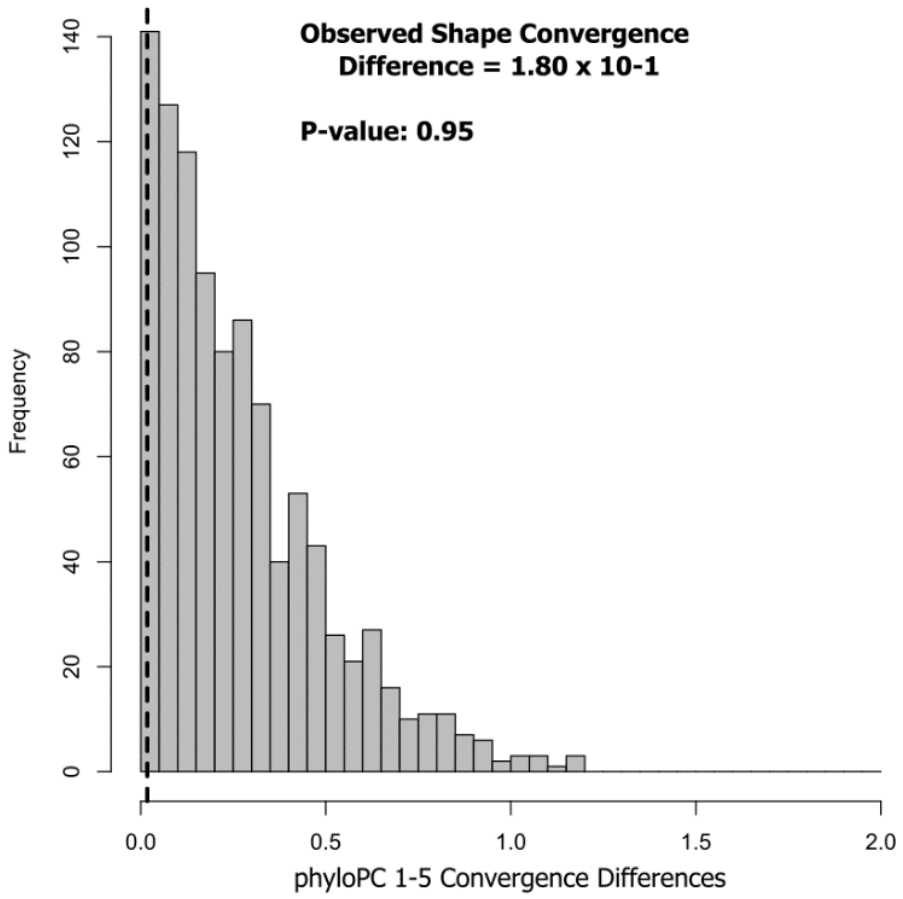

Appendix Figure 2.2. Histogram of differences in clade-wise covariances between Euclidean and patristic distances as a comparison of convergence between clades. The dashed line indicates the observed difference in covariances between Phloeomyini and Chrotomyini, and the gray bars represent differences simulated under a clade-independent Brownian Motion process. The Euclidean distances measured in this figure were calculated from phylogenetically-corrected PC1-5 scores.

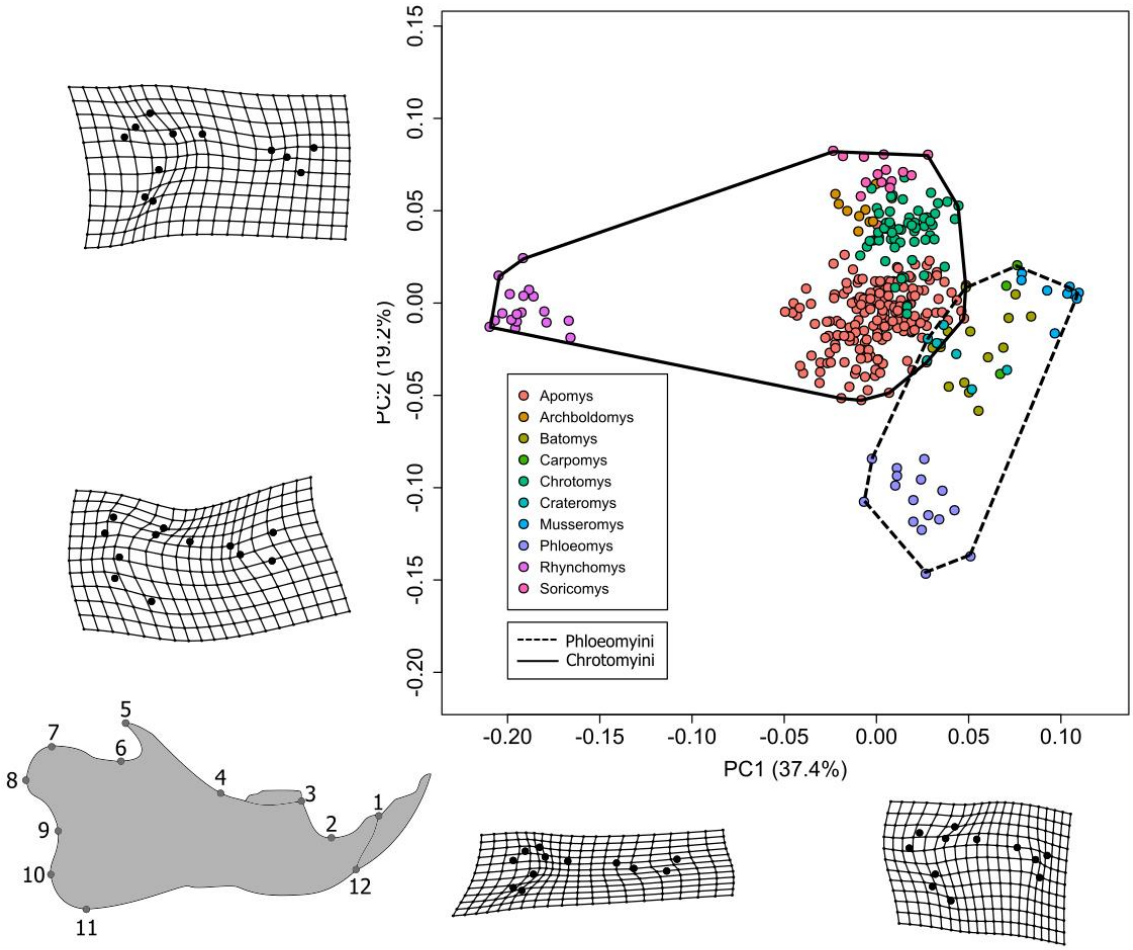

Appendix Figure 2.3. PC1 and PC2 of mandibular morphology for 41 Luzon Old Endemic rodent species (*n* = 337). Specimens are colored according to their placement by genus. Thin-plate splines along axes show specimens with extreme scores and illustrate differences along these axes. Bottom-left: lateral view of mandible indicating landmarks taken. Landmarks taken are as follows: 1. Anterodorsal apex of incisive alveolus; 2. Ventral nadir of diastema between incisor (I1) and first molar (M1); 3. Anterior margin of M1 alveolus; 4. Junction of coronoid process with body of mandible, defined by point at which a straight line following coronoid process first meets the body; 5. Posterodorsal apex of coronoid process; 6. Ventral nadir between coronoid and condyloid processes; 7. Anterodorsal apex of condyloid process; 8. Posterior apex of condyloid process; 9. Anterior nadir between condyloid and angular processes; 10. Posterior apex of angular process; 11. Ventral apex of angular process; 12. Anteroventral apex of incisive alveolus.

Appendix Table 2.1. Specimens and associated metadata used in this study.

Catalog Number	Genus	Species	Sex	Prep	Country	Province	County	Locality	Elevation	Longitude	Latitude	Field Number
FMNH 62750	Apomys	abrae	M	skin,skull	Philippines	Luzon I	Abra Prov	Massisiat	1067	120.8334	17.5834	HH460
FMNH 167254	Apomys	abrae	M	skull,asr, tiss	Philippines	Luzon I	Kalinga Prov	Balbalan Munic, Balbalasang Brgy: Magdallao	1600	121.0683	17.4583	
FMNH 167358	Apomys	abrae	M	skull,skel , tiss	Philippines	Luzon I	Kalinga Prov	Balbalan Munic, Balbalasang Brgy: Magdallao	1600	121.0683	17.4583	LRH6069
FMNH 169055	Apomys	abrae	F	skull,asr	Philippines	Luzon I	Kalinga Prov	Balbalan Munic, Balbalasang Brgy: Mapga	1050	121.075	17.475	LRH6334
FMNH 170919	Apomys	abrae	F	skull,skel , tiss	Philippines	Luzon I	Kalinga Prov	Balbalan Munic, Balbalasang Brgy: Mapga	1050	121.075	17.475	LRH6327
FMNH 188293	Apomys	abrae	F	skull,asr, tiss	Philippines	Luzon I	Mountain Prov	Mt Data; 1.0 km N, 1.25 km E south peak	2231	120.8696	16.8640 2	DSB3963
FMNH 188297	Apomys	abrae	F	skull,asr, tiss	Philippines	Luzon I	Mountain Prov	Mt Data; 0.9 km N, 1.75 km E south peak	2228	120.8744	16.8631 2	DSB3956
FMNH 188437	Apomys	abrae	M	skull,skel , tiss	Philippines	Luzon I	Mountain Prov	Mt Data; 1.0 km N, 1.25 km E south peak	2231	120.8696	16.8640 2	DSB3959
FMNH 193533	Apomys	abrae	M	skull,asr, tiss	Philippines	Luzon I	Mountain Prov	0.4 km N Barlig Munic Hall	1790	121.0985	17.0474	EAR6215
FMNH 193867	Apomys	abrae	M	skull,skel , tiss	Philippines	Luzon I	Mountain Prov	0.4 km N Barlig Munic Hall	1790	121.0985	17.0474	EAR6234
FMNH 193869	Apomys	abrae	M	skull,skel , tiss	Philippines	Luzon I	Mountain Prov	0.6 km N Barlig Munic Hall	1800	121.0998	17.0482	EAR6293
FMNH 214244	Apomys	abrae	F	skull,asr, tiss	Philippines	Luzon I	Mountain Prov	Barlig Munic. 2.15 km N, 1.25 km W Mt Amuyao peak	1650	121.116	17.0327	DSB7909
FMNH 214362	Apomys	abrae	F	skull,skel , tiss	Philippines	Luzon I	Mountain Prov	Barlig Munic. 2.15 km N, 1.25 km W Mt Amuyao peak	1650	121.116	17.0327	DSB7902
FMNH 92755	Apomys	abrae	M	skin,skull	Philippines	Luzon I	Ilocos Norte Prov	Mt Simminublar (Mt Sicapoo)		120.9334	18.0167	DSR1222
FMNH 92760	Apomys	abrae	F	skin,skull	Philippines	Luzon I	Ilocos Norte Prov	Mt Simminublar (Mt Sicapoo)		120.9334	18.0167	DSR1228
FMNH 92761	Apomys	abrae	F	skin,skull	Philippines	Luzon I	Ilocos Norte Prov	Mt Simminublar (Mt Sicapoo)	1311	120.9334	18.0167	DSR1230
USNM 151509	Apomys	abrae	M	skin,skull	Philippines	Luzon I	Benguet Prov	Haights-in-the-Oaks				EAM6498
USNM 399574	Apomys	abrae	F	skull,asr	Philippines	Luzon I	Benguet Prov	Baguio				
USNM 399578	Apomys	abrae	F	skull,asr	Philippines	Luzon I	Benguet Prov	Baguio				
FMNH 190812	Apomys	aurorae	M	skull,asr, tiss	Philippines	Luzon I	Aurora Prov	Dingalan Munic: 2 km S, 2 km W Mingan Peak	1305	121.3842	15.4645 6	PAA864
FMNH 190914	Apomys	aurorae	F	skull,asr	Philippines	Luzon I	Aurora Prov	Dingalan Munic: 2 km S, 2 km W Mingan Peak	1305	121.3842	15.4645 6	DSB4291
FMNH 190919	Apomys	aurorae	M	skull,asr, tiss	Philippines	Luzon I	Aurora Prov	Dingalan Munic: 2.1 km S, 2.9 km W Mingan Peak	902	121.3768	15.4623 3	DSB4300
FMNH 191070	Apomys	aurorae	M	skull,skel , tiss	Philippines	Luzon I	Aurora Prov	Dingalan Munic: 2 km S, 2 km W Mingan Peak	1305	121.3842	15.4645 6	PAA869
FMNH 191076	Apomys	aurorae	F	skull,skel , tiss	Philippines	Luzon I	Aurora Prov	Dingalan Munic: 2 km S, 2 km W Mingan Peak	1305	121.3842	15.4645 6	DSB4281

FMNH 178431	Apomys	banahao	F	skull,asr	Philippines	Luzon I	Quezon Prov	Mt Banahaw, Barangay Lalo	1465	121.5086	14.0665	LRH6962
FMNH 178456	Apomys	banahao	M	skull,asr	Philippines	Luzon I	Quezon Prov	Mt Banahaw, Barangay Lalo	1465	121.5086	14.0663 5	EAR5210
FMNH 178457	Apomys	banahao	M	skull,asr	Philippines	Luzon I	Quezon Prov	Mt Banahaw, Barangay Lalo	1465	121.5086	14.0663 5	EAR5211
FMNH 178459	Apomys	banahao	F	skull,asr	Philippines	Luzon I	Quezon Prov	Mt Banahaw, Barangay Lalo	1465	121.5086	14.0663 5	EAR5213
FMNH 178501	Apomys	banahao	M	skull,asr	Philippines	Luzon I	Quezon Prov	Mt Banahaw, Barangay Lalo	1465	121.5086	14.0663 5	EAR5279
FMNH 183500	Apomys	brownorum	F	skull,asr, tiss	Philippines	Luzon I	Zambales Prov	Palauig Munic: Brgy Salasa: Mt Tapulao peak	2024	120.1196	15.4818 9	DSB3466
FMNH 183504	Apomys	brownorum	F	skull,asr, tiss	Philippines	Luzon I	Zambales Prov	Palauig Munic: Brgy Salasa: Mt Tapulao peak	2024	120.1196	15.4818 9	DSB3482
FMNH 183508	Apomys	brownorum	M	skull,asr, tiss	Philippines	Luzon I	Zambales Prov	Palauig Munic: Brgy Salasa: Mt Tapulao peak	2024	120.1196	15.4818 9	DSB3488
FMNH 183516	Apomys	brownorum	M	skull,asr	Philippines	Luzon I	Zambales Prov	Palauig Munic: Brgy Salasa: Mt Tapulao peak	2024	120.1196	15.4818 9	DSB3504
FMNH 183524	Apomys	brownorum	M	skull,asr	Philippines	Luzon I	Zambales Prov	Palauig Munic: Brgy Salasa: Mt Tapulao peak	2024	120.1196	15.4818 9	DSB3531
FMNH 167246	Apomys	datae	M	skull,asr, tiss	Philippines	Luzon I	Kalinga Prov	Balbalan Munic, Balbalasang Brgy: Magdallao	1600	121.0683	17.4583	LRH5927
FMNH 167249	Apomys	datae	F	skull,asr	Philippines	Luzon I	Kalinga Prov	Balbalan Munic, Balbalasang Brgy: Magdallao	1600	121.0683	17.4583	LRH5935
FMNH 175652	Apomys	datae	M	skull,skel	Philippines	Luzon I	Kalinga Prov	Balbalan Munic, Balbalasang Brgy: Mt Bali-it	1950	121.0017	17.43	LRH6777
FMNH 175662	Apomys	datae	F	skull,skel	Philippines	Luzon I	Kalinga Prov	Balbalan Munic, Balbalasang Brgy: Mt Bali-it	1950	121.0017	17.43	LRH6796
FMNH 188280	Apomys	datae	M	skull,asr, tiss	Philippines	Luzon I	Mountain Prov	Mt Data; 0.75 km N, 1.0 km E south peak	2289	120.8671	16.8623 3	DSB3870
FMNH 188427	Apomys	datae	F	skull,skel , tiss	Philippines	Luzon I	Mountain Prov	Mt Data; 0.75 km N, 0.6 km E south peak	2241	120.8611	16.8628 7	DSB3796
FMNH 188433	Apomys	datae	F	skull,skel , tiss	Philippines	Luzon I	Mountain Prov	Mt Data; 0.75 km N, 0.6 km E south peak	2241	120.8611	16.8628 7	DSB3834
FMNH 188438	Apomys	datae	M	skull,skel , tiss	Philippines	Luzon I	Mountain Prov	Mt Data; 0.1 km E south peak	2310	120.8608	16.8588 8	LRH7397
FMNH 198536	Apomys	datae	M	skull,asr, tiss	Philippines	Luzon I	Benguet Prov	Mt Pulag NP, 0.7 km S, 0.4 km W Mt Babadak peak	2445	120.8781	16.5742 8	LRH7846
FMNH 198799	Apomys	datae	F	skull,skel , tiss	Philippines	Luzon I	Benguet Prov	Mt Pulag NP, 1.2 km S, 1.15 km E Mt Pulag peak	2780	120.9086	16.5879	DSB5296
FMNH 198803	Apomys	datae	M	skull,skel , tiss	Philippines	Luzon I	Benguet Prov	Mt Pulag NP, 1.15 km S, 1.35 km E Mt Pulag peak	2695	120.9096	16.5881 6	DSB5332
FMNH 198841	Apomys	datae	F	skull,skel	Philippines	Luzon I	Benguet Prov	Mt Pulag NP, 1.75 km S, 0.9 km E Mt Pulag peak	2650	120.9051	16.5836 3	LRH7990
FMNH 214274	Apomys	datae	F	skull,asr, tiss	Philippines	Luzon I	Mountain Prov	Barlig Munic. 2.15 km N, 1.25 km W Mt Amuyao peak	1650	121.116	17.0327	DSB7848
FMNH 214276	Apomys	datae	M	skull,asr, tiss	Philippines	Luzon I	Mountain Prov	Barlig Munic. 2.15 km N, 1.25 km W Mt Amuyao peak	1650	121.116	17.0327	DSB7851
FMNH 214278	Apomys	datae	M	skull,asr, tiss	Philippines	Luzon I	Mountain Prov	Barlig Munic. 2.15 km N, 1.25 km W Mt Amuyao peak	1650	121.116	17.0327	DSB7853
FMNH 214292	Apomys	datae	F	skull,asr, tiss	Philippines	Luzon I	Mountain Prov	Barlig Munic. 1.0 km N, 1.0 km W Mt Amuyao peak	2100	121.1179	17.0221 3	LRH8123

USNM 151513	Apomys	datae	F	skin,skull	Philippines	Luzon I	Benguet Prov	Haights-in-the-Oaks				EAM6531
USNM 574889	Apomys	datae	M	skull,asr	Philippines	Luzon I	Cagayan Prov	Baggao, Barrio Via, Sitio Hot Springs, W. Foothills Sierra Madre Mts.		122.02	17.83	RSK1800 96
FMNH 205436	Apomys	iridensis	F	skull,asr, tiss	Philippines	Luzon I	Rizal Prov	Rodriguez Munic., 1.25 km S, 0.5 km W Mt Irid peak	920	121.3212	14.78	DSB5958
FMNH 206321	Apomys	iridensis	M	skull,skel , tiss	Philippines	Luzon I	Rizal Prov	Rodriguez Munic., 1.25 km S, 0.5 km W Mt Irid peak	920	121.3212	14.78	DSB5978
FMNH 206324	Apomys	iridensis	F	skull,skel , tiss	Philippines	Luzon I	Rizal Prov	Rodriguez Munic., 1.25 km S, 0.5 km W Mt Irid peak	920	121.3212	14.78	DSB6010
FMNH 206326	Apomys	iridensis	F	skull,skel , tiss	Philippines	Luzon I	Rizal Prov	Rodriguez Munic., 1.25 km S, 0.5 km W Mt Irid peak	920	121.3212	14.78	DSB6012
FMNH 206335	Apomys	iridensis	M	skull,skel , tiss	Philippines	Luzon I	Rizal Prov	Rodriguez Munic., 1.25 km S, 0.5 km W Mt Irid peak	920	121.3212	14.78	DSB6045
FMNH 178396	Apomys	magnus	F	skull,asr, tiss	Philippines	Luzon I	Quezon Prov	Mt Banahaw, Barangay Lalo	1465	121.5086	14.0663 5	EAR5238
FMNH 183572	Apomys	magnus	F	skull,asr, tiss	Philippines	Luzon I	Quezon Prov	Tayabas Munic: Brgy Lalo: Mt Banahaw, Idoro	765	121.5325	14.0574 7	DSB3601
FMNH 183574	Apomys	magnus	F	skull,asr, tiss	Philippines	Luzon I	Quezon Prov	Tayabas Munic: Brgy Lalo: Mt Banahaw, Hasa-an	1250			DSB3606
FMNH 183577	Apomys	magnus	F	skull,asr, tiss	Philippines	Luzon I	Quezon Prov	Tayabas Munic: Brgy Lalo: Mt Banahaw, Hasa-an	1250			DSB3622
FMNH 183578	Apomys	magnus	M	skull,asr, tiss	Philippines	Luzon I	Quezon Prov	Tayabas Munic: Brgy Lalo: Mt Banahaw, Hasa-an	1250			DSB3623
FMNH 147170	Apomys	microdon	F	skull,asr	Philippines	Luzon I	Isabela Prov	Palanan Municipality, Sitio Dimapnat		122.4	17.15	DSB2040
FMNH 178403	Apomys	microdon	M	skull,asr, tiss	Philippines	Luzon I	Quezon Prov	Mt Banahaw, Barangay Lalo	620	121.5396	14.0518 1	EAR5318
FMNH 178404	Apomys	microdon	M	skull,asr, tiss	Philippines	Luzon I	Quezon Prov	Mt Banahaw, Barangay Lalo	620	121.5396	14.0518 1	LRH7089
FMNH 183326	Apomys	microdon	M	skull,asr, tiss	Philippines	Luzon I	Bataan Prov	0.1 km N Mt Natib peak	1150	120.3989	14.7151 3	LRH7347
FMNH 183478	Apomys	microdon	M	skull,asr, tiss	Philippines	Luzon I	Zambales Prov	Palauig Munic: Brgy Salasa: Mt Tapulao peak	2024	120.1196	15.4818 9	DSB3462
FMNH 183481	Apomys	microdon	F	skull,asr, tiss	Philippines	Luzon I	Zambales Prov	Palauig Munic: Brgy Salasa: Mt Tapulao peak	2024	120.1196	15.4818 9	DSB3478
FMNH 183482	Apomys	microdon	F	skull,asr, tiss	Philippines	Luzon I	Zambales Prov	Palauig Munic: Brgy Salasa: Mt Tapulao peak	2024	120.1196	15.4818 9	DSB3481
FMNH 183483	Apomys	microdon	F	skull,asr, tiss	Philippines	Luzon I	Zambales Prov	Palauig Munic: Brgy Salasa: Mt Tapulao peak	2024	120.1196	15.4818 9	DSB3484
FMNH 189810	Apomys	microdon	M	skull,asr, tiss	Philippines	Luzon I	Camarines Norte Prov	1.0 km N, 0.5 km W east peak of Mt Labo	1115	122.7871	14.0259 6	DSB4001
FMNH 189811	Apomys	microdon	F	skull,asr, tiss	Philippines	Luzon I	Camarines Norte Prov	0.6 km N, 0.5 km W east peak of Mt Labo	1335	122.7878	14.0230 1	DSB4011
FMNH 189812	Apomys	microdon	F	skull,asr, tiss	Philippines	Luzon I	Camarines Norte Prov	0.25 km N, 0.25 km W east peak of Mt Labo	1413	122.7897	14.0188 3	DSB4046
FMNH 189813	Apomys	microdon	M	skull,asr, tiss	Philippines	Luzon I	Camarines Norte Prov	0.25 km N, 0.25 km W east peak of Mt Labo	1413	122.7897	14.0188 3	DSB4047
FMNH 190768	Apomys	microdon	F	skull,asr, tiss	Philippines	Luzon I	Aurora Prov	Dingalan Munic: 3.5 km S, 1.7 km W Mingan Peak	1476	121.3585	15.4662	DSB4258
FMNH 190770	Apomys	microdon	M	skull,asr, tiss	Philippines	Luzon I	Aurora Prov	Dingalan Munic: 2 km S, 2 km W Mingan Peak	1305	121.3842	15.4645 6	DSB4279

FMNH 190771	Apomys	microdon	F	skull,asr, tiss	Philippines	Luzon I	Aurora Prov	Dingalan Munic: 2 km S, 2 km W Mingan Peak	1305	121.3842	15.4645 6	DSB4289
FMNH 190772	Apomys	microdon	F	skull,asr, tiss	Philippines	Luzon I	Aurora Prov	Dingalan Munic: 2.1 km S, 2.9 km W Mingan Peak	902	121.3768	15.4623 3	DSB4313
FMNH 194738	Apomys	microdon	M	skull,asr, tiss	Philippines	Luzon I	Albay Prov	Malinao Munic, 1.4 km E, 0.7 km N Mt Malinao peak	1350	123.62	13.4093 1	DSB4647
FMNH 194739	Apomys	microdon	M	skull,asr, tiss	Philippines	Luzon I	Albay Prov	Malinao Munic, 2 km E, 0.6 km N Mt Malinao peak	1100	123.6255	13.4084 5	DSB4673
FMNH 195017	Apomys	microdon	F	skull,asr, tiss	Philippines	Luzon I	Nueva Vizcaya Prov	Quezon Munic, 1.1 km N, 0.4 km E Mt Palali peak	1443	121.225	16.4378	MRMD465
FMNH 195018	Apomys	microdon	F	skull,asr, tiss	Philippines	Luzon I	Nueva Vizcaya Prov	Quezon Munic, 1.1 km N, 0.4 km E Mt Palali peak	1443	121.225	16.4378	MRMD464
FMNH 195019	Apomys	microdon	M	skull,asr, tiss	Philippines	Luzon I	Nueva Vizcaya Prov	Quezon Munic, 1.1 km N, 0.4 km E Mt Palali peak	1443	121.225	16.4378	PAA1041
FMNH 195020	Apomys	microdon	F	skull,asr, tiss	Philippines	Luzon I	Nueva Vizcaya Prov	Quezon Munic, 1.1 km N, 0.4 km E Mt Palali peak	1443	121.225	16.4378	PAA1061
FMNH 203239	Apomys	microdon	M	skull,asr, tiss	Philippines	Luzon I	Camarines Sur Prov	Caramoan Munic, Caramoan National Park, 0.5 km S, 5 km E Port of Guijalo	50	123.9129	13.7314 5	DSB5390
FMNH 205417	Apomys	microdon	M	skull,asr, tiss	Philippines	Luzon I	Rizal Prov	Rodriguez Munic., 0.5 km S, 0.1 km W Mt Irid peak	1110	121.3246	14.7865 9	DSB6145
FMNH 205418	Apomys	microdon	F	skull,asr, tiss	Philippines	Luzon I	Rizal Prov	Rodriguez Munic., 0.25 km S, 0.15 km W Mt Irid peak	1330	121.3248	14.7887 8	DSB6115
FMNH 205676	Apomys	microdon	F	skull,asr, tiss	Philippines	Luzon I	Quezon Prov	Tayabas Munic., 0.5 km N, 10.25 km E Tayabas town square	300	121.6854	14.0327 5	DSB6158
FMNH 205677	Apomys	microdon	F	skull,asr, tiss	Philippines	Luzon I	Quezon Prov	Tayabas Munic., 0.5 km N, 10.25 km E Tayabas town square	300	121.6854	14.0327 5	DSB6295
FMNH 205678	Apomys	microdon	F	skull,asr, tiss	Philippines	Luzon I	Quezon Prov	Tayabas Munic., 0.5 km N, 10.25 km E Tayabas town square	300	121.6854	14.0327 5	DSB6355
FMNH 209325	Apomys	microdon	M	skull,asr, tiss	Philippines	Luzon I	Cavite Prov	Ternate Munic., 1.4 km N, 1.36 km E Pico de Loro peak	400	120.6627	14.2285 1	DSB7388
FMNH 209327	Apomys	microdon	M	skull,asr, tiss	Philippines	Luzon I	Cavite Prov	Ternate Munic., 0.26 km N, 0.12 km W Pico de Loro peak	550	120.6491	14.218	DSB7451
FMNH 209392	Apomys	microdon	M	skull,asr, tiss	Philippines	Luzon I	Aurora Prov	Dinalungan Munic: 2 km S, 4.5 km E Anacuao Peak	1125	121.9291	16.2369 9	LRH8065
FMNH 209393	Apomys	microdon	F	skull,asr, tiss	Philippines	Luzon I	Aurora Prov	Dinalungan Munic: 1.9 km S, 4 km E Anacuao Peak	1300	121.9291	16.2371 5	LRH8100
FMNH 209397	Apomys	microdon	F	skull,asr, tiss	Philippines	Luzon I	Aurora Prov	Dinalungan Munic: 1.9 km S, 4 km E Anacuao Peak	1300	121.9291	16.2371 5	DSB7107
FMNH 209398	Apomys	microdon	M	skull,asr, tiss	Philippines	Luzon I	Aurora Prov	Dinalungan Munic: 2.25 km S, 4.8 km E Anacuao Peak	940	121.9329	16.2352 9	DSB7143
FMNH 209405	Apomys	microdon	F	skull,asr, tiss	Philippines	Luzon I	Aurora Prov	Dinalungan Munic: 0.2 km E Anacuao Peak	1725	121.889	16.2552 7	DSB7285
FMNH 209548	Apomys	microdon	M	skull,skel, tiss	Philippines	Luzon I	Cavite Prov	Ternate Munic., 1.4 km N, 1.36 km E Pico de Loro peak	400	120.6627	14.2285 1	DSB7354
FMNH 209549	Apomys	microdon	M	skull, tiss	Philippines	Luzon I	Cavite Prov	Ternate Munic., 0.26 km N, 0.12 km W Pico de Loro peak	550	120.6491	14.218	DSB7404
FMNH 214155	Apomys	microdon	M	skull,asr, tiss	Philippines	Luzon I	Cagayan Prov	Peñablanca Munic: 19.4 km N, 9 km E Peñablanca town center	100	121.868	17.8017 5	DSB8360

FMNH 214487	Apomys	microdon	M	skull,skel, tiss	Philippines	Luzon I	Cagayan Prov	Peñablanca Munic: 9.1 km N, 3.5 km E Peñablanca town center	100	121.8174	17.70702	DSB7969
FMNH 216430	Apomys	microdon	F	skull,asr, tiss	Philippines	Luzon I	Cagayan Prov	Peñablanca Munic: 3 km N, 8.75 km W Mt. Cetaceo peak	740	121.9714	17.7343 8	DSB8650
FMNH 216431	Apomys	microdon	M	skull,asr, tiss	Philippines	Luzon I	Cagayan Prov	Peñablanca Munic: 2.33 km N, 7.8 km W Mt. Cetaceo peak	900	121.9794	17.7273 6	DSB8657
USNM 155145	Apomys	microdon	M	skin,skull	Philippines	Catandua nes I	Catanduanes Prov	Biga				DBM6
USNM 458916	Apomys	microdon	M	skull,asr	Philippines	Luzon I	Camarines Sur Prov	Naga, 4 km N, 18 km E, Mt. Isarog, Reforestation Station		123.333	13.6667	LRH3958
USNM 458917	Apomys	microdon	F	skull,asr	Philippines	Luzon I	Camarines Sur Prov	Naga, 4 km N, 18 km E, Mt. Isarog, Reforestation Station		123.333	13.6667	LRH4024
USNM 458918	Apomys	microdon	F	skull,asr	Philippines	Luzon I	Camarines Sur Prov	Naga, 4 km N, 21.5 km E, Mt. Isarog		123.367	13.6667	LRH4154
USNM 458919	Apomys	microdon	M	skull,asr	Philippines	Luzon I	Camarines Sur Prov	Naga, 4 km N, 21.5 km E, Mt. Isarog		123.367	13.6667	LRH4160
FMNH 190878	Apomys	minganensis	F	skull,asr, tiss	Philippines	Luzon I	Aurora Prov	Dingalan Munic: 1.5 km S, 0.5 km W Mingan Peak	1681	121.4004	15.4680 2	DSB4185
FMNH 190949	Apomys	minganensis	M	skull,asr, tiss	Philippines	Luzon I	Aurora Prov	Dingalan Munic: 1.5 km S, 0.5 km W Mingan Peak	1681	121.4004	15.4680 2	MRMD41 6
FMNH 190955	Apomys	minganensis	M	skull,asr, tiss	Philippines	Luzon I	Aurora Prov	Dingalan Munic: Mt Mingan	1540			MVD141
FMNH 190958	Apomys	minganensis	M	skull,asr, tiss	Philippines	Luzon I	Aurora Prov	Dingalan Munic: 1.5 km S, 0.5 km W Mingan Peak	1681	121.4004	15.4680 2	MVD163
FMNH 191065	Apomys	minganensis	F	skull,asr, tiss	Philippines	Luzon I	Aurora Prov	Dingalan Munic: 0.9 km S, 0.3 km W Mingan Peak	1785	121.4007	15.4739	PAA803
FMNH 147171	Apomys	musculus	F	skull,asr	Philippines	Luzon I	Isabela Prov	Bintacan Municipality, Sitio Batong Labang	300	122.07	17.1	DSB2028
FMNH 152024	Apomys	musculus	M	skull,asr	Philippines	Luzon I	Camarines Sur Prov	Mt Isarog, 4 km N, 21.5 km E Naga City	1550	123.37	13.67	DSB3034
FMNH 152027	Apomys	musculus	F	skull,asr	Philippines	Luzon I	Camarines Sur Prov	Mt Isarog, 4 km N, 21.5 km E Naga City	1550	123.37	13.67	DSB3037
FMNH 152029	Apomys	musculus	F	skull,asr	Philippines	Luzon I	Camarines Sur Prov	Mt Isarog, 4 km N, 21.5 km E Naga City	1550	123.37	13.67	DSB3058
FMNH 152030	Apomys	musculus	M	skull,asr	Philippines	Luzon I	Camarines Sur Prov	Mt Isarog, 4 km N, 21.5 km E Naga City	1550	123.37	13.67	DSB3062
FMNH 167241	Apomys	musculus	M	skull,asr, tiss	Philippines	Luzon I	Kalinga Prov	Balbalan Munic, Balbalasang Brgy: Magdallao	1600	121.0683	17.4583	LRH5963
FMNH 167242	Apomys	musculus	M	skull,asr, tiss	Philippines	Luzon I	Kalinga Prov	Balbalan Munic, Balbalasang Brgy: Magdallao	1600	121.0683	17.4583	LRH5997
FMNH 175549	Apomys	musculus	F	skull,asr, tiss	Philippines	Luzon I	Kalinga Prov	Balbalan Munic, Balbalasang Brgy: Mt Bali-it	1950	121.0017	17.43	EAR4963
FMNH 175550	Apomys	musculus	F	skull,asr, tiss	Philippines	Luzon I	Kalinga Prov	Balbalan Munic, Balbalasang Brgy: Mt Bali-it	2150	120.9967	17.4283	LRH6901
FMNH 183488	Apomys	musculus	F	skull,asr, tiss	Philippines	Luzon I	Zambales Prov	Palauig Munic: Brgy Salasa: Mt Tapulao peak	2024	120.1196	15.4818 9	DSB3461
FMNH 183489	Apomys	musculus	F	skull,asr, tiss	Philippines	Luzon I	Zambales Prov	Palauig Munic: Brgy Salasa: Mt Tapulao peak	2024	120.1196	15.4818 9	DSB3493
FMNH 183490	Apomys	musculus	M	skull,asr, tiss	Philippines	Luzon I	Zambales Prov	Palauig Munic: Brgy Salasa: Mt Tapulao peak	2024	120.1196	15.4818 9	DSB3494

FMNH 183492	Apomys	musculus	M	skull,asr, tiss	Philippines	Luzon I	Zambales Prov	Palauig Munic: Brgy Salasa: Mt Tapulao peak	2024	120.1196	15.4818 9	DSB3512
FMNH 188239	Apomys	musculus	M	skull,asr, tiss	Philippines	Luzon I	Mountain Prov	Mt Data; 0.75 km N, 0.6 km E south peak	2241	120.8611	16.8628 7	DSB3839
FMNH 188240	Apomys	musculus	F	skull,asr, tiss	Philippines	Luzon I	Mountain Prov	Mt Data; 0.75 km N, 0.6 km E south peak	2241	120.8611	16.8628 7	DSB3853
FMNH 188244	Apomys	musculus	F	skull,asr, tiss	Philippines	Luzon I	Mountain Prov	Mt Data; 0.1 km E south peak	2310	120.8608	16.8588 8	LRH7481
FMNH 190773	Apomys	musculus	M	skull,asr, tiss	Philippines	Luzon I	Aurora Prov	Dingalan Munic: 1.8 km S, 1.0 km W Mingan Peak	1677	121.3946	15.4658 6	DSB4130
FMNH 193941	Apomys	musculus	M	skull,skel , tiss	Philippines	Luzon I	Mountain Prov	0.4 km N, 0.4 km W Mt Amuyao peak	2480	121.1239	17.0172 7	EAR6345
FMNH 198708	Apomys	musculus	F	skull,asr, tiss	Philippines	Luzon I	Benguet Prov	Mt Pulag NP, 0.6 km S, 0.65 km E Mt Pulag peak	2730	120.9035	16.5937 2	DSB5333
FMNH 198710	Apomys	musculus	F	skull,asr, tiss	Philippines	Luzon I	Benguet Prov	Mt Pulag NP, 0.8 km S, 0.4 km W Mt Babadak peak	2420	120.8788	16.5736 1	LRH7811
FMNH 198712	Apomys	musculus	M	skull,asr, tiss	Philippines	Luzon I	Benguet Prov	Mt Pulag NP, 0.9 km S, 0.9 km W Mt Babadak peak	2335	120.8745	16.5719	LRH7898
FMNH 198853	Apomys	musculus	M	skull,skel , tiss	Philippines	Luzon I	Benguet Prov	Mt Pulag NP, 1.15 km S, 1.35 km E Mt Pulag peak	2695	120.9096	16.5881 6	DSB5374
FMNH 214302	Apomys	musculus	M	skull,asr, tiss	Philippines	Luzon I	Mountain Prov	Barlig Munic. 1.0 km N, 1.0 km W Mt Amuyao peak	2100	121.1179	17.0221 3	DSB7789
FMNH 214303	Apomys	musculus	M	skull,asr, tiss	Philippines	Luzon I	Mountain Prov	Barlig Munic. 2.15 km N, 1.25 km W Mt Amuyao peak	1650	121.116	17.0327	DSB7859
FMNH 214306	Apomys	musculus	F	skull,asr, tiss	Philippines	Luzon I	Mountain Prov	Barlig Munic. 0.5 km N, 0.5 km W Mt Amuyao peak	2530	121.1219	17.0171 7	DSB7796
FMNH 214315	Apomys	musculus	F	skull,asr, tiss	Philippines	Luzon I	Mountain Prov	Barlig Munic. 2.15 km N, 1.25 km W Mt Amuyao peak	1650	121.116	17.0327	DSB7923
FMNH 218387	Apomys	musculus	F	skull,asr, tiss	Philippines	Luzon I	Laguna Prov	Majayjay Munic. 0.05 km N, 0.15 km E Mt. Banahaw peak	2030	121.4901	14.0690 7	LRH8387
FMNH 218523	Apomys	musculus	M	skull,skel , tiss	Philippines	Luzon I	Laguna Prov	Majayjay Munic. 1.0 km N, 0.4 km E Mt. Banahaw peak	1625	121.4926	14.0770 6	LRH8279
FMNH 218524	Apomys	musculus	F	skull,skel , tiss	Philippines	Luzon I	Laguna Prov	Majayjay Munic. 1.0 km N, 0.4 km E Mt. Banahaw peak	1625	121.4926	14.0770 6	LRH8280
FMNH 218529	Apomys	musculus	M	skull,skel , tiss	Philippines	Luzon I	Laguna Prov	Majayjay Munic. 0.05 km N, 0.15 km E Mt. Banahaw peak	2030	121.4901	14.0690 7	LRH8410
USNM 145770	Apomys	musculus	F	skin,skull	Philippines	Luzon I	Benguet Prov	Baguio, Camp John Hay				EAM6409
USNM 145777	Apomys	musculus	M	skin,skull	Philippines	Luzon I	Benguet Prov	Baguio, Lime Kiln, Limestone Hills				EAM6418
USNM 261177	Apomys	musculus	M	skin,skull	Philippines	Luzon I	Benguet Prov	Baguio				AS37-1001
FMNH 212555	Apomys	sacobianus	M	skull,asr, tiss	Philippines	Luzon I	Pampanga Prov	Mabalacat Munic., 7.4 km N, 13 km E Mt. Pinatubo peak	365	120.4621	15.2037 2	DSB7464
FMNH 212562	Apomys	sacobianus	F	skull,asr, tiss	Philippines	Luzon I	Pampanga Prov	Mabalacat Munic., 7.4 km N, 13 km E Mt. Pinatubo peak	365	120.4621	15.2037 2	DSB7491
FMNH 212571	Apomys	sacobianus	M	skull,asr, tiss	Philippines	Luzon I	Pampanga Prov	Mabalacat Munic., 7.4 km N, 13 km E Mt. Pinatubo peak	365	120.4621	15.2037 2	DSB7559
FMNH 212581	Apomys	sacobianus	F	skull,asr, tiss	Philippines	Luzon I	Pampanga Prov	Mabalacat Munic., 7.4 km N, 13 km E Mt. Pinatubo peak	365	120.4621	15.2037 2	DSB7580
USNM 304352	Apomys	sacobianus	M	skin,skull	Philippines	Luzon I	Pampanga Prov	Clark Air Base, water point on Sacobia River				DHJ8555

FMNH 176559	Apomys	sierrae	F	skull,asr	Philippines	Luzon I	Quirino Prov	Nagtipunan Munic, Brgy Disimungal, Sitio Km 18, Mt Lataan	1200	121.7397	16.1725	MGdG1588
FMNH 176561	Apomys	sierrae	M	skull,asr	Philippines	Luzon I	Quirino Prov	Nagtipunan Munic, Brgy Disimungal, Sitio Km 18, Mt Lataan	1200	121.7397	16.1725	MGdG1618
FMNH 176564	Apomys	sierrae	M	skull,asr, tiss	Philippines	Luzon I	Cagayan Prov	Gonzaga Munic, Barangay Magrafil, Mt Cagua, Sitio Masok	800	122.111	18.2186 7	MRMD207
FMNH 176567	Apomys	sierrae	M	skull,asr, tiss	Philippines	Luzon I	Cagayan Prov	Gonzaga Munic, Barangay Magrafil, Mt Cagua, Sitio Masok	800	122.111	18.2186 7	MRMD214
FMNH 176570	Apomys	sierrae	M	skull,asr, tiss	Philippines	Luzon I	Cagayan Prov	Gonzaga Munic, Barangay Magrafil, Mt Cagua, Sitio Masok	800	122.111	18.2186 7	MRMD223
FMNH 180366	Apomys	sierrae	M	skull,asr, tiss	Philippines	Luzon I	Quirino Prov	Nagtipunan Munic, Brgy Matmad, Sitio Mangitagud, Mungiao Mts	450	121.4777	16.0562 5	MVD1
FMNH 180370	Apomys	sierrae	F	skull,asr, tiss	Philippines	Luzon I	Quirino Prov	Nagtipunan Munic, Brgy Matmad, Sitio Mangitagud, Mungiao Mts	450	121.4777	16.0562 5	DSB3440
FMNH 185884	Apomys	sierrae	M	alc, tiss	Philippines	Luzon I	Cagayan Prov	2.0 km SW Mt Cetaceo peak	1500	122.0345	17.6926 4	MRMD354b
FMNH 186821	Apomys	sierrae	M	skull,skel, tiss	Philippines	Luzon I	Nueva Vizcaya Prov	Quezon Munic, 1.3 km NE Mt Palali Peak	1434	121.2234	16.4395 1	PAA629
FMNH 186823	Apomys	sierrae	F	skull,skel, tiss	Philippines	Luzon I	Nueva Vizcaya Prov	Quezon Munic, 1.3 km NE Mt Palali Peak	1434	121.2234	16.4395 1	MRMD373
FMNH 186827	Apomys	sierrae	F	skull,skel, tiss	Philippines	Luzon I	Nueva Vizcaya Prov	Quezon Munic, Mt Palali Peak	1680	121.2208	16.4311 1	PAA656
FMNH 191233	Apomys	sierrae	M	skull,asr, tiss	Philippines	Palaui I	Cagayan Prov	Sta. Ana Munic, Barangay San Vicente, 4.25 km S of Cape Engano Lighthouse	153	122.1352	18.5444 4	PAA702
FMNH 191234	Apomys	sierrae	M	skull,asr, tiss	Philippines	Palaui I	Cagayan Prov	Sta. Ana Munic, Barangay San Vicente, 4.25 km S of Cape Engano Lighthouse	153	122.1352	18.5444 4	PAA703
FMNH 194924	Apomys	sierrae	M	skull,asr, tiss	Philippines	Luzon I	Nueva Vizcaya Prov	Quezon Munic, Mt Palali peak	1700	121.2215	16.4277 7	PAA1009
FMNH 209410	Apomys	sierrae	F	skull,asr, tiss	Philippines	Luzon I	Aurora Prov	Dinalungan Munic: 2 km S, 4.5 km E Anacuao Peak	1125	121.9291	16.2369 9	LRH8076
FMNH 209417	Apomys	sierrae	M	skull,asr, tiss	Philippines	Luzon I	Aurora Prov	Dinalungan Munic: 1.9 km S, 4 km E Anacuao Peak	1300	121.9291	16.2371 5	LRH8114
FMNH 209429	Apomys	sierrae	F	skull,asr, tiss	Philippines	Luzon I	Aurora Prov	Dinalungan Munic: 0.25 km S, 0.65 km E Anacuao Peak	1500	121.8936	16.2530 8	DSB7195
FMNH 209433	Apomys	sierrae	M	skull,asr, tiss	Philippines	Luzon I	Aurora Prov	Dinalungan Munic: 0.25 km S, 0.65 km E Anacuao Peak	1500	121.8936	16.2530 8	DSB7199
FMNH 216434	Apomys	sierrae	F	skull,asr, tiss	Philippines	Luzon I	Cagayan Prov	Peñablanca Munic: 3 km N, 8.75 km W Mt. Cetaceo peak	740	121.9714	17.7343 8	DSB8592
FMNH 216443	Apomys	sierrae	F	skull,asr, tiss	Philippines	Luzon I	Cagayan Prov	Peñablanca Munic: 2.33 km N, 7.8 km W Mt. Cetaceo peak	900	121.9794	17.7273 6	DSB8658
FMNH 216447	Apomys	sierrae	M	skull,asr, tiss	Philippines	Luzon I	Cagayan Prov	Peñablanca Munic: 2.33 km N, 7.8 km W Mt. Cetaceo peak	900	121.9794	17.7273 6	DSB8665

FMNH 216464	Apomys	sierrae	M	skull,asr, tiss	Philippines	Luzon I	Cagayan Prov	Peñablanca Munic: 2.65 km N, 9.15 km W Mt. Cetaceo peak	490	121.9672	17.7309 5	DSB8743
FMNH 214157	Apomys	sp. karst	M	skull,asr, tiss	Philippines	Luzon I	Cagayan Prov	Peñablanca Munic: 9.5 km N, 3.7 km E Peñablanca town center	200	121.8187	17.7121 3	DSB8147
FMNH 178283	Apomys	zambalensis	M	skull,asr, tiss	Philippines	Luzon I	Zambales Prov	Mt High Peak, Palauig Munic, Barangay Salasa	1200	120.084	15.4617 2	DSB3195
FMNH 178287	Apomys	zambalensis	M	skull,asr, tiss	Philippines	Luzon I	Zambales Prov	Mt High Peak, Palauig Munic, Barangay Salasa	1200	120.084	15.4617 2	DSB3202
FMNH 178303	Apomys	zambalensis	F	skull,asr	Philippines	Luzon I	Zambales Prov	Mt High Peak, Palauig Munic, Barangay Salasa	1690	120.107	15.4675	DSB3323
FMNH 178314	Apomys	zambalensis	F	skull,asr	Philippines	Luzon I	Zambales Prov	Mt High Peak, Palauig Munic, Barangay Salasa	1690	120.107	15.4675	DSB3343
FMNH 183420	Apomys	zambalensis	F	skull,asr, tiss	Philippines	Luzon I	Bataan Prov	0.1 km N Mt Natib peak	1150	120.3989	14.7151 3	LRH7339
FMNH 183625	Apomys	zambalensis	F	skull,skel , tiss	Philippines	Luzon I	Bataan Prov	0.3 km N, 0.1 km W Mt Natib peak	1000	120.3981	14.7157 4	EAR5722
FMNH 183629	Apomys	zambalensis	F	skull,skel	Philippines	Luzon I	Bataan Prov	0.3 km N, 0.1 km W Mt Natib peak	1000	120.3981	14.7157 4	EAR5742
FMNH 183631	Apomys	zambalensis	M	skull,skel , tiss	Philippines	Luzon I	Bataan Prov	0.1 km N Mt Natib peak	1150	120.3989	14.7151 3	LRH7343
FMNH 183637	Apomys	zambalensis	M	skull,skel	Philippines	Luzon I	Bataan Prov	0.1 km N Mt Natib peak	1150	120.3989	14.7151 3	EAR5747
FMNH 212573	Apomys	zambalensis	M	skull,asr, tiss	Philippines	Luzon I	Pampanga Prov	Mabalacat Munic., 7.4 km N, 13 km E Mt. Pinatubo peak	365	120.4621	15.2037 2	DSB7562
FMNH 212622	Apomys	zambalensis	F	skull,asr, tiss	Philippines	Luzon I	Pampanga Prov	Mabalacat Munic., 3.2 km N, 11.5 km E Mt. Pinatubo peak	670	120.4501	15.1779 6	DSB7712
FMNH 216278	Apomys	zambalensis	M	skull,asr, tiss	Philippines	Luzon I	Pampanga Prov	Mabalacat Munic., 2 km N, 6.2 km E Mt. Pinatubo peak	1080	120.3986	15.1555 3	DSB8936
FMNH 216279	Apomys	zambalensis	M	skull,asr, tiss	Philippines	Luzon I	Pampanga Prov	Mabalacat Munic., 2 km N, 6.2 km E Mt. Pinatubo peak	1080	120.3986	15.1555 3	DSB8937
FMNH 147172	Archboldomys	luzonensis	M	skull,asr	Philippines	Luzon I	Camarines Sur Prov	Mt Isarog National Park	1700	123.38	13.67	DSB2057
FMNH 147173	Archboldomys	luzonensis	M	skull,asr	Philippines	Luzon I	Camarines Sur Prov	Mt Isarog National Park	1800	123.38	13.67	DSB2061
FMNH 95122	Archboldomys	luzonensis	M	skin,skull	Philippines	Luzon I	Camarines Sur Prov	Mt Isarog, Curry, Pili	732	123.35	13.65	DSR1449
USNM 573505	Archboldomys	luzonensis	M	skull,skel	Philippines	Luzon I	Camarines Sur Prov	Naga, 4 km N, 22 km E, Mt. Isarog		123.37	13.67	EAR1998
USNM 573838	Archboldomys	luzonensis	F	skull,asr	Philippines	Luzon I	Camarines Sur Prov	Naga, 4 km N, 22 km E, Mt. Isarog		123.37	13.67	EAR1837
FMNH 193522	Archboldomys	maximus	M	skull,asr, tiss	Philippines	Luzon I	Mountain Prov	Barlig Munic. 0.5 km N, 0.5 km W Mt Amuyao peak	2530	121.1219	17.0171 7	LRH7572
FMNH 193526	Archboldomys	maximus	M	skull,asr, tiss	Philippines	Luzon I	Mountain Prov	0.4 km N, 0.4 km W Mt Amuyao peak	2480	121.1239	17.0172 7	EAR6356
FMNH 193528	Archboldomys	maximus	F	skull,asr, tiss	Philippines	Luzon I	Mountain Prov	0.75 km W Mt Amuyao peak	2300	121.122	17.0148 7	DSB4436
FMNH 193531	Archboldomys	maximus	M	skull,asr, tiss	Philippines	Luzon I	Mountain Prov	1.75 km N, 0.4 km W Mt Amuyao peak	1885	121.1237	17.0292 9	DSB4540
FMNH 193944	Archboldomys	maximus	F	skull,skel , tiss	Philippines	Luzon I	Mountain Prov	1.75 km N, 0.4 km W Mt Amuyao	1885	121.1247	17.0292 9	DSB4577

USNM 151506	Batomys	dentatus	M	skin,skull	Philippines	Luzon I	Benguet Prov	Haights-in-the-Oaks				EAM6484
FMNH 169125	Batomys	granti	M	skull,asr, tiss	Philippines	Luzon I	Kalinga Prov	Balbalan Munic, Balbalasang Brgy: Magdallao	1600	121.075	17.425	EAR4560
FMNH 175722	Batomys	granti	F	skull,skel , tiss	Philippines	Luzon I	Kalinga Prov	Balbalan Munic, Balbalasang Brgy: Mt Bali-it	1950	121.0017	17.43	EAR4977
FMNH 188323	Batomys	granti	M	skull,asr, tiss	Philippines	Luzon I	Mountain Prov	Mt Data; 0.1 km E south peak	2310	120.8608	16.8588	LRH7434
FMNH 214323	Batomys	granti	F	skull,asr, tiss	Philippines	Luzon I	Mountain Prov	Barlig Munic. 0.5 km N, 0.5 km W Mt Amuyao peak	2530	121.1219	17.0171	DSB7820
FMNH 214324	Batomys	granti	M	skull,asr, tiss	Philippines	Luzon I	Mountain Prov	Barlig Munic. 2.15 km N, 1.25 km W Mt Amuyao peak	1650	121.116	17.0327	DSB7888
FMNH 142046	Batomys	uragon	M	skull,asr	Philippines	Luzon I	Camarines Sur Prov	Mt Isarog		123.3834	13.65	DSB639
FMNH 152033	Batomys	uragon	M	skull,asr	Philippines	Luzon I	Camarines Sur Prov	Mt Isarog, 4 km N, 21.5 km E Naga City	1550	123.37	13.67	DSB3054
USNM 458914	Batomys	uragon	F	skull,skel	Philippines	Luzon I	Camarines Sur Prov	Naga, 4 km N, 22 km E, Mt. Isarog		123.37	13.67	EAR1987
USNM 458939	Batomys	uragon	F	skull,asr	Philippines	Luzon I	Camarines Sur Prov	Naga, 4 km N, 21.5 km E, Mt. Isarog		123.367	13.6667	LRH4150
USNM 458941	Batomys	uragon	M	skull,asr	Philippines	Luzon I	Camarines Sur Prov	Naga, 4 km N, 21.5 km E, Mt. Isarog		123.367	13.6667	LRH4165
USNM 458946	Batomys	uragon	M	skull,asr	Philippines	Luzon I	Camarines Sur Prov	Naga, 4 km N, 22 km E, Mt. Isarog		123.37	13.67	EAR1988
USNM 458947	Batomys	uragon	M	skull,asr	Philippines	Luzon I	Camarines Sur Prov	Naga, 4 km N, 22 km E, Mt. Isarog		123.37	13.67	EAR1993
USNM 458949	Batomys	uragon	M	skull,asr	Philippines	Luzon I	Camarines Sur Prov	Naga, 4 km N, 22 km E, Mt. Isarog		123.37	13.67	EAR2004
USNM 102549	Carpomys	melanurus	M	skin,skull	Philippines	Luzon I		Lepanto ?				JW10
FMNH 175565	Carpomys	phaeurus	F	skull,asr, tiss	Philippines	Luzon I	Kalinga Prov	Balbalan Munic, Balbalasang Brgy: Mt Bali-it	2150	120.9967	17.4283	LRH6866
FMNH 62291	Carpomys	phaeurus	F	skin,skull ,skel	Philippines	Luzon I	Mountain Prov	Mt Kapilingan		121.0167	16.8334	HH425
USNM 458953	Chrotomys	gonzalesi	M	skull,asr	Philippines	Luzon I	Camarines Sur Prov	Naga, 4 km N, 22 km E, Mt. Isarog		123.37	13.67	EAR1850
USNM 458956	Chrotomys	gonzalesi	F	skull,asr	Philippines	Luzon I	Camarines Sur Prov	Naga, 4 km N, 21 km E, Mt. Isarog		123.367	13.6667	EAR2013
USNM 458957	Chrotomys	gonzalesi	M	skull,asr	Philippines	Luzon I	Camarines Sur Prov	Naga, 4 km N, 21 km E, Mt. Isarog		123.367	13.6667	EAR2014
USNM 458958	Chrotomys	gonzalesi	F	skull,asr	Philippines	Luzon I	Camarines Sur Prov	Naga, 4 km N, 21 km E, Mt. Isarog		123.367	13.6667	RBU284
FMNH 178257	Chrotomys	mindorensis	M	skull,asr, tiss	Philippines	Luzon I	Zambales Prov	Mt High Peak, Palauig Munic, Barangay Salasa	1690	120.107	15.4675	DSB3316
FMNH 180400	Chrotomys	mindorensis	F	skull,asr, tiss	Philippines	Luzon I	Quirino Prov	Nagtipunan Munic, Brgy Matmad, Sitio Mangitagud, Mungiao Mts	450	121.4777	16.0562 5	DSB3414
FMNH 180403	Chrotomys	mindorensis	F	skull,asr, tiss	Philippines	Luzon I	Quirino Prov	Nagtipunan Munic, Brgy Matmad, Sitio Mangitagud, Mungiao Mts	450	121.4777	16.0562 5	DSB3425
FMNH 180404	Chrotomys	mindorensis	M	skull,asr, tiss	Philippines	Luzon I	Quirino Prov	Nagtipunan Munic, Brgy Matmad, Sitio Mangitagud, Mungiao Mts	450	121.4828	16.0560 6	DSB3438

FMNH 180406	Chrotomys	mindorensis	M	skull,asr, tiss	Philippines	Luzon I	Quirino Prov	Nagtipunan Munic, Brgy Matmad, Sitio Mangitagud, Mungiao Mts	450	121.4828	16.0560 6	DSB3450
FMNH 180437	Chrotomys	mindorensis	F	skull,skel , tiss	Philippines	Luzon I	Quirino Prov	Nagtipunan Munic, Brgy Matmad, Sitio Mangitagud, Mungiao Mts	450	121.4828	16.0560 6	DSB3444
FMNH 183340	Chrotomys	mindorensis	F	skull,asr, tiss	Philippines	Luzon I	Bataan Prov	0.7 km N, 0.2 km W Mt Natib peak	900	120.3968	14.7192 9	LRH7292
FMNH 183549	Chrotomys	mindorensis	M	skull,asr, tiss	Philippines	Luzon I	Zambales Prov	Palauig Munic: Brgy Salasa: Mt Tapulao peak	2024	120.1196	15.4818 9	DSB3520
FMNH 183551	Chrotomys	mindorensis	M	skull,asr, tiss	Philippines	Luzon I	Zambales Prov	Palauig Munic: Brgy Salasa: Mt Tapulao	925	120.0663	15.4626 9	DSB3558
FMNH 183639	Chrotomys	mindorensis	M	skull,skel , tiss	Philippines	Luzon I	Bataan Prov	0.7 km N, 0.2 km W Mt Natib peak	900	120.3968	14.7192 9	EAR5703
FMNH 195051	Chrotomys	mindorensis	M	skull,asr, tiss	Philippines	Luzon I	Nueva Vizcaya Prov	Quezon Munic, 3.75 km N, 0.5 km W Mt Palali peak	700	121.2186	16.4621 6	PAA1118
FMNH 205488	Chrotomys	mindorensis	M	skull,asr, tiss	Philippines	Luzon I	Rizal Prov	Rodriguez Munic., 1.5 km S, 1 km W Mt Irid peak	700	121.3162	14.7766	DSB5909
FMNH 206030	Chrotomys	mindorensis	M	skull,asr, tiss	Philippines	Luzon I	Cagayan Prov	Peñablanca Munic: 9.1 km N, 3.5 km E Peñablanca town center	100	121.8174	17.7070 2	MVD320
FMNH 206031	Chrotomys	mindorensis	F	skull,asr, tiss	Philippines	Luzon I	Cagayan Prov	Peñablanca Munic: 9.1 km N, 3.5 km E Peñablanca town center	100	121.8174	17.7070 2	MVD321
FMNH 212644	Chrotomys	mindorensis	M	skull,asr, tiss	Philippines	Luzon I	Pampanga Prov	Mabalacat Munic., 7.4 km N, 13 km E Mt. Pinatubo peak	365	120.4621	15.2037 2	DSB7570
FMNH 212649	Chrotomys	mindorensis	F	skull,asr, tiss	Philippines	Luzon I	Pampanga Prov	Mabalacat Munic., 3.2 km N, 11.5 km E Mt. Pinatubo peak	670	120.4501	15.1779 6	DSB7743
FMNH 222104	Chrotomys	mindorensis	F	skull,asr, tiss	Philippines	Mindoro I	Oriental Mindoro Prov	Baco Munic., 9 km N, 0.85 km E Mt. Halcon peak	500	121.0181	13.3454 2	DSB9307
FMNH 222277	Chrotomys	mindorensis	F	skull,skel , tiss	Philippines	Mindoro I	Occidental Mindoro Prov	Paluan Munic., 1.8 km S, 1.05 km E Mt. Calavite peak	900	120.4115	13.4663 4	DSB9857
FMNH 222280	Chrotomys	mindorensis	M	skull,skel , tiss	Philippines	Mindoro I	Occidental Mindoro Prov	Paluan Munic., 1.3 km S, 0.85 km E Mt. Calavite peak	1100	120.4099	13.4713 4	DSB9929
FMNH 183336	Chrotomys	mindorensis	F	skull,asr, tiss	Philippines	Luzon I	Bataan Prov	0.3 km N, 0.1 km W Mt Natib peak	1000	120.3981	14.7157 4	EAR5728
FMNH 209343	Chrotomys	mindorensis	M	skull,asr, tiss	Philippines	Luzon I	Cavite Prov	Ternate Munic., 1.4 km N, 1.36 km E Pico de Loro peak	400	120.6627	14.2285 1	DSB7387
FMNH 209345	Chrotomys	mindorensis	F	skull,asr, tiss	Philippines	Luzon I	Cavite Prov	Ternate Munic., 0.26 km N, 0.12 km W Pico de Loro peak	550	120.6491	14.218	DSB7418
FMNH 222105	Chrotomys	mindorensis	M	skull,asr, tiss	Philippines	Mindoro I	Oriental Mindoro Prov	Baco Munic., 9 km N, 0.85 km E Mt. Halcon peak	500	121.0181	13.3454 2	DSB9308
FMNH 180399	Chrotomys	mindorensis	M	skull,asr	Philippines	Luzon I	Cagayan Prov	Baggao Munic, Brgy Sta Margarita, Sitio Matulang, Mt Twin Peaks	100	122.1119	17.8811 1	PAA463
FMNH 191005	Chrotomys	mindorensis	F	skull,asr, tiss	Philippines	Luzon I	Nueva Ecija Prov	Gabaldon Munic: Nueva Ecija University of Science and Technology campus	100			MRMD440
FMNH 195050	Chrotomys	mindorensis	M	skull,asr, tiss	Philippines	Luzon I	Nueva Vizcaya Prov	Quezon Munic, 3.75 km N, 0.5 km W Mt Palali peak	700	121.2186	16.4621 6	PAA1117
FMNH 195056	Chrotomys	mindorensis	F	skull,asr, tiss	Philippines	Luzon I	Nueva Vizcaya Prov	Quezon Munic, 3.75 km N, 0.5 km W Mt Palali peak	700	121.2186	16.4621 6	PAA1120

FMNH 195058	Chrotomys	mindorensis	M	skull,asr, tiss	Philippines	Luzon I	Nueva Vizcaya Prov	Quezon Munic, 3.75 km N, 0.5 km W Mt Palali peak	700	121.2186	16.4621 6	MRMD49 3
USNM 536800	Chrotomys	mindorensis	F	skin,skull , skel	Philippines	Luzon I	Laguna Prov	College, International Rice Research Institute				LOU36
USNM 536801	Chrotomys	mindorensis	F	skin,skull , skel	Philippines	Luzon I	Laguna Prov	College, International Rice Research Institute				LOU37
USNM 536802	Chrotomys	mindorensis	M	skin,skull	Philippines	Luzon I	Laguna Prov	College, International Rice Research Institute				
FMNH 175726	Chrotomys	silaceus	M	skull,skel , tiss	Philippines	Luzon I	Kalinga Prov	Balbalan Munic, Balbalasang Brgy: Mt Bali-it	2150	120.9967	17.4283	LRH6903
FMNH 170971	Chrotomys	silaceus	F	skull,skel , tiss	Philippines	Luzon I	Kalinga Prov	Balbalan Munic, Balbalasang Brgy: Am-licao	1800	121.0708	17.4417	PAA810
FMNH 193731	Chrotomys	silaceus	F	skull,asr, tiss	Philippines	Luzon I	Mountain Prov	1.0 km N, 1.0 km W Mt Amuyao peak	2150	121.1179	17.0221 3	DSB4524
FMNH 193950	Chrotomys	silaceus	M	skull,skel , tiss	Philippines	Luzon I	Mountain Prov	0.4 km N, 0.4 km W Mt Amuyao peak	2480	121.1239	17.0172 7	EAR6366
FMNH 193951	Chrotomys	silaceus	F	skull,skel , tiss	Philippines	Luzon I	Mountain Prov	0.4 km N, 0.4 km W Mt Amuyao peak	2480	121.1239	17.0172 7	EAR6371
FMNH 193955	Chrotomys	silaceus	M	skull,skel , tiss	Philippines	Luzon I	Mountain Prov	0.75 km W Mt Amuyao peak	2300	121.122	17.0148 7	DSB4404
FMNH 198726	Chrotomys	silaceus	M	alc, tiss	Philippines	Luzon I	Mountain Prov	1.0 km N, 1.0 km W Mt Amuyao peak	2150	121.1179	17.0221 3	DSB5308
FMNH 198864	Chrotomys	silaceus	M	skull,skel , tiss	Philippines	Luzon I	Benguet Prov	Mt Pulag NP, 0.5 km S, 0.4 km W Mt Babadak peak	2480	120.8783	16.5764 5	LRH7952
FMNH 198865	Chrotomys	silaceus	M	skull,skel , tiss	Philippines	Luzon I	Benguet Prov	Mt Pulag NP, 0.5 km S, 0.4 km W Mt Babadak peak	2480	120.8783	16.5764 5	LRH7974
FMNH 198869	Chrotomys	silaceus	F	skull,skel , tiss	Philippines	Luzon I	Benguet Prov	Mt Pulag NP, 1.75 km S, 0.9 km E Mt Pulag peak	2650	120.9051	16.5836 3	LRH8047
FMNH 169140	Chrotomys	whiteheadi	F	skull,asr, tiss	Philippines	Luzon I	Kalinga Prov	Balbalan Munic, Balbalasang Brgy: Mapga	1050	121.075	17.425	EAR4565
FMNH 170972	Chrotomys	whiteheadi	M	skin,skull ,skel, tiss	Philippines	Luzon I	Kalinga Prov	Balbalan Munic, Balbalasang Brgy: Mapga	1050	121.075	17.425	EAR4536
FMNH 175728	Chrotomys	whiteheadi	F	skull,skel , tiss	Philippines	Luzon I	Kalinga Prov	Balbalan Munic, Balbalasang Brgy: Mt Bali-it	1950	121.0017	17.43	LRH6710 b
FMNH 175729	Chrotomys	whiteheadi	M	skull,skel , tiss	Philippines	Luzon I	Kalinga Prov	Balbalan Munic, Balbalasang Brgy: Mt Bali-it	1950	121.0017	17.43	LRH6813
FMNH 188456	Chrotomys	whiteheadi	M	skull,skel , tiss	Philippines	Luzon I	Mountain Prov	Mt Data; 0.75 km N, 0.6 km E south peak	2241	120.8611	16.8628 7	DSB3847
FMNH 188458	Chrotomys	whiteheadi	M	skull,asr, tiss	Philippines	Luzon I	Aurora Prov	Dinalungan Munic: 0.2 km E Anacuao Peak	1725	121.889	16.2552 7	LRH7406
FMNH 188462	Chrotomys	whiteheadi	F	skull,skel , tiss	Philippines	Luzon I	Mountain Prov	Mt Data; 0.75 km N, 1.0 km E south peak	2289	120.8671	16.8623 3	LRH7456
FMNH 188463	Chrotomys	whiteheadi	F	skull,skel , tiss	Philippines	Luzon I	Mountain Prov	Mt Data; 0.75 km N, 0.75 km E south peak	2289	120.865	16.8608 2	LRH7464
FMNH 195026	Chrotomys	whiteheadi	F	skull,asr, tiss	Philippines	Luzon I	Nueva Vizcaya Prov	Quezon Munic, Mt Palali peak	1700	121.2215	16.4277 7	MRMD46 0
FMNH 195045	Chrotomys	whiteheadi	M	skull,asr, tiss	Philippines	Luzon I	Nueva Vizcaya Prov	Quezon Munic, 3.5 km N, 0.1 km W Mt Palali peak	839	121.2222	16.4595 5	MVD199
FMNH 195048	Chrotomys	whiteheadi	F	skull,asr, tiss	Philippines	Luzon I	Nueva Vizcaya Prov	Quezon Munic, 3.5 km N, 0.1 km W Mt Palali peak	839	121.2222	16.4595 5	MVD202
FMNH 209520	Chrotomys	whiteheadi	M	skull,asr, tiss	Philippines	Luzon I	Aurora Prov	Dinalungan Munic: 0.2 km E Anacuao Peak	1725	121.889	16.2552 7	DSB7286

FMNH 209521	Chrotomys	whiteheadi	F	skull,asr, tiss	Philippines	Luzon I	Aurora Prov	Dinalungan Munic: 0.2 km N Anacuao Peak	1805	121.8879	16.2576 8	DSB7347
AMNH 146562	Crateromys	schadenbergi	F	skull,skel	Philippines	Luzon I						
FMNH 198871	Crateromys	schadenbergi	M	skull,skel , tiss	Philippines	Luzon I	Benguet Prov	Mt Pulag NP, 1.15 km S, 1.35 km E Mt Pulag peak	2695	120.9096	16.5881 6	DSB5361
FMNH 62294	Crateromys	schadenbergi	M	skin,skull ,skel	Philippines	Luzon I	Mountain Prov	Mt Kapilingan		121.0167	16.8334	HH404
FMNH 62296	Crateromys	schadenbergi	F	skin,skull ,skel	Philippines	Luzon I	Mountain Prov	Mt Kapilingan	2438	121.0167	16.8334	HH441
USNM 102544	Crateromys	schadenbergi	F	skin,skull	Philippines	Luzon I		Lepanto ?				JW3
USNM 102546	Crateromys	schadenbergi	M	skin,skull	Philippines	Luzon I		Lepanto ?				JW4
USNM 102554	Crateromys	schadenbergi	F	skin,skull	Philippines	Luzon I		Lepanto ?				JW13
USNM 282646	Crateromys	schadenbergi	M	skin,skull,skel				Locality Unknown				NZP1072 2
FMNH 209522	Musseromys	anacuao	F	skull,asr, tiss	Philippines	Luzon I	Aurora Prov	Dinalungan Munic: 0.2 km E Anacuao Peak	1725	121.889	16.2552 7	DSB7267
FMNH 209523	Musseromys	anacuao	M	skull,asr, tiss	Philippines	Luzon I	Aurora Prov	Dinalungan Munic: 0.2 km E Anacuao Peak	1725	121.889	16.2552 7	DSB7287
FMNH 198714	Musseromys	beneficus	F	skull,asr, tiss	Philippines	Luzon I	Benguet Prov	Mt Pulag NP, 1.15 km S, 1.35 km E Mt Pulag peak	2695	120.9096	16.5881 6	DSB5326
FMNH 198857	Musseromys	beneficus	M	skull,skel , tiss	Philippines	Luzon I	Benguet Prov	Mt Pulag NP, 1.15 km S, 1.35 km E Mt Pulag peak	2695	120.9096	16.5881 6	DSB5357
FMNH 178405	Musseromys	gulantang	M	skull,asr, tiss	Philippines	Luzon I	Quezon Prov	Mt Banahaw, Barangay Lalo	620	121.5396	14.0518 1	DSB3408
FMNH 193838	Musseromys	inopinatus	M	skull,asr	Philippines	Luzon I	Mountain Prov	0.75 km W Mt Amuyao peak	2300	121.122	17.0148 7	DSB4386 b
FMNH 193839	Musseromys	inopinatus	M	skull,asr, tiss	Philippines	Luzon I	Mountain Prov	1.0 km N, 1.0 km W Mt Amuyao peak	2150	121.1179	17.0221 3	DSB4477
FMNH 193840	Musseromys	inopinatus	F	skull,asr, tiss	Philippines	Luzon I	Mountain Prov	1.75 km N, 1.5 km W Mt Amuyao peak	1950	121.113	17.0259 5	DSB4555
FMNH 214333	Musseromys	inopinatus	M	skull,asr, tiss	Philippines	Luzon I	Mountain Prov	Barlig Munic. 2.15 km N, 1.25 km W Mt Amuyao peak	1650	121.116	17.0327	DSB7937
FMNH 148187	Phloeomys	cumingi		man	Philippines	Luzon I	Camarines Sur Prov	Mt Isarog National Park, Ocampo Munic, Del Rosario	350	123.38	13.67	DSB2148
FMNH 148188	Phloeomys	cumingi		man	Philippines	Luzon I	Camarines Sur Prov	Mt Isarog National Park, Ocampo Munic, Del Rosario	350	123.38	13.67	DSB2149
USNM 573151	Phloeomys	cumingi	M	skin,skull ,skel	Philippines	Catandua nes I	Catanduanes Prov	Barrio Summit		124.32	13.78	LRH3847
USNM 573152	Phloeomys	cumingi	F	skull,skel	Philippines	Catandua nes I	Catanduanes Prov	Barrio Summit		124.32	13.78	EAR1684
USNM 573153	Phloeomys	cumingi	F	skull,skel	Philippines	Catandua nes I	Catanduanes Prov	Barrio Summit		124.32	13.78	EAR1689
USNM 573506	Phloeomys	cumingi	F	skull,skel	Philippines	Luzon I	Camarines Sur Prov	Mt. Isarog				LRH4045
USNM 573508	Phloeomys	cumingi	F	skin,skull ,skel	Philippines	Luzon I	Camarines Sur Prov	Naga, 4 km N, 15 km E, Yabo River, Mt. Isarog				LRH3962
AMNH 242103	Phloeomys	pallidus	?	skull,skel	Philippines	Luzon I	Kalinga Prov	Balbalan				

FMNH 175730	Phloeomys	pallidus		skull,skel	Philippines	Luzon I	Kalinga Prov	vicinity of Saltan	1400			EAR5063
FMNH 193967	Phloeomys	pallidus	F	skin,skull ,skel, tiss	Philippines	Luzon I	Mountain Prov	Barlig Munic: north slope Mt Amuyao				LRH7514
FMNH 62297	Phloeomys	pallidus	M	skin,skull ,skel	Philippines	Luzon I	Abra Prov	Baay		120.8834	17.55	HH466
MCZ 35041	Phloeomys	pallidus	M	skin,skull ,skel	Philippines	Luzon I	Mountain Prov	near Baguio				
MCZ 38780	Phloeomys	pallidus	M	skin,skull ,skel	Philippines	Luzon I	Tayabas Province					
MCZ 39759	Phloeomys	pallidus	?	skin,skull ,skel	Philippines	Luzon I	Tayabas Province	North part of Tayabas Province				
USNM 151519	Phloeomys	pallidus	F	skin,skull	Philippines	Luzon I	Benguet Prov	Haights-in-the-Oaks				EAM6513
USNM 151520	Phloeomys	pallidus	F	skin,skull	Philippines	Luzon I	Benguet Prov	Haights-in-the-Oaks				EAM6475
FMNH 178429	Rhynchomys	banahao	M	skull,asr, tiss	Philippines	Luzon I	Quezon Prov	Mt Banahaw, Barangay Lalo	1465	121.5086	14.0665	LRH7020
FMNH 183590	Rhynchomys	banahao	M	skull,asr, tiss	Philippines	Luzon I	Quezon Prov	Tayabas Munic: Brgy Lalo: Mt Banahaw, Hasa-an	1250			D. S. Balete
FMNH 189840	Rhynchomys	isarogensis	F	skull,asr, tiss	Philippines	Luzon I	Camarines Norte Prov	0.25 km N, 0.25 km W east peak of Mt Labo	1413	122.7897	14.0188 3	DSB4059
FMNH 95123	Rhynchomys	isarogensis	M	skin,skull	Philippines	Luzon I	Camarines Sur Prov	Mt Isarog, Curry, Pili	1676	123.35	13.65	DSR1434
USNM 573573	Rhynchomys	isarogensis	F	skin,skull ,skel	Philippines	Luzon I	Camarines Sur Prov	Naga, 4 km N, 21 km E, Mt. Isarog		123.37	13.67	EAR2005
USNM 573575	Rhynchomys	isarogensis	M	skin,skull ,skel	Philippines	Luzon I	Camarines Sur Prov	Naga, 4 km N, 21 km E, Mt. Isarog		123.37	13.67	EAR2012
FMNH 169171	Rhynchomys	soricoides	M	skull,asr, tiss	Philippines	Luzon I	Kalinga Prov	Balbalan Munic, Balbalasang Brgy: Am-licao	1800	121.0708	17.4417	EAR4586
FMNH 170981	Rhynchomys	soricoides	M	skull,skel , tiss	Philippines	Luzon I	Kalinga Prov	Balbalan Munic, Balbalasang Brgy: Am-licao	1800	121.0708	17.4417	LRH6438 b
FMNH 175619	Rhynchomys	soricoides	F	skull,asr, tiss	Philippines	Luzon I	Kalinga Prov	Balbalan Munic, Balbalasang Brgy: Mt Bali-it	2150	120.9967	17.4283	EAR5036
FMNH 193980	Rhynchomys	soricoides	F	skull,skel , tiss	Philippines	Luzon I	Mountain Prov	Mt Amuyao peak	2690	121.1281	17.0133	LRH7671
FMNH 198886	Rhynchomys	soricoides	F	skull,skel , tiss	Philippines	Luzon I	Benguet Prov	Mt Pulag NP, 0.5 km S, 0.4 km W Mt Babadak peak	2480	120.8783	16.5764 5	LRH7889
FMNH 198887	Rhynchomys	soricoides	M	skull,skel , tiss	Philippines	Luzon I	Benguet Prov	Mt Pulag NP, 0.5 km S, 0.4 km W Mt Babadak peak	2480	120.8783	16.5764 5	LRH7927
FMNH 214423	Rhynchomys	soricoides	F	skull,skel , tiss	Philippines	Luzon I	Mountain Prov	Barlig Munic. 1.0 km N, 1.0 km W Mt Amuyao peak	2100	121.1179	17.0221 3	LRH8158
FMNH 191043	Rhynchomys	sp Mingan	M	skull,asr, tiss	Philippines	Luzon I	Aurora Prov	Dingalan Munic: 1.8 km S, 1.0 km W Mingan Peak	1677	121.3946	15.4658 6	DSB4108
FMNH 191045	Rhynchomys	sp Mingan	M	skull,asr, tiss	Philippines	Luzon I	Aurora Prov	Dingalan Munic: 1.8 km S, 1.0 km W Mingan Peak	1677	121.3946	15.4658 6	MRMD39 7
FMNH 183553	Rhynchomys	tapulao	F	skull,asr, tiss	Philippines	Luzon I	Zambales Prov	Palauig Munic: Brgy Salasa: Mt Tapulao peak	2024	120.1196	15.4818 9	DSB3472
FMNH 183554	Rhynchomys	tapulao	M	skull,asr, tiss	Philippines	Luzon I	Zambales Prov	Palauig Munic: Brgy Salasa: Mt Tapulao peak	2024	120.1196	15.4818 9	DSB3480
FMNH 183555	Rhynchomys	tapulao	M	skull,asr, tiss	Philippines	Luzon I	Zambales Prov	Palauig Munic: Brgy Salasa: Mt Tapulao peak	2024	120.1196	15.4818 9	DSB3505

FMNH 167304	Soricomys	kalinga	M	skull,asr, tiss	Philippines	Luzon I	Kalinga Prov	Balbalan Munic, Balbalasang Brgy: Magdallao	1600	121.0683	17.4583	EAR4575
FMNH 167307	Soricomys	kalinga	F	skull,asr, tiss	Philippines	Luzon I	Kalinga Prov	Balbalan Munic, Balbalasang Brgy: Magdallao	1600	121.0683	17.4583	LRH5995
FMNH 175555	Soricomys	kalinga	M	skull,asr, tiss	Philippines	Luzon I	Kalinga Prov	Balbalan Munic, Balbalasang Brgy: Mt Bali-it	1950	121.0017	17.43	EAR5001
FMNH 190963	Soricomys	leonardocoi	M	skull,asr, tiss	Philippines	Luzon I	Aurora Prov	Dingalan Munic: 1.8 km S, 1.0 km W Mingan Peak	1677	121.3946	15.4658 6	DSB4122
FMNH 190964	Soricomys	leonardocoi	F	skull,asr, tiss	Philippines	Luzon I	Aurora Prov	Dingalan Munic: 1.8 km S, 1.0 km W Mingan Peak	1677	121.3946	15.4658 6	PAA792
FMNH 190972	Soricomys	leonardocoi	M	skull,asr, tiss	Philippines	Luzon I	Aurora Prov	Dingalan Munic: 0.9 km S, 0.3 km W Mingan Peak	1785	121.4007	15.4739	DSB4160
FMNH 188314	Soricomys	montanus	M	skull,asr, tiss	Philippines	Luzon I	Mountain Prov	Mt Data; 0.75 km N, 0.6 km E south peak	2241	120.8611	16.8628 7	DSB3788
FMNH 188319	Soricomys	montanus	M	skull,asr, tiss	Philippines	Luzon I	Mountain Prov	Mt Data; 0.75 km N, 0.75 km E south peak	2289	120.865	16.8608 2	LRH7463
FMNH 193520	Soricomys	montanus	M	skull,asr, tiss	Philippines	Luzon I	Mountain Prov	1.0 km N, 1.0 km W Mt Amuyao peak	2150	121.1179	17.0221 3	DSB4529
FMNH 193521	Soricomys	montanus	F	skull,asr, tiss	Philippines	Luzon I	Mountain Prov	1.75 km N, 1.5 km W Mt Amuyao peak	1950	121.113	17.0259 5	DSB4570
FMNH 198715	Soricomys	montanus	M	skull,asr, tiss	Philippines	Luzon I	Benguet Prov	Mt Pulag NP, 0.5 km S, 0.4 km W Mt Babadak peak	2480	120.8783	16.5764 5	LRH7897
FMNH 147176	Soricomys	musseri	M	skull,asr	Philippines	Luzon I	Cagayan Prov	Callao Municipality, Mt Cetaceo	1450	122.03	17.7	DSB2092
FMNH 185908	Soricomys	musseri	F	skull,asr, tiss	Philippines	Luzon I	Cagayan Prov	2.0 km SW Mt Cetaceo peak	1500	122.0345	17.6926 4	DSB3704
FMNH 185909	Soricomys	musseri	M	skull,asr, tiss	Philippines	Luzon I	Cagayan Prov	2.0 km SW Mt Cetaceo peak	1500	122.0345	17.6926 4	DSB3711

Appendix Table 2.2. Summary statistics for *arbutus* model adequacy testing along PC1-2 and centroid size for Phloeomyini and Chrotomyini. An asterisk indicates the statistic deviates significantly from the simulated distribution at $\alpha = 0.05$.

Phloeomyini	M_{SIG}	C_{VAR}	S_{VAR}	S_{ASR}	S_{HGT}	D_{CDF}
PC1	1.100	1.082	-13.52	0.4671	-12.16	0.1693
PC2	1.100	0.7829	-17.07	11.91	-227.5	0.1908
Centroid Size	1.100	0.8539	1.983	0.3859	5.0261	0.2121
Chrotomyini	M_{SIG}	C_{VAR}	S_{VAR}	S_{ASR}	S_{HGT}	D_{CDF}
PC1	1.038	0.9672	0.9111	6.129	25.63	0.1345
PC2	1.038	0.7841	-10.06	-1.849	40.27	0.1023
Centroid Size	1.038	0.7568	-0.06279	1.131	-0.5331	0.1802

Appendix Table 2.3. Average model support for 100 simulated character histories of Brownian Motion morphological evolution of PC 1 and 2.

Shape Model	**Single-Rate**	**Two-rate by clade**	**Three-rate by clade + *Rhy*[a]**	**Two-rate *Rhy*[b]**
ln(L)	172.6	181.6	197.0	193.3
k	5	8	11	8
AICc	-333.4	-342.4	-362.1	-365.8
ΔAICc	33.43	24.36	4.665	0.9716
Weight	6.181×10^{-8}	7.030×10^{-6}	0.3700	0.6301
Parameter Values	**Three-rate (PC1)**	**Three-rate (PC2)**	**Two-rate (PC1)**	**Two-rate (PC2)**
Phloeomyini	6.78×10^{-5}	4.85×10^{-4}	4.69×10^{-5}	2.22×10^{-4}
Chrotomyini	4.37×10^{-4}	9.76×10^{-5}	4.69×10^{-5}	2.22×10^{-4}
Rhynchomys	3.23×10^{-3}	4.15×10^{-4}	6.18×10^{-3}	3.14×10^{-4}

Appendix Table 2.4. Average model support for 100 simulated character histories of Brownian Motion morphological evolution of centroid size.

	Single-Rate	**Two-rate by clade**	**Three-rate by clade + *Rhy***	**Two-rate *Rhy***
ln(L)	12.10	16.55	16.89	12.25
k	2	3	4	3
AICc	-19.87	-26.41	-24.61	-17.81
ΔAICc	6.555	0.01681	1.814	8.611
Weight	2.601×10^{-2}	0.6814	0.2832	9.327×10^{-3}
Parameter Values	**Two-Rate Centroid Size**			
Phloeomyini	2.24×10^{-2}			
Chrotomyini	5.30×10^{-3}			

Appendix Table 2.5. Likelihood ratio tests (LRT) of decelerating morphological evolution fitted to phylogenetically-transformed PC1-2 of mandibular shape. Statistically significant result of LRT suggests a decelerating rate model of evolution better describes the rate of evolution in the given clade. An asterisk indicates the likelihood ratio D is statistically significant at $\alpha = 0.05$.

Clade	**Phloeomyini**		**Chrotomyini**	
$\ln(L)_{BM}$	37.85		126.4	
$\ln(L)_{EB}$	37.85		127.5	
D	0		2.23	
d.f.	1		1	
Parameter values	**pPC1**	**pPC2**	**pPC1**	**pPC2**
σ_0^2 (initial rate)	8.91×10^{-4}	1.63×10^{-4}	2.91×10^{-4}	1.99×10^{-4}
$\bar{\sigma}^2$(average rate)	8.91×10^{-4}	1.63×10^{-4}	2.91×10^{-4}	1.99×10^{-4}
θ (ancestral state)	-1.50×10^{-16}	-8.24×10^{-15}	-1.92×10^{-16}	4.03×10^{-17}
β (deceleration parameter)	N/A		N/A	

Appendix Table 2.6. Summary statistics for *arbutus* model adequacy testing along phylogenetically corrected PC1-2 for Phloeomyini and Chrotomyini. An asterisk indicates the statistic deviates significantly from the simulated distribution at $\alpha = 0.05$.

Phloeomyini	M_{SIG}	C_{VAR}	S_{VAR}	S_{ASR}	S_{HGT}	D_{CDF}
PC1	1.100	1.557*	-16.49	-2.993	-78.27	0.2742
PC2	1.100	0.7881	3.163	9.610	94.54	0.1405
Chrotomyini	M_{SIG}	C_{VAR}	S_{VAR}	S_{ASR}	S_{HGT}	D_{CDF}
PC1	1.038	1.213*	13.07	-3.692	370.0	0.239
PC2	1.038	0.6061	-4.269	-6.890	-66.15	0.1581

Appendix Table 2.7. Average model support for 100 simulated character histories of Brownian motion morphological evolution of phylogenetically corrected PC 1-2.

Shape Model	**Single-Rate**	**Two-rate by clade**	**Three-rate by clade + *Rhy*[a]**	**Two-rate *Rhy***
ln(L)	164.4	182.2	190.6	175.5
k	5	8	11	8
AICc	-317.1	-343.6	-349.3	-330.1
ΔAICc	33.05	6.559	0.7775	19.97
Weight	4.305×10^{-7}	0.2043	0.7952	4.941×10^{-4}

a: average parameters for 3-rate model: $r(\text{PC1})_P = 7.74 \times 10^{-4}$, $r(\text{PC2})_P = 1.62 \times 10^{-4}$, $r(\text{PC1})_C = 5.77 \times 10^{-5}$, $r(\text{PC2})_C = 9.96 \times 10^{-5}$, $r(\text{PC1})_R = 9.77 \times 10^{-4}$, $r(\text{PC2})_R = 1.24 \times 10^{-3}$.

APPENDIX 3. SUPPLEMENTARY MATERIAL FOR CHAPTER 3.

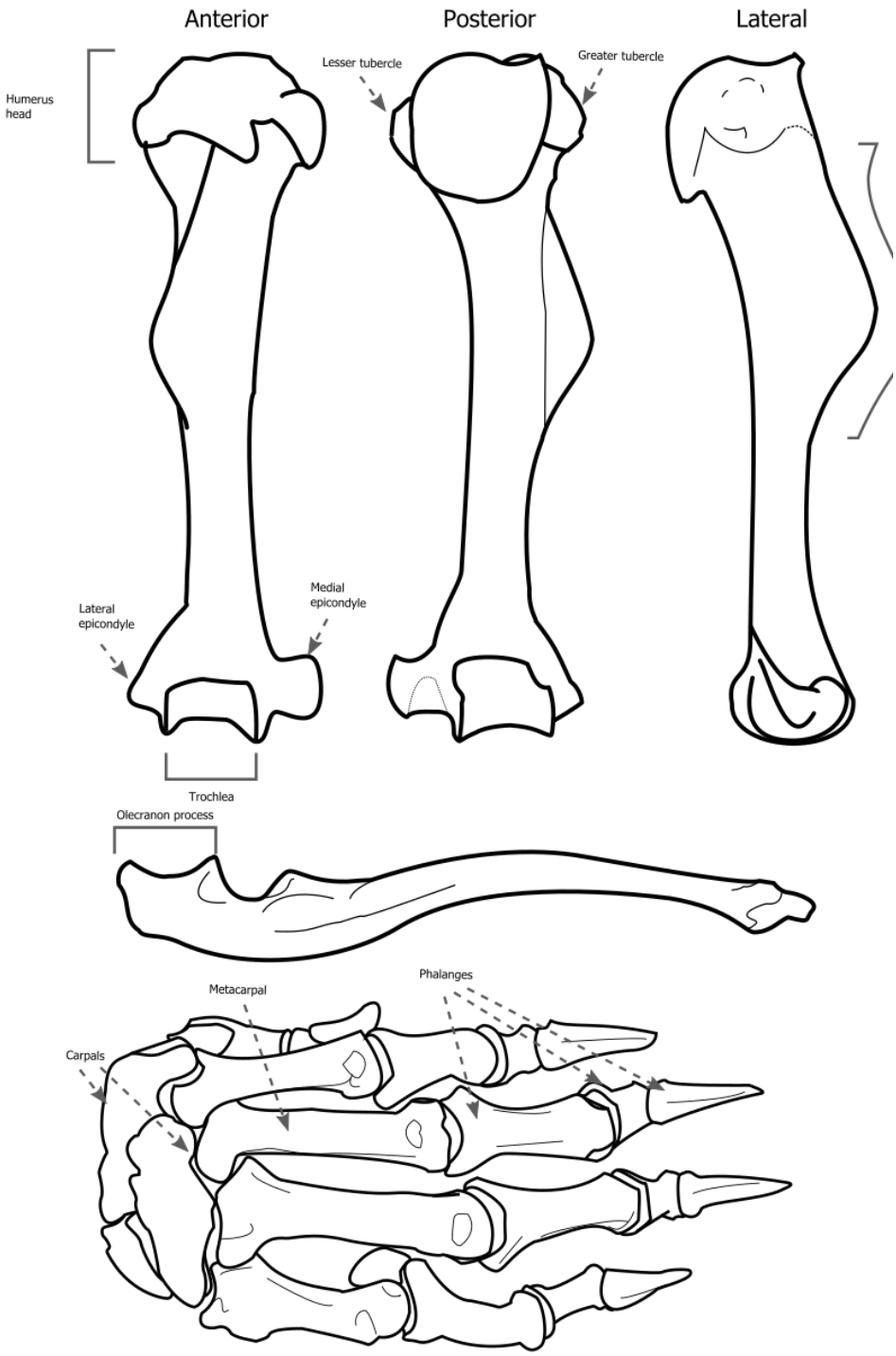

Appendix Figure 3.1 (Previous). Forelimb illustrations labeled with anatomical terms discussed in the manuscript.

Appendix Figure 3.2 (Left). Mean shape for locomotory categories (black) relative to mean for the entire dataset (gray). Left: lateral view; right: posterior view.

Apomys (gray) vs. *Rhynchomys* (black)

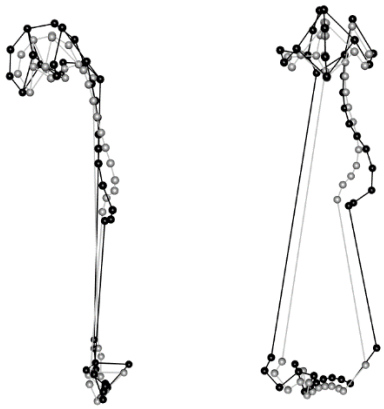

Phloeomys/Crateromys (gray) vs.
Musseromys (black)

Batomys (gray) vs.
Soricomys kalinga and *S. montanus* (black)

Appendix Figure 3.3 (Left). Mean shape for genera with divergent humerus shapes within the same locomotory category based on residuals of linear models including humerus shape as response variable. Left: lateral view; right: posterior view.

Appendix Table 3.1. Specimens examined and associated metadata

Taxon	Catalog Number	Sex	Item Scanned	Province	Locality	Elevation (m)	Latitude	Longitude
Apomys abrae	FMNH 167358	Male	forelimb	Kalinga Prov	Balbalan Munic, Balbalasang Brgy: Magdallao	1600	17.4583	121.0683
Apomys abrae	FMNH 170929	Female	forelimb	Kalinga Prov	Balbalan Munic, Balbalasang Brgy: Mapga	1050	17.475	121.075
Apomys aurorae	FMNH 191068	Female	forelimb	Aurora Prov	Dingalan Munic: 2 km S, 2 km W Mingan Peak	1305	15.464561	121.384211
Apomys aurorae	FMNH 191070	Male	forelimb	Aurora Prov	Dingalan Munic: 2 km S, 2 km W Mingan Peak	1305	15.464561	121.384211
Apomys aurorae	FMNH 191072	Male	forelimb	Aurora Prov	Dingalan Munic: 2 km S, 2 km W Mingan Peak	1305	15.464561	121.384211
Apomys banahao	FMNH 179452	Male	forelimb	Quezon Prov	Mt Banahaw, Barangay Lalo	1465	14.0665	121.50858
Apomys banahao	FMNH 179456	Female	forelimb	Quezon Prov	Mt Banahaw, Barangay Lalo	1465	14.06635	121.50855
Apomys brownorum	FMNH 183504	Female	carcass	Zambales Province	Palauig Munic: Brgy Salasa: Mt Tapulao peak	2024	15.48189	120.11956
Apomys brownorum	FMNH 183516	Male	carcass	Zambales Province	Palauig Munic: Brgy Salasa: Mt Tapulao peak	2024	15.48189	120.11956
Apomys datae	FMNH 175662	Female	forelimb	Kalinga Prov	Balbalan Munic, Balbalasang Brgy: Mt Bali-it	1950	17.43	121.0017
Apomys datae	FMNH 175692	Male	forelimb	Kalinga Prov	Balbalan Munic, Balbalasang Brgy: Mt Bali-it	2150	17.4283	120.9967
Apomys iridensis	FMNH 206324	Female	forelimb	Rizal Prov	Rodriguez Munic., 1.25 km S, 0.5 km W Mt Irid peak	920	14.78	121.32116
Apomys iridensis	FMNH 206325	Male	forelimb	Rizal Prov	Rodriguez Munic., 1.25 km S, 0.5 km W Mt Irid peak	920	14.78	121.32116

Taxon	Catalog Number	Sex	Item Scanned	Province	Locality	Elevation (m)	Latitude	Longitude
Apomys magnus	FMNH 183578	Male	carcass	Quezon Prov	Tayabas Munic: Brgy Lalo: Mt Banahaw, Hasa-an	1250		
Apomys microdon	FMNH 189874	Female	forelimb	Camarines Norte Prov	1.5 km N, 0.75 km W east peak of Mt Labo	910	14.031731	122.785069
Apomys microdon	FMNH 189875	Male	forelimb	Camarines Norte Prov	1.5 km N, 0.75 km W east peak of Mt Labo	910	14.031731	122.785069
Apomys microdon	FMNH 209585	Male	forelimb	Aurora Prov	Dinalungan Munic: 0.2 km S, 1.15 km E Anacuao Peak	1360	16.25456	121.89861
Apomys minganensis	FMNH 190955	Male	carcass	Aurora Prov	Dingalan Munic: Mt Mingan	1540		
Apomys minganensis	FMNH 191065	Female	carcass	Aurora Prov	Dingalan Munic: 0.9 km S, 0.3 km W Mingan Peak	1785	15.4739	121.400661
Apomys musculus	FMNH 214410	Female	forelimb	Mountain Prov	Barlig Munic. 1.0 km N, 1.0 km W Mt Amuyao peak	2100	17.022131	121.117911
Apomys musculus	FMNH 214411	Male	forelimb	Mountain Prov	Barlig Munic. 1.0 km N, 1.0 km W Mt Amuyao peak	2100	17.022131	121.117911
Apomys sacobianus	FMNH 216359	Male	forelimb	Pampanga Prov	Mabalacat Munic., 2 km N, 6.2 km E Mt. Pinatubo peak	1080	15.15553	120.39856
Apomys sacobianus	FMNH 216367	Female	forelimb	Pampanga Prov	Mabalacat Munic., 2 km N, 6.2 km E Mt. Pinatubo peak	1080	15.15553	120.39856
Apomys sierrae	FMNH 186821	Male	forelimb	Nueva Vizcaya Prov	Quezon Munic, 1.3 km NE Mt Palali Peak	1434	16.439511	121.22339
Apomys sierrae	FMNH 186823	Female	forelimb	Nueva Vizcaya Prov	Quezon Munic, 1.3 km NE Mt Palali Peak	1434	16.439511	121.22339

Taxon	Catalog Number	Sex	Item Scanned	Province	Locality	Elevation (m)	Latitude	Longitude
Apomys zambalensis	FMNH 183629	Female	forelimb	Bataan Prov	0.3 km N, 0.1 km W Mt Natib peak	1000	14.715739	120.398069
Apomys zambalensis	FMNH 183637	Male	forelimb	Bataan Prov	0.1 km N Mt Natib peak	1150	14.715131	120.398919
Archboldomys luzonensis	USNM 573505	Male	forelimb	Camarines Sur Province	Naga, 4 km N, 22 km E, Mt. Isarog		13.67	123.37
Archboldomys luzonensis	USNM 573838	Female	carcass	Camarines Sur Province	Naga, 4 km N, 22 km E, Mt. Isarog		13.67	123.37
Archboldomys maximus	FMNH 193943	Male	forelimb	Mountain Prov	0.75 km W Mt Amuyao peak	2300	17.014869	121.121961
Archboldomys maximus	FMNH 193944	Female	forelimb	Mountain Prov	1.75 km N, 0.4 km W Mt Amuyao	1885	17.029289	121.124661
Batomys granti	FMNH 175722	Female	forelimb	Kalinga Prov	Balbalan Munic, Balbalasang Brgy: Mt Bali-it	1950	17.43	121.0017
Batomys granti	FMNH 188321	Male	carcass	Mountain Prov	Mt Data; 0.75 km N, 0.6 km E south peak	2241	16.862869	120.861081
Batomys granti	FMNH 62504	Male	forelimb	Mountain Prov	Mt Data		16.85	120.8666
Batomys uragon	USNM 458914	Female	forelimb	Camarines Sur Province	Naga, 4 km N, 22 km E, Mt. Isarog		13.6667	123.367
Batomys uragon	USNM 458941	Male	carcass	Camarines Sur Province	Naga, 4 km N, 21.5 km E, Mt. Isarog		13.6667	123.367
Carpomys melanurus	FMNH 198723	Male	carcass	Benguet Prov	Mt Pulag NP, 0.8 km S, 0.9 km W Mt Babadak peak	2285	16.572989	120.874319

Taxon	Catalog Number	Sex	Item Scanned	Province	Locality	Elevation (m)	Latitude	Longitude
Carpomys phaeurus	FMNH 175565	Female	carcass	Kalinga Prov	Balbalan Munic, Balbalasang Brgy: Mt Bali-it	2150	17.4283	120.9967
Carpomys phaeurus	FMNH 62291	Female	forelimb	Mountain Prov	Mt Kapilingan		16.8334	121.0167
Chrotomys gonzalesi	USNM 458957	Male	carcass	Camarines Sur Province	Naga, 4 km N, 21 km E, Mt. Isarog		13.6667	123.367
Chrotomys gonzalesi	USNM 458958	Female	carcass	Camarines Sur Province	Naga, 4 km N, 21 km E, Mt. Isarog		13.6667	123.367
Chrotomys mindorensis	FMNH 180437	Female	forelimb	Quirino Prov	Nagtipunan Munic, Brgy Matmad, Sitio Mangitagud, Mungiao Mts	450	16.05606	121.48278
Chrotomys mindorensis	FMNH 183639	Male	forelimb	Bataan Prov	0.7 km N, 0.2 km W Mt Natib peak	900	14.719289	120.396769
Chrotomys silaceus	FMNH 198864	Male	forelimb	Benguet Prov	Mt Pulag NP, 0.5 km S, 0.4 km W Mt Babadak peak	2480	16.57645	120.8783
Chrotomys silaceus	FMNH 214416	Female	forelimb	Mountain Prov	Barlig Munic. 2.15 km N, 1.25 km W Mt Amuyao peak	1650	17.0327	121.11604
Chrotomys whiteheadi	FMNH 188458	Male	forelimb	Mountain Prov	Mt Data; 0.1 km E south peak	2310	16.858881	120.860781
Chrotomys whiteheadi	FMNH 188460	Female	forelimb	Mountain Prov	Mt Data; 0.1 km E south peak	2310	16.858881	120.860781
Crateromys schadenbergi	FMNH 62294	Male	forelimb	Mountain Prov	Mt Kapilingan		16.8334	121.0167
Crateromys schadenbergi	FMNH 62296	Female	forelimb	Mountain Prov	Mt Kapilingan	2438	16.8334	121.0167

Taxon	Catalog Number	Sex	Item Scanned	Province	Locality	Elevation (m)	Latitude	Longitude
Crateromys schadenbergi	FMNH 198871	Male	forelimb	Benguet Prov	Mt Pulag NP, 1.15 km S, 1.35 km E Mt Pulag peak	2695	16.588161	120.9096
Musseromys anacuao	FMNH 209523	Male	carcass	Aurora Prov	Dinalungan Munic: 0.2 km E Anacuao Peak	1725	16.25527	121.88896
Musseromys anacuao	FMNH 209524	Female	carcass	Aurora Prov	Dinalungan Munic: 0.2 km E Anacuao Peak	1725	16.25527	121.88896
Musseromys beneficus	FMNH 198713	Female	carcass	Benguet Prov	Mt Pulag NP, 1.15 km S, 1.35 km E Mt Pulag peak	2695	16.588161	120.9096
Musseromys beneficus	FMNH 198857	Male	forelimb	Benguet Prov	Mt Pulag NP, 1.15 km S, 1.35 km E Mt Pulag peak	2695	16.588161	120.9096
Musseromys inopinatus	FMNH 193838	Male	carcass	Mountain Prov	0.75 km W Mt Amuyao peak	2300	17.014869	121.121961
Musseromys inopinatus	FMNH 193840	Female	carcass	Mountain Prov	1.0 km N, 1.0 km W Mt Amuyao peak	2150	17.022131	121.117911
Phloeomys cumingi	USNM 573506	Female	forelimb	Camarines Sur Province	Mt. Isarog			
Phloeomys cumingi	USNM 573508	Female	forelimb	Camarines Sur Province	Naga, 4 km N, 15 km E, Yabo River, Mt. Isarog			
Phloeomys pallidus	FMNH 175730	Female	forelimb	Kalinga Prov	vicinity of Saltan	1400		
Phloeomys pallidus	FMNH 193967	Female	forelimb	Mountain Prov	Barlig Munic: north slope Mt Amuyao			
Rhynchomys banahao	FMNH 183590	Male	carcass	Quezon Prov	Tayabas Munic: Brgy Lalo: Mt Banahaw, Hasa-an	1250		
Rhynchomys banahao	FMNH 218404	Female	carcass	Laguna Prov	Majayjay Munic. 1.0 km N, 0.4 km E Mt. Banahaw peak			
Rhynchomys isarogensis	USNM 573573	Female	forelimb	Camarines Sur Province	Naga, 4 km N, 21 km E, Mt. Isarog		13.67	123.37
Rhynchomys isarogensis	USNM 573575	Male	forelimb	Camarines Sur Province	Naga, 4 km N, 21 km E, Mt. Isarog		13.67	123.37

Taxon	Catalog Number	Sex	Item Scanned	Province	Locality	Elevation (m)	Latitude	Longitude
Rhynchomys soricoides	FMNH 198886	Female	forelimb	Benguet Prov	Mt Pulag NP, 0.5 km S, 0.4 km W Mt Babadak peak	2480	16.57645	120.8783
Rhynchomys soricoides	FMNH 198887	Male	forelimb	Benguet Prov	Mt Pulag NP, 0.5 km S, 0.4 km W Mt Babadak peak	2480	16.57645	120.8783
Rhynchomys tapulao	FMNH 183553	Female	carcass	Zambales Province	Palauig Munic: Brgy Salasa: Mt Tapulao peak	2024	15.48189	120.11956
Rhynchomys tapulao	FMNH 183554	Male	carcass	Zambales Province	Palauig Munic: Brgy Salasa: Mt Tapulao peak			
Soricomys kalinga	FMNH 170966	Female	forelimb	Kalinga Prov	Balbalan Munic, Balbalasang Brgy: Am-licao	1800	17.4417	121.0708
Soricomys kalinga	FMNH 175721	Male	forelimb	Kalinga Prov	Balbalan Munic, Balbalasang Brgy: Mt Bali-it	2150	17.4283	120.9967
Soricomys leonardocoi	FMNH 190963	Male	carcass	Aurora Prov	Dingalan Munic: 1.8 km S, 1.0 km W Mingan Peak	1677	15.465861	121.394569
Soricomys leonardocoi	FMNH 190964	Female	carcass	Aurora Prov	Dingalan Munic: 1.8 km S, 1.0 km W Mingan Peak	1677	15.465861	121.394569
Soricomys montanus	FMNH 188449	Male	forelimb	Mountain Prov	Mt Data; 0.75 km N, 1.0 km E south peak	2289	16.862331	120.8671
Soricomys montanus	FMNH 193521	Female	carcass	Mountain Prov	1.75 km N, 1.5 km W Mt Amuyao peak	1950	17.02595	121.113011
Soricomys musseri	FMNH 185908	Female	carcass	Cagayan Province	2.0 km SW Mt Cetaceo peak	1500	17.692639	122.034461
Soricomys musseri	FMNH 185909	Male	carcass	Cagayan Province	2.0 km SW Mt Cetaceo peak	1500	17.692639	122.034461

APPENDIX 4. SUPPLEMENTARY MATERIAL FOR CHAPTER 4.

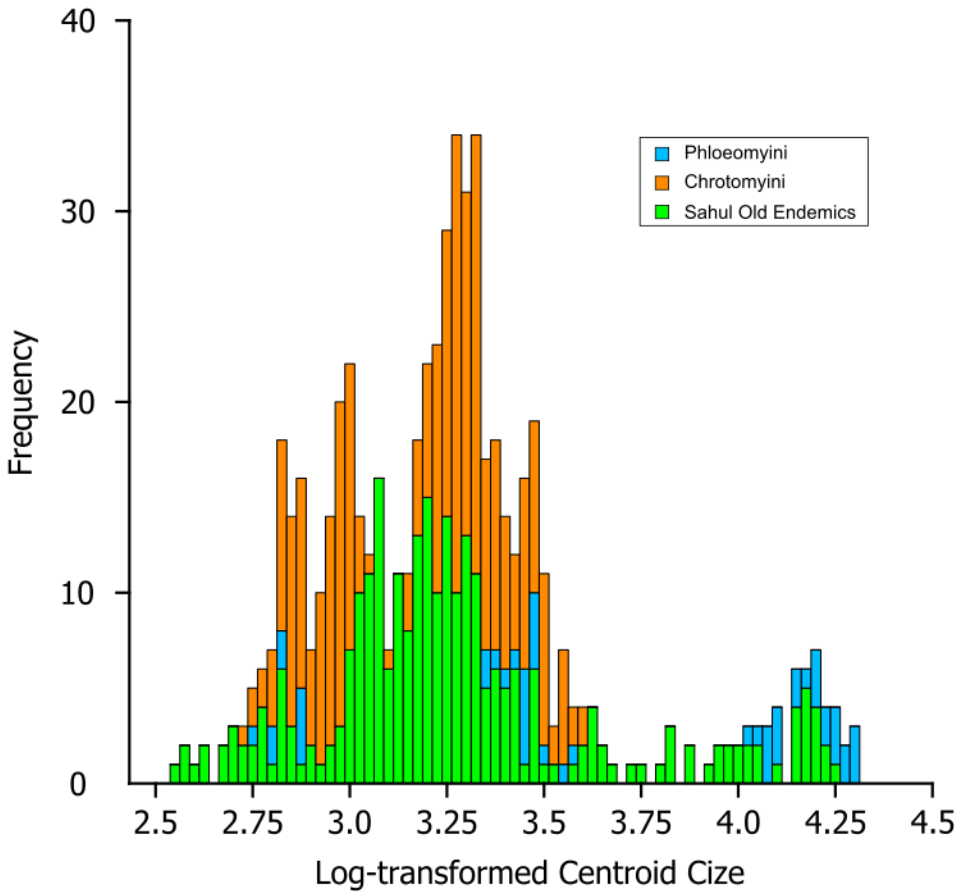

Appendix Figure 4.1. Histogram of specimen-level data of log-transformed centroid size, or the average within-configuration distance between each landmark and the center of the landmark configuration.

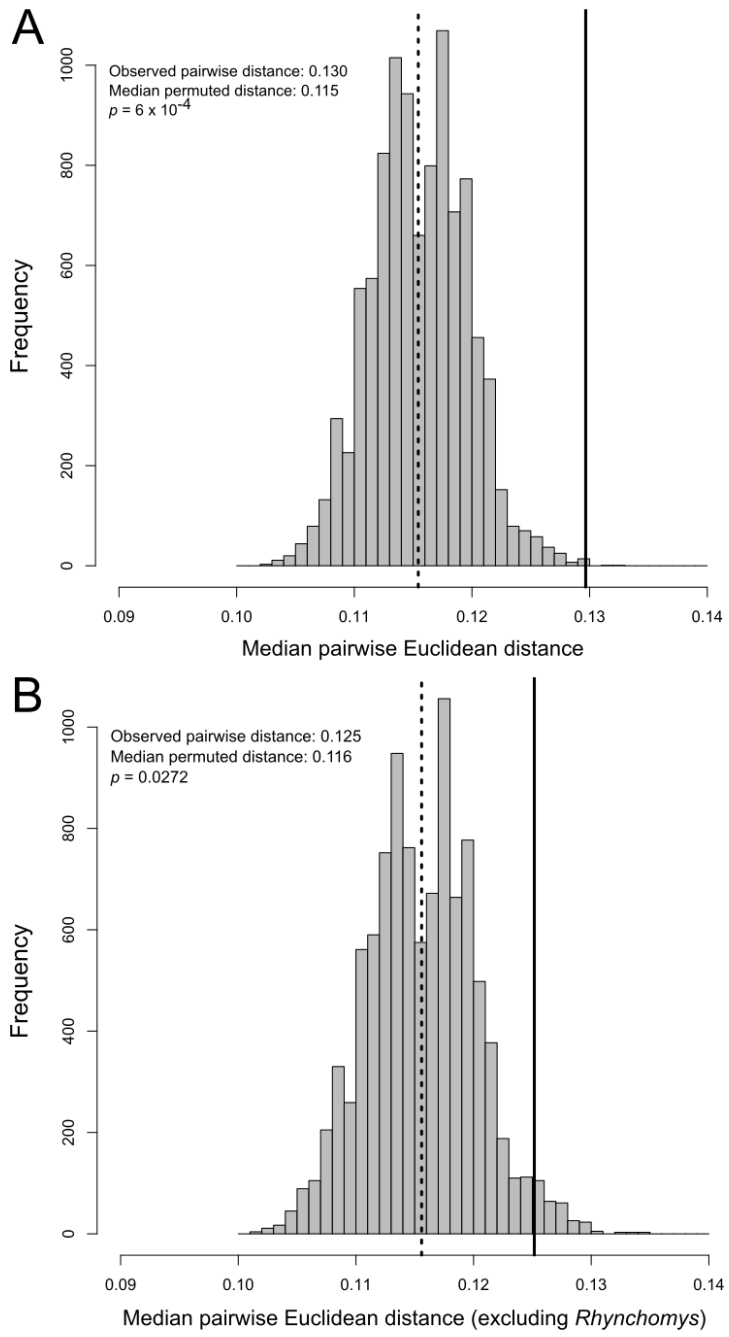

Appendix Figure 4.2. Histograms comparing average Euclidean distance in mandible principal component scores along PC1-2 between Chrotomyini and Phloeomyini (solid black line) to the distribution of 10,000 average distances between Phloeomyini and permutations of Sahul Old Endemics (gray bars, median: dashed line). (*A*) *Rhynchomys* included, (*B*) *Rhynchomys* excluded.

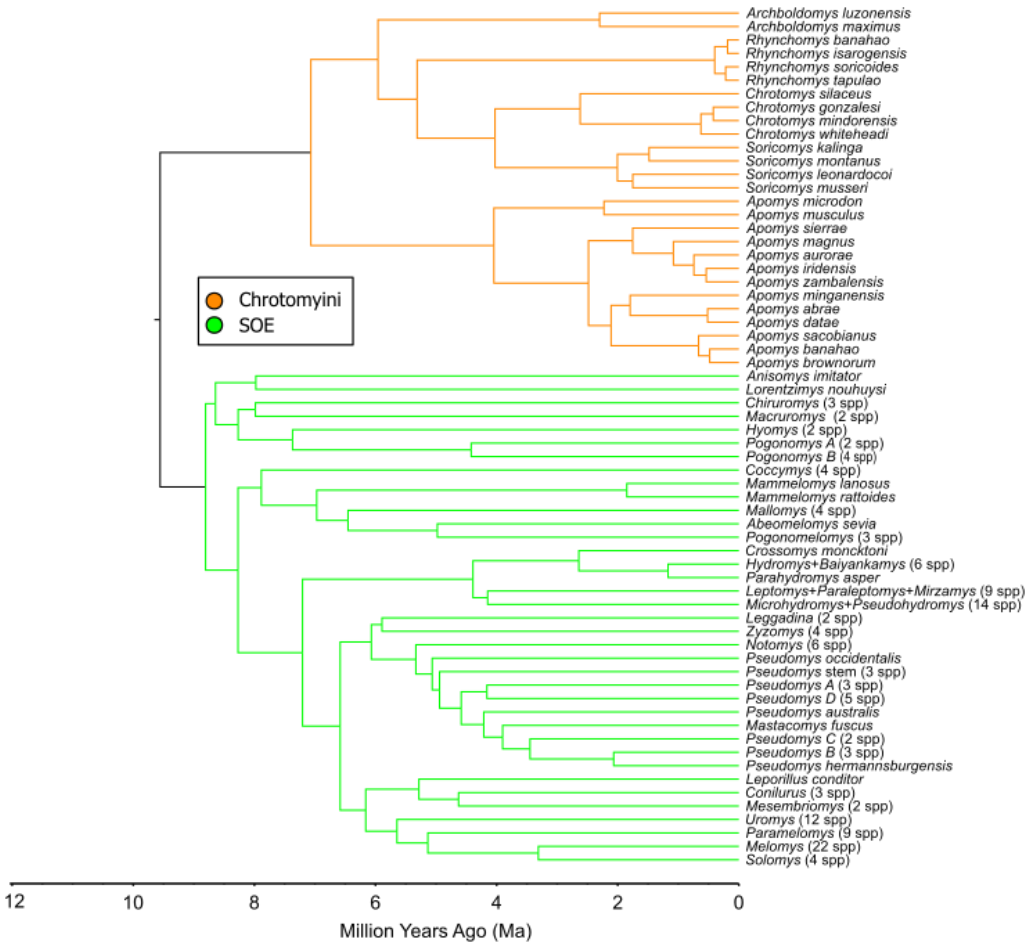

Appendix Figure 4.3. Tree used in MECCA analysis. SOE clades with incomplete sampling list the estimated number of species in that clade based on the taxonomic accounts of (Denys et al. 2017) in parentheses after the clade name. The ancestral state inferred by this analysis corresponds to the root node of this tree.

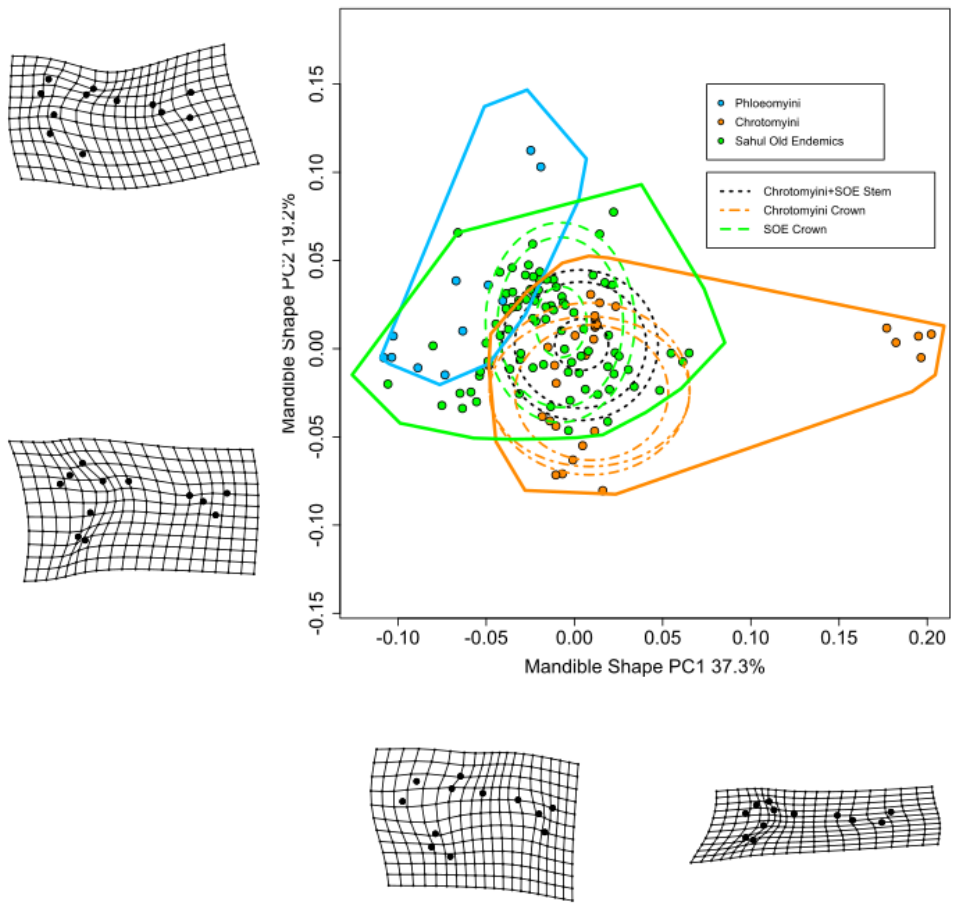

Appendix Figure 4.4. Principal components 1 and 2 of LOE rodent variation with SOE projected in based on LOE rotation matrix. Reference warps along axes illustrate the extreme shapes along each axis. Points indicate species averages, and the specimen-level extremes of each clade are indicated with convex hulls. Ancestral state estimates are given in dashed ellipses, with increasing radius for each ancestor indicating 50%, 90%, and 95% highest posterior density.

Appendix Table 4.1. Primers used in this study, accompanied by the source of the primer sequence.

Locus & Sequence	Forward Primer	Reverse Primer
GHR	GHRF1 (GHREXON10 in Adkins *et al*. 2001)	GHREND (Adkins *et al*. 2001)
	GGRAARTTRGAGGAGGRGAACACMATCTT	CTACTGCATGATTTTGTTCAGTTGGTCTGTGCTCAC
IRBP	IRBPA (Stanhope *et al*. 1996)	IRBPB (Stanhope *et al*. 1996)
	ATGGCCAAGGTCCTCTTGGATAACTACTGCTT	CGCAGGTCCATGATGAGGTGCTCCGTGTCCTG
CYTB	MVZ05A (Smith and Patton 1991, Jansa *et al*. 1999)	UMMZ04 (Smith and Patton 1991, Jansa *et al*. 1999)
	GAAAAATCATCGTTGTAATTCAACT	TCTTCATTTYWGGTTTACAAGAC
BRCA1 – part 1	BRCA1 F19 (this study)	BRCA1 R1141 (this study)
	TGGGCTGAAAGTAAAGAAACATG	GCCAGCTTTGTTCATTAATTTCTC
BRCA1 – part 2	BRCA1 F958 (this study)	BRCA1 R2021 (this study)
	GAACTTCAAATCGATAGTTGTGG	CTCAAATTGTCCCTCTGTCAGAG
BRCA1 – part 3	BRCA1 F1871 (this study)	BRCA1 R2380 (this study)
	CTGGAGTTTCTAGGCTTTGTC	TCTTACCACTTCTCATAGGTTG